Using exceptional points and non-Hermitian topology to simulate fractional charges and apparent event horizons in superconducting circuits

vorgelegt von

Mohammad Atif Javed
geboren am 04.02.1997 in Jhansi, India

Inaugural-Dissertation

zur
Erlangung des Doktorgrades
der Mathematisch-Naturwissenschaftlichen Fakultät
der Universität zu Köln

Januar 2025

Erklärung

„Hiermit versichere ich an Eides statt, dass ich die vorliegende Dissertation selbstständig und ohne die Benutzung anderer als der angegebenen Hilfsmittel und Literatur angefertigt habe. Alle Stellen, die wörtlich oder sinngemäß aus veröffentlichten und nicht veröffentlichten Werken dem Wortlaut oder dem Sinn nach entnommen wurden, sind als solche kenntlich gemacht. Ich versichere an Eides statt, dass diese Dissertation noch keiner anderen Fakultät oder Universität zur Prüfung vorgelegen hat; dass sie - abgesehen von unten angegebenen Teilpublikationen und eingebundenen Artikeln und Manuskripten - noch nicht veröffentlicht worden ist sowie, dass ich eine Veröffentlichung der Dissertation vor Abschluss der Promotion nicht ohne Genehmigung des Promotionsausschusses vornehmen werde. Die Bestimmungen dieser Ordnung sind mir bekannt. Darüber hinaus erkläre ich hiermit, dass ich die Ordnung zur Sicherung guter wissenschaftlicher Praxis und zum Umgang mit wissenschaftlichem Fehlverhalten der Universität zu Köln gelesen und sie bei der Durchführung der Dissertation zugrundeliegenden Arbeiten und der schriftlich verfassten Dissertation beachtet habe und verpflichte mich hiermit, die dort genannten Vorgaben bei allen wissenschaftlichen Tätigkeiten zu beachten und umzusetzen. Ich versichere, dass die eingereichte elektronische Fassung der eingereichten Druckfassung vollständig entspricht."

Teilpublikationen:

1. Mohammad Atif Javed, Jakob Schwibbert, and Roman-Pascal Riwar. "Fractional Josephson effect versus fractional charge in superconducting–normal metal hybrid circuits". In: *Phys. Rev. B* 107 (3 Jan. 2023), p. 035408. DOI: `10.1103/PhysRevB.107.035408`. URL: `https://link.aps.org/doi/10.1103/PhysRevB.107.035408`.

2. M. A. Javed et al. *Utilizing and extending superconducting circuit toolbox to simulate analog quantum gravity.* 2024. arXiv: `2406.01261 [cond-mat.mes-hall]`. URL: `https://arxiv.org/abs/2406.01261`.

Mohammad Atif Javed
Jülich, 10.01.2025

Unterschrift: ...., Datum: 10.01.2025

Acknowledgements

I would like to express my gratitude to my advisor, Dr. Roman-Pascal Riwar, for his guidance and support throughout my PhD. I am also thankful to my colleagues, both past and present, in the group for valuable and insightful discussions. My deepest thanks go to my family and friends for their support throughout the years.

Abstract

Conventional superconductors are one of the most well known example of macroscopic quantum phenomena, therefore superconducting circuits have emerged as a promising platform for qubits, quantum information processing and simulating light-matter interactions. The endeavor of simulating exotic physics on superconducting circuits is also accompanied with search of new circuit elements, apart from already existing elements such as capacitors, inductors and Josephson junctions, that can help in reproducing these novel phenomena experimentally. In this thesis we discuss three different projects that are unified by presence of exceptional points and non-Hermitian topology, that touch on one or both of these aspects of superconducting circuits. In the first project we study a system with both supercurrents and lossy currents in order to unify the two distinct ways of detecting fractional charges. We find that charge quantization is here a conserved property of the detector basis of the Lindbladian, while charge fractionalization is a topological property of its complex-valued eigenspectrum. We show that already conventional superconductor-normal metal hybrid circuits exhibit a variety of topological phases, including an open quantum system version of a fractional Josephson effect, due to the presence of exceptional points in its spectrum. In the second project we study topology of a dissipative system, that can mimic some essential features of an Andreev bound state spectrum of a multi-terminal Josephson junction. We find that this system indeed has topological properties that are encoded in an open system version of Chern number. We also find the full counting statistics for this toy model and conclude that this Chern number is not measurable via any regular transport experiment. Finally in the third project we show how superconducting circuit hardware can implement a variety of classical and quantum spacetime geometries on lattices, by both using established circuit elements and introducing new ones. We demonstrate the possibility of a metric sharply changing within a single lattice point, thus entering a regime where the modulation of system parameters is (in a sense) trans-Planckian, and the Hawking temperature ill-defined. In fact, our approach suggests that stable, thermal event horizons are incompatible with strictly discrete lattice models. Contrary to regular Hawking radiation (nonzero boson occupation number), the instability manifests as an accumulation of charge and phase quantum fluctuations over short time scales – a robust signature even in the presence of an environment. Moreover, we present a loop-hole for the typical black/white hole ambiguity in lattice simulations: exceptional points in the dispersion relation allows for the creation of pure black (or white) hole horizons, at the expense of radically changing the interior wormhole dynamics.

Contents

List of Figures

List of Tables

1. Introduction

1.1. Superconducting circuits: fractional charges, dissipation and event horizons

The recent push to implement quantum computation and construct usable technology for communication based on quantum effects, has brought forth superconducting circuits as a promising platform [Les+20; Bac+21; Cle+20; Lac+19]. This is due to the fact that superconductors are one of the most well-understood examples of a macroscopic quantum phenomenon, with a coherent many-body state of electrons condensed into Cooper pairs. This state is characterized with a complex-valued order parameter $\Delta e^{i\phi}$, where the superconducting phase ϕ represents in a sense a counting field for the number of Cooper pairs stored in the condensate [Tin04]. In short, the order parameter being 2π-periodic in ϕ expresses the fact that the condensate hosts an integer number of Cooper pairs, in a very similar way to solid state band structure theory, where any discrete lattice gives rise to a Brillouin zone. Also, superconducting circuits provide a high degree of tunability since they can be fabricated on a chip using standard lithographical technologies [Gao+21]. These circuits consists of superconductors (called superconducting islands) connected via Josephson junctions or any other element that does not destroy the supercurrent. The study of superconducting circuits for simulating light-matter interactions is termed circuit quantum electrodynamics (circuit QED) [BGO23] in analogy with cavity QED [Kim98]. Just like cavity QED, circuit QED (cQED) also serves as a platform to simulate exotic physics. Studying dynamical Casimir effect [Wil+11], soliton dynamics [Ust98], topologically protected qubits [Gla+09] and quantum phase transitions [Fv01] are just a few examples of superconducting circuits being used to simulate novel phenomena in condensed matter physics. Simulating the aforementioned exotic phenomena often requires devising the energy dependence of the superconducting circuit on its parameters in a specific manner, this leads us to another aspect of research in cQED, which is to design and implement new circuit elements apart from the standard toolbox of resistors, capacitors and inductors. The Josephson junction (JJ) is one famous example of such a circuit element, more currently, there are proposals to implement a whole host of other circuit elements with different energy contributions:: Majorana junctions [FK09], quantum version of gyrators [VD14], multi-stable JJs [Smi+22] etc.

The Josephson junction can be described by an energy contribution to the circuit, of the form of $-E_J \cos(\phi)$ (where E_J is the Josephson energy, and ϕ here denotes the difference of superconducting phases of the two bulks connected by the junction). In alignment with the above Brillouin zone analogy, the 2π-periodic $\cos(\phi)$ energy describes sequential tunneling of integer Cooper pairs across the junction. On the other hand the Majorana junctions are predicted to show a 4π-periodic ($\sim \cos \phi/2$) Josephson effect [FK09], this is due to the fact that Majorana particles carry a fraction of charge of a Cooper pair (half to be specific). While Cooper pairs are composite particles (half a Cooper pair is simply a single electron), it may at a first glance seem unproblematic to fractionalize the Cooper pair, it nonetheless has to be noted that unpaired electrons cannot be part of the actual superconducting condensate – at least when implementing the topological superconductor by proximitizing a given material, such as nanowires [KOB19] or topological insulators [FK08] with a regular s-wave superconductor. Moreover, there exist generalizations to junctions with parafermions [ZK14b; Ort+15] where not only Cooper pairs, but the actual fundamental electron charge seems broken. As a matter of fact, charge quantisation is also seemingly violated if one naively tries to quantise the classical description of a regular, linear inductor, with an energy of the form $\sim \phi^2$, which thus, strangely, provides a quasiparticle with *infinitely* small fractional charge [Koc+09]. Hence cQED is not only a tool to put quantum effects to practical use, it also compels us to look closely at some fundamental aspects of condensed matter physics. Charge franctionalization and how to reconcile it with charge quantization [RB82] is not only of interest within the realm of superconducting circuits, but also connects to a very large body of work in strongly correlated quantum systems, for instance fractionally charged anyons in the fractional quantum Hall effect [KF94], or Luttinger liquid theory [GGM10]. In the absence of superconductivity (and thus of a superconducting phase ϕ), one first of all needs a different transport quantity to describe fractional charges, such as charge counting fields [Riw19], and one needs to include dissipative transport. A generalized understanding of charge franctionalization and quantization in hybrid systems containing both supercurrents and lossy currents (which was so far missing in the existing literature) is the main accomplishment of the first project of this thesis (Ch. 2). A 2π-periodic phase is not only rooted in the physical concept of charge quantization, but can also be regarded as providing a closed base manifold, on which a given topological number, such as the Chern number (see further below for a definition/further details) can be defined. In fact, as shown in [Riw+16a], one does not need topological superconductors to engineer a topological state in a circuit: regular 4-terminal Josephson junctions naturally provide the necessary degrees of freedom to realize Weyl points in the Brillouin zone defined by 3D space of the three independent superconducting phase differences. The Chern number, defined in a 2D slice in ϕ-space, can be nonzero due to the topological charge carried by the Weyl points, and lead to a quantized supercurrent response. However, once again, dissipative processes add considerable complexity, and even threaten to thwart a direct observation of the topological effect: poisoning by non-equilibrium quasiparticles leads to fluctuations of the Chern number, thus washing out the quantization of the current response. This leads to the second project, where nonequilibrium generalizations of Chern numbers in the context of quasiparticle poisoning in multiterminal junctions are studied (Ch. 3).

In the first two projects of this thesis (chapters 2 and 3), we will work with dissipative systems i.e. systems that are connected to an external environment. Taking into account dissipation results in a more realistic modelling of superconducting circuits, which is essential if we ever hope to use them as a basis for realistic devices. Additionally in the last decade non-equilibrium systems, which include both externally driven systems and dissipative systems, have received increasing attention as they offer a whole new range of phenomena that are impossible in equilibrium systems. Such as the realisation of continuous time crystals [Kon+22; Liu+23], Floquet states (achieved by periodic driving of a system) [Tsu24], observation of topological properties in dissipative systems that are topologically trivial in the closed limit [MPS15] etc.

Fractional charges in condensed matter systems are primarily studied in two different ways, first in case of non-equilibrium transport by finding the full counting statistics (FCS) of the system, second in case of coherent transport (supercurrent) by studying the phase picked up by the fractional charge when moving through a magnetic field. As alluded to earlier, studying charge fractionalization in presence of both supercurrents and lossy currents is the goal of the first project of this thesis (Ch. 2), therefore we will study a superconducting circuit that hosts both coherent and dissipative currents, and therefore aim to unify the two methods of studying fractional charges. As we will see, the existence of fractional charges, regardless of which approach we take to study them, will have an intimate connection with the existence of *exceptional points* in the spectrum of the Lindbladian superoperator that encodes the transport properties of the system. In the last section of this project we will also provide a proposal to experimentally observe a 4π-periodic Josephson effect using weak measurements.

Exceptional points are defined as points in parameter space where two eigenvalues and eigenvectors of a system coalesce into one. They are an important feature of open quantum systems where the generator of time evolution, unlike a closed system, is a non-Hermitian operator. Exceptional points are a widely studied topic in context of topology of non-equilibrium systems [Li+23], and their appearance in our work does imply presence of topological properties in the system, which will be discussed in chapter 2. Taking a cue from this result, we will further explore different notions of topology in open quantum systems in Ch.3 with multi terminal Josephson junction as the model system. Multi terminal Josephson junctions, which consist of more than two superconductors connected to a central scattering region, have emerged as a promising platform for simulating condensed matter models with topological properties [Riw+16a; XVL17; XVL18]. In particular our focus will be to extend the result of Riwar et. al. ([Riw+16a]), we will use the proposed extension of the tenfold way for quadratic Lindbladians [LMC20], to study the topology of a multi terminal Josephson junction in presence of quasiparticle poisoning which acts as a source of dissipation. We will find that a notion of topological invariant can indeed be defined even in the presence of dissipation.

The third and final project of this thesis (Ch. 4) is concerned with simulation of analog event horizons. While this may superficially seem like quite a rift from above subjects regarding superconducting circuits, topology, dissipation, and exceptional points, the results presented below will show remarkable parallels. The study of analog event horizons in condensed matter system is a long standing area of research, since it is more experimentally accessible than the study of astrophysical horizons. There have been both theoretical [Unr81; KBW20; STW20; De +21; Gar+00; Gar+01] and experimental [Ste14; Muñ+19; RBF22] works on the subject, some of which indeed use superconducting circuits [Nat+09; KHF20; TD19; Lan15]. Our proposal differs in a number of manners from existing works. One of the main differences is that we do not go to a continuous limit but rather fully embrace the discreteness of the circuit network, such that the lattice nature of the simulation gives us some unexpected results such as unavoidable dynamical instabilities and ambiguity about the nature of the event horizon (i.e. whether it is a black hole or a white hole). The issue of dynamical instabilities can actually be attributed to the appearance of exceptional points, which occur despite the system Hamiltonian being Hermitian. While the full explanation for this is quite involved and will be dealt with in the main text of the thesis, we here sketch a simplified picture. First, note that the emergence of an event horizon (in the same spirit as the original Unruh proposal [Unr81]) in a lattice model requires in essence a chain with inverted (negative) spring constants. Take for instance the circuit version of a harmonic oscillator, the LC resonator, where inverting the sign of the spring constant can be regarded as making the inductance L negative. The resonance frequency $1/\sqrt{LC}$ thus becomes imaginary – a transition that can be described simply as passing through an exceptional point (see also the square root discussion of exceptional points above). Such an instability can be avoided, and the system stabilized to real eigenvalues, when adding nonreciprocal interactions in the circuit which imitate a Lorentz boost. As it turns out, such a nonreciprocal process can be provided by the Chern number of multiterminal junctions. However, the stabiliziation of the full lattice, especially for inhomogeneous systems requires a delicate fine-tuning of system parameters, and can thus in general only be approximately satisfied, leading to latent generic instabilities.

There is a second way, in which periodicity breaking and exceptional points enter – and fundamentally connect to black and white holes. Namely, in lattice models, and event horizon can never be purely black or white hole [De +21], but is always a combination of both. This fact is straightforwardly related to the Nielsen-Ninomiya theorem [NN81]. In 3D lattice systems, it guarantees that Weyl points always emerge as pairs with opposite topological charge. In 1D lattices (the focus of Ch. 4), the dispersion relation of a massless field always has to cross zero energy at least twice within the Brillouin zone. As we show, under appropriate arrangement of the circuit elements within the lattice, one can engineer dispersion relations with exceptional points, leading to a periodicity breaking in the dispersion relation, where at least a part of the spectrum is complex-valued. In this case, event horizons can be true black or white holes, at the cost of severe instabilities within the wormhole interior. Overall this project uses existing elements of cQED in novel ways, like inductors, capacitors, and nonreciprocal elements, and proposing new elements, like negative inductors (by using transient flux quench in Josephson junctions), as well as quantum inductors. The latter, though, not studied in this thesis, is a part of the larger work that contains the final project.

This thesis is organised as follows

1. The remaining sections of this introductory chapter contains preliminary reviews of basic notions and mathematical methods relevant this thesis.
2. Chapter 2 contains the first project, where we study how fractional charges appear in a conventional superconducting-normal metal hybrid circuit.
3. In chapter 3 we investigate a toy model realisable using superconducting circuits that hosts topological properties in presence of dissipation.
4. Finally in chapter 4 we use existing elements of circuit QED and propose new ones in order to realise an analog event horizon in a superconducting circuit.
5. Finally appendices A, B, C, D, E, F and G provide additional important calculations to support the work in the main thesis.

Further introduction to the topics mentioned above and their relevance in superconducting circuits will be given at the beginning of the corresponding chapter. Chapters 2 and 4 contain works that have either appeared as a publication or are being prepared as such, and include a high degree of collaboration with the coauthors of the corresponding papers. The coauthors will be credited in the beginning of the corresponding chapters and specifically in sections of the chapters.

Note on notations: We will denote many body operators with a hat, for example an annihilation operator will be represented as $\hat{a}$, while the operators that act on single particle spaces do not have any special notation, it should be clear from the context of the equation. Also $\hbar = 1$ in this thesis unless stated otherwise.

1.2. Circuit QED: a quick review

In this section we will give a quick overview of cQED by going over how one begins to study superconducting circuits using Lagrangians and Hamiltonians. For a more detailed and thorough introduction to the subject, the e-book by Ciani et. al. [CDT24] and the review paper by Blais et. al. [Bla+21] are recommended, these also serve as the main references for this section. The approach to dealing with general electrical circuits in cQED is to first write down the Lagrangian, that corresponds to the classical equations of motion i.e. Kirchhoff's laws for currents and voltages. Then, find the Hamiltonian and finally promote the classical variables to quantum operators by imposing commutation relations on them. We will focus on the following three circuit elements: capacitors, inductors and Josephson junctions, since they are not only the most commonly occurring ones, but they also serve as building blocks for new and more complicated circuit elements.

The circuits generally consists of branches and nodes, where each branch is a two terminal circuit element and nodes are points where two or more branches meet. We

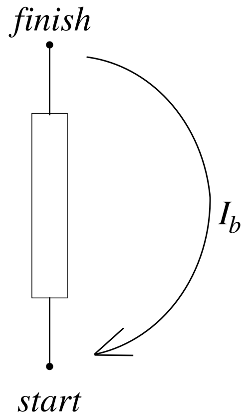

Figure 1.1.: Schematic of a branch with a two terminal circuit element, represented by a rectangle, connected to two nodes. The arrow represents the direction of flow of the current in the branch I_b.

can also have four terminal circuit elements, we are going to discuss one such element, called gyrator, near the end of this section. Lastly to be precise we need to assign a direction to the branches, we do this by calling one of the nodes, for a given branch, as *finish* and the other one as *start* (see Fig.1.1). As per convention positive current flows from the *finish* node to the *start* node and we define the branch voltage as $V_b = V_{finish} - V_{start}$. Instead of working with currents and voltages we will define the branch-flux variables $\Phi_b(t)$ as

$$V_b(t) = \frac{d\Phi_b}{dt}. \tag{1.1}$$

We will assume that at $t \to -\infty$ all electromagnetic fields and potentials were zero, hence we can write

$$\Phi_b(t) = \int_{-\infty}^{t} V_b(t)dt. \tag{1.2}$$

Like voltages we can also define node fluxes as $\Phi_b = \Phi_{finish} - \Phi_{start}$. For superconducting circuits the branch-flux variable also directly relates to the superconducting phase drop over the piece of superconducting material representing the branch.

1.2.1. Capacitors, inductors and LC oscillators

Now we will construct the Lagrangian for linear capacitors and linear inductors in terms of the branch-flux Φ_b and its time derivative $\dot{\Phi}_b$, which will play the role of position and velocity (of a mechanical system) respectively. First let us consider an inductive branch with current $I_b(t)$ at some time t, then for an infinitesimal time dt the charge transported from *finish* node to *start* node is $I_b(t)dt$. If the branch voltage is $V_b(t)$, the work done on the element is $dW = V_b(t)I_b(t)dt$. The total energy stored in the inductive element can be written as

$$U_b(t) = \int_{-\infty}^{t} V_b(t')I_b(t')dt'. \tag{1.3}$$

For a linear inductor the current can be written as

$$I_b(t) = \frac{\Phi_b(t)}{L}, \tag{1.4}$$

where L denotes its inductance. Hence the total energy is

$$U_b(t) = \frac{\Phi_b^2(t)}{2L}. \tag{1.5}$$

For a linear capacitor, we use the relation $Q = CV$ in the following form

$$I_b(t) = C\frac{dV_b}{dt}, \tag{1.6}$$

where C is its capacitance. We get the following expression for energy

$$U_b(t) = \frac{1}{2}CV_b^2(t) = \frac{1}{2}C\dot{\Phi}_b^2(t). \tag{1.7}$$

As a concrete example for circuit quantisation let us take a look at the example of an LC oscillator. It consists of a capacitor and an inductor in parallel (Fig.1.2), since they are connected in parallel the voltages in both the branches must be equal by Kirchhoff's law of voltages. Hence we only have a single independent branch-flux $\Phi_b = \Phi - \Phi_{\text{ground}}$, which we can write in terms of node fluxes. Since the only thing that matters is the difference of the node fluxes we can set $\Phi_{\text{ground}} = 0$ without loss of generality to get $\Phi_b = \Phi$. As stated earlier the branch flux and its time derivative play the role of position and velocity respectively, therefore when writing the Lagrangian we associate the energy of the inductive element with potential energy and the energy of the capacitive element with kinetic energy. Further below, we will discuss a special case of a nonreciprocal element, a gyrator, which cannot be categorized as purely kinetic nor purely potential energy, as its energy depends on both ϕ and $\dot{\phi}$. Hence the Lagrangian for an LC circuit is

$$\mathcal{L} = \frac{1}{2}C\dot{\Phi}^2(t) - \frac{\Phi^2(t)}{2L}, \tag{1.8}$$

where we have already substituted the branch flux with the node flux. To get the Hamiltonian, we first define the conjugate variable

$$q = \frac{\partial \mathcal{L}}{\partial \dot{\Phi}} = C\dot{\Phi}, \tag{1.9}$$

which has the dimensions of charge hence the symbol. Using Legendre transformation we get

$$\mathcal{H} = q\dot{\Phi} - \mathcal{L} = \frac{q^2(t)}{2C} + \frac{\Phi^2(t)}{2L}. \tag{1.10}$$

Now we promote the variables to Hermitian quantum operators $q \to \hat{q}$ and $\Phi \to \hat{\Phi}$ and impose the commutation relation

$$\left[\hat{\Phi}, \hat{q}\right] = i\hbar. \tag{1.11}$$

The Hamiltonian along with the commutation relation is clearly a quantum harmonic oscillator and can be easily solved by using the method of ladder operators.

Now we introduce some dimensionless variables to work with that will be used for the rest of this thesis

$$\begin{aligned} \phi &= \frac{2\pi\Phi}{\Phi_0}, \\ n &= \frac{q}{2e}, \end{aligned} \tag{1.12}$$

where $\Phi_0 = h/2e$ is the superconducting flux quantum and the variable n measures the number of charges in units of two times the elementary charge e, this definition is appropriate for superconducting circuits since the relevant "particles" are the Cooper pairs which carry a charge of $2e$. The Hamiltonian becomes

$$\mathcal{H} = E_C\hat{n}^2 + E_L\hat{\phi}^2, \tag{1.13}$$

where we have introduced the charging energy

$$E_C = \frac{(2e)^2}{2C}, \tag{1.14}$$

and the inductive energy

$$E_L = \frac{\Phi_0^2}{8\pi^2 L}, \tag{1.15}$$

also the commutation relation now reads

$$\left[\hat{\phi}, \hat{n}\right] = i. \tag{1.16}$$

Next, we replace the linear inductor in the LC circuit with a Josephson junction. Josephson junction is characterised by two relations

$$I_b = I_c \sin\varphi, \tag{1.17}$$

$$\frac{d\varphi}{dt} = \frac{2\pi V_b}{\Phi_0}, \tag{1.18}$$

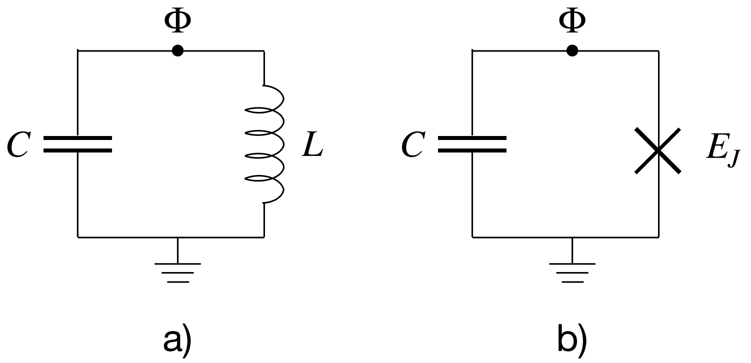

Figure 1.2.: a) Figure showing a schematic of an LC oscillator with one independent node flux Φ. b) Here the linear inductor of the LC oscillator is replaced by a Josephson junction.

where I_b and V_b are the branch current and voltage respectively. Also I_c is the critical current, which depends on properties of the junction like the material, thickness, area etc. Most importantly, φ is the superconducting phase difference between the two superconductors that form the Josephson junction and lies in the interval $[0, 2\pi)$, which is different from the branch flux variable Φ_b or its dimensionless counterpart $\phi_b = \Phi_b/\Phi_0$ that takes any value in $\mathbb{R}$. Nonetheless, here we are going to make the identification $\varphi = \phi_b$, the mathematical justification for this identification is too involved for this quick review, therefore we refer to the section 4.1.1 in [CDT24]. With this identification we can write the first Josephson relation as

$$I_b = I_c \sin \phi_b, \tag{1.19}$$

and get the energy associated with the Josephson junction

$$U_J = \int_{-\infty}^{t} V_b(t') I_b(t') dt' = I_c \Phi_0 \int_{\phi_b(t'=-\infty)}^{\phi_b(t'=t)} \sin \phi_b d\phi_b = -E_J \cos \phi_b. \tag{1.20}$$

Here we have defined the Josephson energy as

$$E_J = \frac{I_c \Phi_0}{2\pi}, \tag{1.21}$$

and dropped a constant term that arises out of our assumption that $\phi_b(t' = -\infty) = 0$.

Finally we can write down the Lagrangian for the circuit in Fig. 1.2(b) as

$$\mathcal{L} = \frac{C}{2}\dot{\Phi}^2 + E_J \cos \frac{\Phi}{\Phi_0}, \tag{1.22}$$

where we have again set the ground flux to zero and replaced the branch flux with the node flux. The conjugate variable is $q = \partial\mathcal{L}/\partial\dot{\Phi} = C\dot{\Phi}$ and therefore the quantised Hamiltonian is

$$\mathcal{H} = \frac{\hat{q}^2}{2C} - E_J \cos \frac{\hat{\Phi}}{\Phi_0}, \tag{1.23}$$

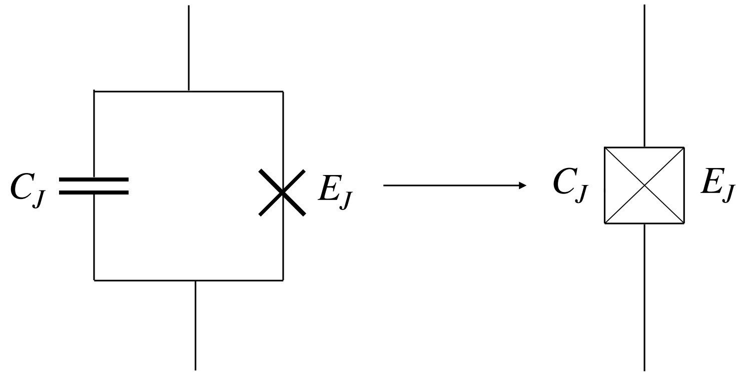

Figure 1.3.: Every Josephson junction has an intrinsic capacitance, in circuits this fact is conveyed by drawing a box around the two crosses that denotes a JJ.

and in terms of dimensionless variables it can be written as

$$\mathcal{H} = E_C \hat{n}^2 - E_J \cos \hat{\phi}. \tag{1.24}$$

This Hamiltonian is taken to be the one that describes a general Josephson junction since every junction comes with an intrinsic capacitance, this capacitance is often denoted as C_J. In fact the compact circuit symbol for a JJ is designed with this fact in mind (see Fig. 1.3). If a JJ is additionally shunted by another capacitor C_s then the effective capacitance of the system will be $C = C_s + C_J$.

Our work will also feature a nonreciprocal four terminal circuit elements, called gyrators. Classical gyrators, are already widely in use in circuit engineering and signal processing [Abd+13; KSA20; MC15; MC17], whose consistent circuit theoretical description goes back to the work by Tellegen [Tel48]. These are however generally large clunky objects operating in a finite frequency window. Various recent works strive towards a realisation and a consistent description of quantum mechanical gyrators [VD14; Rym+21; Sel+23; VH24]. As defined by Tellegen, the fundamental equation of a gyrator is

$$\begin{pmatrix} I_1 \\ I_2 \end{pmatrix} = \begin{pmatrix} 0 & -G \\ G & 0 \end{pmatrix} \begin{pmatrix} V_1 \\ V_2 \end{pmatrix}, \tag{1.25}$$

where I_1, I_2 are the currents flowing through port 1 and port 2 respectively, and V_1, V_2 are the voltages across port 1 and port 2 respectively, see Fig. 1.4. We will use the gyrator as an effective two terminal element, by grounding the nodes with fluxes Φ_3 and Φ_4, as shown in Fig. 1.5, which is an example of a minimal circuit that contains gyrator as a two terminal element. The Lagrangian for this circuit can be written as

$$\mathcal{L} = \frac{1}{2} C \dot{\Phi}_1^2 + \frac{1}{2} C \dot{\Phi}_2^2 + \frac{G}{2} \left(\Phi_1 \dot{\Phi}_2 - \dot{\Phi}_1 \Phi_2 \right). \tag{1.26}$$

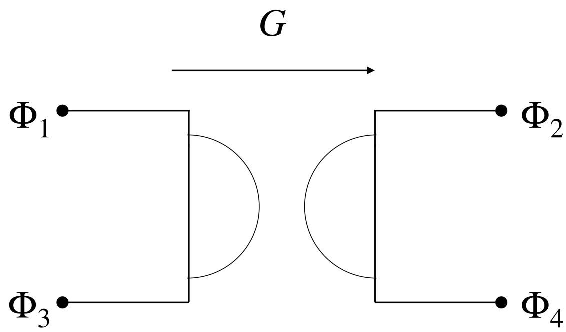

Figure 1.4.: Schematic of a gyrator, a four terminal and two-port element, the left port (port 1) contains two nodes with node fluxes Φ_1 and Φ_3, while the right port (port 2) contains two nodes with node fluxes Φ_2 and Φ_4.

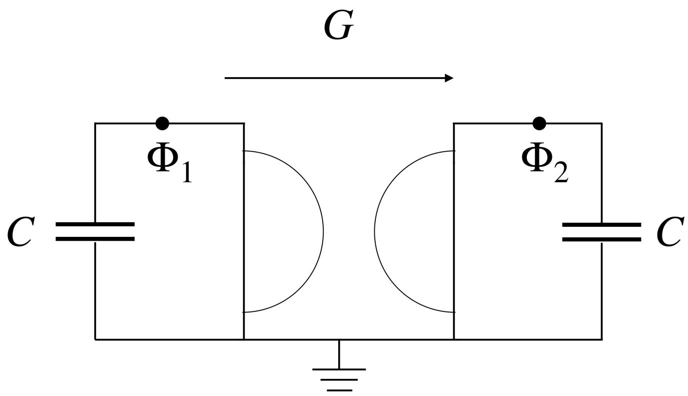

Figure 1.5.: A minimal circuit containing a gyrator and capacitors. The nodes with fluxes Φ_3 and Φ_4 (in Fig. 1.4) have been grounded. Hence the node fluxes Φ_1 and Φ_2 are equal to the branch fluxes.

The contribution of the gyrator element to this Lagrangian is such that when we write the equations of motion in terms of currents and voltages, we get back the defining equation for the gyrator (Eq. (1.25)). The Hamiltonian of this minimal circuit is

$$\mathcal{H} = \frac{\left(\hat{q}_1 + 0.5 * G\hat{\Phi}_2\right)^2}{2C} + \frac{\left(\hat{q}_2 - 0.5 * G\hat{\Phi}_1\right)^2}{2C}. \tag{1.27}$$

Gyrator will play an indispensable role in Ch. 4, where we will need it to tilt the dispersion relation of a JJ array. A connection to the work of Riwar et. al. [Riw+16a] can also be made, the Chern number that quantizes the transconductance of the multi-terminal Josephson junction essentially provides a source of gyration (see Eq. (3.5)).

Before ending this section we will just state the following facts without going into any mathematical details:

1. if a circuit has a constant voltage source V, then we define a line as a path in the circuit that starts from the branch that is grounded and ends at the branch that is connected to the voltage source without any breaks. Then we have the following constraint for the branch fluxes across a line

$$\sum_{b\in\text{line}} \dot{\Phi}_b = V, \tag{1.28}$$

which is just the Kirchhoff's law of voltages.

2. If instead of forming a line we choose the branches such that they form a closed loop, then we have the following constraint on the branch fluxes

$$\sum_{b\in\text{loop}} \Phi_b = \Phi_{\text{ext.}}, \tag{1.29}$$

where $\Phi_{\text{ext.}}$ is the (time independent) external flux passing through the loop in question.

In our discussion above we associated the energy of capacitive element with kinetic energy and that of inductive elements with potential energy. It is worth pointing out that there is no fundamental reason to make this association, in fact for the case of quantum phase-slip junctions this approach fails due to the Lagrangian being non-convex (hence the Legendre transform to the Hamiltonian is no longer possible). We also did not deal with the case of time dependent external fluxes as it is still a topic of current research, for some approaches to this problem see [Bla+21; RD22].

1.3. POVMs and weak measurements

In this section we give a brief introduction to weak measurements, that will be useful for section 2.6 when we use them to simulate a counting field (χ) and give an experimentally realisable way to observe a 4π-periodic Josephson effect. First let us begin by stating the measurement postulate of quantum mechanics [Bru02]:

Postulate 1. A physical observable of a quantum system is represented by a Hermitian operator that acts on the elements of the Hilbert space of the quantum system. The only possible outcome of the measurement of an observable are the eigenvalues of the corresponding operator.

Let us consider a quantum system described by the state $|\psi\rangle$, and a Hermitian operator O that corresponds to some physical observable. The possible results of the measurement are the eigenvalues, $\{o_n\}$, of O. The probability of measuring a particular eigenvalue is given by

$$p(o_n) = \mathrm{tr}\left(P_n \rho\right), \tag{1.30}$$

where ρ describes the state of the system and P_n is the projection operator for the eigenspace of o_n. After the measurement the system is in the state

$$\tilde{\rho} = \frac{P_n \rho P_n^\dagger}{\mathrm{tr}\left(P_n \rho\right)}. \tag{1.31}$$

The projection operators corresponding to a Hermitian observable are orthogonal (Hermitian) and have the following properties $P_n P_{n'} = \delta_{nn'} P_n$ and $\sum_n P_n = \mathbb{I}$, where $\mathbb{I}$ is the identity operator on the Hilbert space. The second property is just a restatement of the fact that summing over all probabilities for a measurement gives unity, the measurements described by this postulate are called projective or von Neumann measurements. So far we have just repeated what is taught to undergraduates in an introductory quantum mechanics course, albeit in terms of density operator instead of state vectors, in the next paragraph we are going to reformulate the measurement postulate.

Now, consider a case where the system of interest (S) is coupled to an auxillary system (A), such that the composite system is described by the state $\rho = \rho_{\mathrm{S}} \otimes \rho_{\mathrm{A}}$. Then following the measurement postulate the probability to obtain an experimental value m can be specified with an orthogonal projection operator P_m

$$\begin{aligned} p(m) &= \mathrm{tr}\left(P_m \rho\right), \\ p(m) &= \mathrm{tr}_{\mathrm{S}}\left(E_m \rho_{\mathrm{S}}\right). \end{aligned} \tag{1.32}$$

Here $E_m = \mathrm{tr}_{\mathrm{A}}\left(P_m \rho_{\mathrm{A}}\right)$ is an operator that acts only on the Hilbert space of the system (S), the subscripts in the trace operation indicate over which Hilbert space the trace is being taken. Using the properties of the projection operator it can be easily deduced that E_m is a positive operator and again due to probability conservation $\sum_m E_m = \mathbb{I}_{\mathrm{S}}$. If we have a set of projection operators on the composite system $\{P_m\}$ from that we can deduce the set of positive operators $\{E_m\}$ that can be used to obtain the measurement probabilities. The operators E_m are called POVM (positive operator valued measure) elements and the whole set of $\{E_m\}$ is called the POVM. This example provides us a way to generalise the measurement postulate with the help of POVMs [Bru02].

Postulate 2. Quantum measurement is defined by a collection of positive operators $\{E_m\}$ acting on the Hilbert space of the system that satisfy $\sum_m E_m = \mathbb{I}$. The index m refers to the possible outcomes of the experiment. If a system is in a state ρ then the probability that the result of the experiment is m is given by

$$p(m) = \mathrm{tr}\left(E_m \rho\right). \tag{1.33}$$

Note that the second measurement postulate does not add anything fundamentally new to quantum mechanics since we reached it by using the postulate of projective measurements and the idea of composite quantum systems. Indeed given any POVM on a Hilbert space ($\mathcal{H}$) it is always possible to construct a set of orthogonal projection operators that act on a space obtained by extending $\mathcal{H}$ and gives us the correct measurement probabilities by using the projective measurement postulate, this is the statement of Neumark's theorem (section 9-6 of [Per95]) whose proof we are not going to present here. But despite this, POVM formalism is quite helpful, since extending the Hilbert space of a system to cast every measurement in form of orthogonal projections just adds complexity and shields us from understanding the physics.

One might immediately see an important fact missing from the POVM approach to measurements, we cannot write the state of the system after the measurement in terms of elements of POVM. First we would like to point out that in many real world experiments only the measurement statistics is of interest and not the state of the system after the measurement. Secondly, if we further know a set of operators M_{mk} such that $E_m = \sum_k M_{mk}^\dagger M_{mk}$ then we can write the state of the system after measurement as

$$\tilde{\rho} = \frac{\sum_k M_{mk} \rho M_{mk}^\dagger}{p(m)}. \tag{1.34}$$

Here, M_{mk} are called measurement operators, for the special case of $E_m = M_m^\dagger M_m$, i.e index k only takes one value, the measurement preserves the purity of the states.

1.3.1. Weak measurements

After reviewing the POVM formalism of the measurement postulate we are in position to discuss weak measurements. Broadly speaking there are two distinct ways we can call a measurement weak [Bru02]. To see this let us consider a two level system with states $|0\rangle$ and $|1\rangle$ and the following POVM

$$\begin{aligned} E_0 &= |0\rangle\langle 0| + (1-\epsilon)|1\rangle\langle 1|, \\ E_1 &= \epsilon |1\rangle\langle 1|, \end{aligned} \tag{1.35}$$

where $\epsilon \ll 1$. We can define the following measurement operators

$$\begin{aligned} M_0 &= |0\rangle\langle 0| + \sqrt{1-\epsilon}\,|1\rangle\langle 1|, \\ M_1 &= \sqrt{\epsilon}\,|1\rangle\langle 1|. \end{aligned} \tag{1.36}$$

It is easy to check that E_0 and E_1 are positive operators and $E_0 + E_1 = \mathbb{I}$. If the system is in the state $|\psi\rangle = \alpha|0\rangle + \beta|1\rangle$ such that $|\alpha|^2 + |\beta|^2 = 1$, then the probability of the outcome labelled 0 is given by $p(0) = 1 - \epsilon|\beta|^2$ and the probability of obtaining the outcome labelled 1 is $p(1) = \epsilon|\beta|^2$. Hence for most experiments the measurement outcome 0 will be obtained and the state of the system changes very little

$$\left|\tilde{\psi}\right\rangle = \frac{\alpha|0\rangle + \beta\sqrt{1-\epsilon}|1\rangle}{\sqrt{1-\epsilon|\beta|^2}}. \tag{1.37}$$

But with a small probability we obtain the the outcome labelled 1, in this case the state of the system is drastically changed to $\left|\tilde{\psi}\right\rangle = |1\rangle$. Therefore this measurement is weak in the sense that for most replication of this process we obtain very little information about the system and the state of the system is changed very little about but on rare occasions the state of the system is drastically changed and we obtain ample information about the system.

On the other hand we can also construct the following POVM

$$\begin{aligned}
E_0 &= \frac{1+\epsilon}{2}|0\rangle\langle 0| + \frac{1-\epsilon}{2}|1\rangle\langle 1|, \\
E_1 &= \frac{1-\epsilon}{2}|0\rangle\langle 0| + \frac{1+\epsilon}{2}|1\rangle\langle 1|, \\
M_0 &= \sqrt{\frac{1+\epsilon}{2}}|0\rangle\langle 0| + \sqrt{\frac{1-\epsilon}{2}}|1\rangle\langle 1|, \\
M_1 &= \sqrt{\frac{1-\epsilon}{2}}|0\rangle\langle 0| + \sqrt{\frac{1+\epsilon}{2}}|1\rangle\langle 1|.
\end{aligned} \tag{1.38}$$

Starting with the same state of the two level system as in the last example, the probabilities for outcomes labelled 0 and 1 are

$$\begin{aligned}
p(0) &= \frac{1}{2} + \epsilon\frac{|\alpha|^2 - |\beta|^2}{2}, \text{ and} \\
p(1) &= \frac{1}{2} - \epsilon\frac{|\alpha|^2 - |\beta|^2}{2}.
\end{aligned} \tag{1.39}$$

The states of the system after these measurements are (up to first order in ϵ)

$$\begin{aligned}
\left|\tilde{\psi}_0\right\rangle &\approx \alpha\left(1 + \epsilon|\beta|^2\right)|0\rangle + \beta\left(1 - \epsilon|\alpha|^2\right)|1\rangle, \\
\left|\tilde{\psi}_1\right\rangle &\approx \alpha\left(1 - \epsilon|\beta|^2\right)|0\rangle + \beta\left(1 + \epsilon|\alpha|^2\right)|1\rangle.
\end{aligned} \tag{1.40}$$

Since the probability of the two measurement outcomes are almost equal and the state of the system changes very little, an individual measurement represented by this POVM does not contain much useful information. To get a good understanding of the state of the system the measurements have to be repeated sufficient amount of times so that the state of the system eventually drifts towards either $|0\rangle$ or $|1\rangle$ depending on $|\alpha|^2$ and $|\beta|^2$.

Before finishing this review of weak measurements we would like to state a result for a system that is under continuous measurement from [Cre+06]. Suppose a system that evolves autonomously due to its own Hamiltonian H is under continuous measurement, where the measurement outcomes can be described by a set of measurement operators $\{M_i\}$ that can be used to construct a POVM. By continuous measurement we mean that the measurements take place instantaneously and randomly in time at an average rate R, hence this result will only be true for time scales $> 1/R$. Consider a short time interval δt (that is still large compared to $1/R$), during this time interval the probability that a measurement takes place is $R\delta t$ we also assume that the time interval is short enough so that the possibility of two or more measurements can be neglected. If a measurement takes place then the density operator evolves as

$$\rho(t+\delta t) = \sum_i M_i \rho(t) M_i^\dagger, \tag{1.41}$$

and in absence of a measurement taking place the system evolves under its own Hamiltonian

$$\rho(t+\delta t) = \rho(t) - i\,[H, \rho(t)]\,\delta t. \tag{1.42}$$

To lowest order in δt we can write down the total change in the density operator by adding the two processes, weighted by their probabilities of occurrence

$$\begin{aligned} \rho(t+\delta t) &= (1 - R\delta t)\,(\rho(t) - i\,[H, \rho(t)]\,\delta t) + R\delta t \left(\sum_i M_i \rho(t) M_i^\dagger\right), \\ \frac{\rho(t+\delta t) - \rho(t)}{\delta t} &= -i\,[H, \rho(t)] + R\left(\sum_i M_i \rho(t) M_i^\dagger - \rho(t)\right). \end{aligned} \tag{1.43}$$

Taking the limit $\delta t \to 0$ we get the differential equation

$$\frac{d\rho}{dt} = -i\,[H, \rho(t)] + R\sum_i \left(M_i \rho(t) M_i^\dagger - \frac{1}{2}\{M_i^\dagger M_i, \rho(t)\}\right), \tag{1.44}$$

where we have used the fact that $\sum_i M_i^\dagger M_i = \mathbb{I}$ to write the equation in Lindblad form. As we will see in Sec. 1.4, Lindblad equation is a generic master equation for systems that evolve under a Hamiltonian and a weak dissipative environment, hence continuous measurements seem to simulate the effect of weak dissipation. This result is in general true for any kind of (continuous) measurement but we will use it in section 2.6 specifically for weak measurement.

1.3.2. Full counting statistics

So far we have talked about how POVMs provide a way to obtain measurement statistics for a system, a related and very useful concept is that of full counting statistics (FCS), which has been widely used in mesoscopic physics [LLL96; BS01; BN03; Bel05; Gus+06; Mat+14; YTW16]. Consider a detector connected to a system of interest, where the measurement operators are given by Eq. (1.35), such that the detector registers a click every time a projective measurement happens (i.e. outcome corresponding to M_1). This information about the detector can be included in the density matrix $\rho(t) \to \rho(n,t)$ by introducing a new variable n, that tells us how many times the detector has registered clicks up to time t.

We can find the probability of registering n clicks up to time t as

$$P(n,t) = \mathrm{tr}\left(\rho(n,t)\right), \tag{1.45}$$

note that $\rho(n,t)$ contains a degree of freedom for detector as well therefore it does not completely fit the definition of a density matrix, hence its trace is not necessarily unity. To get the FCS we define the following Fourier transform

$$m(\chi,t) = \sum_n P(n,t) e^{in\chi}, \tag{1.46}$$

where χ is called the counting field. It should be noted that, although we introduced FCS by using an example of weak measurement it is not a necessity, all one needs to define an FCS is some form of measurement statistics (here it was $P(n,t)$). For example in [LLL96] it is the electron counting statistics and in [LRS14] it is the number of photons counted by the detector. It might seem a little artificial to introduce this quantity, but for charge transport one can obtain quantities like the average current and average noise as follows

$$\begin{aligned}\langle I \rangle &= -i \lim_{t\to\infty} \frac{1}{t} \left.\frac{\partial \ln m(\chi,t)}{\partial \chi}\right|_{\chi=0}, \\ \langle S \rangle &= i^2 \lim_{t\to\infty} \frac{1}{t} \left.\frac{\partial^2 \ln m(\chi,t)}{\partial \chi^2}\right|_{\chi=0}, \end{aligned} \tag{1.47}$$

as well as higher moments. One can equivalently introduce the quantity $\rho(\chi,t) = \sum_n \rho(n,t) e^{in\chi}$ and find its equation of motion of the form

$$\partial_t \rho(\chi,t) = K(\chi,t)\rho(\chi,t), \tag{1.48}$$

where $K(\chi,t)$ in general is non-Hermitian (especially if we include continuous measurements). As pointed out in [RD22] and [Li+23], the eigenvalues of $K(\chi,t)$ can undergo braid phase transitions and introduce topological properties in otherwise conventional systems. We will build on this result in the first project in Ch. 2, especially on the result in the former paper.

1.4. Open quantum systems and third quantisation

We have mentioned about how taking dissipation into account for quantum systems results in more realistic models, and the fact that open (dissipative) quantum systems sometimes display features that are absent from their non-dissipative counterparts. In this section we give a brief introduction to how open quantum systems are dealt with mathematically, this will lead us through topics like Lindblad equation, exceptional points and finally to the work of Tomaz Prosen about specifically dealing with Lindblad equations that are quadratic in fermionic operators, sometimes termed as "third quantization". As shown by [LMC20] Prosen's formalism allows one to easily extend the famous ten-fold classification of topological insulators and superconductors to the systems governed by quadratic Lindblad equations, this will be of particular use to us in Ch. 3 where we study such a system and try to find some notion of topology that can be associated with it.

The fact that the time evolution of an isolated quantum system is governed by a Hermitian Hamiltonian, is necessary to conserve the norm of the wave function. Hence when discussing open systems, where some loss of information is expected, lifting the condition of Hermiticity is an obvious way forward. This leads us to the first approach used in working with dissipative systems, where the governing equation is Schrödinger-like but the Hamiltonian is no longer Hermitian. This approach arises naturally in gain loss systems [KYZ16; FEG17; El-+18], one aspect that makes this approach rather useful is that if the non-Hermitian Hamiltonian has combined parity-time ($\mathcal{PT}$) symmetry then the eigenvalues are guaranteed to be real even in absence of Hermiticity. We won't go into much detail about this approach here since it will not be of much use to us, but it is a very interesting and active area of research, for a thorough review see [YU20].

The second approach to studying open quantum systems is via the Gorini Kossakowski Sudarshan Lindblad equation (GKSL equation) or just Lindblad equation, which is a quantum master equation. Consider a composite system that consists of the system of interest denoted by S and other system that acts as the environment. The Hamiltonian of the composite system can be written in the following form

$$H = H_S + H_{\text{env.}} + H_{\text{int.}}, \tag{1.49}$$

where H_S and $H_{\text{env.}}$ are free Hamiltonians of the system and bath respectively, and $H_{\text{int.}}$ is the interaction Hamiltonian between them. The complete mathematical model of the total system is often much too complicated. The environment can be, for example a reservoir (environment with infinite degree of freedoms) or a bath (reservoir in thermal equilibrium state), in which case the exact solution would require solving an infinite hierarchy of coupled equations of motion. We regard an open system S to be singled out by the fact that all observations of interest refer to this subsystem. If the total system is described by the density matrix ρ then we define $\rho_S = \text{tr}_{\text{env.}}\rho$ as the reduced density matrix for S. At time t we can find the reduced density matrix by

$$\rho_S(t) = \text{tr}_{\text{env.}}\left(U(t,t_0)\rho(t_0)U^\dagger(t,t_0)\right) \tag{1.50}$$

where $U(t,t_0)$ is the time evolution operator of the composite system.

Let us assume that it is possible to prepare the initial state of the composite system as a product state, i.e.

$$\rho(t_0) = \rho_S(t_0) \otimes \rho_{\text{env.}}(t_0). \tag{1.51}$$

Since $\rho_{\text{env.}}(t_0)$ is positive and has a unit trace, there always exist a set of orthonormal eigenvectors $\{|\nu\rangle\}$ such that

$$\rho_{\text{env.}}(t_0) = \sum_{\nu} \lambda_\nu |\nu\rangle \langle\nu| , \tag{1.52}$$

where λ_ν are the non-negative eigenvalues. Hence we get

$$\begin{aligned}
\rho_S(t) &= \text{tr}_{\text{env.}} \left(U(t,t_0)\rho(t_0)U^\dagger(t,t_0)\right), \\
\rho_S(t) &= \sum_{\mu} \langle\mu| \left(U(t,t_0)\rho_S(t_0) \otimes \sum_{\nu} \lambda_\nu |\nu\rangle \langle\nu| U^\dagger(t,t_0)\right) |\mu\rangle , \\
\rho_S(t) &= K_{\mu\nu}(t,t_0)\rho_S(t_0)K^\dagger_{\mu\nu}(t,t_0),
\end{aligned} \tag{1.53}$$

where the operators $K_{\mu\nu}(t)$ that only act on the Hilbert space of S are called Kraus operators and are given by

$$K_{\mu\nu}(t,t_0) = \sqrt{\lambda_\nu} \langle\mu| (U(t,t_0) |\nu\rangle . \tag{1.54}$$

The representation of the equation of motion in terms of these Kraus operators is called Kraus operator sum representation (OSR). Since we want the reduced density matrix $\rho_S(t)$ to have a unit trace, this imposes the following condition on the Kraus operators

$$\sum_{\mu\nu} K^\dagger_{\mu\nu}(t,t_0)K_{\mu\nu}(t,t_0) = \mathbb{I}, \tag{1.55}$$

where $\mathbb{I}$ is the identity operator on the reduced Hilbert space. This is reminiscent of the measurement operators we came across while discussing POVMs in Sec. 1.3, indeed OSR can capture, among other things, the descrition of non-selective measurements and therefore the measurement operators are sometimes called Kraus operators. If we consider the Kraus OSR as a map that maps a density matrix from some initial time to final time, $F(\rho(t_0)) \to \rho(t)$, then it can be shown to have following properties: trace preserving, linear, and completely positive [Lid20].

Our goal is to write a differential equation for time evolution of the density matrix, for that we will first make two assumptions:

1. first, the system we are interested in is time translationally invariant, hence the term t_0 that has appeared so far can be set to zero.

2. secondly, we make the Markovian approximation i.e., the system has no memory.

Using Taylor expansion near $t = 0$ we can write

$$\rho_S(dt) = \rho_S(0) + \dot{\rho}_S dt + O(dt^2), \tag{1.56}$$

and from the Kraus OSR we get

$$\rho_S(dt) = \sum_{\alpha} K_\alpha(dt)\rho_S(0)K^\dagger_\alpha(dt), \tag{1.57}$$

where we hve collected the indices μ and ν into one index α. Next we have to find the Kraus operators such that the OSR time evolution matches the Taylor expansion, for this one of the Kraus operators will need to contain the identity operator. Hence we can write

$$K_0(dt) = \mathbb{I} + L_0 dt, \tag{1.58}$$

this gives us

$$K_0(dt)\rho_S(0)K_0^\dagger(dt) = \rho_S(0) + \left[L_0\rho_S(0) + \rho_S(0)L_0^\dagger\right]dt + O(dt^2). \tag{1.59}$$

Thus we pick all other Kraus operators as

$$K_\alpha = \sqrt{dt}L_\alpha, \quad \alpha \geq 1, \tag{1.60}$$

which acts on the density matrix as

$$K_\alpha\rho_S(0)K_\alpha^\dagger = L_\alpha\rho_S(0)L_\alpha^\dagger dt. \tag{1.61}$$

We now also impose the condition for trace preservation $\sum_{\alpha\geq 0} K_\alpha^\dagger K_\alpha = \mathbb{I}$ up to $O(dt^2)$, which gives

$$\mathbb{I} = \mathbb{I} + \left[L_0 + L_0^\dagger + \sum_{\alpha\geq 1} L_\alpha^\dagger L_\alpha\right]dt + O(dt^2). \tag{1.62}$$

Next we write L_0 as a sum of a Hermitian and anti-Hermitian operator $L_0 = A - iH$ where $A^\dagger = A$ and $H^\dagger = H$. This gives the following identity

$$A = -\frac{1}{2}\sum_{\alpha\geq 1} L_\alpha^\dagger L_\alpha. \tag{1.63}$$

Finally putting all this in the OSR time evolution equation and defining $\dot{\rho}_S|_{t=0} = (\rho_S(dt) - \rho_S(0))/dt$, we get

$$\dot{\rho}_S|_{t=0} = -i\left[H, \rho_S(0)\right] + \sum_{\alpha\geq 1}\left(L_\alpha\rho_S(0)L_\alpha^\dagger - \frac{1}{2}\{L_\alpha^\dagger L_\alpha, \rho_S(0)\}\right). \tag{1.64}$$

Now we make use of the Markov approximation and claim that this equation is true for all times, since for every small time step the rate of change of the system will only depend on its current state, we also re-scale the L_α operators as $L_\alpha \to \sqrt{\gamma'_\alpha}L_\alpha$ to make them dimensionless. Hence the final equation we get is

$$\dot{\rho}_S(t) = -i\left[H, \rho_S(t)\right] + \sum_{\alpha\geq 1}\gamma_\alpha\left(L_\alpha\rho_S(t)L_\alpha^\dagger - \frac{1}{2}\{L_\alpha^\dagger L_\alpha, \rho_S(t)\}\right), \tag{1.65}$$

where $\gamma_\alpha = \sqrt{|\gamma'_\alpha|^2}$. The generator of the evolution, $\mathcal{L}$ from the equation $\dot{\rho}_S = \mathcal{L}\dot{\rho}_S$, is called the Lindbladian. The L_α are called the Lindblad or dissipation operators. The operator H is Hermitian and can be interpreted as the Hamiltonian of the system plus a correction called the Lamb shift, this detail becomes obvious if we derive the Lindblad equation microscopically which can be found in Ch. 3 of [BP07].

1.4.1. Exceptional points

Hermitian matrices, at least the ones that are finite dimensional, can always be diagonalized, which means they have as many linearly independent eigenvectors as the number of eigenvalues (this is just the spectral theorem for finite dimensions). Non-Hermitian matrices have no such guarantee, sometimes they can be defective i.e. the number of linearly independent eigenvectors are less than the number of eigenvalues. Keeping this in mind let us consider the following non-Hermitian Hamiltonian [Li+23]

$$H = \begin{pmatrix} \omega_0 - i\gamma & \kappa \\ \kappa & \omega_0 + i\gamma \end{pmatrix}, \tag{1.66}$$

which is a simple model of two coupled resonators with same frequency (ω_0), such that the loss of one resonator is equal to the gain of the other one ($\pm\gamma$), and κ is the coupling strength. The eigenvalues of this (non-Hermitian) Hamiltonian are

$$E_\pm = \omega_0 \pm \sqrt{\kappa^2 - \gamma^2}, \tag{1.67}$$

if the system parameters can be externally controlled then we see that for $\kappa > \gamma$ both eigenvalues are real while for $\kappa < \gamma$ both of them become complex. For $\kappa = \gamma$, both the eigenvalues are same $E_+ = E_- = \omega_0$, this is not the ordinary degeneracy that one might encounter working with a Hermitian Hamiltonian, this becomes clear if we try to find its eigenvectors, of which it only has one $\begin{pmatrix} 1 & i \end{pmatrix}^T$.

If we were to look at the above Hamiltonian as a function of one of parameters (say γ), then at the point $\kappa = \gamma$ in the parameter space it will appear as if the two eigenvalues and eigenvectors are coalescing into each other. This is how we define exceptional points (EPs), i.e. as points in parameter space where two or more eigenvalues and eigenvectors coalesce. The points where more than two eigenvalues (and eigenvectors) meet are called higher order EPs, although they have recently started become subject of interest [Bud+19; OY19], most works concerning EPs still focus on the case of only two eigenvalues and eigenvectors, therefore that is what we will discuss here.

EPs have been studied in areas of physics such as optics [Hlu+21; Xia+21],acoustics [Din+18] and quantum mechanics [Özt+21; Lia+21], but here we will focus on the effect the presence EPs has on the topology of the spectrum of the corresponding non-Hermitian system. For this purpose we will consider the following $2 * 2$ non-Hermitian Hamiltonian [DFM22]

$$H(z) = \begin{pmatrix} 0 & 1 \\ 1 & z \end{pmatrix}, \tag{1.68}$$

where $z \in \mathbb{C}$. The eigenvalues of this Hamiltonian are

$$E_\pm(z) = \frac{z \pm \sqrt{z^2 + 4}}{2}, \tag{1.69}$$

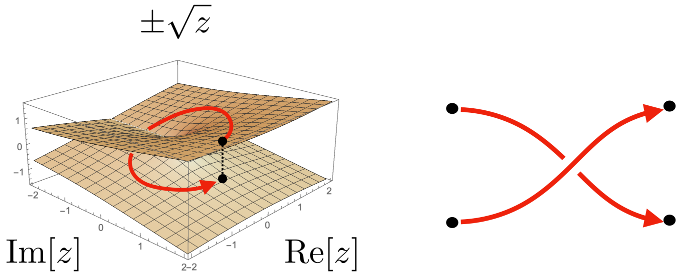

Figure 1.6.: If two eigenvalues go around a branch point, i.e. an exceptional point, then they braid around each other.

to find the exceptional points we set $E_+(z) = E_-(z)$ and find that at points $z = \pm 2i$ in the parameter space the eigenvalues and eigenvectors coalesce. Note that in the expression for eigenvalues we have a square root of a complex function, which we know is multi-valued function that is dealt with by introducing branch cuts. The end point of a branch cut is called branch point and in context of non-Hermitian matrices it is precisely the EP. An interesting thing to consider is the behavior of eigenvalues near the EPs, we can do this by expanding the parameter z near one of the EPs, $z = 2i(1 + \delta z/2)$, where δz is small. The difference of eigenvalues near the EP looks as follows

$$|E_+ - E_-| = 2\left|\sqrt{\delta z}\right|, \tag{1.70}$$

up to the leading order. As it turns out this square root behavior is generic for EPs where two eigenvalues and eigenvectors meet.

In simplified terms, the vicinity of an exceptional point can be described by the two solutions of the square root function $\pm\sqrt{\lambda}$ of a complex number λ. To foreshadow the connection to charge fractionalization, we make the following observation: when following a circle around the singular point $z = 0$, after one revolution around the origin, one adiabatically connexts $+\sqrt{\lambda}$ with $-\sqrt{\lambda}$ (and vice versa), and only returns to the origin after a second turn (see Fig. 1.6). This behaviour can be regarded as a braid, breaking periodicity in the circle, which (as we will show in Ch. 2) can be connected to fractional charges, if the parameters appearing in λ are connected to transport quantities, such as the superconducting phase or the counting field.

Since eigenvalues of non-Hermitian Hamiltonians are complex, and therefore two dimensional, there is a possibility of forming loops by changing the parameters of the system in an appropriate way. This fact is captured by defining the eigenvalue winding number as

$$w = \frac{1}{2\pi i}\oint_C dz \partial_z \ln\det\left(H(z) - E_r\right), \tag{1.71}$$

where C denotes a closed path generated by varying the parameter z that maps to a closed loops for eigenvalues in the complex plane and E_r is arbitrary reference energy, this definition can be expanded if more than one parameter is involved. By Stokes theorem we know that the above integral will vanish unless the path C encloses some singularities. Note that winding number is also defined for Hermitian systems, for example in the SSH model, but it is not defined for eigenvalues since real eigenvalues cannot form closed loops. For the simple example we have used so far the winding number reduces to

$$\begin{aligned} w &= v_{\pm} + v_{\mp}, \\ w &= \frac{1}{2\pi}\oint_C dz\partial_z\left(\arg\left(E_+ - E_-\right)\right) + \frac{1}{2\pi}\oint_C dz\partial_z\left(\arg\left(E_- - E_+\right)\right), \end{aligned} \tag{1.72}$$

where we have set the reference energy E_r equal to the energy at the EP and $v_{\pm(\mp)}$ is called the eigenvalue vorticity. If we vary the parameter z such that the eigenvalues form two separate closed loops then the winding number comes out to be 0, but if the eigenvalues form a single closed loop then it comes out to be -1, hence indicating a topological transition in the spectrum. In the second case there is only one loop becuase it encloses an EP and the eigenvalues have braided around each other. The topological distinction between the two loops has to do with the fact that if a loop does not pass through a branch cut it can be reduced to a single point with smooth deformations but if a loop does pass through a branch cut (if it contains an EP it will necessarily has to) it cannot be reduced to a single point.

1.4.2. Third quantisation

Here we review the approach to solving Lindblad master equation that is quadratic in fermionic operators, developed by Prosen in [Pro08; Pro10], called third quantisation. We will use this in Sec.3.4 to study topology of a system described by a quadratic Lindbladian.

Let us consider a system of n Fermions, described by a quadratic Lindblad equation

$$\dot{\rho} = -i\left[\hat{H}, \rho\right] + \sum_{\mu}\left(\hat{L}_\mu \rho \hat{L}_\mu^\dagger - \frac{1}{2}\left\{\hat{L}_\mu^\dagger \hat{L}_\mu, \rho\right\}\right). \tag{1.73}$$

First we write the n fermionic operators in terms of $2n$ Majorana operators, hence we can write the Hamiltonian and dissipation operators as

$$\hat{H} = \sum_{i,j=1}^{2n} \hat{\alpha}_i H_{ij} \hat{\alpha}_j, \tag{1.74}$$

and

$$\hat{L}_\mu = \sum_{i=1}^{2n} l_{\mu,i} \hat{\alpha}_i, \tag{1.75}$$

where

$$\left\{\hat{\alpha}_i, \hat{\alpha}_j\right\} = 2\delta_{i,j}, \tag{1.76}$$

because of the above commutation relation we can always write the first quantized Hamiltonian as an anti-symmetric matrix, i.e. $H^T = -H$ this also makes it a purely imaginary matrix.

Next step is to assign a Hilbert space structure to the space of operators $\mathcal{K}$, which is a $2^{2n} = 4^n$ dimensional space. We define the canonical basis for this space $|P_w\rangle$, where

$$P_w = \prod_{i=1}^{2n} \hat{\alpha}_i^{w_i}, w_i \in \{0,1\}, \tag{1.77}$$

the inner product is defined as

$$\langle x | y \rangle = 4^{-n} \mathrm{tr}\left(x^\dagger y\right). \tag{1.78}$$

We also define creation and annihilation operators on this space of operators, as follows

$$\hat{c}_j |P_w\rangle = \delta_{w_j,1} |\hat{\alpha}_j P_w\rangle, \tag{1.79}$$
$$\hat{c}_j^\dagger |P_w\rangle = \delta_{w_j,0} |\hat{\alpha}_j P_w\rangle, \tag{1.80}$$

these operators follow the standard fermionic anti-commutation relations.

Now we are ready to write the Lindblad operator in the canonical basis we just defined, we start with the commutator part of the Lindblad equation

$$\hat{\mathcal{L}}_0 \rho = \left[\hat{H}, \rho\right]. \tag{1.81}$$

Since $\mathcal{K}$ is a Lie algebra, one defines the adjoint representation of a Lie derivative for an arbitrary $A \in \mathcal{K}$ back on $\mathcal{K}$ as, $\mathrm{ad}A|B\rangle = |[A,B]\rangle$. It is now straightforward to compute the action of a Lie derivative of a product of two Majorana operators on an arbitrary basis element

$$\begin{aligned}\mathrm{ad}\hat{\alpha}_j\hat{\alpha}_k |P_w\rangle &= |\hat{\alpha}_j\hat{\alpha}_k P_w\rangle - |P_w \hat{\alpha}_j \hat{\alpha}_k\rangle \\ &= 2\left(\delta_{w_j,1}\delta_{w_k,0} + \delta_{w_j,0}\delta_{w_k,1}\right) |\hat{\alpha}_j\hat{\alpha}_k P_w\rangle \\ &= 2\left(\hat{c}_j^\dagger \hat{c}_k - \hat{c}_k^\dagger \hat{c}_j\right) |P_w\rangle. \end{aligned} \tag{1.82}$$

Hence for the Hamiltonian we get

$$\hat{\mathcal{L}}_0 = 4 \sum_{j,k=1}^{2n} \hat{c}_j^\dagger H_{jk} \hat{c}_k. \tag{1.83}$$

Now let us consider the action of dissipation operators

$$\hat{\mathcal{L}}_\mu \rho = 2\hat{L}_\mu \rho \hat{L}_\mu^\dagger - \left\{\hat{L}_\mu^\dagger \hat{L}_\mu, \rho\right\} = \sum_{j,k=1}^{2n} l_{\mu,j} l_{\mu,k}^* \hat{\mathcal{L}}_{j,k} \rho, \tag{1.84}$$

where

$$\hat{\mathcal{L}}_{j,k}\rho = \hat{\alpha}_j\rho\hat{\alpha}_k - \{\hat{\alpha}_k\hat{\alpha}_j, \rho\}. \tag{1.85}$$

Again we proceed by computing the actions of $\hat{\mathcal{L}}_{j,k}$ on elements of the canonical basis of operator Fock space $\mathcal{K}$. In order to do so, it is crucial to observe that the question whether $\hat{\alpha}_j$ commutes or anticommutes with P_w depends on the number of a-fermions $|w| = \sum_i w_i$ in P_w, namely $P_w\hat{\alpha}_j = (-1)^{|w|+w_j}\,\hat{\alpha}_j P_w$, and hence

$$\hat{\mathcal{L}}_{j,k}\,|P_w\rangle = \left[2\,(-1)^{|w|+w_j}\,\hat{\alpha}_j\hat{\alpha}_k - \hat{\alpha}_k\hat{\alpha}_j - (-1)^{w_k+w_j}\,\hat{\alpha}_k\hat{\alpha}_j\right]|P_w\rangle\,. \tag{1.86}$$

Observing that

$$\begin{aligned}
|\hat{\alpha}_j P_w\rangle &= \left(\hat{c}_j^\dagger + \hat{c}_j\right)|P_w\rangle\,,\\
(-1)^{w_j}\,|\hat{\alpha}_j P_w\rangle &= \left(\hat{c}_j^\dagger - \hat{c}_j\right)|P_w\rangle\,,\\
(-1)^{|w|}\,|\hat{\alpha}_j P_w\rangle &= \exp\left(i\pi\hat{N}\right)|P_w\rangle\,,
\end{aligned} \tag{1.87}$$

where $\hat{N} = \sum_j \hat{c}_j^\dagger\hat{c}_j$. One can derive that

$$\hat{\mathcal{L}}_{j,k} = \left(1 + \exp\left(i\pi\hat{N}\right)\right)\left(2\hat{c}_j^\dagger\hat{c}_k^\dagger - \hat{c}_j^\dagger\hat{c}_k - \hat{c}_k^\dagger\hat{c}_j\right) + \left(1 - \exp\left(i\pi\hat{N}\right)\right)\left(2\hat{c}_j\hat{c}_k - \hat{c}_j\hat{c}_k^\dagger - \hat{c}_k\hat{c}_j^\dagger\right). \tag{1.88}$$

Obviously, the maps $\hat{\mathcal{L}}_{j,k}$, and hence also the total Lindblad part of Liouvillean $\sum_\mu \mathcal{L}_\mu$, do not conserve the number of a-fermions. But they conserve its parity, i.e. the product of any two creation/annihilation a-Fermi maps commutes with the parity operation $\hat{\mathcal{P}} = \exp\left(i\pi\hat{N}\right)$, with respect to which the operator space can be decomposed into a direct sum $\mathcal{K} = \mathcal{K}^+ \oplus \mathcal{K}^-$, and even/odd operator spaces are orthogonally projected as $\mathcal{K}^\pm = \left(1 \pm \exp\left(i\pi\hat{N}\right)\right)\mathcal{K}$. Thus, the positive parity subspace $\mathcal{K}^+$ is a linear space spanned by $|P_w\rangle$ with even $|w|$. All the maps $\hat{\mathcal{L}}_{j,k}$ now act separately on $\mathcal{K}^\pm$ and $\hat{\mathcal{L}}_{j,k}\mathcal{K}^\pm \subseteq \mathcal{K}^\pm$. For example, the maps defined on even parity subspace are indeed quadratic in a-fermions

$$\hat{\mathcal{L}}_{j,k}\Big|_{\mathcal{K}^+} = 4\hat{c}_j^\dagger\hat{c}_k^\dagger - 2\hat{c}_j^\dagger\hat{c}_k - 2\hat{c}_k^\dagger\hat{c}_j. \tag{1.89}$$

We shall focus on physical observables which are products of an even number of Majorana fermions, so we shall in the following discuss only Liouville dynamics on the subspace $\mathcal{K}^+$. Putting the previous results together we get

$$\begin{aligned}
\hat{\mathcal{L}}_+ &= -2\underline{\hat{c}}^\dagger\cdot\left(2iH + M + M^T\right)\underline{\hat{c}} + 2\underline{\hat{c}}^\dagger\cdot\left(M - M^T\right)\underline{\hat{c}}^\dagger,\\
\hat{\mathcal{L}}_+ &= 4\underline{\hat{c}}^\dagger\cdot\left(-iH - \mathrm{Re}\left[M\right]\right)\underline{\hat{c}} + 4i\underline{\hat{c}}^\dagger\cdot\mathrm{Im}\left[M\right]\underline{\hat{c}}^\dagger,
\end{aligned} \tag{1.90}$$

where M is a complex Hermitian matrix parametrizing the Lindblad operators

$$M_{jk} = \sum_\mu l_{\mu,j}l_{\mu,k}^*. \tag{1.91}$$

Using the fact that M is Hermitian we can write

$$\hat{\mathcal{L}}_+ = \begin{pmatrix} \underline{\hat{c}}^\dagger & \underline{\hat{c}} \end{pmatrix} \begin{pmatrix} -X^T & Y \\ 0 & X \end{pmatrix} \begin{pmatrix} \underline{\hat{c}} \\ \underline{\hat{c}}^\dagger \end{pmatrix}, \tag{1.92}$$

where

$$\begin{aligned} X &= -2iH + 2\mathrm{Re}\left[M\right], \\ Y &= 4i\mathrm{Im}\left[M\right]. \end{aligned} \tag{1.93}$$

Here we take a side step to prove some results that will be useful later, first let us look at the definition of the Hermitian matrix $M_{jk} = \sum_\mu l_{\mu,j} l^*_{\mu,k}$ and consider the case where $\mu = 1$, then keeping in mind that we started with a system of n Fermions we can write

$$M = \begin{pmatrix} 0 & \cdots & l_1 \\ \vdots & \cdots & \vdots \\ 0 & \cdots & l_n \end{pmatrix} \begin{pmatrix} 0 & \cdots & 0 \\ \vdots & \cdots & \vdots \\ l_1^* & \cdots & l_n^* \end{pmatrix} = \begin{pmatrix} 0 & \cdots & l_1 \\ \vdots & \cdots & \vdots \\ 0 & \cdots & l_n \end{pmatrix} \begin{pmatrix} 0 & \cdots & l_1 \\ \vdots & \cdots & \vdots \\ 0 & \cdots & l_n \end{pmatrix}^\dagger . \tag{1.94}$$

This is the sufficient condition for M to be positive semi-definite, if we generalise to the case $\mu > 1$, then it can be straight forwardly argued that M is a sum of positive semi-definite matrices, hence in turn itself is positive semi-definite. , this also implies that $X + X^T = 4\mathrm{Re}[M] \geqslant 0$. Consider an eigenvalue β and the corresponding eigenvector $|v\rangle$ of X, then

$$\begin{aligned} X\,|v\rangle &= \beta\,|v\rangle\,, \\ X\,|v\rangle^* &= \beta^*\,|v\rangle^*\,, \end{aligned} \tag{1.95}$$

since X is purely real. Taking appropriate dot products we show that

$$|v\rangle^\dagger \left(X + X^T\right)|v\rangle = 2\mathrm{Re}[\beta]\,|v\rangle^\dagger\,|v\rangle\,, \tag{1.96}$$

then the strict positivity of $|v\rangle^\dagger\,|v\rangle$ and non negativity of $|v\rangle^\dagger\left(X + X^T\right)|v\rangle$ imply $\mathrm{Re}[\beta] \geq 0$.

Our next goal is to write the Lindbladian operator obtained in Eq.(1.92) in a form similar to a diagonalised second quantised operator. To that end, define

$$\begin{aligned} \hat{a}_{1,j} &= \frac{1}{\sqrt{2}}\left(\hat{c}_j + \hat{c}_j^\dagger\right), \\ \hat{a}_{2,j} &= \frac{i}{\sqrt{2}}\left(\hat{c}_j - \hat{c}_j^\dagger\right). \end{aligned} \tag{1.97}$$

These follow the anti-commutation relations $\{\hat{a}_{\mu,j}, \hat{a}_{\nu,k}\} = \delta_{\mu\nu}\delta_{jk}$, where $\mu, \nu = 1, 2$. Hence the Lindbladian can be written as

$$\hat{\mathcal{L}}_+ = \underline{\hat{a}}^T \cdot A \cdot \underline{\hat{a}} - A_0\hat{\mathbb{I}}, \tag{1.98}$$

where $\underline{\hat{a}} = \begin{pmatrix} \hat{a}_{1,1} & \cdots & \hat{a}_{1,2n} & \hat{a}_{2,1} & \cdots & \hat{a}_{2,2n} \end{pmatrix}^T$ and A is a complex anti-symmetric $4n * 4n$ matrix with

$$\begin{aligned} A &= \begin{pmatrix} -2iH + 2i\mathrm{Im}[M] & 2iM \\ -2iM^T & -2iH - 2i\mathrm{Im}[M] \end{pmatrix}, \\ &= -2i\mathbb{I}_2 \otimes H - 2\sigma_2 \otimes \mathrm{Re}[M] - 2(\sigma_1 - i\sigma_3) \otimes \mathrm{Im}[M], \\ A_0 &= 2\sum_j M_{jj}. \end{aligned} \tag{1.99}$$

We can define the following unitary transformation

$$\tilde{A} = UAU^\dagger, \tag{1.100}$$

$$= \begin{pmatrix} -X^T & Y \\ 0 & X \end{pmatrix}, \tag{1.101}$$

where

$$U = \frac{1}{\sqrt{2}} \begin{pmatrix} 1 & -i \\ 1 & i \end{pmatrix} \otimes \mathbb{I}_{2n}. \tag{1.102}$$

Since $\tilde{A}$ and A are connected by a unitary transformation, they will have the same eigenvalues. Using the formula for a special case of determinant of a block matrix

$$\det \begin{pmatrix} P & Q \\ 0 & S \end{pmatrix} = \det(P)\det(S),$$

we can deduce that the set of eigenvalues of A will be the union of the sets of eigenvalues of X and $-X$, hence we have shown that the eigenvalues of A come in pairs of $(\beta_i, -\beta_i)$.

In order to diagonalise the Lindbladian we have to diagonalise the matrix A, in general there is no guarantee that this matrix will be diagonalisable but here we will assume that to be the case. We will arrange the eigenvalues of A as follows $\begin{pmatrix} \beta_1 & \cdots & \beta_{2n} & -\beta_1 & \cdots & -\beta_{2n} \end{pmatrix}$, such that $\mathrm{Re}[\beta_1] \geq \mathrm{Re}[\beta_2] \geq \cdots \mathrm{Re}[\beta_{2n}] \geq 0$, this ordering allows us to conclude that $\{\beta_i\}_{i=1}^{2n}$ are the eigenvalues of X. Due to our assumption of diagonalisability, the matrix A will have $4n$ linearly independent eigenvectors and as a result of the matrix being anti-symmetric these eigenvectors can be normalised as follows

$$|v_i\rangle^T |v_j\rangle = J_{ij}, \text{ where } J = \sigma_1 \otimes \mathbb{I}_{2n} \tag{1.103}$$

Let V be a matrix such that its rows are the eigenvectors of A, combined with how we have arranged our eigenvalues the first $2n$ rows of V will contain eigenvectors corresponding to the eigenvalues $\begin{pmatrix} \beta_1 & \cdots & \beta_{2n} \end{pmatrix}$ and the last $2n$ rows will contain eigenvectors corresponding to the eigenvalues $\begin{pmatrix} -\beta_1 & \cdots & -\beta_{2n} \end{pmatrix}$, hence we can write

$$AV^T = V^T D,$$

$$VV^T = J, \tag{1.104}$$

where $D = \text{diag}\begin{pmatrix} \beta_1 & \cdots & \beta_{2n} & -\beta_1 & \cdots & -\beta_{2n} \end{pmatrix}$. Combining the above two equations we get

$$A = V^T \Lambda V, \text{ where } \Lambda = DJ. \tag{1.105}$$

Define new operators as

$$\begin{aligned} \hat{b}_j &= |v_j\rangle^T \underline{\hat{a}}, \text{ for } 1 \le j \le 2n \\ \hat{b}'_j &= |v_j\rangle^T \underline{\hat{a}}, \text{ for } 2n+1 \le j \le 4n. \end{aligned} \tag{1.106}$$

These operators follow the almost canonical anti-commutation relations $\{\hat{b}_j, \hat{b}_k\} = 0$, $\{\hat{b}'_j, \hat{b}'_k\} = 0$, $\{\hat{b}_j, \hat{b}'_k\} = \delta_{jk}$, this is a direct consequence of the second line of Eq.(1.104) and the commutation relations of the Majorana operators defined in Eq.(1.97). We can finally write the Lindbladian as

$$\hat{\mathcal{L}}_+ = -2\sum_{j=1}^{2n} \beta_j \hat{b}'_j \hat{b}_j + \left(\sum_{j=1}^{2n} \beta_j - A_0\right)\hat{\mathbb{I}}. \tag{1.107}$$

Now we will show that the last term in Eq.(1.107) is actually 0. We can write

$$A_0 = 2\text{tr}\left(M\right) = 2\text{tr}\left(\text{Re}[M]\right), \tag{1.108}$$

since the imaginary part of a Hermitian matrix is always anti-symmetric. Also since $\{\beta_i\}_{i=1}^{2n}$ are eigenvalues of X, we can write

$$\sum_{i=1}^{2n} \beta_i = \text{tr}\left(X\right) = 2\text{tr}\left(\text{Re}[M]\right), \tag{1.109}$$

here we have used the fact that $H^T = -H$. Finally,

$$\hat{\mathcal{L}}_+ = -2\sum_{j=1}^{2n} \beta_j \hat{b}'_j \hat{b}_j. \tag{1.110}$$

We can write the eigenvalues of the Lindbladian superoperator $\hat{\mathcal{L}}_+$ in term of eigenvalues of Z as

$$\lambda_{\underline{\nu}} = -2\sum_{j=1}^{2n} \beta_j \nu_j, \tag{1.111}$$

where $\nu_j \in \{0,1\}$ and $\underline{\nu} = \{\nu_1, \nu_2, \cdots, \nu_{2n}\}$.

1.5. Introduction to the tenfold way

Here we will review the famous tenfold way, that classifies topological insulators (TIs) and topological superconductors (TSCs) into ten symmetry classes [Sch+08; Ryu+10; Kit09; Chi+16], depending on which symmetry the system possesses. This will serve as the jumping off point to discuss the extension of this classification for non-Hermitian systems in the next section, the results of which we will use in Ch. 3 to find topological properties of an open system.

To begin consider a second quantised free fermionic Hamiltonian

$$\hat{H} = \sum_{J,K} \hat{c}_J^\dagger H_{JK} \hat{c}_K, \tag{1.112}$$

where the fermionic creation and annihilation operators follow the canonical anti-commutation relations $\{\hat{c}_J^\dagger, \hat{c}_K\} = \delta_{JK}$, the capitalised indices represent collection of quantum numbers for e.g. site index, spin or other relevant quantum numbers for the system and H_{JK} is the gapped first quantised Hamiltonian. The framework of tenfold way uses the two anti-unitary symmetries of H, namely time-reversal and particle-hole symmetry, to classify the first quantised Hamiltonian into ten symmetry classes. To understand this classification better, first we need to understand how these symmetries act on the Hamiltonian.

1. **Time-reversal symmetry (TRS):** Time reversal $\hat{\mathcal{T}}$ is an anti-unitary operator that acts on the fermionic annihilation operators as follows

$$\begin{aligned} \hat{\mathcal{T}} \hat{c}_J \hat{\mathcal{T}}^{-1} &= \sum_K (U_T)_{JK} \hat{c}_K, \\ \hat{\mathcal{T}} i \hat{\mathcal{T}}^{-1} &= -i, \end{aligned} \tag{1.113}$$

where U_T must be a unitary matrix to preserve the canonical anti-commutation relations. For this operation to be a symmetry of the system, the operator must commute with the second quantised Hamiltonian $\hat{\mathcal{T}} \hat{H} \hat{\mathcal{T}}^{-1} = \hat{H}$, this leads to the following condition for the first quantised Hamiltonian

$$U_T^\dagger H^* U_T = H. \tag{1.114}$$

Applying the time-reversal operator twice we get

$$(U_T^* U_T)^\dagger H (U_T^* U_T) = H, \tag{1.115}$$

since first quantised Hamiltonian can always be written in the irreducible representation, the above condition in conjunction with Schur's lemma implies that $U_T^* U_T = e^{i\alpha}\mathbb{I}$, using the fact that U_T is unitary it can be deduced that

$$U_T^* U_T = \pm\mathbb{I}. \tag{1.116}$$

Applying the time-reversal operator twice on a fermionic annihilation operator we see that $\hat{\mathcal{T}}^2\hat{c}_J\hat{\mathcal{T}}^{-2} = \sum_K \left(U_T^* U_T\right)_{JK} \hat{c}_K = \pm\hat{c}_J$, hence in a fermionic system the time-reversal operator squares to

$$\hat{\mathcal{T}}^2 = (\pm 1)^{\hat{N}} \text{ when } U_T^* U_T = \pm\mathbb{I}, \tag{1.117}$$

where $\hat{N} = \sum_J \hat{c}_J^\dagger \hat{c}_J$ is the number operator.

2. **Particle-hole symmetry (PHS):** Particle-hole transformation $\hat{\mathcal{C}}$ is a unitary transformation that transforms fermionic annihilation operators into creation operators

$$\hat{\mathcal{C}}\hat{c}_J\hat{\mathcal{C}}^{-1} = \sum_K \left(U_C^*\right)_{JK} \hat{c}_K^\dagger, \tag{1.118}$$

and vice-versa, again to preserve the canonical anti-commutation relations U_C must be a unitary matrix. If this transformation is a symmetry of the system, i.e. $\hat{\mathcal{C}}\hat{H}\hat{\mathcal{C}}^{-1} = \hat{H}$, then for the first quantised Hamiltonian we get

$$U_C^\dagger H^T U_C = -H, \tag{1.119}$$

and $\mathrm{tr}H = 0$. Using similar arguments as for the time-reversal operator, we can deduce that

$$\hat{\mathcal{C}}^2 = (\pm 1)^{\hat{N}} \text{ when } U_C^* U_C = \pm\mathbb{I}. \tag{1.120}$$

3. **Chiral symmetry (CS):** This symmetry is defined as the combination of time-reversal and particle-hole symmetries, a system might not fulfill the criteria for the two symmetries discussed above, but it can still have the symmetry that is the combination of the two, the so called chiral symmetry

$$\hat{\mathcal{S}} = \hat{\mathcal{T}} \cdot \hat{\mathcal{C}}. \tag{1.121}$$

This transformation acts as follows on the fermionic annihilation operators

$$\hat{\mathcal{S}}\hat{c}_J\hat{\mathcal{S}}^{-1} = \sum_K \left(U_C^* U_T^*\right)_{JK} \hat{c}_K^\dagger, \tag{1.122}$$

and if the transformation satisfies $\hat{\mathcal{S}}\hat{H}\hat{\mathcal{S}}^{-1} = \hat{H}$, then the conditions on the first quantised Hamiltonian are

$$U_S^\dagger H U_S = -H, \text{ where } U_S = U_C U_T, \tag{1.123}$$

and $\mathrm{tr}H = 0$. Using the same reasoning that we used to derive $\hat{\mathcal{T}}^2 = \hat{\mathcal{C}}^2 = (\pm 1)^{\hat{N}}$, we can deduce that $U_S^2 = e^{i\alpha}\mathbb{I}$. Redefining $U_S \to e^{i\alpha/2}U_S$, the conditions on the single particle Hamiltonian for chiral symmetry simplifies to

$$\{H, U_S\} = 0, \quad U_S^2 = U_S^\dagger U_S = \mathbb{I}. \tag{1.124}$$

As a final remark, the analysis in this section does not apply to TSCs, since the second quantised Hamiltonian does not contain any pairing terms (for e.g. $\hat{c}_J\hat{c}_K$), but a similar analysis can be repeated by writing the superconductor Hamiltonian in BdG form and using Nambu operators instead of fermionic operators.

1.5.1. Periodic table of TIs and TSCs

After the above discussion, we are now in position to classify the gapped single particle Hamiltonians into symmetry classes in terms of non-unitary symmetries. It should be noted that using unitary symmetries that commute with the first quantised Hamiltonian, we can write it in a block diagonal form, such that the unitary symmetries will act trivially on each block. It is these irreducible blocks, without any unitary symmetries, that we wish to classify. So far we have discussed the following

$$\begin{aligned} T^{-1}HT &= H, \quad T = U_T\mathcal{K}, \quad U_T^* U_T = \pm\mathbb{I}, \\ C^{-1}HC &= -H, \quad C = U_C\mathcal{K}, \quad U_C^* U_C = \pm\mathbb{I}, \\ S^{-1}HS &= -H, \quad S = U_S, \quad U_S^2 = \mathbb{I}, \end{aligned} \tag{1.125}$$

where U_T, U_C and U_S are unitary matrices and $\mathcal{K}$ is the complex conjugation operator. As it turns out this list is exhaustive, i.e. without loss of generality we can assume there is only one operator T representing TRS and only one operator C representing PHS. If this was not the case, say there were two operators C_1 and C_2 that represented PHS, then their combination $C_1 \cdot C_2$ will act as unitary symmetry and it would be possible to bring H into a block diagonal form such that $U_{C_1} \cdot U_{C_2}^*$ will act trivially on each block. Thus on each block U_{C_1} and U_{C_2} will be trivially related to each other, hence we can just use a single operator corresponding to PHS, similar argument can be used to prove uniqueness of the TRS operator. On the other hand, the combination of TRS and PHS ($T \cdot C$), the chiral symmetry, is indeed a unitary operator but instead of commuting with H it anti-commutes, hence it is necessary to take it into account separately.

It is easy to see, why the above three symmetries lead to ten symmetry classes for the single particle Hamiltonians. Let us begin with how H transforms under TRS(T), first option is that H is not invariant under T, second option is that it is invariant under T and $T^2 = +\mathbb{I}$ and the third option is that H is invariant under T and $T^2 = -\mathbb{I}$. Similarly we get three cases for PHS, hence the combination of both gives us $3 * 3 = 9$ cases. For chiral symmetry, in the eight out of nine cases mentioned above it is easy to deduce its presence or absence just by looking at how the Hamiltonian transforms under TRS and PHS. For the ninth case where both TRS and PHS are absent, the chiral symmetry can be absent or present, resulting in $(3 * 3) - 1 + 2 = 10$ cases.

The table 1.1 lists the ten symmetry classes that are used to classify TIs and TSCs, these symmetry classes were first described by Altland and Zirnbauer [Zir96; AZ97] in context of disordered fermionic systems, and are therefore sometimes called Altland-Zirnbauer (AZ) classes. The table 1.1 also is written in such a way as to separate the so called *complex* classes A and AIII from the rest of the so called *real* classes. This nomenclature is due to the fact that these eight classes have at least one anti-unitary symmetry which imposes a relation between the real and imaginary part of the corresponding Hamiltonian, while for the two complex classes the real and imaginary part of the corresponding Hamiltonians are completely independent.

Before ending this section we say a few words about topological invariants, they play the same role for classification of topological phases of matter as the order pa-

Class	TRS	PHS	CS	d=0	d=1	d=2	d=3	d=4	d=5	d=6	d=7
Complex classes											
A	0	0	0	$\mathbb{Z}$	0	$\mathbb{Z}$	0	$\mathbb{Z}$	0	$\mathbb{Z}$	0
AIII	0	0	1	0	$\mathbb{Z}$	0	$\mathbb{Z}$	0	$\mathbb{Z}$	0	$\mathbb{Z}$
Real classes											
AI	+	0	0	$\mathbb{Z}$	0	0	0	$2\mathbb{Z}$	0	$\mathbb{Z}_2$	$\mathbb{Z}_2$
BDI	+	+	1	$\mathbb{Z}_2$	$\mathbb{Z}$	0	0	0	$2\mathbb{Z}$	0	$\mathbb{Z}_2$
D	0	+	0	$\mathbb{Z}_2$	$\mathbb{Z}_2$	$\mathbb{Z}$	0	0	0	$2\mathbb{Z}$	0
DIII	−	+	1	0	$\mathbb{Z}_2$	$\mathbb{Z}_2$	$\mathbb{Z}$	0	0	0	$2\mathbb{Z}$
AII	−	0	0	$2\mathbb{Z}$	0	$\mathbb{Z}_2$	$\mathbb{Z}_2$	$\mathbb{Z}$	0	0	0
CII	−	−	1	0	$2\mathbb{Z}$	0	$\mathbb{Z}_2$	$\mathbb{Z}_2$	$\mathbb{Z}$	0	0
C	0	−	0	0	0	$2\mathbb{Z}$	0	$\mathbb{Z}_2$	$\mathbb{Z}_2$	$\mathbb{Z}$	0
CI	+	−	1	0	0	0	$2\mathbb{Z}$	0	$\mathbb{Z}_2$	$\mathbb{Z}_2$	$\mathbb{Z}$

Table 1.1.: Listed in this table are ten symmetry classes for fermionic gapped first quantised Hamiltonians. The time evolution operator constructed from the single particle Hamiltonian e^{itH} belongs to a symmetric space, the first column in the table denotes the name given to this symmetric space by Élie Cartan in his classification. The labels TRS, PHS and CS represent the time-reversal, particle-hole and the chiral symmetries respectively. For TRS and PHS the label 0 means that the Hamiltonian is not invariant under that transformation, while the ± signs mean that the transformation is a symmetry and the corresponding operators square to $\pm\mathbb{I}$. For CS the labels 0 and 1 denote its absence or presence respectively. The columns labelled with different values of d (spatial dimension), tells us if for a given d there exist a topologically non-trivial ground state. The symbols $\mathbb{Z}$, $2\mathbb{Z}$ and $\mathbb{Z}_2$ represent the nature of topological invariant that characterises a symmetry class, and the symbol '0' represents that all the ground states are topologically trivial.

rameter in the Landau-Ginzburg theory of phase transitions. Hence the value of the topological invariant is an indication of the phase of the matter, which can be calculated experimentally by observing a quantity that is proportional to the said topological invariant, for example: transverse conductivity in integer quantum hall effect [Hat97]. As shown in Table 1.1, topological invariants can take variety of different values depending on the symmetry class and the spatial dimension of the system, the ones in the table means the following:

1. topological invariants in $\mathbb{Z}$ can take integer values $(0, \pm 1, \pm 2, ...)$,
2. topological invariants in $2\mathbb{Z}$ can take even integer values $(0, \pm 2, \pm 4, ...)$,
3. topological invariants in $\mathbb{Z}_2$ can take two values, generally denoted as $\{-1, +1\}$.

Some well known topological invariants are the winding number in the SSH model [MAG16] and the Chern number for the Haldane model [Hal88]. Chern number, or its modified version for non-Hermitian Hamiltonians, will be the relevant topological invariant in the second project in Ch. 3, for a dissipative toy model that is realised via multi-terminal Josephson junction. Chern number for closed systems is defined by Berry curvature, consider a gapped quantum system described by a wave function $|\psi(\mathbf{k})\rangle$, then the Berry connection is defined as follows

$$\mathbf{A}(\mathbf{k}) = i \langle\psi(\mathbf{k})| \nabla_{\mathbf{k}} |\psi(\mathbf{k})\rangle, \tag{1.126}$$

and Berry curvature is

$$\mathbf{B}(\mathbf{k}) = \nabla_{\mathbf{k}} \times \mathbf{A}(\mathbf{k}), \tag{1.127}$$

finally the Chern number can be written as

$$C = \frac{1}{2\pi} \iint_{BZ} \mathbf{B}(\mathbf{k}) \cdot d\mathbf{S}, \tag{1.128}$$

where the integral is taken over the entire Brillouin zone.

1.6. Extending the tenfold classification

It will be in our interest in Ch. 3 to discuss the topology of a non-Hermitian system described by Lindblad equation, hence in this section we review the proposed extension of the classification of TIs and TSCs to non-Hermitian systems. Characterising non-Hermitian systems with topological properties has been a focus of research for more than a decade now [RL09; HH11]. Here we focus on the work of Kawabata et. al. [Kaw+19a] where the authors claim to develop a complete theory of symmetry and topology in non-Hermitian physics and show that presence of non-Hermiticity ramifies the ten symmetry classes to 38 symmetry classes, and on the work of Lieu et. al. [LMC20] where the authors use the work by Kawabata et. al. to show that the fermionic systems described by quadratic Lindbladians can be classified into ten symmetry classes that reduce to the Altland-Zirnbauer classes in the absence of dissipation.

We start with the observation that for non-Hermitian matrices the operation of complex conjugation is not equal to the operation of transpose unlike the case of Hermitian matrices. Hence if we take the example of TRS for closed systems which is given by

$$U_T^\dagger H^* U_T = H, \quad U_T^* U_T = \pm\mathbb{I}, \tag{1.129}$$

the complex conjugation can be replaced by a transpose but if we want to extend this condition to include non-Hermtian matrices we will have to make a choice between the two operations. Similar problem arises when extending the concept of PHS and CS. To develop the expression for the action of symmetries we define the second quantised time reversal and particle hole transformation as in Eqs. (1.113) and (1.118) respectively, then we follow a similar procedure as for the closed system (except there no constraint due to Hermiticity) and end up with the following definitions of TRS, PHS and CS for single particle non-Hermitian Hamiltonians respectively

$$\begin{aligned} T_+^\dagger H^* T_+ = H, \quad T_+^\dagger T_+ = \mathbb{I}, \quad T_+^* T_+ = \pm\mathbb{I}, \\ C_-^\dagger H^T C_- = -H, \quad C_-^\dagger C_- = \mathbb{I}, \quad C_-^* C_- = \pm\mathbb{I}, \\ \Gamma^\dagger H^\dagger \Gamma = -H, \quad \Gamma^\dagger = \Gamma, \quad \Gamma^2 = \mathbb{I}. \end{aligned} \tag{1.130}$$

Here, as with the closed system, chiral symmetry is defined as the combination of time reversal and particle hole symmetries. The equations in (1.130) serve as a natural extension of symmetry operations that give us Altland-Zirnbauer (AZ) classes, we can also define a variant of TRS with transpose and a variant of PHS with complex conjugation as

$$\begin{aligned} C_+^\dagger H^T C_+ = H, \quad C_+^\dagger C_+ = \mathbb{I}, \quad C_+^* C_+ = \pm\mathbb{I}, \\ T_-^\dagger H^* T_- = -H, \quad T_-^\dagger T_- = \mathbb{I}, \quad T_-^* T_- = \pm\mathbb{I}. \end{aligned} \tag{1.131}$$

These new variants of TRS and PHS are termed TRS† and PHS† respectively, also it is easy to notice that combining TRS and PHS gives the same result as combining TRS† and PHS†, hence we don't need to define a new chiral symmetry operator. TRS†, PHS† and CS also generate ten symmetry classes that are called AZ† symmetry classes (see table 1.2). We also define a new symmetry the sublattice symmetry (SLS)

$$SHS^\dagger = -H, \quad S^\dagger S = \mathbb{I}, \quad S^2 = \mathbb{I}, \tag{1.132}$$

which is equivalent to CS for the Hermitian case. The symmetries discussed in Eqs. (1.130), (1.131) and (1.132) results in 38 distinct symmetry classes, which can be counted as follows: the original 10 AZ symmetry classes, 6 additional AZ† symmetry classes and 22 symmetry classes originating by combining AZ classes with SLS, any other combination of the aforementioned symmetries can be expressed in terms of these 38 classes [Kaw+19a]. The reason AZ† only result in six new classes is due to the fact that the classes A and AIII are common to both AZ and itself, furthermore the class AI in AZ class and class D† in AZ† class are equivalent due to the fact that when a non-Hermitian Hamiltonian H respects TRS another non-Hermitian Hamiltonian iH respects PHS† [Kaw+19b], similarly class AII is equivalent to class C†.

Another aspect of tenfold classification is the presence of a gap in the spectrum of the first quantised Hamiltonian, which in the case of non-Hermitian Hamiltonians becomes a little complicated since in general they can have complex eigenvalues. The energy gap of a closed system can be contracted to a point since the spectrum is one dimensional, this point is generally termed the Fermi energy E_F, thus naturally and uniquely a system can be said to have a energy gap if no energy bands cross the point $E = E_F$. For the case of open systems, the energy gap is not necessarily contractible to a point since the spectrum is two dimensional, hence the energy gap can be either a forbidden point (point gap) or a forbidden line (line gap) in the complex plane. Importantly the definitions of of the two energy gaps are independent of each other, the choice of the gap depends on the physical problem. The topological classification also depends on the kind of the gap in the system, two systems with same symmetries and same dimensions can have different topological characterisations if the type of gaps they exhibit are different (table III in [Kaw+19a]). The precise definition of the gaps are as follows:

Point gap: A non-Hermitian Hamiltonian $H(\mathbf{k})$ is said to have a point gap if and only if it is invertible, i.e. $\det H(\mathbf{k}) \neq 0, \forall\ \mathbf{k}$, and all the eigenenergies are nonzero, i.e. $E(\mathbf{k}) \neq 0, \forall\ \mathbf{k}$.
In principle the point gap can exist at any arbitrary value in the complex plane, but the presence of symmetries often restrict the eigenvalues. For example in presence of TRS the eigenenergies must come in pairs of (E, E^*) and in presence of SLS they must come in pairs of $(E, -E)$, thus zero energy is a convenient choice for the definition of the point gap.

Line gap: A non-Hermitian Hamiltonian $H(\mathbf{k})$ is said to have a real (imaginary) line gap if and only if it is invertible, i.e. $\det H(\mathbf{k}) \neq 0, \forall\ \mathbf{k}$, and the real (imaginary) part of the eigenenergies is nonzero, i.e. $\mathrm{Re}E(\mathbf{k}) \neq 0, \forall\ \mathbf{k}$ ($\mathrm{Im}E(\mathbf{k}) \neq 0, \forall\ \mathbf{k}$).
Again the choice of real and imaginary axes as the defining lines in the complex plane instead of an arbitrary line has to do with the restrictions imposed by symmetries on the eigenvalues.

Kawabata et. al. provided the topological classification of non-Hermitian Hamiltonians based on 38 symmetry classes, different types of gap and spatial dimensions. The different phases of topologically nontrivial non-Hermitian Hamiltonians are distinguished by topological invariants such as winding numbers and Chern numbers. We will not go into detail of how to calculate these invariants for each case, but we will expand upon the Chern number later in section 3.4 when discussing our specific model.

So far we have discussed general open systems described by a non-Hermitian Hamiltonian, now we discuss the work of Lieu et. al. [LMC20] which specializes the work of Kawabata et. al. to dissipative fermionic systems described by quadratic Lindbla-

Class	TRS	PHS	TRS†	PHS†	CS	d=0	d=1	d=2	d=3
Complex classes									
A	0	0	0	0	0	$\mathbb{Z}$	0	$\mathbb{Z}$	0
AIII	0	0	0	0	1	0	$\mathbb{Z}$	0	$\mathbb{Z}$
Real AZ classes									
AI	+	0	0	0	0	$\mathbb{Z}$	0	0	0
BDI	+	+	0	0	1	$\mathbb{Z}_2$	$\mathbb{Z}$	0	0
D	0	+	0	0	0	$\mathbb{Z}_2$	$\mathbb{Z}_2$	$\mathbb{Z}$	0
DIII	−	+	0	0	1	0	$\mathbb{Z}_2$	$\mathbb{Z}_2$	$\mathbb{Z}$
AII	−	0	0	0	0	$2\mathbb{Z}$	0	$\mathbb{Z}_2$	$\mathbb{Z}_2$
CII	−	−	0	0	1	0	$2\mathbb{Z}$	0	$\mathbb{Z}_2$
C	0	−	0	0	0	0	0	$2\mathbb{Z}$	0
CI	+	−	0	0	1	$\mathbb{Z}$	0	$\mathbb{Z}$	0
Real AZ† classes									
AI†	0	0	+	0	0	$\mathbb{Z}$	0	0	0
BDI†	0	0	+	+	1	$\mathbb{Z}_2$	$\mathbb{Z}$	0	0
D†	0	0	0	+	0	$\mathbb{Z}_2$	$\mathbb{Z}_2$	$\mathbb{Z}$	0
DIII†	0	0	−	+	1	0	$\mathbb{Z}_2$	$\mathbb{Z}_2$	$\mathbb{Z}$
AII†	0	0	−	0	0	$2\mathbb{Z}$	0	$\mathbb{Z}_2$	$\mathbb{Z}_2$
CII†	0	0	−	−	1	0	$2\mathbb{Z}$	0	$\mathbb{Z}_2$
C†	0	0	0	−	0	0	0	$2\mathbb{Z}$	0
CI†	0	0	+	−	1	0	0	0	$2\mathbb{Z}$

Table 1.2.: Listed in this table are 16 distinct symmetry classes out of 38 symmetry classes found by Kawabata et. al. while extending the tenfold classification to non-Hermitian systems. The topological equivalence of classes D†(C†) and AI(AII) and the fact that the classes A and AIII are common to both AZ and AZ† results in 16 distinct classes instead of 20. The labels ± and 0 here have the same meaning as in the table 1.1. The columns labelled with different values of d (spatial dimension), tells us if for a given d there exist a topologically non-trivial non-Hermitian Hamiltonian in presence of a *real* line gap. The complete topological classification is much richer than what we have presented here, since it contains more symmetry classes that arise by combining AZ classes with SLS and additional types of gaps namely, point gap and imaginary line gap. For a detailed description of topological classifiction of non-Hermitian Hamiltonians one can look at the original work [Kaw+19a].

dians. Consider a system described by the Lindblad equation

$$i\frac{d\rho}{dt} = \hat{\mathcal{L}}(\rho) = [\hat{H},\rho] + i\sum_{\mu}\left(2\hat{L}_{\mu}\rho\hat{L}_{\mu}^{\dagger} - \{\hat{L}_{\mu}^{\dagger}\hat{L}_{\mu},\rho\}\right), \tag{1.133}$$

this equation describes the non-unitary time evolution of the density matrix. Here, the Hamiltonian $\hat{H}$ encodes to the coherent time evolution, while the so called jump or dissipation operators $\hat{L}_{\mu}$ describe the gains and losses in the system. Also the above Lindblad equation is written in a non-standard form, since we have multiplied i on both sides, this was done so that in absence of dissipation operators the equation will reduce to the standard Schrödinger equation.

In general a Lindblad equation can be solved by vectorising the density matrix and writing the Lindbladian superoperator $\hat{\mathcal{L}}$ as a matrix. For a system of n fermions this amounts to diagonalising a $2^{2n}\times 2^{2n}$ matrix, which can get very numerically expensive. But for the case when the Hamiltonian $\hat{H}$ is quadratic and the dissipation operators $\hat{L}_{\mu}$ are linear in fermionic operators the problem becomes much simpler. In his work on quadratic Lindblad equations, Prosen [Pro08; Pro10] has been able to show that for such systems we can work with $4n \times 4n$ matrix. We have given a detailed review of Prosen's approach in Sec. 1.4, here we will just use the results.

Using Prosen's formalism the Linbladian superoperator can be written as

$$\hat{\mathcal{L}} = 2\begin{pmatrix} \underline{\hat{c}}^{\dagger} & \underline{\hat{c}} \end{pmatrix}\begin{pmatrix} -Z^T & -2\mathrm{Im}\,[M] \\ 0 & Z \end{pmatrix}\begin{pmatrix} \underline{\hat{c}} \\ \underline{\hat{c}}^{\dagger} \end{pmatrix} - 2i\mathrm{tr}\,[M] \tag{1.134}$$

where $Z = H + i\mathrm{Re}\,[M]$ and $\underline{\hat{c}} = (\hat{c}_1,\cdots,\hat{c}_{2n})$. The $\hat{c}_i^{(\dagger)}$ superoperators follow the fermionic canonical anti-commutation relations (CAR) $\{\hat{c}_i,\hat{c}_j^{\dagger}\} = \delta_{ij}$, $\{\hat{c}_i^{\dagger},\hat{c}_j^{\dagger}\} = 0$ and $\{\hat{c}_i,\hat{c}_j\} = 0$. The upper diagonal form of the Lindbladian implies that its spectrum only depends on the eigenvalues of Z, it can be diagonalised in terms of quasiparticles

$$\hat{\mathcal{L}} = -4\sum_{i=1}^{4}\lambda_i\hat{b}_i'\hat{b}_i, \tag{1.135}$$

where the quasiparticles follow the *almost* CAR $\{\hat{b}_i,\hat{b}_j'\} = \delta_{ij}$, $\{\hat{b}_i',\hat{b}_j'\} = 0$ and $\{\hat{b}_i,\hat{b}_j\} = 0$. The eigenvalues of Z have to follow some generic restrictions: i) $\mathrm{Im}[\lambda_i] \geq 0$ since elements of density matrix can only decay and not amplify with time, and ii) the eigenvalues always come in pairs of $(\lambda,-\lambda^*)$ in order to preserve the Hermiticity of the density matrix at all times.

The eigenvalues of the non-Hermitian matrix Z plays the same role for quadratic Lindbladians as the eigenvalues of the single particle Hamiltonian play for the second quantised Hamiltonian in the case of closed systems. Hence, while investigating the topological properties of a system described by a quadratic Lindbladian it is natural to look at the symmetry classification of the matrix Z. As discussed earlier in this section, for non-Hermitian matrices the time-reversal and particle-hole symmetries can be generalised in two ways given by Eqs. (1.130) and (1.131). Let us assume that for Z the correct way to generalise time-reversal is via complex conjugation

($T_+^\dagger Z^* T_+ = Z$), then this would imply that every eigenvalue of Z will have a conjugate partner, this implies that for every decaying mode ($\mathrm{Im}[\lambda] \geq 0$) of Z there will be an amplifying mode ($\mathrm{Im}[\lambda^*] \leq 0$), which is unphysical. Similarly using the transpose for particle-hole symmetry ($C_-^\dagger Z^T C_- = -Z$) implies the eigenvalues always come in pairs of $(\lambda, -\lambda)$, which again leads to an amplifying mode. Hence for Z the unique way to generalise symmetries is given by Eq. (1.131)

$$\begin{aligned}
\text{Time-reversal:} \quad & C_+^\dagger Z^T C_+ = Z, \quad C_+^\dagger C_+ = \mathbb{I}, \quad C_+^* C_+ = \pm\mathbb{I}, \\
\text{Particle-hole:} \quad & T_-^\dagger Z^* T_- = -Z, \quad T_-^\dagger T_- = \mathbb{I}, \quad T_-^* T_- = \pm\mathbb{I}, \\
\text{Chiral:} \quad & \Gamma^\dagger Z^\dagger \Gamma = -Z, \quad \Gamma^\dagger = \Gamma, \quad \Gamma^2 = \mathbb{I}.
\end{aligned} \tag{1.136}$$

The fact that for quadratic Lindbladians the time-reversal symmetry takes the form of the first line in Eq. (1.136) can also be ascertained from the microscopic derivation of Lindblad equation, as shown in supplementary material of [LMC20]. The restriction that all eigenvalues of Z should follow $\mathrm{Im}[\lambda] \geq 0$, also allows us to rule out the possibility of using either a point gap or an imaginary line gap to determine its symmetry class. This is due to the fact that for both, the point gap and imaginary line gap, the eigenvalues of Z can be deformed to a single point without closing the gap. Hence to determine the symmetry class of Z, we should ascertain if it satisfies the conditions in Eq. (1.136) and if its spectrum has a real line gap.

2. Fractional charges and fractional Josephson effect in superconductor-normal metal hybrid circuits

2.1. Introduction

The notion of fractional charges plays an omnipresent role in condensed matter physics, especially in lower dimensional systems, such as in 1D Luttinger liquids [PGL00; Imu+02; Tra+04; Ste+07; GGM10], or in the 2D fractional quantum Hall effect [TSG82; Lau83; KF94; Sam+97; de-+97], as well as in topological superconductors, where the presence of Majorana- or parafermions gives rise to a fractional Josephson effect [Kit01; FK09; ZK14a; Ort+15]. While the literature on how to define and detect a fractional charge $e^* \neq e$ (e being the elementary charge) is of course much vaster than we could possibly account for in this small introduction, we can nonetheless identify two main and seemingly distinct flavours, which we here intend to unify. As we argue below, this attempt of a unification is deeply rooted in the understanding, that fundamentally, charge of any electronic system must be quantized in integer units of the elementary charge e, such that any charge fractionalization effect can only be meaningfully defined in terms of the topological properties of the time evolution of a system coupled to a transport detector.

In a non-equilibrium transport situation, e^* may be extracted from the transport statistics. This idea was pioneered by Kane and Fisher [KF94], who showed that the Fano factor (the noise-to-current ratio) returns e^*/e, provided that the transport statistics is Poissonian. Very recently, this idea was generalized to a generic non-Poissonian transport regime, when considering the topological properties [Riw19] of the entire full-counting statistics (FCS) [LLL96]. This definition hinges on the time-dependent dynamics of the moment generating function $m(\chi) = \sum_N e^{i\chi N} P(N)$, where χ is the so-called counting field, and $P(N)$ is the probability of having transported N electrons. If N is integer, then m is obviously 2π-periodic in χ for all times. Effective quantum field theories hosting fractionally charged excitations may in principle predict a moment generating function m with broken periodicity. However, it was understood already, that the elementary charge being fundamental for any electronic system, this broken periodicity must be artificial. That is, such effective field theories must have a limited validity for sufficiently high cumulants, and the 2π-periodicity of

$m(\chi)$ must be restored [Ari98; GGM10; IAC13; Riw19; Riw21]. On the other hand, generic open quantum systems with a transport detector were shown to undergo dynamical phase transitions [Pis04; Ubb+12; FG13; Bra+17] leading to a braiding of the complex eigenspectrum of the Lindbladian along the counting field [RS13; LRS14]. The main nontrivial contribution of [Riw19] is the realization, that the resulting breaking of the 2π-periodicity of the complex eigenspectrum, which governs the time evolution of $P(N)$, and thus of $m(\chi)$, should be interpreted as transport carrying fractional charges in the same sense as the known examples from strongly correlated systems. In short, fundamental charge quantization is thus a property of the detector basis, whereas fractional charges are a property of the open system eigenspectrum. Based on this realization, Ref. [Riw19] argued that fractional charges are already observable for standard sequential electron tunneling through a quantum dot in a purely dissipative transport regime, not requiring any material-specific properties or interactions.

Fractional charges can also be defined without the explicit need for nonequilibrium transport (and transport statistics measurements) by the phase picked up when travelling through a magnetic field, $\phi = e^* \int dx A(x)/\hbar$, where for anyonic excitations, e^* can be directly linked to the nontrivial exchange statistics [LM77; Wil82; ASW84; Bar+20; 20]. This notion of fractional charges is at the heart of the fractional Josephson effect due to the presence of exotic excitations, such as Majorana- or parafermions [Kit01; FK09; ZK14a; Ort+15; Kap+19]. Here, e^* defines the periodicity with which the supercurrent depends on the superconducting phase bias ϕ, since in superconducting transport, the phase enters as $e^{\pm i\phi}$. For a pure superconducting regime, it is usually possible to describe the dissipation-free current in the form of a low-energy Hamiltonian $H(\phi)$. It may therefore be tempting to just equip H with the periodicity in ϕ given by the fractional Josephson effect. However, also in the context of superconducting circuits, there is a lingering question about the importance of charge quantization in various contexts, such as for charge noise sensitivity of the fluxonium [Koc+09; Man+09; MY20], when coupling Josephson junctions to an electromagnetic environment [Mur+20; HS21; Mur+21; Kau+21], or when considering the physics of quantum phase slip junctions [KR23]. Specifically for topological superconductors, the presence of Majorana fermions provides a degenerate ground state with even and odd fermion parity, allowing for coherent transport processes which transport a single elementary charge e instead of the Cooper pair charge $2e$ in the ordinary Josephson effect. However, there is a fundamental incompatibility between charge stored in the topological part of the circuit (integer multiples of e) and the charge stored in the trivial parts of the device (integer multiples of $2e$). This interplay can lead to instabilities of the fractional Josephson effect for certain circuit configurations [Hec+11]. The relevance of this incompatibility has also been recently studied for time-dependent driving and capacitive coupling [KHR22], giving rise to a purely geometric correction term. Generally it was argued [Riw21], that for superconducting systems, the periodicity in ϕ of a Hamiltonian (describing a given circuit element) is defined by the unit of charge which a detector, a magnetic field or another circuit element couples to, whereas fractional Josephson effects, and the associated fractional charges, are defined in the periodicity of the eigenspectrum. This argument thus corresponds to a quantum mechanical counterpart to the statement made for purely dissipative systems in Ref. [Riw19].

The question which has, to the best of our knowledge, not yet been addressed, is how exactly the fractional Josephson effect and fractional charges measured in the transport statistics are related, and importantly, how to generalize to a situation where dissipative non-equilibrium currents and equilibrium supercurrents coexist. When combining supercurrents and FCS [RN04], the counting field χ appears as a shift in ϕ, suggesting that the fractional charge in the moment generating function is directly inherited from the periodicity of the Josephson relation. However, we show that the picture becomes much more complex when including nonequilibrium currents, and that in the most generic situation, charge fractionalization expresses itself as exceptional points (EP) in the 2D space spanned by the independent superconducting phase ϕ and the counting field χ. Charge fractionalization in the current statistics and the fractional Josephson effect are thus in general related, but nonetheless distinct effects. Moreover, and similar in spirit to Ref. [Riw19], we can show that in a generic open system context, no exotic materials are required to engineer topological phase transitions giving rise to fractional charges, and a fractional Josephson effect. Curiously, we find that poisoning due to out-of-equilibrium quasiparticles, usually a nuisance for superconducting circuits [LGL05; Sha+08; Cat+11; LM12; FK09; Hec+11; RL12; GC11; BWT12; Pek+13]), is in the particular case studied here a necessary ingredient driving the topological transitions.

For concreteness, we consider a minimal heterostructure model of a single-level quantum dot coupled to two phase-biased superconductors (S) allowing for a supercurrent to flow, and an additional normal metal (N), providing a nonequilibrium electron source. Quantum dot heterostructures have been widely studied in the past both theoretically [FR98; Kan98; CAH00; CLM01; PGK07; Sot+10; Hil+11; Fut+13; Sot+14; WK17] and experimentally [Her+10; Hof+10; Dir+11], with a recently revived interest in connection with a possible probing of the Higgs mode [HS22], and observation of transition from normal Josephson junction to a π junction [SMH22]. In particular, the inclusion of a counting field has been discussed in Ref. [SK14].

While all of our results have been obtained specifically for this model, we believe that our findings regarding the connection between the fractional Josephson effect and fractional charges are generic, so long as the dynamics is described by a Lindbladian. In particular, we find that the aforementioned EPs give rise to phase transitions which can carry a trivial or fractional charge in χ (along the lines of [Riw19]) for different values of ϕ, and at the same time a conventional or fractional Josephson effect for different values of χ. Our work can thus be seamlessly embedded in a larger currently ongoing effort to generalize the notion of topological phase transitions to open quantum systems [RL09; RL10; Die+11; Bar+13; BD15; RLL; Eng+17; Bar+18; MC18; EKB19; Kaw+19a; MC19; KR19; LMC20], especially when expressed via EPs in the open system eigenspectrum [Hei04; Hei12; Kun+18; Kaw+19a; WJS19; MB21; BBK21; Avi+19; San+16], by here assigning them the explicit role of generators of fractional charges and a fractional Josephson effect.

Let us take some time here to comment on our choice of considering the Lindbladian approach for an open quantum system. In particular, the time-local approximation allows us to classify the open system dynamics in a formally similar way as the closed system, by analyzing the topological properties of the eigenspectrum of the Lindbladian superoperator. On the one hand we stress that there are a number of examples, where this approach proved to be very successful to accurately model real experimental systems, such as time dependently driven electron pumps [Roc+13], or the full-counting statistics in quantum dots [Fli+09], notably even at finite frequency [Ubb+12]. On the other hand, it would of course be desirable to not be restricted to weak coupling, and work towards a classification scheme of quantum systems strongly coupled to the environment. Here, the most general way of describing a dissipative system would be via a time non-local kernel that incorporates memory effects, as in the Nakajima-Zwanzig quantum master equation [Nak58; Zwa60]. It might thus seem, that our topological analysis may be restricted to weak coupling to an environment. However, we would like to point out a recent important work by Nestmann et. al. [NBW21], which shows that it is possible to establish a connection between the above time non-local master equation, and a time-local one (which still captures the strong coupling to the environment), via a fixed point relation. It is therefore perceivable that our classification approach is in principle generalisable to systems with strong coupling to the environment. However such an effort is well beyond the scope of the present work, and would likely be envisaged as a future project.

Finally, we explicitly illuminate the role of transport detectors, for different transport measurement schemes. For instance, a generic model of a charge meter constantly entangling with the measured transport processes [PWS17; PWS; SKB09] suppresses all supercurrents, but nonetheless provides a new type of fractional transport phase, which was not yet predicted in Ref. [Riw19], consisting of a statistical mix of trivial and fractional charges. This is constrasted with a complementary understanding of FCSs, where the cumulant generating function is reconstituted by measuring individual cumulants of the current statistics (in the spirit of the FCS as defined in Ref. [RN04]), where supercurrents persist, and the aforementioned EP phase-transitions are (at least in principle) measurable. However, because the materials in the here considered circuit are trivial, the fractional Josephson effect is only visible at finite counting fields χ, and its unambiguous observation would thus in principle require the measurement of cumulants of arbitrarily high order. In order to circumvent this issue, we study alternatively quantum weak measurements of the supercurrent. While weak measurement of the current could be envisaged by means of Faraday rotation (explicitly proposed to weakly measure spins, e.g., in Ref. [Liu+10]), we strive to propose an "all-circuit" realization of weak measurement using SQUID detectors, inspired by Ref. [Ste+01]. We show in particular that a certain post-processing of the classical information obtained by the weak measurement allows to simulate the influence of a finite counting field, and thus induces the protected fractional Josephson effect. This principle can to some extend be understood as a new paradigm of the information of a weak detector being used to "filter out" transport processes with integer Cooper pairs in favour of fractional Cooper pair processes, importantly, without the need of real-time feedback [Vij+12].

This work was done in collaboration with J. Schwibbert and R.-P. Riwar and has appeared as a paper in PRB [JSR23], the part of the work done by them will be explicitly stated. This chapter of the thesis is organized as follows. In Sec. 2.2 we set the stage by reviewing generic features of conventional and fractional Josephson effects by comparing the quantum dot circuit with a Majorana-based circuit. In the same section we define a notion of an open system fractional Josephson effect in presence of a generic coupling to a bath. This is followed by Sec. 2.3 where we explicitly introduce dissipation by means of a coupling between normal metal-induced dissipative mechanism for the quantum dot circuit. In Sec. 2.4 two common versions of full-counting statistics are introduced and the relevant features with respect to topological transport are elucidated. In Sec. 2.5 we discuss various topological phase transitions which arise due to the interplay of dissipation and transport measurement, and argue how they can be interpreted as fractional charges and a fractional Josephson effect, respectively. Based on these results, we investigate in Sec. 2.6 how continuous weak measurement of the current can serve as a means to reach the part of the phase space with finite counting field, where the fractional Josephson effect can be observed. The conclusions are presented in Sec. 2.7. Finally, the appendices A and B detail the derivation of how to extract higher cumulants of all eigenmodes and the calculation of the scattering properties of the SQUID detector used for weak measurement respectively. In the original paper there are two more appendices, credited to Schwibbert and Riwar, that include important derivations and intermediate results, such as the computation of the open system eigenmodes and their interpretation, the calculation of the position of exceptional points. They are not included in the thesis but will be referenced in the text as their results show up. Finally some of the calculations for [JSR23] are part of J. Schwibbert's master thesis [Sch20], it will also be referenced in the relevant parts.

2.2. Integer versus fractional Josephson effect and open quantum system generalization

Consider two superconducting contacts with a phase difference ϕ (which may be controlled, e.g., by a magnetic field). These superconductors may be brought into electrical contact through various ways, for instance by an insulating barrier (the SIS junction) [Jos74] or via more general weak links [Bee91]. In this work, we consider for concreteness weakly coupled tunnel junctions, which have a single quantum dot level [Kön99][1] sandwiched in between, see Fig. 2.1a. The quantum dot itself is described by a single level at energy ϵ, which can be at most doubly occupied (due to

[1]Note however, that we expect our conclusions qualitatively hold also for other systems providing a single-level charge level in between the superconductors, such as a superconducting charge island (Cooper pair transistor in the regime of large charging energies, see, e.g., [Cot02]).

spin degeneracy). The double occupation comes in addition with the energy cost U due to Coulomb interactions. The Hamiltonian thus reads

$$H_{\text{dot}} = \epsilon\widehat{n} + U\frac{\widehat{n}\left(\widehat{n}-1\right)}{2}, \tag{2.1}$$

the total occupation number on the single level being $\widehat{n} = \sum_\sigma d_\sigma^\dagger d_\sigma$, where $d_\sigma^{(\dagger)}$ annihilates (creates) an electron with spin $\sigma = \uparrow, \downarrow$. The eigenstates of H_{dot} are $|0\rangle$, $|1\rangle_\sigma = d_\sigma^\dagger |0\rangle$, and $|2\rangle = d_\uparrow^\dagger d_\downarrow^\dagger |0\rangle$, where $|0\rangle$ is the empty state, $d_\sigma |0\rangle = 0$. The coupling to the superconductors will in leading order introduce coherent transitions between the $|0\rangle$ and $|2\rangle$ states, such that the transport can be captured in terms of the Hamiltonian (detailed calculation of this result can be found in Appendix B of [Sch20])

$$H\left(\phi\right) = H_{\text{dot}} + H_J\left(\phi\right), \tag{2.2}$$

where the exchange of Cooper pairs is described by

$$H_J\left(\phi\right) = \frac{E_{JL} + E_{JR}e^{i\phi}}{2} d_\uparrow^\dagger d_\downarrow^\dagger + \text{h.c.} \tag{2.3}$$

The origin of this additional pairing term is the proximity effect, here considered in the limit of large superconducting gaps Δ [RA00; VMY03; Cho+04; Fut+09; Sot+10], such that $E_{J\alpha} = \Gamma_{S\alpha}$ where $\Gamma_{S\alpha}$ is the normal state tunneling rate between the quantum dot and the corresponding contact α = L,R. That is, the relevant correlation time of the superconducting reservoir is Δ^{-1}. In some sense, the tunnel coupling to the superconductor reservoirs already represent an opening of the local quantum system to a reservoir. However, since supercurrents are mediated entirely without dissipation (at least in this approximation) this effect can be captured by a low-energy Hamiltonian. Hence, the dissipation-free circuit constitutes our "closed" quantum system.

While these individual processes each give rise to single Cooper pair tunneling processes ($\sim e^{\pm i\phi}$), the presence of the quantum dot level modifies the overall transport behaviour. Namely, the Hamiltonian $H\left(\phi\right)$ has the even eigenstates $|\pm\rangle = \frac{1}{\sqrt{2}}\sqrt{1\pm\delta}\,|0\rangle \pm \frac{1}{\sqrt{2}}e^{i\phi_J}\sqrt{1\mp\delta}\,|2\rangle$ with

$$\delta = -\frac{2\epsilon + U}{\sqrt{\left(2\epsilon+U\right)^2 + |E_{JL} + E_{JR}e^{i\phi}|^2}}, \tag{2.4}$$

and the corresponding eigenenergies

$$\epsilon_\pm\left(\phi\right) = \frac{-2\epsilon - U \pm \sqrt{\left(2\epsilon+U\right)^2 + |E_{JL} + E_{JR}e^{i\phi}|^2}}{2}. \tag{2.5}$$

Since the odd parity states $|1_\sigma\rangle$ cannot partake in the Cooper pair transport, they remain eigenstates also for the full H, with the unchanged eigenenergy ϵ. The above energies $\epsilon_\pm\left(\phi\right)$ are no longer a pure cosine (as for instance for the standard Josephson effect), but the spectrum remains in general 2π-periodic, see Fig. 2.1c, signifying integer multiple Cooper pair tunnelings as explained initially in this paragraph.

There is however one special point in parameter space, where the 2π-periodicity is broken: for $\epsilon = -U/2$ and $E_{JL} = E_{JR} \equiv E_J$, the minigap closes, such that $\epsilon_\pm = \pm E_J \cos(\phi/2)$, and the eigenvalues exchange places when progressing ϕ by 2π, see Fig. 2.1d. Here, it seems that the transport can be described by means of a fractional transport of Cooper pairs, transferred in half-integer portions.

This is highly reminiscent of topological Josephson junctions based on Majorana fermions, where the fractional Josephson effect hinges upon the topological contacts having an even and odd ground state [FK09]. Here, the Hamiltonian is commonly given in the form

$$H_M = iE_M \cos(\phi/2)\, \gamma_{1,\mathrm{L}}\gamma_{2,\mathrm{R}} \ , \tag{2.6}$$

describing the coupling of Majorana edge states on the left and right $\gamma_{1/2,\alpha}$ via a junction, see Fig. 2.1b (see, e.g., Ref. [12]). This Hamiltonian has the exact same 4π-periodic eigenvalues $\epsilon_\pm(\phi) = \pm E_M \cos(\phi/2)$ (see again Fig. 2.1d), which we associate to the eigenvectors $|\pm\rangle$ [2]. Note that of course, the eigenstates $|\pm\rangle$ of the Majorana circuit are different from the eigenstates $|\pm\rangle$ of the quantum dot circuits. We nonetheless choose the same notation for simplicity - the reason for this will become obvious below.

Now, the reader might perhaps be surprised by such seemingly naive (or even slightly brazen) juxtaposition of a regular quantum dot circuit and a Majorana-based junction. Indeed, one might for instance argue that no experiment could ever tune both $E_{JL,JR}$ and ϵ to such perfection as to make the mini-gap disappear completely. However, it should be noted that in Majorana circuits, finite size effects are known to induce a small gapping, due to a coupling of the Majoranas on the same chain (i.e., terms of the form $\sim \gamma_{2,\mathrm{L}}\gamma_{1,\mathrm{L}}$ or $\sim \gamma_{2,\mathrm{R}}\gamma_{1,\mathrm{R}}$) [Kit01; LSD10; Wan+]. A gapping and thus a restoring of a 2π-periodic spectrum was also predicted when a Majorana-junction and a regular Josephson junction are coupled in parallel to form a SQUID [Hec+11]. As a consequence, the line between fractional and regular Josephson effect starts to blur, as a minigap may likely be present for both trivial and topological circuits.

Alternatively, one might have tried to argue that while the energy spectrum of both systems looks similar, the Hamiltonian has a fundamentally different periodicity in ϕ, with Eq. (2.3) being 2π-periodic whereas Eq. (2.6) appears genuinely 4π-periodic. Such arguments can however likewise be easily defused. If the phase bias ϕ is stationary, the periodicity of the Hamiltonian is a simple gauge choice and not of relevance. For instance, we could have redistributed the phase drop in Eq. (2.3) symmetrically over both junctions with a factor $e^{\pm i\phi/2}$, thus achieving a 4π-periodic Hamiltonian. However, this basis choice becomes relevant (i.e., it ceases to be a mere gauge choice) if ϕ becomes time-dependent due to driving with magnetic fields [YSK19a; RD22], or a dynamical quantum operator due to the addition of a capacitor [KHR22], or

[2] We note that for the open Majorana circuit, each of the eigenvalues is two-fold degenerate, corresponding to overall even and odd parity. For our purposes, this distinction is of no further importance.

if non-local correlation measurements are performed [Riw21]. Here, the appropriate rule of thumb [Riw21] is that the relevant charge (and the corresponding charge unit) is the charge that a magnetic field, a capacitor, or a detector couple to. For instance, for the Majorana circuit, Eq. (2.6), a detector could measure the charge being transported across the actual Majorana junction, marked with an arrow in Fig. 2.1b. Then, the 4π-periodic basis choice given in Eq. (2.6) is correct, since the Majorana wires physically exchange the charge e. If the same detector would however measure the charge entering one of the s-wave superconductor bulks, which proximitize the topological nanowire (the green bulks in Fig. 2.1b), then the correct basis choice must be a 2π-periodic one (e.g. via the unitary transformation proposed by Ref. [Hec+11]), to account for the fact, that the trivial, s-wave part of the circuit can in its ground state only accept integer Cooper pairs with charge $2e$.

The above short review leads us to two conclusions. First, whether a system provides a fractional or regular Josephson effect should be best described exclusively by the periodicity of the eigenspectrum, and not of the Hamiltonian, as the latter is either a gauge choice (for constant phase bias), or fixed by external factors. Second, even if a system consists of topological superconductors, there are many nontrivial factors that may lead to an instability of the fractional Josephson effect, by introducing a minigap, and restoring 2π-periodicity. In the following, we will show with the example of the trivial quantum dot system, that the inclusion of a non-equilibrium quasiparticle reservoir, and the addition of a transport detector can as a matter of fact undo the gapping, and restore an open system version of the fractional Josephson effect, without the need for fine-tuning any system parameters. As already stated in the introduction, this effort will furthermore shed light on the intricate relationship between the fractional Josephson effect and fractional charges, as defined in the transport statistics [Riw19].

However, before continuing, we need to develop as a next preparatory step a generalization of the notion of a fractional Josephson effect for open systems. To this end, we consider either the quantum dot circuit, Eq. (2.2), or the Majorana circuit described in Eq. (2.6), and add a generic open system dynamics to it. For this purpose, we take as the basis the two closed system eigenstates $|\pm\rangle$ with eigenenergies $\epsilon_\pm(\phi)$, where $\epsilon_\pm$ can now either be 2π-periodic or 4π-periodic, see Fig. 2.1c and d. In the next section, we discuss a concrete model for open system dynamics for the quantum dot circuit; here, on this general, illustrative level, we are merely concerned with simple generic open system processes, which consists of stochastic transitions between the $|+\rangle$ and $|-\rangle$ states. Such processes can be described by a Lindblad quantum master equation for the density matrix $\rho = \sum_{\eta,\eta'=\pm} P_{\eta\eta'} |\eta\rangle \langle\eta'|$,

$$\dot{\rho} = -i\left[H(\phi), \rho\right] + \sum_{j=\pm} \Gamma_j \left(a_j \rho a_j^\dagger - \frac{1}{2}\left\{a_j^\dagger a_j, \rho\right\}\right), \tag{2.7}$$

with $a_\pm = |\pm\rangle\langle\mp|$, such that $\Gamma_\pm$ represents the rate for a stochastic jump from $|\mp\rangle$ to $|\pm\rangle$.

While in the closed system, we had the real eigenvalues $\epsilon_\pm(\phi)$, the Lindblad equation gives rise to a set of complex eigenvalues $\{\lambda_n\}$, describing both the coherent and

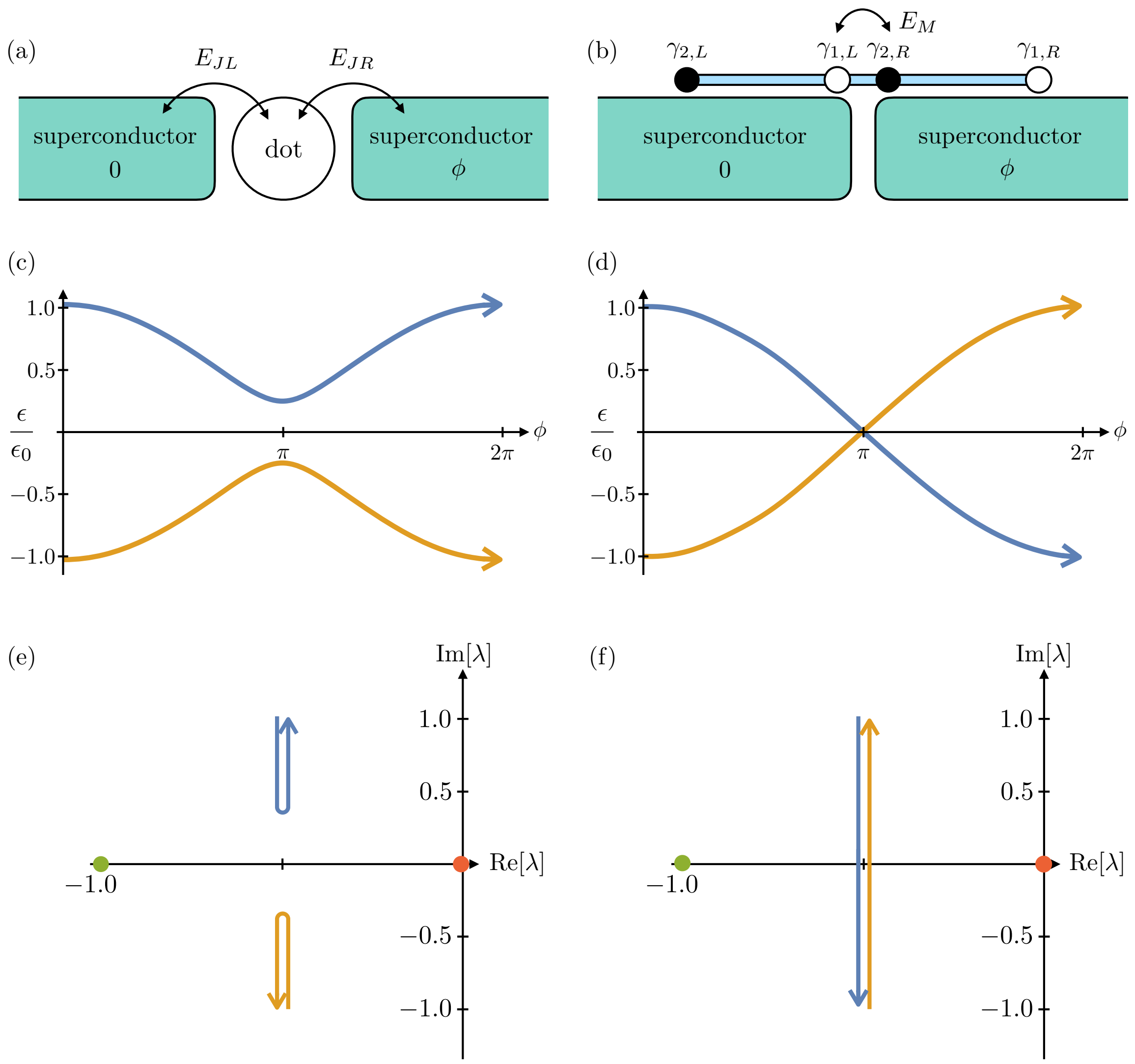

Figure 2.1.: Generalization of integer versus fractional Josephson effect for open quantum systems. We compare a conventional circuit, such as the quantum dot proximitized with two superconductors (essentially a Cooper pair transistor) (a), with a topological circuit, hosting Majorana fermions (b). Both circuits are subject to the phase bias ϕ. For the closed system, the regular and fractional Josephson effect can be distinguished by either a 2π-periodic (c), or a 4π-periodic (d) energy spectrum as a function of ϕ. When including a simple, generic open system dynamics, see Eq. (2.7), the purely real spectrum in (c,d) gets replaced by a complex spectrum $\lambda(\phi)$ (e,f), where the real part describes dissipation and decoherence, whereas the imaginary part represents the coherent dynamics. When drawing the complex spectrum of the open system parametrically with respect to ϕ (from 0 to 2π, in the sense indicated by the arrow), we see that in the regular Josephson effect, the eigenvalues with finite imaginary part return to their initial values after a progression of ϕ from 0 to 2π (e). For the fractional Josephson effect, these two eigenvalues swap places (f).

dissipative dynamics, see Fig. 2.1e and f. In addition, while the closed system could be described by just two eigenvalues, due to the two degrees of freedom + and −, for the open system, we have four eigenvalues due to the enlarged structure of the density matrix. The eigenvalue 0 represents the fact that there is a unique stationary state, $\rho_{\mathrm{st}} = (\Gamma_- |-\rangle\langle-| + \Gamma_+ |+\rangle\langle+|) / (\Gamma_+ + \Gamma_-)$. The eigenvalue $-(\Gamma_+ + \Gamma_-)$ corresponds to the decay of the diagonal density matrix elements (if the states $|\pm\rangle$ encode a qubit, this would be the T_1 time). Finally, there are the eigenvalues $\pm i(\epsilon_+ - \epsilon_-) - (\Gamma_+ + \Gamma_-)/2$, belonging to the eigenoperators $|\pm\rangle\langle\mp|$ which describe the coherent oscillations, including the decoherence rate $(\Gamma_+ + \Gamma_-)/2$ (T_2 time). Only this last pair of eigenvalues depends on ϕ, such that the integer and fractional Josephson effects can be characterized by means of their ϕ-dependence. In order to represent the (now) complex eigenspectrum, we choose a parametric plot, where the real and imaginary parts of λ are shown as two independent axes, and the resulting curves are parametrized by ϕ (in Figs. 2.1e and f). In the regular Josephson effect the eigenvalues with finite imaginary part (coherent dynamics) map onto themselves when running ϕ from 0 to 2π, see Fig. 2.1e. This is in contrast to the fractional Josephson effect, where the same two eigenvalues swap places, see Fig. 2.1f. The two resulting open system spectra are thus still topologically distinct, as one cannot continuously map from one to the other. This allows for a straightforward topological classification of the open system dynamics.

2.3. The model: superconductor-normal metal hybrid circuit

Let us now introduce a microscopic model for the open system dynamics of the quantum dot circuit. In addition to the two superconductors, we include a tunnel coupling to a third, normal metal reservoir, see Fig. 2.2a. This coupling introduces dissipative, stochastic transport events. Since pairing (Δ) is absent in the normal metal, it can in lowest order only introduce processes which flip the parity within the quantum dot. We here focus on the regime where the chemical potential of the normal metal is large with respect to the system dynamics ($\mu \gg \epsilon, U, E_{J\alpha}$). Therefore, for the computation of the dynamics due to the normal metal (by means of a standard sequential tunneling approximation, see Ref. [Kön99]), we may disregard the internal coherent dynamics. Consequently, the normal metal will mainly act as a source of quasiparticles, thus inducing the nonequilibrium stochastic transitions, $|0\rangle \to |1_\sigma\rangle$ and $|1_\sigma\rangle \to |2\rangle$. Including the stochastic processes, the dynamics of the system is described by the quantum master equation $\dot{\rho} = L\rho$, with

$$L(\phi)\cdot = -i[H(\phi), \cdot] + W_N\cdot, \tag{2.8}$$

where $H(\phi)$ is the Hamiltonian given in Eq. (2.2), and the kernel due to the normal metal processes, W_N, is of the Lindblad form

$$W_N\cdot = \Gamma_N \sum_\sigma \left(d_\sigma^\dagger \cdot d_\sigma - \frac{1}{2}\left\{ d_\sigma d_\sigma^\dagger, \cdot \right\} \right), \tag{2.9}$$

the calculation to obtain this form of the kernel W_N can be found in Appendix B of [Sch20]. We note that strictly speaking, the superconductors themselves should likewise contribute to parity switches due to a finite quasiparticle population. However, even though quasiparticles are known to occur with a much higher concentration that what is expected from a thermal equilibrium distribution [MAA09; Ris+13], they are nonetheless dilute (with a concentration of typically $10^{-6} \sim 10^{-5}$ with respect to the Cooper pair density [RC19]), such that the normal metal influence may be expected to be dominant, even when $E_J > \Gamma_N$, especially due to the large chemical potential.

The processes $|0\rangle \to |1_\sigma\rangle$ and $|1_\sigma\rangle \to |2\rangle$ both occur with the same rate. This is in particular due to $\mu \gg U$, such that effectively, the many-body interaction is no longer visible within the dissipative dynamics. This is why, for the remainder of this work, we will set $U = 0$ without loss of generality. As another important observation, let us point out that contrary to the generic open system discussion in the previous section, the kernel W_N here gives rise to relaxation and decoherence in a basis which is different from the eigenbasis of the local dynamics H. This will render the dynamics much more complex, especially when including a transport detector, as we show in what follows.

However, before we continue with transport measurements and transport statistics, let us briefly describe the system dynamics of ρ. As already introduced in Sec. 2.2 the system dynamics is governed by the set of generally complex eigenvalues $\{\lambda_n\}$ of the superoperator L, Eq. (2.8), with the corresponding eigenoperators. In absence of the parity drive, $\Gamma_N = 0$, the dynamics of the density matrix is given by the eigenmodes of $-i[H,\cdot]$ alone. The eigenoperators $|+\rangle\langle+|, |-\rangle\langle-|, |1_\sigma\rangle\langle 1_\sigma|$, all have eigenvalues 0, meaning that they correspond to the eigenstates of H. The eigenoperators $|\pm\rangle\langle\mp|$ with the eigenvalues $-i(\epsilon_\pm - \epsilon_\mp)$ indicate the coherent dynamics. With finite Γ_N, the even and odd subsectors couple. The eigenvalues are now $0, -\Gamma_N, -2\Gamma_N, -i(\epsilon_\pm - \epsilon_\mp) - \Gamma_N$, where $-\Gamma_N$ is doubly degenerate, see Fig. 2.2b. These eigenvalues can be interpreted as the decay of physical quantities as discussed in Refs. [Spl+10; Con+12; SW12]. For this purpose, one needs to consider the structure of the corresponding eigenoperators. While it is possible to find a closed form for the eigenoperators for arbitrary system parameters, the expressions are quite cumbersome and thus not very instructive. We therefore consider the here relevant limit $\Gamma_N \ll |\epsilon_+ - \epsilon_-|$, where we may simplify the expressions considerably (done explicitly by Schwibbert and Riwar in Appendix A of [JSR23]). Namely, we find that the eigenoperators belonging to $\lambda_\pm = -i(\epsilon_\pm - \epsilon_\mp) - \Gamma_N$ are still approximately given by $|\pm\rangle\langle\mp|$, which now represent the coherent oscillations damped with the decoherence rate Γ_N. The eigenvalue $\lambda_0 = 0$ corresponds to the stationary state of the quantum master equation,

$$\widehat{\rho}^{\text{st}} \approx \frac{(1-\delta)^2}{4}|+\rangle\langle+| + \frac{1-\delta^2}{4}\sum_\sigma |1_\sigma\rangle\langle 1_\sigma| + \frac{(1+\delta)^2}{4}|-\rangle\langle-|. \tag{2.10}$$

We observe that even though the parity switching rate is small, the occupation of the odd state is of the same order as the even state in ρ^{st}. This is simply due to the fact that while parity switches from even to odd are rare, the same is true for the reversed process from odd to even. Hence the system spends an approximately equal amount of time in either parity sector. The eigenvalue $\lambda_p = -2\Gamma_N$ indicates the decay of the fermion parity, given by the operator $\widehat{p} = e^{i\pi\widehat{n}}$, as discussed also in Ref. [SW12]. The doubly degenerate eigenvalue $\lambda_{s,c} = -\Gamma_N$ relates to two processes. For one, to the decay of spin, $\widehat{s} = \sum_\sigma \sigma \left|1_\sigma\right\rangle \left\langle 1_\sigma\right|$, and for another, to the decay of what we refer to as the pseudo-charge number $\widehat{c} = \left|+\right\rangle \left\langle +\right| - \left|-\right\rangle \left\langle -\right|$. We baptize it in this way because in the absence of the proximity effect, $E_J \to 0$, we find $\widehat{c} \to \left|2\right\rangle \left\langle 2\right| - \left|0\right\rangle \left\langle 0\right| = \widehat{n} - 1$.

With respect to the Josephson effect, note that the normal metal itself merely introduces relaxation and decoherence, but does not alter the periodicity of the eigenspectrum with respect to ϕ: the coherent oscillations still occur with the frequency $\epsilon_+ - \epsilon_-$, which, as discussed above, are usually 2π periodic in ϕ (unless the system parameters are tuned to very special values). Hence, in the generic case of a spectrum with a minigap, the complex open system spectrum has the same topology as the one shown in Fig. 2.1e. This will change now, when considering the combination of open system dynamics and transport measurements. Let us point out though, that while the transport measurement is indispensable, the presence of a *nonequilibrium* drive due to the voltage-biased normal metal is equally important. For a pure equilibrium drive, the kernel L would satisfy an equivalent of a PT symmetry, where braid phase transitions are forbidden even in the presence of a counting field [RS13; Riw19].

2.4. Different flavors of full-counting statistics

Generally, for a superconducting junction described by a Hamiltonian $H(\phi)$, the operator for the supercurrent across the junction can be defined as $I = 2e\partial_\phi H(\phi)$. In Eq. (2.3), the phase bias is attached to the right contact, such that the operation ∂_ϕ actually returns the current to the right,

$$I \equiv ieE_{JR}e^{i\phi}d_\uparrow^\dagger d_\downarrow^\dagger + \text{h.c.} = I_{SR}. \tag{2.11}$$

By means of a simple unitary transformation, the Josephson energy could be modified as $E_{JL} + E_{JR}e^{i\phi} \to E_{JL}e^{-i\phi} + E_{JR}$, such that here, the current at the left interface would be measured. In accordance with what we stated in the introduction and in Sec. 2.2, the position of measurement is not a mere gauge choice, and gives rise to different predictions. Here, this difference is in particular due to the addition of a third (normal metal) contact, which injects an additional dissipative displacement current. For the remainder of this thesis we will stick for concreteness to the explicit example where the current is measured at the right contact (see also Fig. 2.2a). In order to map these results to the case where the detector is on the left, one has to mirror the entire device (that is exchange $E_{JL} \leftrightarrow E_{JR}$). Let us note that yet another physically distinct scenario would be to distribute the phase bias across both junctions with a factor ζ, i.e., $E_{JL} + E_{JR}e^{i\phi} \to E_{JL}e^{-i\zeta\phi} + E_{JR}e^{i(1-\zeta)\phi}$. This would express the situation when a current detector couples to both currents at the left and right junction with this prefactor. Our results would certainly be sensitive to the value of ζ. We disregard

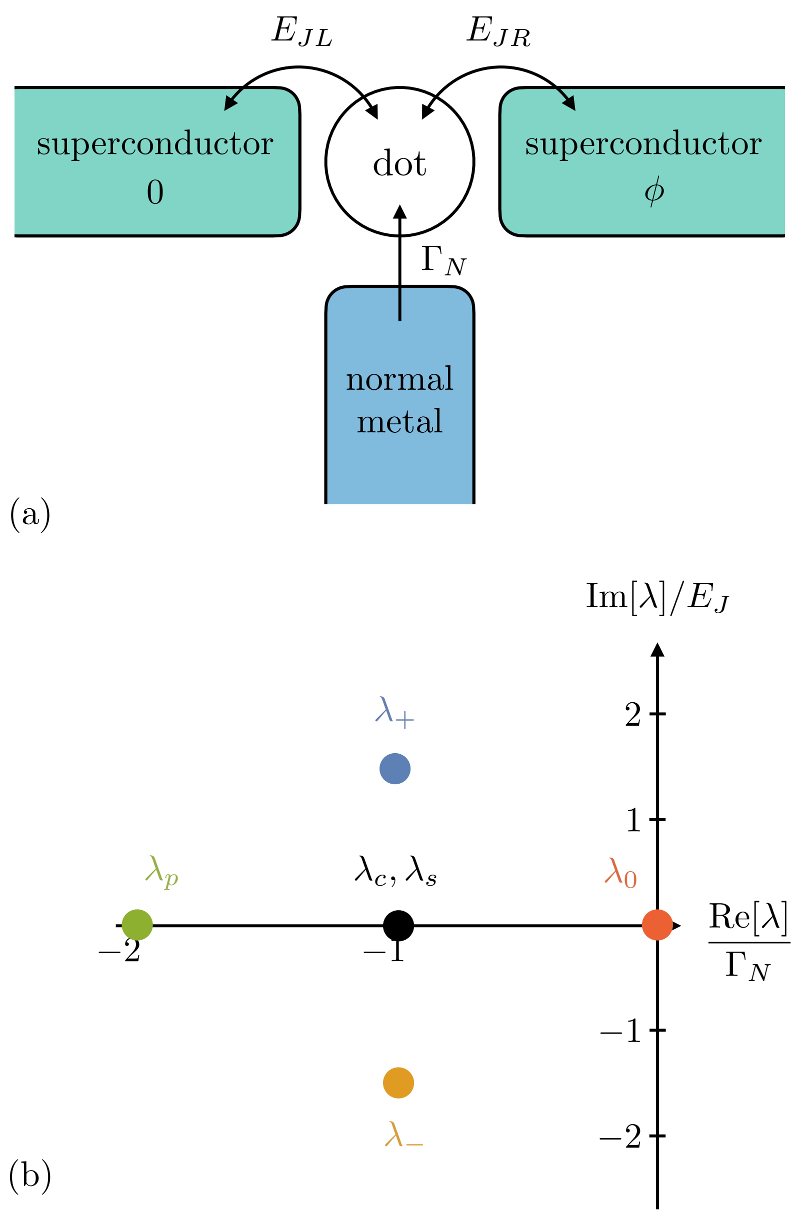

Figure 2.2.: (a) Sketch of the system under consideration. A central charge island (quantum dot) is connected to a left and right superconductor, with a phase bias ϕ. The normal metal pumps quasiparticles into the system with the rate Γ_N. A detector with counting field χ measures current into the right superconductor. (b) The complex eigenspectrum of the quantum master equation $\{\lambda\}$ for $\chi = 0$. The eigenmodes can be interpreted as follows. There is a stationary state related to the eigenvalue $\lambda_0 = 0$. The nonzero eigenvalues can be associated to the decay of the parity, pseudocharge (see main text) and spin, $\lambda_{p,\bar{c},s}$, respectively, and to the coherent dynamics $\lambda_\pm$.

this option for simplicity, assuming that it is physically possible to build a current detector which couples only to the right contact.

For starters, let us point out that in the absence of the normal metal, the even parity eigenstates $|\pm\rangle$ exhibit a dc Josephson effect,

$$\langle I \rangle_{\pm} = 2e\partial_{\phi}\epsilon_{\pm}. \tag{2.12}$$

In the odd parity sector, the system is "poisoned", and no supercurrent flows, see also discussion after Eq. (2.5). For the current expectation value, the main influence of the normal metal is a reduction of the supercurrent in the stationary state, due to the finite occupation of the poisoned state, see Eq. (2.10).

In the following, we now want to go way beyond the current expectation value, and describe the entire FCS of the transport, where the interplay between quasiparticle-induced dissipation and current measurement will give rise to a plethora of nontrivial effects. However, before going down that road, we have to explicitly address the fact that there are several different ways to define the FCS, which correspond to different measurement schemes. While these differences do not play a role for purely dissipative transport, in the presence of supercurrents, these different "flavours" of FCS give rise to markedly different results, and in particular to different interpretations of the observed topological transitions.

2.4.1. Averaging time-resolved current measurements

In the context of superconducting transport, a straightforward access to FCS is due to [RN04], whereby the quantum master equation is supplemented with a counting field χ, $\dot{\rho}(\chi) = L(\chi, \phi)\rho(\chi)$, such that

$$L(\chi,\phi)\cdot = -i\left[H(\phi-\chi)\cdot - \cdot H(\phi+\chi)\right] + W_N \cdot . \tag{2.13}$$

The cumulant generating function for the transported charges after a measurement (integration) time τ, $c(\chi,\tau)$, is then computed via the moment generating function $m(\chi,\tau)$, defined as

$$m(\chi,\phi,\tau) = \mathrm{tr}\left[e^{L(\chi,\phi)\tau}\rho_0\right] \equiv e^{\tau c(\chi,\phi,\tau)}, \tag{2.14}$$

where ρ_0 is the initial state (which becomes irrelevant for large measurement times τ). Derivatives of the cumulant generating function provide the cumulants C_k. For instance, the average current is given as

$$\langle I \rangle = C_1 = -ie\partial_{\chi}c\big|_{\chi\to 0}, \tag{2.15}$$

and the current noise (usually denoted by the letter S) is given as

$$S = C_2 = (-i)^2 e^2 \partial_{\chi}^2 c\big|_{\chi\to 0}, \tag{2.16}$$

and so forth. In order to appreciate the difference to the other important notion of FCS (explained below), we have to go beyond this formal definition, and recapitulate

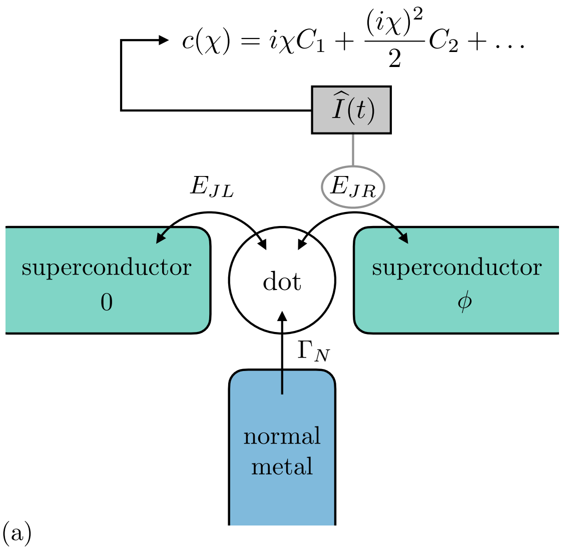

(a)

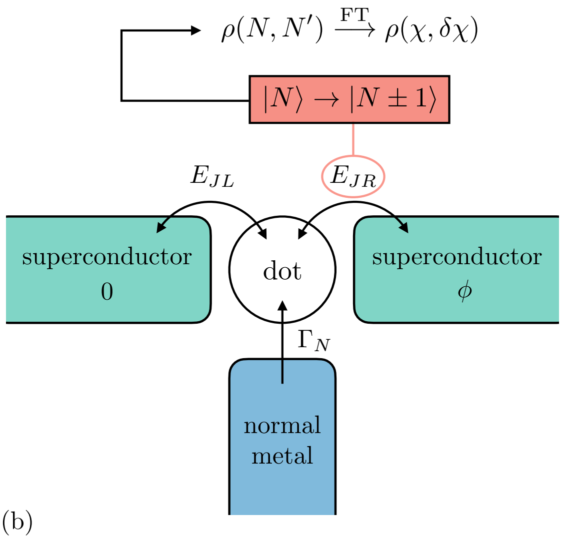

(b)

Figure 2.3.: Different approaches to FCS. (a) The current at the right junction may be projectively measured at a given time t, and current measurements at different times can be correlated and integrated over time, in order to obtain the cumulants C_k. In between measurements, the system propagates freely. The cumulant generating function can then be reconstructed in a Taylor series. In this approach, the counting field χ is a fictitious quantity. (b) An ideal detector may be coupled at the right contact, such that for each transported Cooper pair, the detector changes its state $|N\rangle \to |N \pm 1\rangle$ where N stands for the number of transported Cooper pairs. The detector thus continuously entangles with the system. As a consequence, the counting field χ is here an actual physical quantity: the detector momentum, related to N by a Fourier transform (FT). However, after a projective measurement of the detector state, the information of the dissipation-free supercurrent is lost.

in detail, *how* the current is actually measured in order to obtain the above cumulants. For this purpose, let us examine the first couple of statistical moments a little more closely. The first moment (giving rise to the current expectation value $I = C_1$) returns

$$-ie\partial_\chi \left. m\right|_{\chi\to 0} = -ie\mathrm{tr}\left[\int_0^\tau dt_1 e^{L(\phi)(\tau-t_1)} \left.\partial_\chi L(\phi)\right|_{\chi\to 0} e^{L(\phi)t_1}\rho_0\right] \tag{2.17}$$

where

$$-ie\,\partial_\chi \left. L\right|_{\chi\to 0}\cdot = e\left\{\partial_\phi H(\phi),\cdot\right\} = \frac{1}{2}\left\{I,\cdot\right\}, \tag{2.18}$$

with the anticommutator $\{\cdot,\cdot\}$. As we see, the FCS as defined above corresponds to a system evolving freely (that is, without any detection event) for most of the time, and a projective current measurement at a precise time step t_1, and subsequently, integrating over all times t_1 from 0 to a total measurement time τ, as schematically represented in Fig. 2.3a. The zero-frequency limit of the FCS is when the measurement time approaches infinity, $\tau \to \infty$. The picture becomes even more detailed, when going to the next moment, providing the current-current correlations,

$$\begin{aligned}(-i2e)^2\,\partial_\chi^2 \left. m\right|_{\chi\to 0} &= (-i2e)^2\,\mathrm{tr}\left[\int_0^\tau dt_1 e^{L(\phi)(\tau-t_1)}\,\partial_\chi^2 \left. L(\phi)\right|_{\chi\to 0} e^{L(\phi)t_1}\rho_0\right]\\ &+ 2\mathrm{tr}\left[\int_0^\tau dt_1\int_0^{t_1} dt_2 e^{L(\phi)(\tau-t_1)}\left\{I,\cdot\right\} e^{L(\phi)(t_1-t_2)}\left\{I,\cdot\right\} e^{L(\phi)t_2}\rho_0\right].\end{aligned} \tag{2.19}$$

While both the first and second line now indicate two current measurements, the time difference between these two measurements is of the essence. While the second line accounts for projective current measurements at times t_1 and t_2, which are sufficiently far apart (with an unimpeded system evolution for the rest of the time interval), the first line describes two current measurements that occur within time intervals which are short with respect to the superconductor correlation time Δ^{-1} (see also previous section). For the interested reader, we refer to the diagrammatic language for noise, which was first developed for time-independent systems [Thi+03; Thi+05a; Thi+05b], subsequently generalized to time-dependent systems [RSK13] as well as finite frequency noise [DS18]. In this language, measurements according to the first line are represented by diagrams where the two current operators appear within the same irreducible block.

At any rate, it is interesting to note that if the current detector fails to measure time-resolved currents on a time-scale smaller than Δ^{-1}, the first line will be absent altogether. This can be understood as a high-frequency cut-off for the FCS. Such a deficient detector would return a different moment generating function, given as

$$m_{\text{cut-off}}(\chi,\phi,\tau) = \mathrm{tr}\left[e^{L_{\text{cut-off}}(\chi,\phi)\tau}\rho_0\right], \tag{2.20}$$

with

$$L_{\text{cut-off}}(\chi,\phi) = L(\phi) + i\frac{\chi}{2e}\left\{I,\cdot\right\}, \tag{2.21}$$

which is nothing but a first order in χ approximation of the full $L(\phi, \chi)$. Thus, while the eigenspectrum of $L_{\text{cut-off}}(\phi, \chi)$ asymptotically approaches the one for the full $L(\phi, \chi)$ for low values of χ (low cumulants), the global properties (arbitrarily high cumulants) differ decisively. In particular, while the full L is 2π-periodic in χ, $L(\phi, \chi + 2\pi) = L(\phi, \chi)$, reflecting the fact that the detector measures the supercurrent in integer portions of Cooper pairs, this information is lost in $L_{\text{cut-off}}$. Likewise, we cannot in general hope to see the same topological phase transitions along χ for the two scenarios. We conclude that if we are interested in understanding and measuring the global properties of the FCS with respect to χ (relevant for fractional charges as defined in [Riw19]) by means of projective current measurements, a current detector which can resolve beyond the time-scale Δ^{-1} is required.

2.4.2. Continuous entanglement with a charge transport detector

This subsection is credited to Schwibbert. There is a different approach to FCS, whereby an explicit detector is included in the model description of the system [LLL96; SKB09; PWS; PWS17], keeping track of the number of charges exchanged at a given interface. Hence, the counting field χ is here not merely an auxiliary mathematical object without any physical meaning. To the contrary, it has a well-defined precise interpretation: χ is the detector momentum [PWS; PWS17]. Because of this, the global properties defined in χ-space are much more tangible compared to the notion described in the above section, where large χ can only be reached by measuring a sufficiently high number of cumulants. Here, an analysis (read-out) of the detector state may directly provide the moment generating function for finite χ, in contrast to the previously introduced approach, where m as a function of χ would have to be reconstructed essentially by analytic continuation, starting from $\chi = 0$.

Following the lines of [SKB09; PWS; PWS17], a detector measuring transport at the interface to the right superconductor can be modeled by supplementing the proximity Hamiltonian H_J with the detector degrees of freedom $|N\rangle$ indicating the number N of measured Cooper pair transport events,

$$\rightarrow H_J = \frac{1}{2}\left(E_{JL} + E_{JR}e^{i\phi}\sum_N |N-1\rangle\langle N|\right) d_\uparrow^\dagger d_\downarrow^\dagger + \text{h.c.} \tag{2.22}$$

Thus, the detector state changes as $|N\rangle \rightarrow |N \pm 1\rangle$, for each Cooper pair leaving or entering the right contact, see also Fig. 2.3b. Note that the detector itself is ideal in the sense that it does not have any internal dynamics apart from this coupling (i.e., the Hamiltonian of the isolated detector is zero). The quantum system plus detector have a much larger state space, described by the density matrix $\rho_{S+D} = \sum_{N,N'} \rho(N, N') \otimes |N\rangle\langle N'|$, illustrating the fact that the detector will be entangled with the system during the measurement. Similar to the previous notion of FCS, τ here stands for the total measurement time. Whereas in Sec. 2.4.1 τ represented the total time interval over which the current measurements should be averaged, here τ stands for the total time elapsed since the coupling to the detector (and thus the build up of entanglement) started. Also for continuous entanglement, a related zero-frequency FCS can be defined, by analyzing the asymptotic behaviour for $\tau \to \infty$.

The additional detector degree of freedom can be compactified by a double Fourier transform,

$$\rho(\chi, \delta\chi) = \sum_N \sum_{N'} e^{i\chi(N+N')} e^{i\delta\chi(N-N')} \rho(N, N'), \tag{2.23}$$

resulting in the quantum master equation

$$\dot{\rho}(\chi, \delta\chi) = L_{\mathrm{CE}}(\chi, \delta\chi, \phi)\, \rho(\chi, \delta\chi) \ . \tag{2.24}$$

We note that the Lindbladian describing the continuous entanglement with the detector, L_{CE}, is related to the above, first version of FCS, described by $L(\chi, \phi)$ in Eq. (2.13), as

$$L_{\mathrm{CE}}(\chi, \delta\chi, \phi) = L(\chi, \phi - \delta\chi). \tag{2.25}$$

The variables χ and $\delta\chi$ can be thought of as the classical and quantum component of the detector momentum. As we see, the classical detector momentum corresponds to the counting field introduced in the FCS of Ref. [RN04].

The quantum part $\delta\chi$ on the other hand simply enters as a shift in the superconducting phase, and may therefore at first sight seem innocuous. It is however this shift, which makes all the difference. Namely, for the continuously entangling detector, the moment generating function is defined as the Fourier transform of a projective measurement of the detector state in its eigenbasis $|N\rangle$,

$$m_{\mathrm{CE}}(\chi, \tau) = \sum_N e^{i2N\chi} \mathrm{tr}\left[\rho(N, N, \tau)\right] = \int_0^{2\pi} \frac{d\delta\chi}{2\pi} \mathrm{tr}\left[\rho(\chi, \delta\chi, \tau)\right], \tag{2.26}$$

where for the second identity, we used the fact that the integration over $\delta\chi$ results in the projection onto the diagonal elements $\rho(N, N') \to \rho(N, N)$. Importantly, due to $\delta\chi$ appearing as a shift in ϕ, we can relate this moment generating function to the first one, Eq. (2.14), as follows

$$m_{\mathrm{CE}}(\chi, \tau) = \int_0^{2\pi} \frac{d\phi}{2\pi} m(\chi, \phi, \tau). \tag{2.27}$$

Overall, we note that since L_{CE} and likewise m_{CE}, Eqs. (2.25) and (2.27), can be constructed from L and m respectively, Eqs. (2.13) and (2.14), we consider L to be the more fundamental construction of FCS. Therefore, it will suffice to analyse the topological properties of $L(\chi, \phi)$.

However, the above phase shift $\delta\chi$ plays an important role when it comes to analyzing the topological eigenspectrum of L, due to the presence of supercurrents. If supercurrents were absent, there would be no phase-dependence of the transport $m(\chi, \phi) = m(\chi)$, such that m and m_{CE} are equivalent. However, for supercurrents being present, the two notions of FCS differ, in that the supercurrents are averaged out in m_{CE}. One can convince oneself of this fact, simply by means of the Josephson relations given in Eq. (2.12), where $\int_0^{2\pi} d\phi I_{S\pm} \sim \epsilon_\pm(2\pi) - \epsilon_\pm(0)$ must be zero, due to the 2π-periodicity of the eigenspectrum $\epsilon_\pm$ in ϕ. This cancellation of the supercurrent is a consequence of the detector always being ideally coupled to the interface at which it counts the number of transported Cooper pairs. It thus entangles with the coherent transport (and the entanglement continuously increases as the measurement goes on), such that when projectively reading out the detector state, the information about the supercurrent is destroyed. Nonetheless, such a continuously entangled detector may serve for an understanding of the topology of the dissipative part of transport. Moreover, as we will show below, such a detector will give rise to a novel transport phase, which can be interpreted as a statistical mix between a fractional and a trivial transport.

Let us conclude this section by pointing out the following. In this work, we aim at understanding the topological properties of the eigenspectrum of L along both the χ and ϕ coordinates. While this is endeavour is formally well-defined, thanks to Eq. (2.13), from a more practical point of view, we see that both of the above flavours of FCS come with their advantages and disadvantages. Ultimately we have the choice between measuring individual cumulants without destroying the supercurrent information (in accordance with the construction of L), which however allows us to only explore the vicinity of $\chi \approx 0$ (since the measurement of arbitrarily high cumulants is experimentally challenging), or, via L_{CE}, explore the full χ-space (since the detector and thus χ are here physical) but at the expense of losing the supercurrent information, and thus losing the ϕ-dependence. Moreover, realistically, a detector measuring the charge that arrived at one of the superconducting contacts most likely involves supplementing said contact with a capacitance, which thus renders the detector nonideal (its Hamiltonian is no longer zero). This leads us to consider below a third variation to obtain information about the transport statistics: continuous weak measurement. However, this approach is very challenging to cast into a general form, which is why we first present our results for the topology of L, and identify a particularly interesting topological regime, for which we formulate a specifically tailored version of weak transport measurement.

2.5. Fractional charge versus fractional Josephson effect

This section is credited to Schwibbert and Riwar. We have so far established a framework to describe the open system dynamics of a superconductor-normal metal hybrid circuit, including the FCS, based on the Lindbladian $L(\chi, \phi)$ in Eq. (2.13). Let us now explore the topological properties of the eigenspectrum of $L(\chi, \phi)$, $\{\lambda_n(\chi, \phi)\}$. In order to analyze the topology of the eigenspectrum, keeping track of the eigenvalue labelling will be important. In Sec. 2.3, we have already introduced the labelling $\{\lambda_0, \lambda_\pm, \lambda_p, \lambda_{s,c}\}$, motivated by the physical interpretation of the decay processes of the corresponding eigenmodes. When including the counting field χ, the eigenspectrum will be modified, $\lambda_n(\phi) \to \lambda_n(\chi, \phi)$. For finite χ we will still use the same labelling of indices, which is however somewhat tricky because of braid phase transitions, whereby certain eigenvalues swap places. We therefore use the convention, that the labelling n shall be done according to Sec. 2.3 at the reference point $\chi = 0$.

As detailed in the previous section, the counting field and the superconducting phase difference appear per se as independent parameters. Similarly to Refs. [RS13; LRS14; Riw19], it turns out that the nonequilibrium drive via the normal metal will give rise to topological transitions in the spectrum λ_n. However, in Refs. [RS13; LRS14; Riw19] only the counting field χ was considered as a relevant coordinate. Here, we have the 2D space (χ, ϕ). In 2D, exceptional points appear, as we will explain in more detail below. When considering cuts of the complex spectrum along either χ or ϕ, these exceptional points generate a braid phase transition, and a resulting broken periodicity in either χ or ϕ. We will interpret phases with a broken periodicity along χ as a transport with fractional charges (along the lines of Ref. [Riw19]). Intriguingly, including here the superconducting phase ϕ, our theory also predicts braid phase transitions in ϕ. There are several nontrivial phases, which can be classified as a fractional Josephson effect, in the sense of having a spectrum with broken periodicity in ϕ. We will refine this statement in the following. Importantly, since transitions along both coordinates appear due to exceptional points in the 2D space (χ, ϕ), we conclude that the fractional charge defined in the transport statistics (χ) and the fractional Josephson effect (ϕ) are intimately related, but distinct concepts in a generic open system context.

2.5.1. Braid phase transitions due to exceptional points in counting field and superconducting phase

In order to describe the topological phase transitions in the spectrum of $L(\chi, \phi)$, we first have to establish some technical details regarding braid theory. As already stated, in general, the eigenspectrum of $L(\chi, \phi)$, $\{\lambda_n(\chi, \phi)\}$, is complex. Considering the space spanned by (χ, ϕ), we can think of the eigenspectrum as a complex band in a 2D Brillouin zone (where χ and ϕ are coordinates of the 2D torus). Therefore, the touching of two complex bands, $\lambda_n = \lambda_{m \neq n}$, leads to two independent conditions, which may be satisfied for particular values of both χ and ϕ. That is, a touching of two complex bands occurs in isolated points on the 2D torus. In Fig. 2.4a, we show the location of exceptional points for a chosen parameter set. As it turns out, band degeneracy points can occur for typical system parameters (see caption of Fig. 2.4). Locally, at the degeneracy points, the two eigenvalues partaking in the degeneracy can be described by a complex square root function $\pm\sqrt{z}$ (where $z \sim \chi + i\phi$). In the literature of topological transitions in open quantum systems, these touching points are commonly referred to as exceptional points, see, e.g., Ref. [BBK21] (and references therein).

When choosing a closed path in (χ, ϕ) around an exceptional point, the two eigenvalues which touch at the exceptional points, perform a braid. Thus, to each of the exceptional points, one may assign generators of the braid group; the braid generator may be considered as a generalization of the notion of a topological charge carried by a degeneracy point (see, e.g., [Riw19]). Given a certain ordering of the eigenvalues, the index j of the braid generator σ_j (see Fig. 2.4b) indicates, which two eigenvalues perform a braid. We here choose the order of the labels as $\lambda_0, \lambda_+, \lambda_-, \lambda_p$, see, e.g., Fig. 2.6. For instance, the braid generator σ_1 thus braids λ_0 with λ_+, σ_2 braides λ_+ with λ_- and finally σ_3 braids λ_- with λ_p. Note that the eigenvalues $\lambda_{s,c}$ are inert, in the sense that they depend neither on χ nor ϕ, and do not partake in braiding. This is why we do not have to include them for the analysis of the topology of the eigenspectrum. While $\partial_\chi \lambda_s = 0$ can be understood by the complete symmetry of the system with respect to spin, $\partial_\chi \lambda_{\overline{n}} = 0$ stems from the effective elimination of the many-body interactions within the dissipative (quasiparticle-induced) processes, due to $\mu \gg U$. At any rate, we only have to consider braid generators with four strands. For four strands, the set of three braid generators, σ_1, σ_2, and σ_3, see Fig. 2.4b, is complete and describes the whole braid group. For convenience, we have furthermore introduced a braid generator to directly braid the first and fourth strand (λ_0 and λ_p), $\sigma_4 = \sigma_1^{-1}\sigma_3^{-1}\sigma_2\sigma_1\sigma_3$. This generator is however non-fundamental in the sense that it can be constructed out of $\sigma_{1,2,3}$.

Due to the 2π-periodicity of L in χ and ϕ, there must be an overall conservation of the "braid charge" (similar to [Riw19], where this was discussed for complex χ). As a consequence, to each exceptional point with a given braid generator σ_j (see Fig. 2.4b), there must exist a partner point, with the inverse braid generator. These two partner points are connected by a line, see 2.4a. In fact, since the exceptional points are locally described by the square root function, these lines can be understood as the corresponding branch cuts, with the two partner points as origin points for the branch cut. When considering the spectrum along one particular parameter (either χ or ϕ, see red arrows in Fig. 2.4a), the braid word for the spectrum can be constructed as follows. One simply has to add for each branch cut which is crossed, the corresponding braid generator in the order it is crossed. In order to know the chirality of the braid generator (i.e., whether one has to add a given σ_j or σ_j^{-1}) one may follow a "right hand rule": take the cross product of the tangential vector indicating the path taken (red arrow in Fig. 2.4a) and the tangential vector of the branch cut, at the given point, where these two lines cross. The direction of the cross product vector decides the chirality. In Fig. 2.4a, we show two examples of paths (as red arrows), one along χ for a fixed value of ϕ, and conversely one along ϕ with fixed χ. Along these paths, the topological phases discussed below emerge (marked with a star and an inverse star symbol, cf Secs. 2.5.2 and 2.5.3).

At this point, let us comment on the importance of the fact that the dissipative processes due to W_N relax into a basis different from the eigenbasis of H. If the coupling to the environment would be such that the dissipative processes occurred in the basis of H, as is the case, e.g. in Eq. (2.7), then the addition of the counting field χ would not give rise to any interesting topological transitions. Here, the eigenvalues $\lambda_\pm(\phi) = \pm i[\epsilon_+(\phi) - \epsilon_-(\phi)] - (\Gamma_+ + \Gamma_-)/2$ would simply receive a χ-dependence as $\lambda_\pm(\chi, \phi) = \mp i[\epsilon_+(\phi + \chi) - \epsilon_-(\phi - \chi)] - (\Gamma_+ + \Gamma_-)/2$. Due to $\epsilon_\pm$ being gapped for the quantum dot circuit, the complex spectrum eigenspectrum would here be trivial for all values of (χ, ϕ). The normal metal providing an out-of-equilibrium electron source thus plays an essential role as the driver of topological phase transitions. We note that usually, processes which change the parity of superconducting circuits are considered detrimental (referred to as quasiparticle poisoning, see, e.g., Refs. [LGL05; Sha+08; Cat+11; LM12; FK09; Hec+11; RL12; GC11; BWT12; Pek+13]). Here, we provide a rare counter example, where they are at the origin of an interesting effect.

2.5.2. Fractional charges

Let us now analyze explicitly the plethora of braid phase transitions of the eigenspectrum of $L(\chi, \phi)$ along χ with fixed ϕ. While we could in principle use the information of the exceptional points in (χ, ϕ)-space, as discussed above, we note that for explicit calculations, there is a mathematically more efficient approach, which was discussed in Ref. [Riw19] (and further detailed in Appendix B of [JSR23]). Namely, the trick is to describe braid transitions in $L(\chi)$ (for fixed ϕ) by generalizing to complex counting fields $e^{i\chi} \to z \in \mathbb{C}$ (and $e^{-i\chi} \to 1/z$), such that the real counting fields are represented on the unit circle, $|z| = 1$. The exceptional points now do no longer appear in the 2D space of (χ, ϕ), but in the complex 2D space of z. A braid phase transition in the χ-space occurs when an exceptional point traverses the unit circle. Therefore, in order to keep track of the topological phases, we simply have to compute the number of exceptional points residing within the unit circle. Based on the definition for L in Eq. (2.13), we find that the positions of the exceptional points can be obtained analytically by means of the quartic equations,

$$\sum_{i=0}^{4} p_i z^i = 0 \quad \text{and} \quad \sum_{i=0}^{4} q_i z^i = 0 \ , \tag{2.28}$$

where the coefficients p_i and q_i depend on all the system parameters and ϕ. Their explicit forms are given in Appendix B of [JSR23]. Note that both equations have to be fulfilled individually, such that there are two sets of roots for z, one for the first, and one for the second polynomial equation. As explained above, for a given root z_0, one simply has to test if $|z_0| \lessgtr 1$ and count the total number of roots inside the unit circle, which enables us to draw maps of the topological phases as in Fig. 2.5 as a function of all the system parameters and ϕ. We find overall four different types of braids for the eigenspectrum along χ, which are labelled in Fig. 2.5b with the sphere, triangle, upside down triangle, and star symbols, and explicitly drawn at example points in parameter space in Fig. 2.6. In the upper left corner of each panel in Fig. 2.6, we also provide the braid word describing the topology of the spectrum.

There is a trivial phase, shown in Fig. 2.6a (sphere symbol). Here, the eigenvalues $\{\lambda_0, \lambda_+, \lambda_p, \lambda_-\}$ do not swap places within the entire interval $\chi \in [0, 2\pi)$. There are two topological phases (triangle, and upside-down triangle), shown in Figs. 2.6b and c. In Fig. 2.6b, the eigenvalues related to the stationary state λ_0 and the parity decay λ_p perform a braid. However, this braid does not break the 2π-periodicity in χ, as they braid twice, as indicated by the braid words $\sigma_4\sigma_4$ and $\sigma_2\sigma_2$.

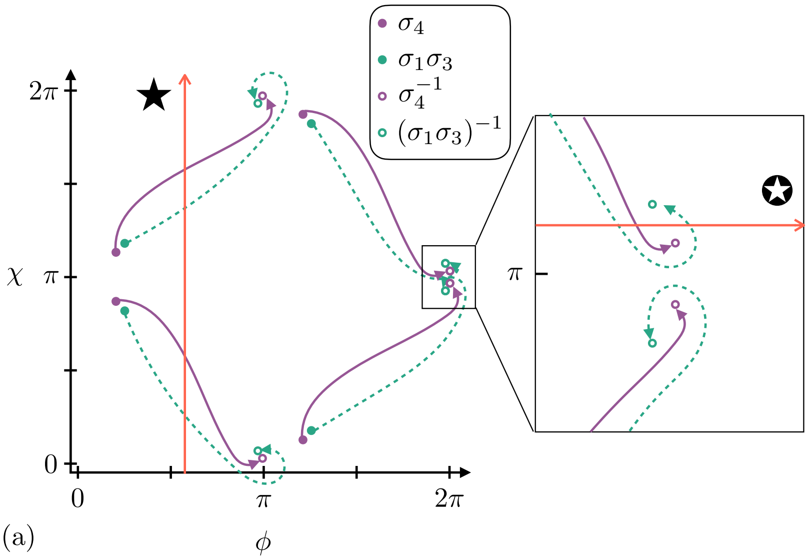

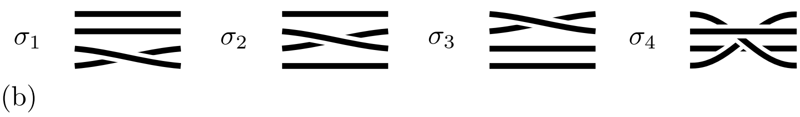

Figure 2.4.: (a) Positions of exceptional points in (χ, ϕ)-space for $E_{JL} = E_{JR} \equiv E_J$, $\epsilon = 0.1E_J$, and $\Gamma_N = 0.5E_J$. To each exceptional point, one may assign braid generators (similar to a topological charge), marked with solid and empty circles. Since four eigenvalues partake in braid phase transitions, we need the braid group for four strands, given in b). In fact, this braid group is complete already with the first three generators, σ_1, σ_2, and σ_3. The fourth braid generator is only added for convenience; it can be expressed as $\sigma_4 = \sigma_1^{-1}\sigma_3^{-1}\sigma_2\sigma_1\sigma_3$. Due to overall "braid charge" conservation, each exceptional point must have its negative counter part, to which the inverse braid generator is assigned. Such a pair of exceptional points is connected via an arrow (solid purple and dashed green). The braids along a particular axis (either χ or ϕ, see two examples marked with red arrows), see subsequent figures, can be constructed from a) by the following rule. To know the topology (i.e., the braid word) of a spectrum along a given path, one needs to assemble all the generators of the connection lines of two exceptional points, in the order they are crossed. For instance, the red arrow along χ, gives rise to the braid word $(\sigma_1\sigma_3\sigma_4)^2 = (\sigma_2\sigma_1\sigma_3)^2$, which corresponds to the topological phase given in Fig. 2.6d. The red line along ϕ [see inset of a)], returns the braid word $\sigma_1\sigma_3\sigma_4\sigma_1^{-1}\sigma_3^{-1} = \sigma_2$, and thus the topological phase from Fig. 2.8d.

Finally, there is a topological phase where the 2π-periodicity in χ is broken, see Fig. 2.6d. After progression of χ by 2π the eigenvalues λ_0 and λ_p, as well as λ_+ and λ_- have swapped places, leading to an overall 4π-periodicity of the spectrum. Along the lines of Ref. [Riw19], such a spectrum can be interpreted as transporting a charge with half the unit as compared to the 2π-periodic phases. For the sake of completeness, let us reiterate the arguments of Ref. [Riw19]. First of all, note that as per the two definitions of the FCS, Eqs. (2.13) and (2.25), the charge is counted in units of Cooper pairs, with charge $2e$. The trivial phases with a spectrum 2π-periodic in χ therefore transport charges in units of $2e$. The in the 4π-periodic phase, the transported charge is $e^* = 2e/2 = e$. Charge quantization is broken in the sense that physically, the s-wave superconducting contacts can only accept integer Cooper pairs (due to the large Δ limit). The non-equilibrium drive due to the normal-metal induces the topological phase of Fig. 2.6d, where the contacts seem to accept half-integer Cooper pairs. In fact, this breaking of charge quantization seems already to some extent indicative of a fractional Josephson effect, which we will discuss in detail in moment.

According to Ref. [Riw19], there are two important ways to define fractional charges in χ. Let us first consider the zero-frequency limit of FCS. As already mentioned above, the measurement time τ is here to be taken as infinite, $\tau \to \infty$. Consequently, in the transport statistics, only the eigenvalue with the least negative real part, λ_0 is visible (see also Ref. [NB02; BN03]), as can be seen when considering the definition of the moment generating function m in Eq. (2.14). As τ increases, all higher eigenmodes $\lambda_{n\neq 0}$ become exponentially suppressed. In fact, the cumulant generating function in this limit can be computed simply as

$$\lim_{\tau\to\infty} c(\chi,\tau) = \lambda_0(\chi) \ . \tag{2.29}$$

That is, for a hypothetical experimenter measuring the true zero-frequency FCS, the information of the higher modes would be lost. However, something nontrivial remains. Suppose that we were able to measure a sufficiently large number of cumulants C_k to reconstruct $c(\chi)$, and thus $m(\chi)$, for finite values of χ. This would essentially correspond to analyzing the eigenvalue $\lambda(\chi)$ first close to $\chi \approx 0$ and then analytically continuing to finite χ. If the cumulants C_k are measured up to a sufficiently high (ideally infinitely high) order k, the cumulants could thus be used to reconstruct the periodicity of λ_0 in χ and thus determine unit of the charge being transported. Curiously, when the zero mode λ_0 partakes in a braid phase transision, the analytic continuation would clearly provide a 4π-periodic moment generating function, indicating transport in units of e, in spite of the system physically transporting charges into the superconducting reservoirs in units of $2e$.

The interpretation of the broken periodicity as a fractional charge works also for finite measurement times τ, when the transport statistics still depend on τ, and the decaying modes $\lambda_{n\neq 0}$ are still detectable. Here, Ref. [Riw19] argues, that the spectrum consisting of complex bands with broken periodicity in χ can be exactly mapped to a fictitious open quantum system which transports charges in units given by the periodicity in χ. In the topological phase shown in Fig. 2.6d, both λ_0 and λ_p as well as λ_+ and λ_- merge into two complex bands, each with periodicity 4π. Thus, this corresponds to two fictitious bands transporting charge e instead of $2e$.

There is an additional final point to be discussed. Namely, the spectrum as shown in Fig. 2.6 can only be measured when adopting the first version of FCS, outlined in Sec. 2.4.1, i.e., when projectively measuring the current at local times, and correlating them to obtain the transport statistics. If the FCS is instead measured with a continuously entangling detector, according to Eq. (2.27) the moment generating function is integrated over ϕ. Since the moment generating function is a regular expectation value, the integral over ϕ (including the normalization prefactor $1/2\pi$) can be understood effectively as a statistical average over a homogeneous probability distribution in ϕ. It is in this sense, that the transport statistics obtained via m_{CE} are to be understood as a statistical mix of different topological phases. For instance, in Fig. 2.5 for a given ϵ one can draw a horizontal line along ϕ, and thus evaluate how many distinct topological phase regions the line crosses. In particular, there is thus the possibility to observe a statistical mix of topological phases with different transported charge units, either the charge $2e$ for the phases in Figs. 2.6a, b, and c or the charge e for Fig. 2.6d. Such an effect was not posssible in Ref. [Riw19], where only normal metal contacts were considered, and thus the FCS was ϕ-independent.

2.5.3. Fractional Josephson effect

As we have seen just now, one particular topological phase along χ (Fig. 2.6d) indicated transport with a charge e instead of $2e$ which would be the default charge of the superconducting contact. Here, we want to analyse the topological properties of the eigenspectrum along ϕ for different values of χ. To this end, we proceed similarly as above, this time, by replacing $e^{i\phi} \to \widetilde{z}$ (and $e^{-i\phi} \to 1/\widetilde{z}$) and analyzing the positions of exceptional points in the space of general, complex $\widetilde{z}$. Also here, this position can be evaluated again by means of a quartic equation with the same form as in Eq. (2.28), with $z \to \widetilde{z}$ and the new coefficients $p_i, q_i \to \widetilde{p}_i, \widetilde{q}_i$, depending on χ instead of ϕ. Again, their explicit form is given in Appendix B of [JSR23].

The resulting map of topological phases is shown in Fig. 2.7. Here, there are overall five different phases to be observed, a trivial one, and four topologically nontrivial ones, denoted by the square, diamond, pentagon and inverted star symbols (as indicated in Fig. 2.7b). Here, all of the nontrivial phases break 2π-periodicity along ϕ. Hence, in this broad sense, all of these phases may be interpreted as a fractional Josephson effect. In particular, apart from the 4π-periodic phases in Fig. 2.8a and b (denoted with the square and diamond symbols), there is in fact an 8π-periodic phase (pentagon symbol), where all four non-inert eigenvalues partake in a braid. Here, we can think of the interaction with the magnetic field generating the phase bias ϕ in terms of a charge $e/2$, similar to parafermionic circuits [ZK14a; Ort+15]. Note that a fractional charge $e/2$ could not be observed in the topological properties along χ discussed previously. We can therefore see this as a nice example illustrating why the topological properties along χ and along ϕ should in general be considered distinct effects. Topological transitions along both parameters are related due to their com-

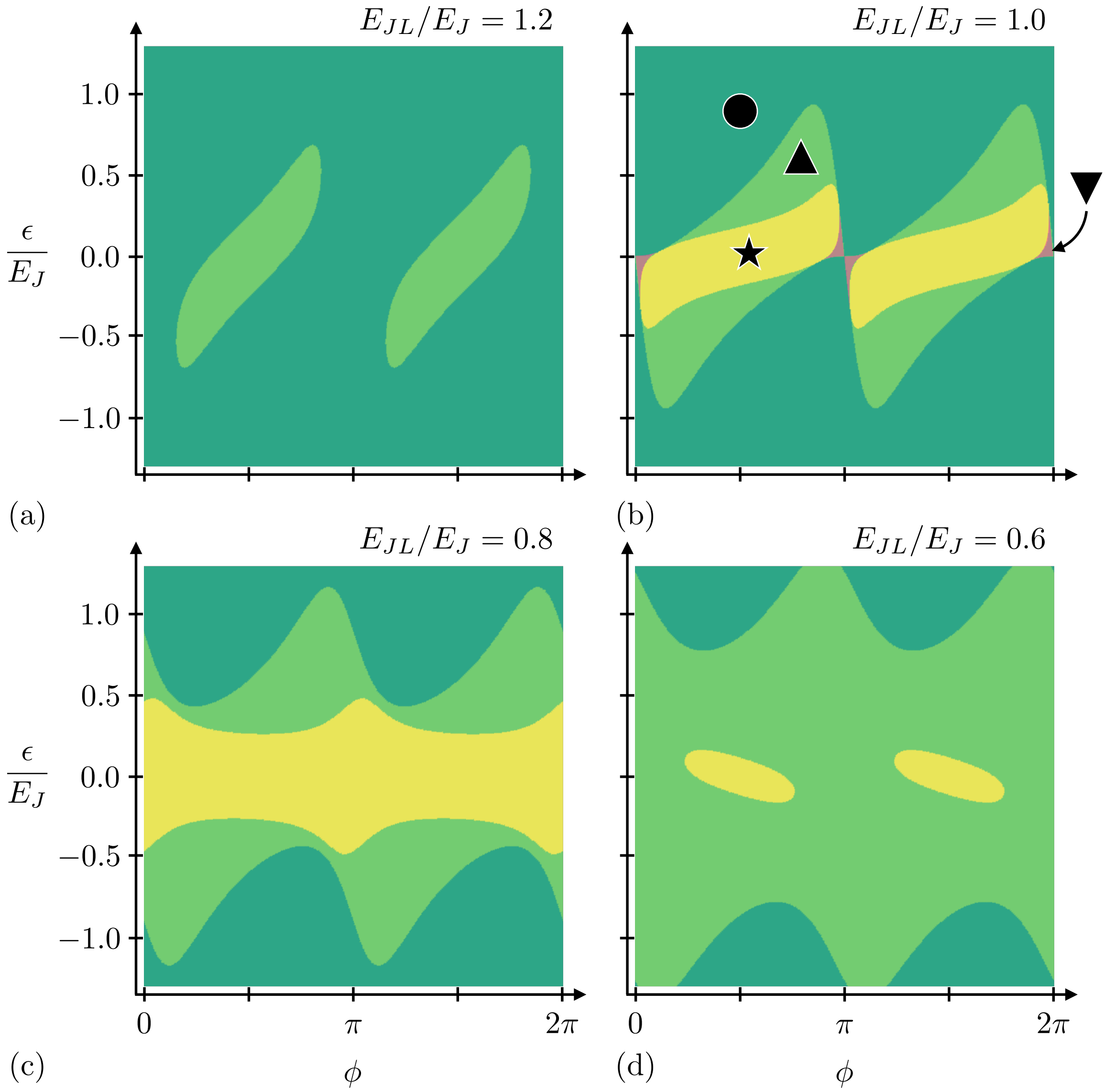

Figure 2.5.: Map of the different topological phases of the eigenspectrum $\lambda_n(\chi)$ (with $n = \{0, +, -, p\}$), as a function of the detuning ϵ, and the phase bias ϕ, for different asymmetries of the Josephson energies, E_{JL}/E_J (a-d). In (b) we mark all four possible topological phases with the symbols of circle, triangle, inverted triangle, and star. Out of those, only the yellow phase (star) is a topological phase with fractional charge $e^* = e/2$. For asymmetric junctions, $E_{JL}/E_J = 0.8$ (see panel c), this phase is connected for all ϕ for a certain interval of ϵ close to 0.

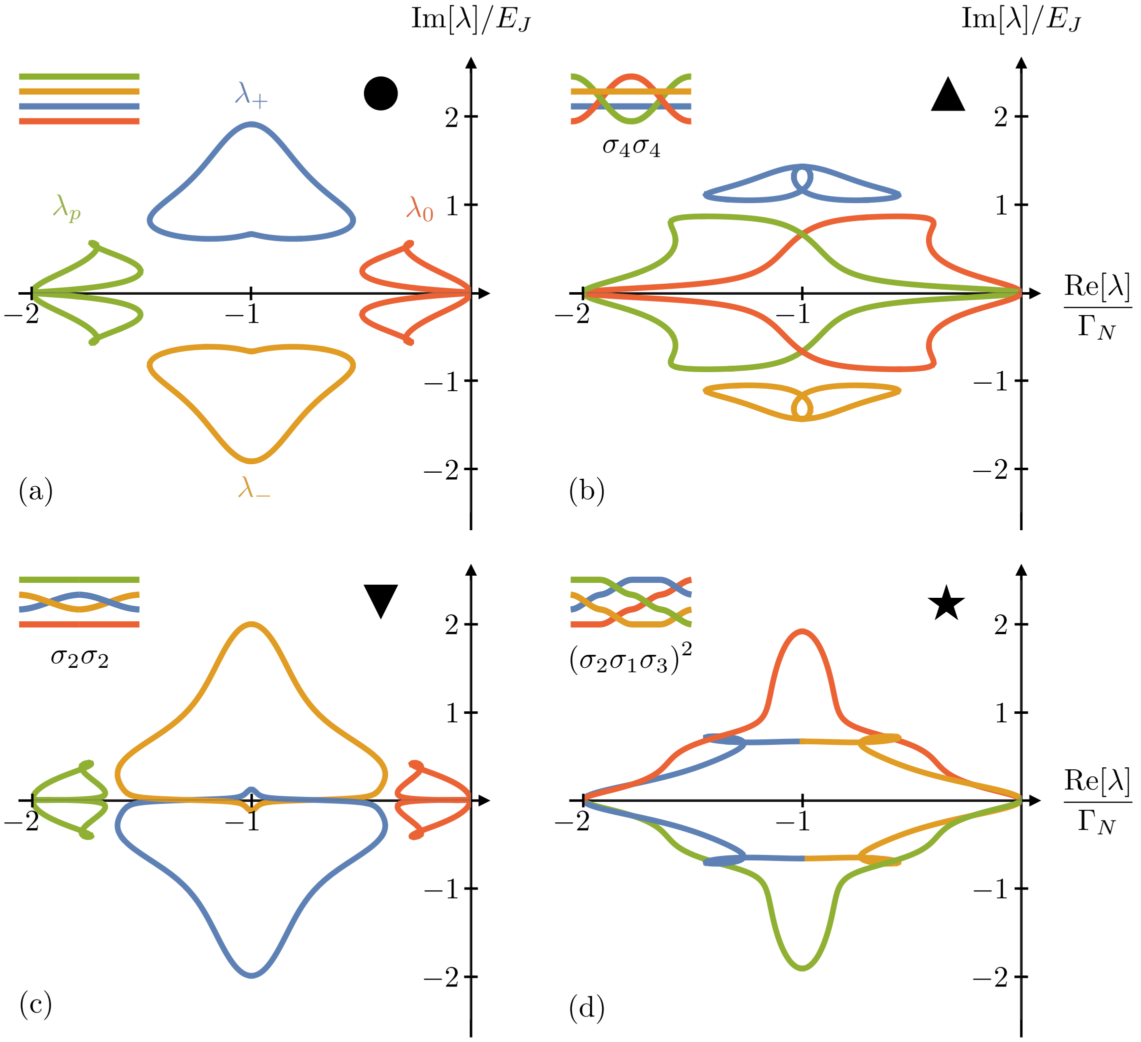

Figure 2.6.: The real and imaginary parts of the spectrum $\lambda_n(\chi)$ (with $n = \{0, +, -, p\}$), drawn parametrically for $\chi = [0, 2\pi)$, for the four different topological phases mapped out in Fig. 2.5 (a-d), and the definitions for the generators of the braid group, $\sigma_{1,2,3}$ (e). The corresponding inverse generators $\sigma_{1,2,3}^{-1}$ can be constructed by braiding with opposite chirality. There is a trivial phase (a), where all complex eigenvalues form separate bands. The corresponding braid word is trivial. In (b) the eigenvalues λ_0 and λ_p braid twice, such that the total spectrum remains 2π-periodic in χ. This spectrum can be described by the braid word $\sigma_4\sigma_4$ with $\sigma_4 = \sigma_1^{-1}\sigma_3^{-1}\sigma_2\sigma_3\sigma_1$. In (c) the same double braiding occurs but with the eigenvalues λ_+ and λ_-, characterized by the braid word $\sigma_2\sigma_2$. Finally, in (d) the braid leads to eigenvalues λ_0 and λ_p, respectively λ_+ and λ_-, swapping places. Here, the eigenspectrum is 4π-periodic in χ, thus breaking the 2π-periodicity of $L(\chi)$. Here, the transport can be described by eigenmodes with fractional charge $e^* = e/2$.

mon generation by means of the exceptional points in (χ, ϕ), as shown in Fig. 2.4, however, as it turns out, their configuration may be such that different braid phases occur along the two parameters.

In addition, there is a topological phase (inverted star symbol in Fig. 2.7b) which deserves the label of a fractional Josephson effect in a more narrow sense. Namely, the complex spectrum here (shown in Fig. 2.8d) can be continuously mapped to the open system spectrum of the actual Majorana-fermion circuit, shown in Fig. 2.1f. That is, the shape of the eigenvalues in Fig. 2.8d permits the explicit interpretation of the spectrum as two eigenvalues related to the coherent (Hamiltonian) dynamics $\lambda_\pm$ which have now a closed minigap, and remaining standard eigenvalues related to decay and stationary state, which do not partake in the braid. Importantly, we note that for a closed system, the gap in the Josephson spectrum can only be closed when using at least four superconducting contacts (and thus three phase differences $\phi_{1,2,3}$) as shown in Ref. [Riw+16b]. As already pointed out in Sec. 2.2, for the circuit considered here, with only two superconducting contacts (and the single phase difference ϕ), the closed system cannot stabilize a closing of the minigap: any deviation from $\epsilon = 0$ or $E_{JL} = E_{JR}$ opens a gap. Here we show, that a gap closing can be stabilized by means of the interplay between a nonequilibrium drive (due to the normal metal) and a measurement of the transport statistics (nonzero χ).

Let us conclude this section by summarizing, that for a generic open quantum circuit, the emergence of fractional charges defined in the FCS (χ) and a fractional Josephson effect, indicating the unit of charge with which the magnetic field interacts (ϕ) are in so far related, as they are generated by exceptional points in the 2D space spanned by (χ, ϕ). They are however also distinct in the sense that these exceptional points produce different braids when analyzing the spectrum either along the χ-space (where either 2π- or 4π-periodic spectra emerge) or along the ϕ-space (where we find 2π-, 4π- and even 8π-periodic spectra). Moreover, we can show that the fractional Josephson effect, and thus a closing of the minigap in the Josephson energy (imaginary part of the complex eigenspectrum) can be stabilized when combining nonequilibrium and transport measurements, a feature which is impossible for a closed (dissipation-free) circuit.

Finally, let us explicitly point out what we have already indicated at the beginning of Sec. 2.4. Namely, there is a left-right asymmetry in the occurrence of topological phases, as can be seen when swapping $E_{JL} \leftrightarrow E_{JR}$, e.g., when comparing Figs. 2.5a and c as well as Figs. 2.7a and c. This is due to the fact, that the current is measured asymmetrically (at the right contact), as we have discussed when defining the current operator, Eq. (2.11). Exact left-right symmetry is only achieved by mirroring the circuit *and* the detector placement.

2.6. Finite counting field as weak measurement

While we have learned above that a trivial circuit with a quantum dot coupled to superconducting and normal metal contacts provide an unexpected wealth of open

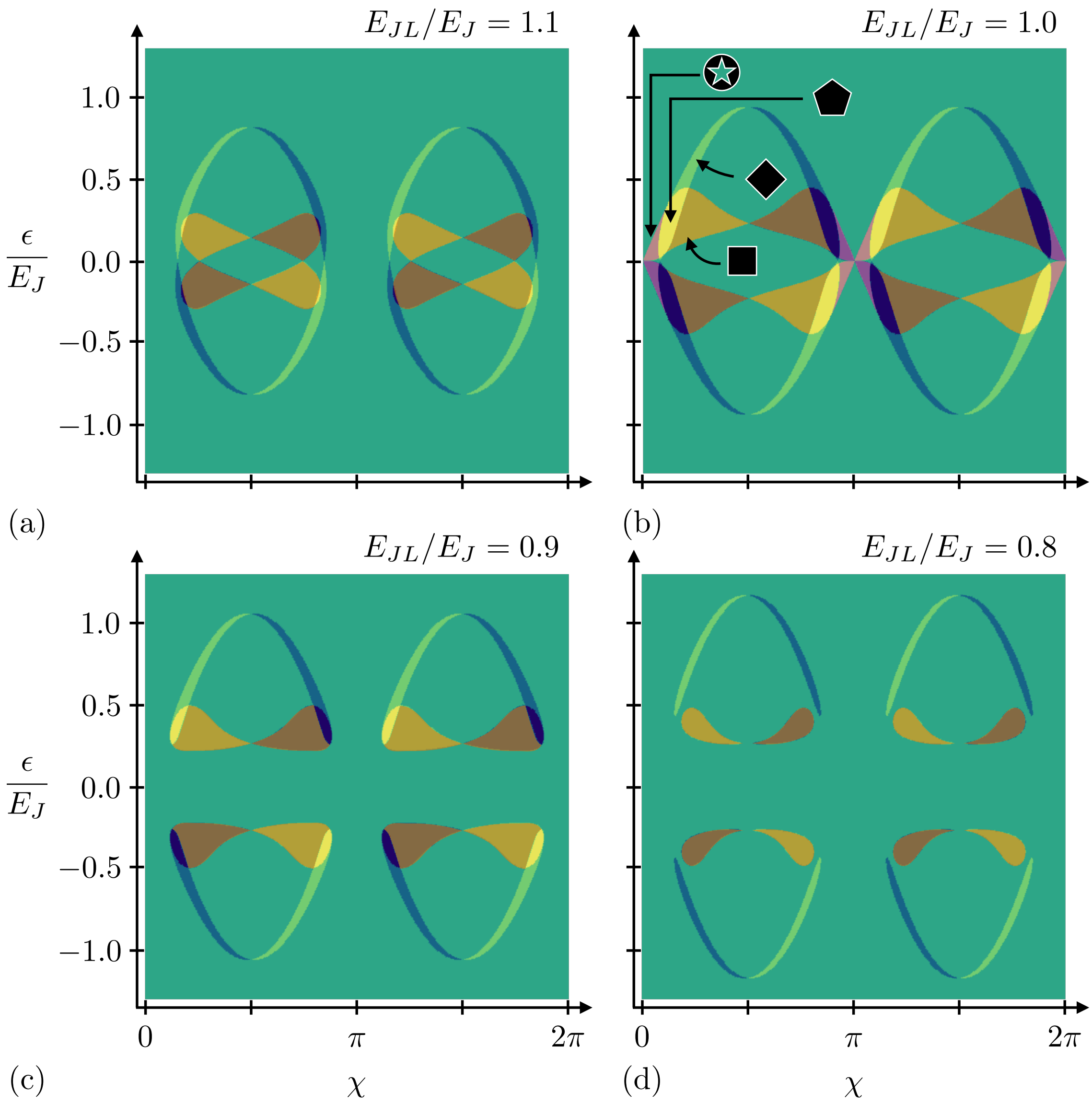

Figure 2.7.: Map of the different topological phases of the spectrum $\lambda_n(\phi)$, as a function of the detuning ϵ, and the counting field χ, for different asymmetries of the Josephson energies, E_{JL}/E_J (a-d). Apart from the trivial phase, there are here four distinct topological phases, marked in (b) with the symbols of square, rhombus, pentagon, and inverted star. For each topological phase at a given (ϵ, χ), there is a partner phase at $(-\epsilon, \chi)$ which can be obtained through complex conjugation of the bands $\lambda_x \to \lambda_x^*$.

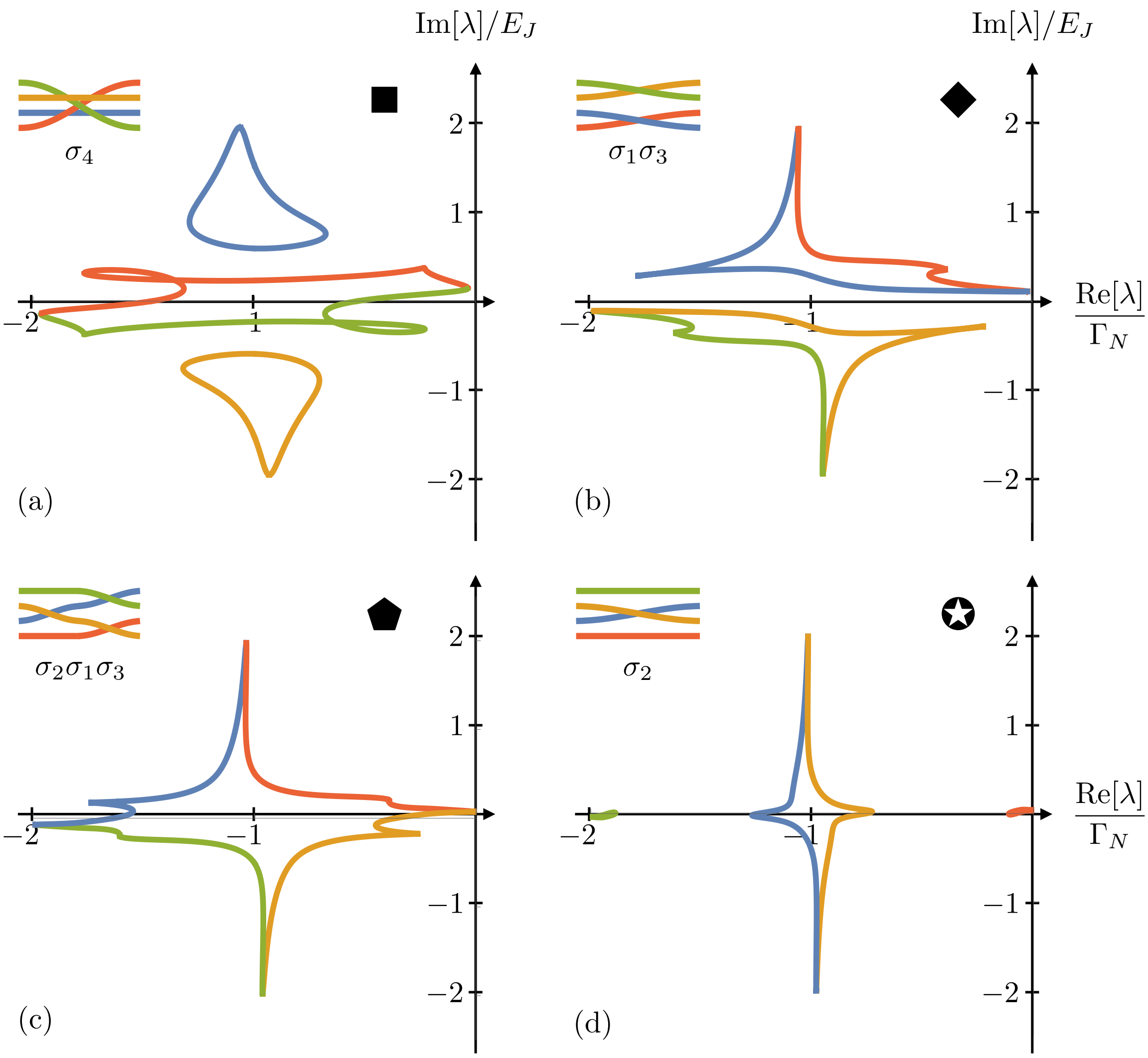

Figure 2.8.: The real and imaginary parts of the spectrum $\lambda_n(\phi)$, drawn parametrically for $\phi = [0, 2\pi)$, for the four different topological phases mapped out in Fig. 2.7 (a-d). In all phases, the 2π-periodicity in ϕ is broken. In (a) and (d), two eigenvalues participate in a braid, either λ_0 and λ_p in (a), or λ_+ and λ_- in (d). In (b), both λ_0 and λ_+ as well as λ_p and λ_- exchange places during a 2π-sweep of ϕ. In (c), all eigenvalues interchange, leading to an 8π-periodic phase. The phase depicted in (d) has a mapping to a closed system fractional Josephson effect including weak dissipation. The other phases (a-c) do not have such a correspondence, since they involve the eigenvalues λ_0 and λ_p (see also main text).

system topological phase transitions, there are some important remaining caveats especially with regard to the nature of the detector. In particular, the observation of the topological phase transitions along ϕ-space (see Figs. 2.8) are in fact virtually impossible, when adhering to the idealized detection schemes depicted in Fig. 2.3. As for the detection scheme with time-local projective current measurements, Fig. 2.3a, the finite χ parameter regime can only be approached, by measuring an increasing number of cumulants C_k of the supercurrent (and, in fact, by including finite measurement times τ in order to extract all the eigenmodes, see Appendix A) and then analytically continuing the eigenmodes $\lambda_n(\chi)$ starting from the extracted $\partial_\chi^k \lambda_n(0)$. It goes without saying that, such a procedure is in and of itself extremely challenging expermentally. Moreover, note also, that there is no convergence if we aim to go across a topological phase transition. Let us explicitly illustrated this fact with the example of the topological spectrum shown in Fig. 2.8d. For $\chi = 0$ (while keeping all other parameters the same) the spectrum is trivial. The analytically continued eigenvalues, starting at $\chi = 0$, are defined as

$$\lambda_i^{\mathrm{ac}}(\chi, \phi) = \lambda_i(0, \phi) + \chi\, \partial_\chi \lambda_i(\chi, \phi)\big|_{\chi=0} + \frac{\chi^2}{2!}\, \partial_\chi^2 \lambda_i(\chi, \phi)\big|_{\chi=0} + \cdots \tag{2.30}$$

Now we can compare the analytically continued eigenspectrum to the exact one (without expansion around $\chi = 0$) to see if they still braid in the same way, keeping all other parameters same. In Fig. 2.9a we compare the parametric plots of the analytically continued eigenvalues to second order and exact eigenvalues for finite counting field, and can easily conclude that analytically continued eigenvalues do not reproduce the same braid. We find that the 4π-periodic fractional Josephson effect only emerges when going to arbitrary high order cumulants, which is an outright prohibitive requirement from an experimental viewpoint.

This issue could be avoided if χ was a real, physical parameter, which it is not when utilizing time-local current correlations (Fig. 2.3a). It would be, if instead an explicit physical detector was present (Fig. 2.3a), however, here there is the aforementioned problem, that the continuous entanglement between system and detector destroys the information of the supercurrent. This prompts us to study alternative measurement schemes, where the transport measurement satisfies both the requirements of the counting field being physical, and at the same time preserving information about the supercurrent. As it turns out, these requirements can be met by a weak continuous measurement of the current.

Weak measurement has been studied extensively in several contexts (for an instructive review, see Ref. [Cle+10]). A weak continuous measurement of the current could for instance be envisaged along similar lines as in Ref. [Liu+10], where it was proposed to weakly measure spins via an incident polarized photon beam and exploiting the Faraday effect. Due to the magnetic field emitted by the supercurrent, it is in principle perceivable to use a similar setup here to obtain information about the transport. However, in the light of massive experimental advances in the interaction and control of superconducting circuits with transmission lines [Wal+04; Gu+17; Wen17], we deem it informative to briefly sketch an “all-circuit” realization of the weak measure-

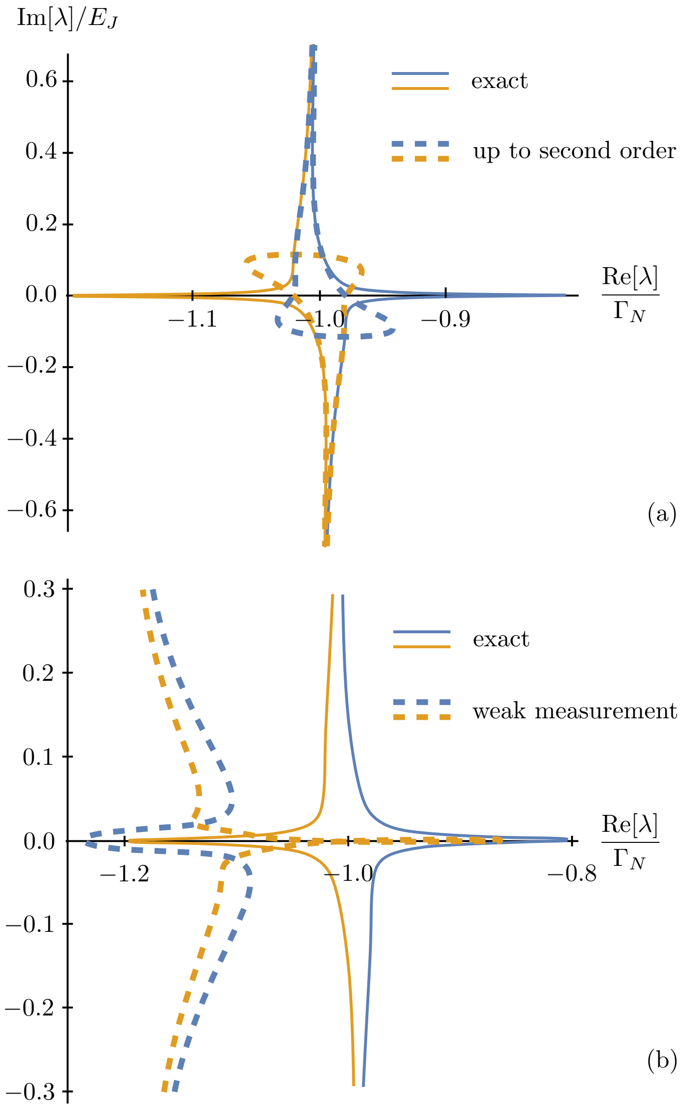

Figure 2.9.: (a) The dashed lines are analytically continued eigenvalues up to second order, while the solid lines are eigenvalues with a finite counting field (see also Fig. 2.8d). The analytically continued eigenvalues match asymptotically only away from $\phi = \pi$. Near $\phi = \pi$ however, they do not perform the same braiding as in Fig. 2.8d, such that the topological phase cannot be observed. (b) The solid lines are again eigenvalues for ideal detector kernel with finite counting field (Fig. 2.8d), and the dashed lines are eigenvalues for the weak measurement kernel. The eigenvalues do not match up exactly (due to a distortion, see main text), but they exhibit the same braiding. These plots are for the following parameter values: $\frac{\epsilon}{E_{JR}} = 0.007$, $\frac{E_{JL}}{E_{JR}} = 1.0$, $\frac{\Gamma_N}{E_{JR}} = 0.2$, $\chi = -0.04$, $\frac{\omega_m \delta r}{E_{JR}} = 0.02$ and $\xi = \pi/2$.

ment (i.e., without relying on polarized photon beams). For this purpose we study coherent scattering in a nearby SQUID inductively coupled to the circuit, loosely inspired by Ref. [Ste+01]. In the following we will provide a highly simplified model of a SQUID detector and its interaction with the circuit, as a proof of principle for a weak measurement of the supercurrent, and show how it can be used to simulate a counting field. Finally, we will investigate as an example, how the topological phase from Fig. 2.8d can be probed with this setup.

2.6.1. SQUID detector for weak current measurement

The SQUID detector consists of two superconducting lines connected via two Josephson junctions (with Josephson energy $E_{J,\mathrm{SQUID}}$) in parallel, see Fig. 2.10. The weak measurement is then implemented by means of the following points. (i) The current from the main circuit produces a magnetic field that can interact with the SQUID. The interaction strength can be estimated based on Ampère's law, see, e.g., Ref. [Riw21]. (ii) If we send a signal from one end of the detector it will be reflected and transmitted at the SQUID. (iii) The reflection and transmission coefficients are sensitive to the flux enclosed by the SQUID and therefore depend on the current from the quantum dot.

As we will develop now, a subsequent evaluation of the scattered state will provide us with classical information about the supercurrent without completely suppressing it. In particular, we will show that the measurement is weak because of a highly reflective nature of the SQUID (i.e., full reflection is the default event, without obtaining any information about the current), and continuous in the sense that there is a repeated initiation of incoming waves after a given time interval, the inverse of which represents the detection frequency.

In order to describe the scattering problem, let us start by writing down the Hamiltonian for the SQUID detector. Overall it is composed of three parts, $H_{\mathrm{SQUID}} = H_L + H_R + V$ describing the left (right) conductor line H_L (H_R) and the SQUID part connecting the two, V. Each of these subparts can be written as

$$H_L = \frac{1}{2C_0}\sum_{j=-\infty}^{0} q_j^2 + \frac{1}{2L_0}\sum_{j=-\infty}^{-1}\left(\frac{\varphi_{j+1}-\varphi_j}{2e}\right)^2 \tag{2.31}$$

$$H_R = \frac{1}{2C_0}\sum_{j=1}^{\infty} q_j^2 + \frac{1}{2L_0}\sum_{j=1}^{\infty}\left(\frac{\varphi_{j+1}-\varphi_j}{2e}\right)^2 \tag{2.32}$$

$$V = -\frac{\gamma}{2e^2}\cos\left(\varphi_1-\varphi_0\right) \approx \gamma\left(\frac{\varphi_1-\varphi_0}{2e}\right)^2 + \text{const.}\ , \tag{2.33}$$

where we chose for convenience a discrete lattice representation of the conductor lines [Poz12], which are characterized by the capacitances C_0 and the inductances L_0. The charge and phase variables q_j and φ_j on the lattice nodes j satisfy the commutation relations $[q_j, \varphi_{j'}] = i2e\delta_{jj'}$. The interaction with the circuit is included via the coupling prefactor in V (which is chosen to have the units of an inverse

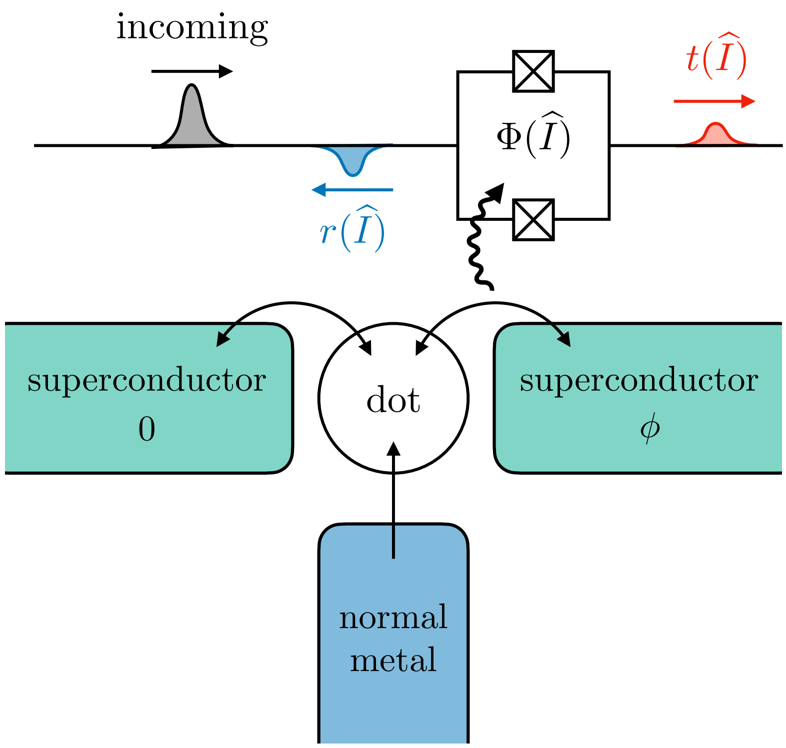

Figure 2.10.: Setup for weak measurement by means of a SQUID detector. An incoming wave packet will be scattered at the SQUID. The inductive coupling between the main circuit and the SQUID shall be tailored such that the outgoing scattered state depends on the supercurrent entering the superconductor on the right. A subsequent projective measurement of the scattered state realizes a form of weak measurement of the supercurrent.

inductance). When tuning the externally applied flux to half flux quantum, we get

$$\gamma = 2e^2\lambda E_{J,\mathrm{SQUID}} I \ , \tag{2.34}$$

where I is the current operator, as defined in Eq. (2.11). The coupling constant λ can be estimated from Ampère's law (as already mentioned, see Ref. [Riw21]). Note that for simplicity, we assume that the signals will have low amplitudes in φ, such that we may expand V up to quadratic order, see Eq. (2.33). The tuning to half-flux makes the SQUID highly reflective; for $I = 0$, the SQUID can be considered as a hard wall from the point of view of an incident wave, and only weakly transmittive for a finite I since the local inductance of the SQUID is very high. Strictly speaking, for two disconnected wires (as for $I = 0$), the phase difference $(\varphi_1 - \varphi_0)$ is not in general guaranteed to remain small. However, one can easily connect the two transmission lines in a loop, so that even when $\gamma = 0$ the phase difference remains small, at least for a sufficiently small loop inductance. Also, note that for simplicity, we assumed the superconductor line to be without resistance. Of course realistically resistance is always present [Sch83; Bul84; HG97]. According to [HG97] the coupling to continuous modes in the loop leads to the renormalization of the Josephson energy, but this does not qualitatively change our idea of using the SQUID detector. The other more drastic effect the dissipation can have is that the superconducting loop itself might undergo a superconductor to insulator phase transition. As predicted in [Sch83; Bul84], this puts a limitation on the transmission line parameters. To be precise if the parameter g, where $g^{-1} = \frac{4e^2}{\hbar\pi}\sqrt{\frac{L_0}{C_0}}$, is below a certain threshold g_c then the superconducting loop will act as a insulator [HG97]. We further note, that the existence of dissipative quantum phase transitions is currently still subject to debate [Mur+20; HS21; Mur+21]. Overall, our specific proposal of a circuit realization of weak current measurement should really only be considered a proof of concept, and may easily serve as blueprint for other (more) feasible realizations.

Let us briefly touch on an important point regarding the spatial resolution of the current measurement. Namely, depending on the circuit geometry and detector placement, the SQUID could in principle couple to both the left and right supercurrents (and thus fails to reproduce the topological phase transitions discussed above, and in general complicate the discussion). In the most generic case, we would thus actually have a nonzero ζ parameter, describing this nonideal coupling, see the discussion in Sec. 2.4 after Eq. (2.11). In order to avoid such subtleties, we assume that the SQUID is placed more towards the right contact than the actual quantum dot. This is fine, because it is plausible to assume that the Cooper pairs, once they enter the right contact, are distributed very fast (according to the group velocity of the Nambu-Goldstone mode within the superconductor bulk, see, e.g., Ref. [AS10]). Hence, the bottleneck current is the tunneling current between dot and superconducting contact, which can be still observed deep within the right contact, neglecting the high-frequency displacement currents inside the bulk.

To continue, we note that the individual Hamiltonians $H_{L,R}$ each have a linear dispersion relation, for bosonic modes propagating in 1D, $E_k \approx \omega_0|k|$ (valid for $|k| \ll 1$), with $\omega_0 = 1/\sqrt{L_0 C_0}$ and the unitless wave vector k. We then assume that one creates an incoming signal at a certain energy E with wave vector $k_E = E/\omega_0$, carried by the conductor lines, which can scatter at the SQUID. The transmission amplitude can be computed by means of the Fisher-Lee formula [FL81],

$$t^{\mathrm{L}}(E) = -iv_E \lim_{j\to\infty, j'\to-\infty} G^{+}_{jj'}(E)e^{-ik_E(j-j')} \tag{2.35}$$

where $v_E = \partial_k E_k|_{E_k=E}$ and $G^{+}_{jj'}(E)$ is the retarded single-particle (here, single-boson) Green's function. We obtain

$$t^{\mathrm{L}}(E) = -i\frac{\gamma L_0}{k_E} \tag{2.36}$$

The explicit calculation is shown in Appendix B. This final result is valid up to first order in γ (in accordance with the assumption that tunneling is weak, $|t| \ll 1$). Importantly, for half flux $\Phi_{\mathrm{ext}} = \Phi_0/2$, which will be our default parameter setting from now on, the transmission coefficient is directly proportional to the current I, see Eq. (2.34). In particular, it changes sign if the current changes sign. Due to left-right symmetry of SQUID detector we can easily deduce that

$$\begin{aligned} t^{\mathrm{L}}(E) &= t^{\mathrm{R}}(E) = t(E) \\ r^{\mathrm{L}}(E) &= r^{\mathrm{R}}(E) = r(E) \end{aligned} \tag{2.37}$$

Thus, the reflection and transmission coefficients can be cast into a standard scattering matrix

$$S = \begin{pmatrix} r^{\mathrm{L}} & t^{\mathrm{R}} \\ t^{\mathrm{L}} & r^{\mathrm{R}} \end{pmatrix} = \begin{pmatrix} r & t \\ t & r \end{pmatrix} \tag{2.38}$$

Since the scattering matrix is unitary ($S^\dagger S = \mathbb{I}$), we can deduce two equations that give us a relation between the reflection and transmission coefficients. The first equation is $r^* t + t^* r = 0$ which leads us to conclude that the reflection coefficient must be real since the transmission coefficient in Eq. (2.36) is imaginary. The other equation, conservation of probability $|t|^2 + |r|^2 = 1$, lets us calculate the amplitude of r.

As already stated above the SQUID is weakly transmitting, therefore most of the signal will be reflected,

$$r = 1 - \delta r \tag{2.39}$$

with $\delta r \ll 1$. From this, we derive

$$|t|^2 = 2\delta r \tag{2.40}$$

upto first order in δr. These identities will help us now in constructing the Master equation including the influence of the SQUID detector.

2.6.2. Master equation including weak measurement

Now we are ready to develop the master equation for the quantum dot system in presence of the SQUID detector and show how it simulates a counting field. To write down the master equation we need Kraus operators that describe the weak measurement process.

For simplicity, we assume that the scattering time of the wave packet at the SQUID is very short, much shorter than the dynamics due to the coupling with the superconductors (defined by the energy scale $\sim E_{JL,JR}$) and the coupling to the normal metal ($\sim \Gamma_N$). Thus, we are entitled to treat the different parts of the system dynamics independently, and add them up for the final Master equation.

Keeping therefore the circuit state constant, let the initial state of the circuit plus detector (no normal metal) before scattering at the SQUID be the factorized state

$$|\Psi_{\text{in}}\rangle = \Big[C_- |I_-\rangle + C_{0\uparrow} |I_{0\uparrow}\rangle + C_{0\downarrow} |I_{0\downarrow}\rangle + C_+ |I_+\rangle\Big] \otimes |\text{in,R}\rangle \tag{2.41}$$

where the states $|I_\mp\rangle, |I_{0\sigma}\rangle$ ($\sigma = \uparrow, \downarrow$) are the eigenvectors of the current operator I and $C_\mp, C_{0\sigma}$ are complex-valued wave function amplitudes, satisfying the normalization condition $|C_-|^2 + |C_{0\uparrow}|^2 + |C_{0\downarrow}|^2 + |C_+|^2 = 1$. The vector $|\text{in,R}\rangle$ represents the normalized state that depicts the incoming signal, without loss of generality assumed to originate from the right end of the conductor line. For the sake of completeness, let us provide the explicit forms of the current operator eigenbasis, in terms of the quantum dot charge basis, $|0\rangle, |1_\sigma\rangle, |2\rangle$, as introduced below Eq. (2.1). The eigenstates with nonzero eigenvalues $I_\mp = \mp e E_{JR}$ are given as $|I_\mp\rangle = \left(|0\rangle \pm i e^{i\phi} |2\rangle\right)/\sqrt{2}$, and the degenerate pair of zero eigenvalues $I_{0\sigma} = 0$ belong to the eigenvectors $|I_{0\sigma}\rangle = |1_\sigma\rangle$.

After scattering, the factorized initial state gets weakly entangled, resulting in the final state

$$|\Psi_{\text{f}}\rangle = \Big[t_- C_- |I_-\rangle + t_+ C_+ |I_+\rangle\Big] \otimes |\text{out,L}\rangle + \Big[r_- C_- |I_-\rangle + \sum_\sigma C_{0\sigma} |I_{0\sigma}\rangle + r_+ C_+ |I_+\rangle\Big] \otimes |\text{out,R}\rangle\ , \tag{2.42}$$

where $r_\pm$ and $t_\pm$ are reflection and transmission coefficients, respectively, corresponding to eigenvalues $I_\pm$. We have furthermore made use of the fact, that for $I_{0\sigma} = 0$, the signal gets completely reflected (due to the half-flux tuning).

In fact, the above final state shown in Eq. (2.42) is meaningful, if the experimenter is merely measuring the presence or absence of a transmitted wave. We note however, that an additional important piece of information can be extracted from the scattered state: the aforementioned sensitivity of the transmission amplitude on the sign of the current, $t_- = -t_+$. In terms of the outgoing signal, this sign change can be understood as a π-phase shift, which could in principle be detected by an appropriate interference setup. Then, we have three instead of two detection outcomes, which should therefore be cast into the final wave function

$$\begin{aligned}|\Psi_{\text{f}}'\rangle &= t_- C_- |I_-\rangle \otimes |\text{out,L}-\rangle + t_+ C_+ |I_+\rangle \otimes |\text{out,L}+\rangle \\ &+ \Big[r_- C_- |I_-\rangle + \sum_\sigma C_{0\sigma} |I_{0\sigma}\rangle + r_+ C_+ |I_+\rangle\Big] \otimes |\text{out,R}\rangle\ ,\end{aligned} \tag{2.43}$$

where the states $|\text{out,L}\mp\rangle$ represent a measurement of a transmitted wave (outgoing to the left) including a determination of its relative phase shift with respect to the initial wave, leading to the extra index $\mp$.

Depending on the two possible detection scenarios, we have either two or three possible measurement outcomes for the ancilla system, denoted by the index $q \in \{0,1\}$, or $q \in \{-,0,+\}$. The projection onto the different measurement outcomes is described in the second scenario by the three Kraus operators

$$M_\mp = t_\mp \left|I_\mp\right\rangle \left\langle I_\mp\right| \tag{2.44}$$

$$M_0 = r_- \left|I_-\right\rangle \left\langle I_-\right| + \sum_\sigma \left|I_{0\sigma}\right\rangle \left\langle I_{0\sigma}\right| + r_+ \left|I_+\right\rangle \left\langle I_+\right| \tag{2.45}$$

For the first scenario, the $\mp$ outcomes are merged into a single Kraus operator $M_1 = M_- + M_+$. Independent of the specific measurement basis, it is easy to check that the requirement $\sum_q M_q^\dagger M_q = \mathbf{1}$ is satisfied. We notice, that due to the highly reflective nature of the SQUID, we may use Eq. (2.39), to express the Kraus operator

$$M_0 = \mathbf{1} + \delta M_0 \ , \tag{2.46}$$

where δM_0 scales linear in δr, and thus quadratic in t, see also Eq. (2.40). The Kraus operators $M_\mp$ on the other hand scale linearly in t. This different scaling behaviour is important now for the derivation of the Master equation including weak measurement

We now assume that there is a repetition of incoming signals according to a measurement frequency ω_m, that is, the weak entanglement and subsequent projective measurement occurs on average every time interval $\sim 1/\omega_m$. The time evolution of the density matrix due to this process (still neglecting the influence from the superconducting and normal metal contacts) can then be given as

$$\dot\rho = \omega_m \left(\sum_q M_q \rho M_q^\dagger - \rho \right) \ . \tag{2.47}$$

The right-hand side can be expanded up to second order in t, resulting in the Master equation

$$\dot\rho = \omega_m \left(K_0 + K_- + K_+ \right) \rho \ , \tag{2.48}$$

with the definitions of the superoperators $K_\mp \cdot = M_\mp \cdot M_\mp$ and $K_0 \cdot = \delta M_0 \cdot + \cdot\, \delta M_0$. This equation is the specific case of the master equation we derived for continuous measurement at the end of Sec. 1.3.

These superoperators can be reexpressed using the quantum dot creation and annihilation operators as follows,

$$\begin{aligned} K_0 \cdot &= -2\delta r \left(1 + d_\uparrow^\dagger d_\downarrow^\dagger d_\downarrow d_\uparrow\right) \cdot \left(1 + d_\uparrow^\dagger d_\downarrow^\dagger d_\downarrow d_\uparrow\right) \\ K_- \cdot &= A \cdot A - \frac{i}{2} \left\{ \delta r e^{i\phi} d_\uparrow^\dagger d_\downarrow^\dagger - \delta r e^{-i\phi} d_\downarrow d_\uparrow, \cdot \right\} \\ K_+ \cdot &= A \cdot A + \frac{i}{2} \left\{ \delta r e^{i\phi} d_\uparrow^\dagger d_\downarrow^\dagger - \delta r e^{-i\phi} d_\downarrow d_\uparrow, \cdot \right\} \end{aligned} \tag{2.49}$$

where A is a Hermitian operator given by

$$A = \sqrt{\delta r} \left(1 + i e^{i\phi} d_\uparrow^\dagger d_\downarrow^\dagger - i e^{-i\phi} d_\downarrow d_\uparrow + d_\uparrow^\dagger d_\downarrow^\dagger d_\downarrow d_\uparrow\right) \ . \tag{2.50}$$

In order to derive the above K superoperators, we have used the property $t_{-1} = -t_1$, which further implies $|t_{-1}|^2 = |t_1|^2 = |t|^2$ and $\delta r_{-1} = \delta r_1 = \delta r$. We notice that $K_\pm$ are actually of the form $K_\pm = A \cdot A \mp \delta r/(2eE_{JR})\{I, \cdot\}$ with the current operator I as defined in Eq. (2.11). This observation will be of great use in a moment.

Let us now reintroduce the dynamics due to the superconducting and normal metal contacts, captured by the Lindbladian $L(\phi)$, see Eq. (2.8). In addition, we keep a register n which stores the classical information of the outcome of the above described weak continuous measurement, $\rho \to \rho(n)$. The full master equation can be written as

$$\dot{\rho}(n) = [L(\phi) + \omega_m K_0]\,\rho(n) + \omega_m K_+ \rho(n \mp 1) + \omega_m K_- \rho(n+1)\ . \tag{2.51}$$

Note that for the K_+-term, we have included both of the above scenarios of either being able to distinguish the current direction or not. The resulting information processing protocols are the following. If the current direction cannot be distinguished, then $K_+\rho(n \mp 1) \to K_+\rho(n+1)$, such that the register n is simply increased by +1, when having measured a nonzero current (events described by $K_\mp$). The absence of a transmitted signal corresponds to a measurement of zero current, resulting in no change in the detector count. If the current direction can be distinguished, we may engage in a different protocol, $K_+\rho(n \mp 1) \to K_+\rho(n-1)$. Here, for a measurement of the eigenvalue I_-, the detector count goes down by one, and and for a measurement of I_+, the detector count goes up by one.

To proceed, let us define the Fourier transform as $\rho(\xi) = \sum_n e^{in\xi}\rho(n)$ with a new counting field ξ, which is distinct from, but (as we show now) to some extent related to, the original counting field χ. The Fourier transformed master equation becomes

$$\dot{\rho}(\xi) = \left[L(\phi) + \omega_m K_0 + \omega_m K_+ e^{i\xi} + \omega_m K_- e^{\mp i\xi}\right]\rho(\xi)\ . \tag{2.52}$$

Crucially, it can be shown that for $\xi = \pi/2$, the weak measurement part in Eq. (2.52) can be brought into a very similar form as the kernel in Eq. (2.21), provided that our detector is able to distinguish between positive and negative currents, $e^{\pm i\xi} \to e^{-i\xi}$ for K_-. Note that setting ξ to a strong nonzero value (i.e., $\xi = \pi/2$) is no problem whatsoever: the detector is here physically realized, and the experimenter will be able to directly access the classical probability distribution of measurements along the space n (the space conjugate to ξ). Hence, the choice $\xi = \pi/2$ simply corresponds to a particular way of evaluating (post-processing) the classical information. At any rate, plugging in $\xi = \pi/2$, we then find

$$\dot{\rho}(\pi/2) = \left[L(\phi) + \omega_m K_0 - i\frac{\omega_m \delta r}{eE_{JR}}\{I, \cdot\}\right]\rho(\pi/2)\ . \tag{2.53}$$

Indeed with the replacement

$$\omega_m \delta r \to -\chi\frac{E_{JR}}{2} \tag{2.54}$$

the kernel including the weak measurement can be mapped (up to the extra term K_0, which we discuss in a moment) onto the kernel with small but finite χ. Of course, we can therefore not hope to probe the global properties of the kernel for all χ. However, this form of weak measurement can be used to "simulate" the presence of a small but finite counting field. Importantly, here the simulated χ enters as a system parameter influencing the dynamics, and is no longer related to the transport measurement (as the latter is encoded in the new classical counting field ξ). Hence, we are no longer required to expand in χ, and can thus avoid any problems related to analytic continuation, and the topological phase transition shown in Fig. 2.8d can now be observed.

Let us now comment on the effect of aforementioned the extra term K_0. While the presence of K_0 does distort the spectrum, we observe that the braid group of the two eigenvalues $\lambda_\pm$ is preserved, when setting the weak measurement parameters (ω_m and δr) to values that correspond to the value of χ [according to Eq.2.54] in Fig. 2.8d. As a proof of principle, we show the new eigenvalues for the weak measurement in comparison with old ones, for finite χ, in Fig. 2.9b. Let us repeat that this recreation of the braid phase transition via weak measurement is only possible if the detector is able to distinguish the sign of the current (see above discussion), as otherwise, the weak measurement kernel cannot be mapped onto $L_{\text{cut-off}}(\phi, \chi)$.

To conclude, let us provide a short interpretation of the above concept. In the absence of the weak current measurement (or transport measurement in general, $\chi = 0$), the complex open system spectrum is trivial, and the eigenvalues belonging to the coherent time evolution, $\lambda_\pm$ are gapped, see Fig. 2.1e. This corresponds to the trivial Josephson effect. The reason why they are gapped is simply because it is in general impossible to tune the system parameters to the perfectly symmetric values $E_{JL} = E_{JR}$ and $\epsilon = 0$ (due to $U = 0$). The weak measurement can close the gap, and thus correct for the "failure" to tune to perfect symmetry. We note that we have to set the new counting field ξ to a precise value ($\pi/2$) to accomplish this. This is however no real limitation: the weak measurement has provided us with an entire array of classical information [encoded in the register n, $\rho(n)$, see Eq. (2.51)], and setting $\xi = \pi/2$ is just a particularly chosen way to evaluate (post-process) this information. Figuratively speaking, this particular choice of post-processing the classical information "filters out" transport processes with integer Cooper pair charge $2e$ in favour of processes with fractional charge e.

2.7. Conclusions

We studied the topology of the transport properties of a generic quantum system where supercurrents and dissipative currents coincide, in terms of the transport degrees of freedom of the counting field χ and the superconducting phase bias ϕ. We found that fractional charges defined in the full-counting statistics are related to fractional charges visible in the Josephson effect in a generic open quantum system via exceptional points defined in the 2D base space (χ, ϕ) – as a matter of fact, the exceptional points can be considered as the generators of these fractional charges. While thus related, the two notions of fractional charges are nonetheless distinct in the sense that they are defined along two independent spaces. By means of the concrete model of a hetero-structure circuit, where a quantum dot is coupled to superconducting and normal metal contacts, we showed that the intricate interplay between transport measurement and nonequilibrium drive gives rise to a plethora of topological phases, surprisingly including a phase which can be interpreted as an open system version of a fractional Josephson effect, in spite of the system being composed of trivial materials.

In addition, we elucidated different flavours of full-counting statistics based on different implementations of the transport detector, and their relevance for observing different topological phases. For a continuously entangling detector, a novel type topological phase emerges, which can be interpreted as a statistical mix of fractional and integer charges defined in the counting field χ. However, as we pointed out, such detectors destroy the information about the supercurrent, and thus cannot directly measure a fractional Josephson effect. A complementary approach for obtaining the full-counting statistics involves time-local measurements of the current, leaving the system be in between measurements. While this approach preserves supercurrents, it cannot detect topological transitions away from zero counting field. This prompted us to develop a third notion of full-counting statistics relying on a continuous weak measurement of the supercurrent. We sketched a proof of principle for an all-circuit implementation of such a weak measurement by means of SQUID detectors. This approach preserves supercurrents, and importantly enables us to reach topological phases at finite counting fields.

As a final note, we believe that the "revival" of a fractional Josephson effect by means of a weak supercurrent measurement might be an interesting effect also for actual Majorana junctions, since the gap closing in the Josephson relation may not be fully protected due to finite size effects. The applicability of weak measurement and nonequilibrium driving to induce topological protection will likely be subject of future research.

3. Topology in dissipative systems

3.1. Introduction

Broadly speaking, two things are said to be topologically similar if they can be mapped to each other by continuous deformations, a famous example that often comes up in popular science communication is the fact that a coffee mug and a torus are topologically similar. It is in this sense that we encountered topological regions in the eigenspectrum of the superconductor-normal metal hybrid circuit in chapter 2, the behaviour of eigenvalues in the topological and trivial regions could not be mapped to one other with only continuous deformations. We also encountered the fact that dissipation played an essential part in realising this topology by helping to avoid the fine-tuning problem. Now we would like to further explore the connection between topology of superconducting circuits and dissipation. A straight forward way would be to consider the same Lindbladian as the last chapter, and investigate it for different notions of topology, for e.g. using Lieu et. al.'s [LMC20] work on extending the tenfold classification to quadratic Lindbladians. Unfortunately it turns out this particular Lindbladian does not show any interesting properties in this regard, but if we make the system two dimensional (i.e. two superconducting phases instead of one) we do get something interesting. Therefore our goal in this chapter is to study a dissipative toy model inspired from our previous work and see what topological properties it holds and how to, if possible, realise it experimentally.

This chapter of the thesis is organised as follows: first we give a brief overview of topology and related concepts in condensed matter systems in Sec. 3.2. Then in Sec. 3.3 we review the work of Riwar et. al. [Riw+16a] on topology of multi terminal Josephson junctions (MTJJs) since they are one of the platforms where our toy model could be experimentally realised. We also argue how the topological properties of MTJJs becomes experimentally inaccessible in presence of dissipation and therefore we need to consider a notion of topology that takes into account open quantum systems. Finally in Sec. 3.4 we study our toy model, the Hamiltonian for which resembles the two dimensional Chern Hamiltonian, and investigate its topological properties using the ideas discussed in Sec. 1.6.

3.2. Topological phases of matter

Characterisation and classification of different phases of matter and the study of phase transitions has always been an essential goal of condensed matter physics, one famous example of which is Ginzburg-Landau theory of continuous phase transitions [HK15].

This theory has two essential ingredients: i) the observation that a phase transition to a more 'ordered state' is accompanied by spontaneous breaking of a symmetry, and ii) a phenomenological order parameter that becomes nonzero as the system transitions to the more ordered state. The discovery of integer quantum Hall effect (IQHE) in 1980 [KDP80] goes against the Ginzburg-Landau paradigm. In this effect the Hall resistance of a 2D electron gas is observed to be quantised $R_{xy} = h/ne^2$, where $n \in \mathbb{N}$. The transition between states of different Hall resistances is not accompanied by breaking of any symmetry, hence indicating presence of a different kind of phase transition.

The explanation of IQHE [Lau81; Tho+82] resulted in a new approach to classify phases of matter, one related to the topology of the wave function. IQHE turned out to be the first observation of a new class of materials called topological insulators (TIs) with many others being predicted and observed [KM05; FKM07; MB07; BHZ06; FK07; Kön+07; Hsi+08]. The topological insulators are defined as free fermionic systems that are gapped in the bulk but host gapless modes at the boundary. These systems are topological in the sense that the states with gapless boundary modes cannot be continuously deformed to a trivial insulating state, i.e. state with no gapless boundary modes, without closing the gap in the bulk or without breaking the symmetries of the Hamiltonian. This indifference to smooth deformation can also help us characterise these topological phases with the help of topological invariants (as in the case of IQHE), which are integrals over the momentum space. Using the analogy between the Bogoliubov de-Gennes (BdG) Hamiltonian for quasiparticles of superconductors and Hamiltonian of a band insulator, the study of TIs can be generalised to study of topological superconductors (TSCs) [Roy08; Qi+09], for a more detailed review of TIs and TSCs the following reviews [HK10; QZ11] are a good starting point.

Currently, the zoo of topological materials is ever growing. By taking into account crystal symmetries in addition to internal symmetries of the Hamiltonian the existence of topological crystalline insulators and topological semi-metals have been predicted and confirmed [Wie+22], superconducting heterostructures have also emerged as a promising platform to construct topological metamaterials [Riw+16a; Eri+17; MH17; XVL17; XVL18; Kle+21; Kle+20; Wei+21], and study of topology in non-equilibrium systems (driven or dissipative) has also led to exciting insight into the role topology can play even in more realistic systems [RL09; Kaw+19a; LMC20; YU20; BBK21; Lin+13; Har+20]. Since topological properties of materials is currently a very active area of research this list of works on topological materials is certainly not exhaustive.

3.3. Multi terminal Josephson junction

Multi terminal Josephson junctions (MTJJs) are a generalisation of Josephson junctions, instead of two junctions being connected by a thin non-superconducting film, MTJJs consist of multiple superconductors connected to a central scattering region. They have emerged as one of the candidates for creating topological metamaterials

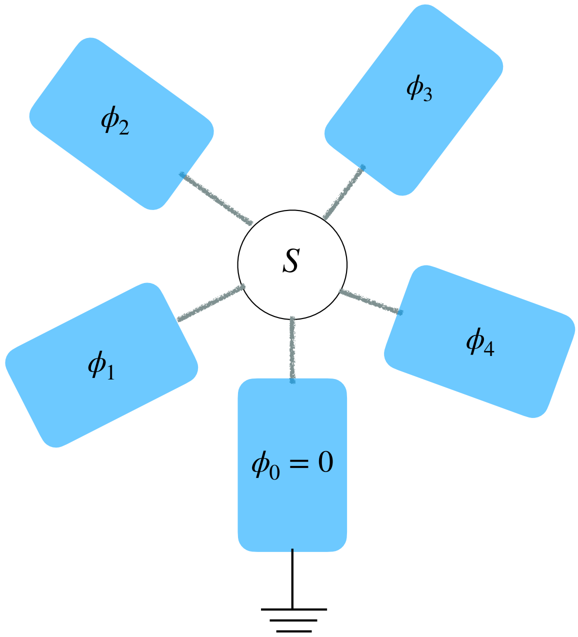

Figure 3.1.: A schematic diagram for a particular case of a multi terminal Josephson junction (MTJJ) with five superconducting islands connected to a central scattering region S. Due to the gauge invariance we set the superconducting phase labelled ϕ_0 to zero (i.e. ground) and all other phases are measured with respect to it.

using superconducting nanostructures [Riw+16a; XVL17; XVL18]. Particularly in the work by Roman et. al. [Riw+16a] the authors were able to show that an n terminal MTJJ can display properties of an $(n-1)$ dimensional topological material. Since this result is relevant for this chapter of the thesis, in this section we will give a brief summary of this paper.

Consider an MTJJ (Fig.3.1) with n superconducting leads connected to a scattering region with the same superconducting gap Δ but with different superconducting phase ϕ_μ. Since due to gauge invariance only the difference of the phases matter, therefore we set one of them, say $\phi_0 = 0$. Andreev bound state (ABS) energy spectrum, that describes the subgap physics of the junction, provides a way to investigate the properties of this junction. Andreev bound states are formed due to Andreev reflections between superconducting and normal regions, and resemble the states of a particle in a box where the role of "walls" is played by the superconductor-normal region interfaces. The ABS energy spectrum is found to have gap closings at some specific points in the space spanned by the superconducting phases. The lowest ABS band can be effectively described by two-by-two Weyl Hamiltonian near these gap closings

$$H_{Weyl} = \sum_{j=1}^{3} h_j \sigma_j,$$

$$h_j = \sum_\alpha \delta\phi_\alpha M_{\alpha j}, \tag{3.1}$$

where σ_j are Pauli matrices, the fields h_j depend on $\delta\phi_j = \phi_j - \phi_j^{(0)}$ via the real matrix M, $\phi_j^{(0)}$ denotes the values of superconducting phases at the gap is closing and, α is the index for superconducting leads.

The structure of the Weyl Hamiltonian implies that we need at least three independent parameters to tune the system to gap closing, hence we need at least a four terminal MTJJ (i.e. three independent phases) to observe Weyl singularities. The presence of Weyl singularities serves as the motivation to study the topology of the junction, which can be characterised by a set of Chern numbers. A Chern number is defined as the integral over the Berry curvature in the subspace spanned by any two of the superconducting phases, say ϕ_α and ϕ_β, where the Berry curvature of a bound state with band index k and spin σ is defined in terms of the wavefunction $|\psi_{k\sigma}\rangle$ as

$$B_k^{\alpha\beta} = -2\mathrm{Im}\left\langle \frac{\partial\psi_{k\sigma}}{\partial\phi_\alpha} \middle| \frac{\partial\psi_{k\sigma}}{\partial\phi_\beta} \right\rangle, \tag{3.2}$$

it turns out to be independent of the spin. The total Chern number associated with phases ϕ_α and ϕ_β is then given by

$$C^{\alpha\beta} = \sum_{k\sigma} C_k^{\alpha\beta}\left(n_{k\sigma} - \frac{1}{2}\right), \tag{3.3}$$

where $n_{k\sigma} = 0, 1$ is the occupation number and

$$C_k^{\alpha\beta} = \int_{-\pi}^{\pi} d\phi_\alpha \int_{-\pi}^{\pi} d\phi_\beta \frac{B_k^{\alpha\beta}}{2\pi}. \tag{3.4}$$

Finally, if the superconducting lead corresponding to the phase ϕ_β is biased by a voltage V_β then the direct current in the superconducting lead α is given by

$$\bar{I}^\alpha = -\frac{4e^2}{h} C^{\alpha\beta} V_\beta, \tag{3.5}$$

hence the transconductance matrix for the D.C. response of the junction can give us information about its topology, this is the main result of Riwar et. al. [Riw+16a].

Let us return to Eq.(3.3) and notice that if the occupation number $n_{k\sigma}$ fluctuates with time then the contribution of the band k to the total Chern number fluctuates as well. This fluctuation is symmetric since the contribution of an empty band is $-C_k^{\alpha\beta}$, $C_k^{\alpha\beta}$ for a completely filled band and zero for a singly occupied band, therefore this will average out to zero. One possible cause for such a fluctuation in occupation number are the quasiparticles in the superconductors with energy higher then the superconducting gap Δ. Hence while obtaining the D.C. response of the junction the total Chern number $C^{\alpha\beta}$ needs to be averaged over as well, since it is fluctuating with time therefore the simple relation between the D.C current and the total

Chern number will disappear and the topology of the junction will be hidden from experiments. To account for the quasiparticles in the junction, without making the problem intractable, we can treat them as a source of dissipation, which leads us to an obvious question. In presence of dissipation is there still some notion of topology of the junction that can be detected by experiments?

To answer the above question we will use the notions of topology that have been developed for non-Hermitian systems, that were discussed in 1.6, and apply those ideas to a dissipative toy model that can be realised in MTJJs and simulates some essential features of ABS, and additionally hosts a non-Hermitian topological invariant, and examine if an experimentally observable quantity that depends on this topological invariant is available.

3.4. Dissipative Chern Hamiltonian

Finally, we come to our original goal of studying a dissipative toy model that could be simulated by an MTJJ. As stated earlier the Hamiltonian we consider is the two dimensional extension of the Hamiltonian in Eq. (2.2) that resembles a 2d Chern insulator Hamiltonian

$$\hat{H} = \Delta(\phi_1, \phi_2)\left(\hat{d}_\uparrow^\dagger \hat{d}_\uparrow + \hat{d}_\downarrow^\dagger \hat{d}_\downarrow - 1\right) + E_{wJ}\left(\sin\phi_1 - i\sin\phi_2\right)\hat{d}_\uparrow^\dagger \hat{d}_\downarrow^\dagger + E_{wJ}\left(\sin\phi_1 + i\sin\phi_2\right)\hat{d}_\downarrow \hat{d}_\uparrow, \tag{3.6}$$

where $\Delta(\phi_1, \phi_2) = \delta + E_{wJ}(\cos\phi_1 + \cos\phi_2)$ and the operators $\hat{d}_\uparrow^{(\dagger)}$, $\hat{d}_\downarrow^{(\dagger)}$ follow standard CAR. This Hamiltonian can be thought of as describing the lowest energy ABS band in a four terminal junction, where one of the three independent superconducting phases is fixed by threading an external flux through a loop (Fig.(3.2)).

As a quick aside, the Hamiltonian in Eq.(3.6) becomes the standard Chern Hamiltonian if we replace the superconducting phases with the pseudo-momenta $\phi_i \to k_i$. But it does not lie in the same symmetry class as the standard Chern Hamiltonian, because the pseudo-momenta are odd under particle-hole transformation ($k_i \to -k_i$) but the superconducting phases are even ($\phi_i \to \phi_i$) [ZK14a] (both are odd under time-reversal). Using the conditions in Eq.(1.125) we can deduce that the Hamiltonian in Eq.(3.6) lies in the symmetry class C. If we calculate the Chern number for this Hamiltonian, we find that it is 0 for $|\delta| > 2$, -1 for $-2 < \delta < 0$ and 1 for $0 < \delta < 2$, this agrees with the information in table 1.1 that tells us that for a Hamiltonian in class C and in two dimensions the topological invariant lies in $\mathbb{Z}$.

The quasiparticles are nothing but the excitations in superconductors that destroy the fermion parity of the ABS, therefore the dissipation can be described by the fermionic operators $\hat{d}_\uparrow^{(\dagger)}$ and $\hat{d}_\downarrow^{(\dagger)}$. Hence the dissipation operators that will enter the Lindblad equation are

$$\hat{L}_1 = \sqrt{\Gamma_1}\hat{d}_\uparrow, \quad \hat{L}_2 = \sqrt{\Gamma_2}\hat{d}_\downarrow, \quad \hat{L}_3 = \sqrt{\Gamma_3}\hat{d}_\uparrow^\dagger, \quad \hat{L}_4 = \sqrt{\Gamma_4}\hat{d}_\downarrow^\dagger. \tag{3.7}$$

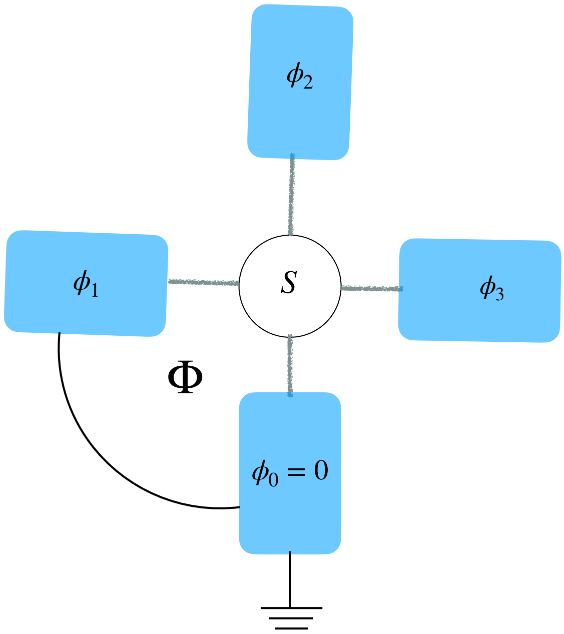

Figure 3.2.: Schematic of a four terminal multi terminal Josephson junction, where one of the three independent superconducting phases is fixed by threading an external flux Φ via a loop.

Γ_1 (Γ_2) and Γ_3 (Γ_4) respectively describe the rate of relaxing and pumping for the particle described by $\hat{d}_\uparrow$ ($\hat{d}_\downarrow$). Writing the fermionic creation and annihilation operators in terms of Majoranas

$$\begin{aligned} \hat{d}_\uparrow^\dagger &= \frac{\hat{\alpha}_1 + i\hat{\alpha}_2}{2} \implies \hat{d}_\uparrow = \frac{\hat{\alpha}_1 - i\hat{\alpha}_2}{2}, \\ \hat{d}_\downarrow^\dagger &= \frac{\hat{\alpha}_3 + i\hat{\alpha}_4}{2} \implies \hat{d}_\downarrow = \frac{\hat{\alpha}_3 - i\hat{\alpha}_4}{2}, \end{aligned} \tag{3.8}$$

the Hamiltonian becomes

$$\hat{H} = \begin{pmatrix} \hat{\alpha}_1 & \hat{\alpha}_2 & \hat{\alpha}_3 & \hat{\alpha}_4 \end{pmatrix} H \begin{pmatrix} \hat{\alpha}_1 \\ \hat{\alpha}_2 \\ \hat{\alpha}_3 \\ \hat{\alpha}_4 \end{pmatrix} \tag{3.9}$$

where

$$H = \frac{\Delta(\phi_1, \phi_2)}{4} \begin{pmatrix} 1 & 0 \\ 0 & 1 \end{pmatrix} \otimes \begin{pmatrix} 0 & -i \\ i & 0 \end{pmatrix} + \begin{pmatrix} 0 & 1 \\ -1 & 0 \end{pmatrix} \otimes \begin{pmatrix} -i\frac{E_{wJ}\sin\phi_2}{4} & i\frac{E_{wJ}\sin\phi_1}{4} \\ i\frac{E_{wJ}\sin\phi_1}{4} & i\frac{E_{wJ}\sin\phi_2}{4} \end{pmatrix}, \tag{3.10}$$

and the Hermitian matrix M that encodes the effect of dissipation operators is

$$M = \begin{pmatrix} 1 & 0 \\ 0 & 0 \end{pmatrix} \otimes \begin{pmatrix} \frac{\Gamma_1+\Gamma_3}{4} & i\frac{\Gamma_1-\Gamma_3}{4} \\ -i\frac{\Gamma_1-\Gamma_3}{4} & \frac{\Gamma_1+\Gamma_3}{4} \end{pmatrix} + \begin{pmatrix} 0 & 0 \\ 0 & 1 \end{pmatrix} \otimes \begin{pmatrix} \frac{\Gamma_2+\Gamma_4}{4} & i\frac{\Gamma_2-\Gamma_4}{4} \\ -i\frac{\Gamma_2-\Gamma_4}{4} & \frac{\Gamma_2+\Gamma_4}{4} \end{pmatrix}. \tag{3.11}$$

Finally the $Z = H + i\text{Re}[M]$ matrix can be written as

$$Z = H + i\frac{\Gamma_\uparrow + \Gamma_\downarrow}{8}\begin{pmatrix} 1 & 0 \\ 0 & 1 \end{pmatrix} \otimes \begin{pmatrix} 1 & 0 \\ 0 & 1 \end{pmatrix} + i\frac{\Gamma_\uparrow - \Gamma_\downarrow}{8}\begin{pmatrix} 1 & 0 \\ 0 & -1 \end{pmatrix} \otimes \begin{pmatrix} 1 & 0 \\ 0 & 1 \end{pmatrix}, \tag{3.12}$$

here we have defined $\Gamma_\uparrow = \Gamma_1 + \Gamma_3$ and $\Gamma_\downarrow = \Gamma_2 + \Gamma_4$ for the sake of convenience.

The eigenvalues of Z are

$$\begin{aligned}
\lambda_1 &= i\frac{\Gamma_\uparrow + \Gamma_\downarrow}{8} - \frac{i}{8}\sqrt{(\Gamma_\uparrow - \Gamma_\downarrow)^2 - 4\Delta^2 - 4E_{wJ}^2\left(\sin^2\phi_1 + \sin^2\phi_2\right) - i4\Delta(\Gamma_\uparrow - \Gamma_\downarrow)}, \\
\lambda_2 &= i\frac{\Gamma_\uparrow + \Gamma_\downarrow}{8} - \frac{i}{8}\sqrt{(\Gamma_\uparrow - \Gamma_\downarrow)^2 - 4\Delta^2 - 4E_{wJ}^2\left(\sin^2\phi_1 + \sin^2\phi_2\right) + i4\Delta(\Gamma_\uparrow - \Gamma_\downarrow)}, \\
\lambda_{-1} &= i\frac{\Gamma_\uparrow + \Gamma_\downarrow}{8} + \frac{i}{8}\sqrt{(\Gamma_\uparrow - \Gamma_\downarrow)^2 - 4\Delta^2 - 4E_{wJ}^2\left(\sin^2\phi_1 + \sin^2\phi_2\right) - i4\Delta(\Gamma_\uparrow - \Gamma_\downarrow)}, \\
\lambda_{-2} &= i\frac{\Gamma_\uparrow + \Gamma_\downarrow}{8} + \frac{i}{8}\sqrt{(\Gamma_\uparrow - \Gamma_\downarrow)^2 - 4\Delta^2 - 4E_{wJ}^2\left(\sin^2\phi_1 + \sin^2\phi_2\right) + i4\Delta(\Gamma_\uparrow - \Gamma_\downarrow)},
\end{aligned} \tag{3.13}$$

the eigenvalues are indexed such that the ones with negative index have negative real part when $\Gamma_\uparrow = \Gamma_\downarrow$. The analysis of these eigenvalues tells us that for $|\delta| < 2$, the topologically interesting regime in absence of dissipation, there is no real line gap. Also, these eigenvalues contain square roots of complex functions therefore appearance of EPs is guaranteed, which makes calculating Berry curvature and other such quantities impossible. Because of these problems and looking at the form of eigenvalues in Eq.(3.13), we specialize to the case $\Gamma_\uparrow = \Gamma_\downarrow = \Gamma$, here the eigenvalues simplify to

$$\begin{aligned}
\lambda_1 = \lambda_2 &= i\frac{\Gamma}{4} + \frac{1}{4}\sqrt{\Delta^2 + E_{wJ}^2\left(\sin^2\phi_1 + \sin^2\phi_2\right)}, \\
\lambda_{-1} = \lambda_{-2} &= i\frac{\Gamma}{4} - \frac{1}{4}\sqrt{\Delta^2 + E_{wJ}^2\left(\sin^2\phi_1 + \sin^2\phi_2\right)}.
\end{aligned} \tag{3.14}$$

Hence the eigenvalues become degenerate, but it can be checked that these are not defective, i.e. we can still find four linearly independent eigenvectors for Z. More importantly we get eigenvalues with a real line gap that closes at $\delta = -2, 0, 2$ for some specific values of ϕ_1 and ϕ_2, taking a cue from the closed system we would expect the topological invariant to change as we move across these points in the parameter regime. But before we can start looking for topological invariants we need to look at the symmetries of Z and determine if it lies in a symmetry class that allows for topological phases in two dimensions.

The matrix Z in the case of symmetric dissipation $\Gamma_\uparrow = \Gamma_\downarrow$ reduces to

$$Z = \begin{pmatrix} 1 & 0 \\ 0 & 1 \end{pmatrix} \otimes \begin{pmatrix} i\frac{\Gamma}{4} & -i\frac{\Delta(\phi_1,\phi_2)}{4} \\ i\frac{\Delta(\phi_1,\phi_2)}{4} & i\frac{\Gamma}{4} \end{pmatrix} + \begin{pmatrix} 0 & 1 \\ -1 & 0 \end{pmatrix} \otimes \begin{pmatrix} -i\frac{E_{wJ}\sin\phi_2}{4} & i\frac{E_{wJ}\sin\phi_1}{4} \\ i\frac{E_{wJ}\sin\phi_1}{4} & i\frac{E_{wJ}\sin\phi_2}{4} \end{pmatrix}, \tag{3.15}$$

the function $\Delta(\phi_1, \phi_2)$ contains cosines of ϕ_1 and ϕ_2 and therefore is an even function of these variables. Below we go case by case and see which of the three conditions in Eq.(1.136) are applicable for our model.

1. Time-reversal symmetry: For Z to have time-reversal symmetry we must find a unitary matrix C_+ such that it can connect $Z^T(-\phi_1,-\phi_2)$ to $Z(\phi_1,\phi_2)$ with a similarity transformation. Writing out $Z^T(-\phi_1,-\phi_2)$ explicitly

$$Z^T(-\phi_1,-\phi_2) = \begin{pmatrix} 1 & 0 \\ 0 & 1 \end{pmatrix} \otimes \begin{pmatrix} i\frac{\Gamma}{4} & i\frac{\Delta(\phi_1,\phi_2)}{4} \\ -i\frac{\Delta(\phi_1,\phi_2)}{4} & i\frac{\Gamma}{4} \end{pmatrix} + \begin{pmatrix} 0 & 1 \\ -1 & 0 \end{pmatrix} \otimes \begin{pmatrix} -i\frac{E_{wJ}\sin\phi_2}{4} & i\frac{E_{wJ}\sin\phi_1}{4} \\ i\frac{E_{wJ}\sin\phi_1}{4} & i\frac{E_{wJ}\sin\phi_2}{4} \end{pmatrix}, \tag{3.16}$$

we see that we need a unitary matrix of the form

$$C_+ = \begin{pmatrix} 1 & 0 \\ 0 & 1 \end{pmatrix} \otimes \begin{pmatrix} w & z \\ -e^{i\theta}z^* & e^{i\theta}w^* \end{pmatrix}, \tag{3.17}$$

where the second matrix in the above equation is a generic 2*2 unitary matrix defined by three numbers w, z, θ such that $|w|^2 + |z|^2 = 1$ and $\theta \in \mathbb{R}$. This generic matrix should satisfy the following two matrix equations

$$\begin{pmatrix} w & z \\ -e^{i\theta}z^* & e^{i\theta}w^* \end{pmatrix} \begin{pmatrix} \Gamma & \Delta \\ -\Delta & \Gamma \end{pmatrix} \begin{pmatrix} w^* & -e^{-i\theta}z \\ z^* & e^{-i\theta}w \end{pmatrix} = \begin{pmatrix} \Gamma & -\Delta \\ \Delta & \Gamma \end{pmatrix}, \tag{3.18}$$

$$\begin{pmatrix} w & z \\ -e^{i\theta}z^* & e^{i\theta}w^* \end{pmatrix} \begin{pmatrix} -\sin\phi_2 & \sin\phi_1 \\ \sin\phi_1 & \sin\phi_2 \end{pmatrix} \begin{pmatrix} w^* & -e^{-i\theta}z \\ z^* & e^{-i\theta}w \end{pmatrix} = \begin{pmatrix} -\sin\phi_2 & \sin\phi_1 \\ \sin\phi_1 & \sin\phi_2 \end{pmatrix}. \tag{3.19}$$

Solving these two equations we conclude that no such unitary matrix exist, hence there is no time-reversal symmetry.

2. Particle-hole symmetry: Since Z is a purely imaginary matrix by construction and the superconducting phases do not change under particle-hole transformation, therefore we have $-Z^*(\phi_1,\phi_2) = Z(\phi_1,\phi_2)$, hence our model trivially satisfies the condition for particle-hole symmetry.

3. Chiral symmetry: Since this is a combination of time-reversal and particle-hole symmetries and time-reversal is absent for this case therefore chiral symmetry is also absent.

From the above discussion and looking at the table 1.2, we conclude that our system lies in the class $\mathrm{D}^\dagger$ which does host topologically nontrivial non-Hermitian matrices in two dimensions, and the corresponding topological invariant lies in $\mathbb{Z}$.

3.4.1. Calculation of the topological invariant

The $\mathbb{Z}$ topological invariants of systems in even spatial dimensions $d = 2n$ with real line gap, are given by the nth Chern number C_n (Appendix H [Kaw+19a]). To define this Chern number we will first discuss diagonalisation of non-Hermitian matrices. Consider a general non-Hermitian square matrix B of dimension $p*p$, if this matrix is diagonalisable (i.e. it has p linearly independent eigenvectors) then we can decompose it as follows

$$B = \sum_{l=1}^{p} \lambda_p \left| u_p \right\rangle \langle\langle u_p | \,, \tag{3.20}$$

where $|u_p\rangle$ and $\langle\langle u_p|$ are right and left eigenvectors of B corresponding to the eigenvalue λ_p. These are defined as follows

$$\begin{aligned} B \left| u_p \right\rangle &= \lambda_p \left| u_p \right\rangle , \\ B^\dagger \left| u_p \right\rangle\rangle &= \lambda_p^* \left| u_p \right\rangle\rangle . \end{aligned} \tag{3.21}$$

The left and right eigenvectors satisfy the following orthonormality conditions

$$\langle\langle u_p | \, u_q \rangle = \delta_{pq}, \quad \langle u_p \, | u_q \rangle\rangle = \delta_{pq}, \tag{3.22}$$

and the following completeness relations

$$\sum_p |u_p\rangle \langle\langle u_p| = \sum_p |u_p\rangle\rangle \langle u_p| = \mathbb{I}. \tag{3.23}$$

The indices p and q in the above formulas are band indices, we will use the convention such that bands below the real line gap are denoted by negative integers and the ones above the gap are denoted by positive integers.

In order to define the nth Chern number we first define the non-Abelian Berry connection as a matrix-valued one-form, for the bands below the gap, whose components are defined as

$$\mathcal{A}_{pq} = \sum_{i=1}^{2n} \langle\langle u_p | \, \partial_{k_i} u_q \rangle \, dk_i, \quad p, q < 0. \tag{3.24}$$

The Berry curvature is a matrix-valued two-form whose components are given by

$$\mathcal{F}_{pq} = d\mathcal{A}_{pq} + \sum_{m<0} \mathcal{A}_{pm} \wedge \mathcal{A}_{mq}, \quad p, q < 0, \tag{3.25}$$

expanding the above expression in terms of eigenvectors we obtain

$$\begin{aligned} \mathcal{F}_{pq} &= \sum_{i,j=1}^{2n} \left(\langle\langle \partial_{k_i} u_p | \, \partial_{k_j} u_q \rangle + \sum_{m<0} \langle\langle u_p | \, \partial_{k_i} u_m \rangle \langle\langle u_m | \, \partial_{k_j} u_q \rangle \right) dk_i \wedge dk_j, \\ \mathcal{F}_{pq} &= \sum_{i,j=1}^{2n} \langle\langle \partial_{k_i} u_p | \left(1 - \sum_{m<0} |u_m\rangle \langle\langle u_m| \right) \left| \partial_{k_j} u_q \right\rangle dk_i \wedge dk_j, \end{aligned} \tag{3.26}$$

where we have used the fact that $\partial_{k_i} \langle\langle u_p | \, u_q \rangle = 0 \implies \langle\langle u_p | \, \partial_{k_i} u_q \rangle = - \langle\langle \partial_{k_i} u_p | \, u_q \rangle$. The Chern number can now be computed using the following expression

$$C_n = \frac{1}{n!} \left(\frac{i}{2\pi} \right)^n \int_{\mathrm{BZ}} \mathrm{tr} \left(\mathcal{F}^n \right), \tag{3.27}$$

since the Berry curvature is a matrix-valued two-form, the expression $\mathcal{F}^n$ implies matrix multiplication with the caveat that the components of the matrix are multiplied by exterior product. The above definitions of Berry connection, curvature and therefore the Chern number can equivalently be defined for bands with positive indices, in that case the change in topological invariant as we go from one phase to the other will have the same absolute value but sign will be flipped.

For our model, a system with two spatial dimensions and four bands (two above the real line gap and two below), the relevant topological invariant is the first Chern number, which simplifies to

$$C_1 = \sum_{p=-2}^{-1} \frac{i}{2\pi} \int_{\phi_1=0}^{2\pi} \int_{\phi_2=0}^{2\pi} \left(\langle\langle \partial_{\phi_1} u_p |\, \partial_{\phi_2} u_p \rangle - \langle\langle \partial_{\phi_2} u_p |\, \partial_{\phi_1} u_p \rangle \right) d\phi_1 d\phi_2. \tag{3.28}$$

To compute this Chern number numerically we use the algorithm described in Fukui et. al. [FHS05], we present a modified version of the algorithm here for the case of non-Hermitian Hamiltonians. Let us say we have to calculate the Chern number for the band $|u(\phi_{j_1}, \phi_{j_2})\rangle$ (with $\langle\langle u(\phi_{j_1}, \phi_{j_2})|$ as the corresponding left eigenvector), we begin by discretising the Brillouin zone into lattice points denoted by the ordered pair (ϕ_{j_1}, ϕ_{j_2}), where

$$\phi_{j_\mu} = \frac{2\pi j_\mu}{N_\mu}, \quad j_\mu = (0, 1, \cdots, N_\mu - 1), \tag{3.29}$$

hence the total number of lattice points in the Brillouin zone are $N_1 N_2$. We assume that the state $|u(\phi_{j_1}, \phi_{j_2})\rangle$ is periodic on the lattice, $|u(\phi_{j_1} + 2\pi, \phi_{j_2})\rangle = |u(\phi_{j_1}, \phi_{j_2})\rangle = |u(\phi_{j_1}, \phi_{j_2} + 2\pi)\rangle$.

Now we define the $U(1)$ link variable as follows

$$\begin{aligned} U_1(\phi_{j_1}, \phi_{j_2}) &= \frac{\langle\langle u(\phi_{j_1}, \phi_{j_2})|\, u(\phi_{j_1} + 2\pi/N_1, \phi_{j_2})\rangle}{|\langle\langle u(\phi_{j_1}, \phi_{j_2})|\, u(\phi_{j_1} + 2\pi/N_1, \phi_{j_2})\rangle|}, \\ U_2(\phi_{j_1}, \phi_{j_2}) &= \frac{\langle\langle u(\phi_{j_1}, \phi_{j_2})|\, u(\phi_{j_1}, \phi_{j_2} + 2\pi/N_2)\rangle}{|\langle\langle u(\phi_{j_1}, \phi_{j_2})|\, u(\phi_{j_1}, \phi_{j_2} + 2\pi/N_2)\rangle|}. \end{aligned} \tag{3.30}$$

The link variable is defined as long as the expressions in the denominator do not become zero, if this happens it can be avoided by shifting the lattice infinitesimally. From the link variable we define the lattice field strength by

$$\tilde{F}(\phi_{j_1}, \phi_{j_2}) = \ln\left[U_1(\phi_{j_1}, \phi_{j_2})\, U_2(\phi_{j_1} + 2\pi/N_1, \phi_{j_2})\, U_1(\phi_{j_1}, \phi_{j_2} + 2\pi/N_2)^{-1}\, U_2(\phi_{j_1}, \phi_{j_2})^{-1}\right]. \tag{3.31}$$

Note that the field strength is defined within the principal branch of logarithm i.e. $-\pi < \tilde{F}(\phi_{j_1}, \phi_{j_2})/i < \pi$. It can also be easily shown that this field strength is invariant under the gauge transformation $|u(\phi_{j_1}, \phi_{j_2})\rangle \to e^{i\lambda(\phi_{j_1}, \phi_{j_2})} |u(\phi_{j_1}, \phi_{j_2})\rangle$. Finally the Chern number associated with the band $|u(\phi_{j_1}, \phi_{j_2})\rangle$ is given by

$$\tilde{C}_1 = \frac{i}{2\pi} \sum_{\phi_{j_1}, \phi_{j_2}} \tilde{F}(\phi_{j_1}, \phi_{j_2}) \tag{3.32}$$

The above algorithm has to be modified to include the case of degenerate eigenvalues, let us assume that the following states are degenerate $|u_1\rangle, |u_2\rangle, \cdots, |u_M\rangle$, then we define the following multiplets

$$\begin{aligned}\psi &= \begin{pmatrix} |u_1\rangle & |u_2\rangle & \cdots & |u_M\rangle \end{pmatrix},\\ \widetilde{\psi} &= \begin{pmatrix} \langle\langle u_1| \\ \vdots \\ \langle\langle u_M| \end{pmatrix},\end{aligned} \tag{3.33}$$

now the $U(1)$ link variables are defined as

$$\begin{aligned}U_1(\phi_{j_1}, \phi_{j_2}) &= \frac{\det\left(\widetilde{\psi}(\phi_{j_1}, \phi_{j_2})\,\psi(\phi_{j_1} + 2\pi/N_1, \phi_{j_2})\right)}{\left|\det\left(\widetilde{\psi}(\phi_{j_1}, \phi_{j_2})\,\psi(\phi_{j_1} + 2\pi/N_1, \phi_{j_2})\right)\right|},\\ U_2(\phi_{j_1}, \phi_{j_2}) &= \frac{\det\left(\widetilde{\psi}(\phi_{j_1}, \phi_{j_2})\,\psi(\phi_{j_1}, \phi_{j_2} + 2\pi/N_2)\right)}{\left|\det\left(\widetilde{\psi}(\phi_{j_1}, \phi_{j_2})\,\psi(\phi_{j_1}, \phi_{j_2} + 2\pi/N_2)\right)\right|}.\end{aligned} \tag{3.34}$$

The definition of field strength remains the same and the Chern number follows from that. The numerically calculated Chern number $\tilde{C}_1$ converges to the analytical value C_1 the smaller we make the lattice spacing. The figure (3.3) shows the Chern number for our system with respect to the parameter δ.

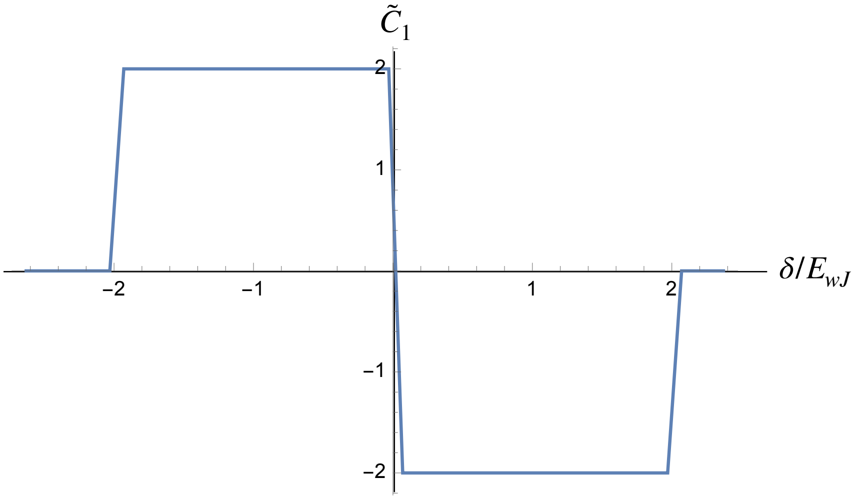

Figure 3.3.: Plot of the Chern number versus the parameter δ that varies from $-2.5E_{wJ}$ to $2.5E_{wJ}$. Other energy scale in the system is the dissipation rate which is set to $\Gamma = 0.3E_{wJ}$, while the lattice spacing is set by using the following parameters $N_1 = N_2 = 100$. We see that as expected the Chern number is zero for $|\delta| > 2$ indicating that the system is topologically trivial, and is finite for $|\delta| < 2$. Additionally there are two distinct topological regions marked by $\tilde{C}_1 = \pm 2$.

3.4.2. Preliminary result for measurement

After confirming that our model indeed hosts a non-Hermitian topological invariant, the next step is to find an experimentally measurable quantity that reflects this topology. As a first step, taking inspiration from our previous work on superconductor-normal metal hybrid circuit, we introduce a counting field in the system to model a detector, this allows us to access the full counting statistics of the junction which can then be used to obtain experimental observables. The counting field (χ) modifies the Lindbladian as follows

$$\begin{aligned} i\frac{d\rho}{dt} &= \left(\hat{H}\left(\phi_1+\chi,\phi_2\right)\rho - \rho\hat{H}\left(\phi_1-\chi,\phi_2\right)\right) + i\sum_{\mu=\uparrow,\downarrow}\left(2L_\mu\rho L_\mu^\dagger - \left\{L_\mu^\dagger L_\mu,\rho\right\}\right), \\ i\frac{d\rho}{dt} &= \cos\chi\left[\hat{H}\left(\phi_1,\phi_2\right),\rho\right] + \sin\chi\left\{\partial_{\phi_1}\hat{H}\left(\phi_1,\phi_2\right),\rho\right\} + i\sum_{\mu=\uparrow,\downarrow}\left(2L_\mu\rho L_\mu^\dagger - \left\{L_\mu^\dagger L_\mu,\rho\right\}\right), \end{aligned} \tag{3.35}$$

the choice to add the counting field to the phase ϕ_1 is arbitrary. Once we have the modified form of the Lindblad equation, we can reapply the formalism proposed by Prosen to write the Lindbladian superoperator in following form

$$\hat{\mathcal{L}} = 2\begin{pmatrix} \underline{\hat{c}}^\dagger & \underline{\hat{c}} \end{pmatrix}\begin{pmatrix} H\cos(\chi) - i\mathrm{Re}\left[M\right] & \sin(\chi)\,\partial_{\phi_1}H - 2\mathrm{Im}\left[M\right] \\ -\sin(\chi)\,\partial_{\phi_1}H & H\cos(\chi) + i\mathrm{Re}\left[M\right] \end{pmatrix}\begin{pmatrix} \underline{\hat{c}} \\ \underline{\hat{c}}^\dagger \end{pmatrix} - 2i\mathrm{tr}\left[M\right], \tag{3.36}$$

here H and M matrices are the same ones that were defined in absence of the counting field, the dependence of the Hamiltonian on the superconducting phases have been hidden to make the equation more readable.

We can clearly see from Eq.(3.36) that inclusion of counting field in the system removes the straight forward dependence of the spectrum of the Lindbladian on the block matrix on the main diagonal. Hence the topology of the complete Lindbladian can no longer be ascertained by just looking at the topology of the block matrix on the main diagonal.

3.5. Conclusion

Unfortunately due to time constraints this project had to be paused here, and the question of if there exist a measurement that can reflect the topology of this dissipative system remains open. One possibility of confirming at least some part of our result is via direct observation of the eigenspectrum of the Lindbladian and looking for the gap closing. We can obtain the eigenvalues of the Lindbladian from the eigenvalues of Z (Eq.(1.111))

$$\begin{aligned} &\lambda_1 = 0, \lambda_2 = -4i\Gamma, \lambda_3 = \lambda_4 = \lambda_5 = \lambda_6 = -2i\Gamma, \\ \lambda_7 =&\lambda_8 = -i\Gamma - \sqrt{\left(\delta + E_{wJ}\left(\cos\phi_1 + \cos\phi_2\right)\right)^2 + E_{wJ}^2\left(\sin^2\phi_1 + \sin^2\phi_2\right)}, \end{aligned}$$

$$\begin{aligned}
\lambda_9 =&\lambda_{10} = -i\Gamma + \sqrt{(\delta + E_{wJ}(\cos\phi_1 + \cos\phi_2))^2 + E_{wJ}^2(\sin^2\phi_1 + \sin^2\phi_2)},\\
\lambda_{11} =&\lambda_{12} = -3i\Gamma - \sqrt{(\delta + E_{wJ}(\cos\phi_1 + \cos\phi_2))^2 + E_{wJ}^2(\sin^2\phi_1 + \sin^2\phi_2)},\\
\lambda_{13} =&\lambda_{14} = -3i\Gamma + \sqrt{(\delta + E_{wJ}(\cos\phi_1 + \cos\phi_2))^2 + E_{wJ}^2(\sin^2\phi_1 + \sin^2\phi_2)},\\
\lambda_{15} =& - 2i\Gamma - 2\sqrt{(\delta + E_{wJ}(\cos\phi_1 + \cos\phi_2))^2 + E_{wJ}^2(\sin^2\phi_1 + \sin^2\phi_2)},\\
\lambda_{16} =& - 2i\Gamma + 2\sqrt{(\delta + E_{wJ}(\cos\phi_1 + \cos\phi_2))^2 + E_{wJ}^2(\sin^2\phi_1 + \sin^2\phi_2)}.
\end{aligned}$$

We see that at the point of gap closing the eigenvalues of the Lindbladian become imaginary (except for λ_1). The real gap closing is shown for the eigenvalues λ_7 and λ_9 is shown in Fig.

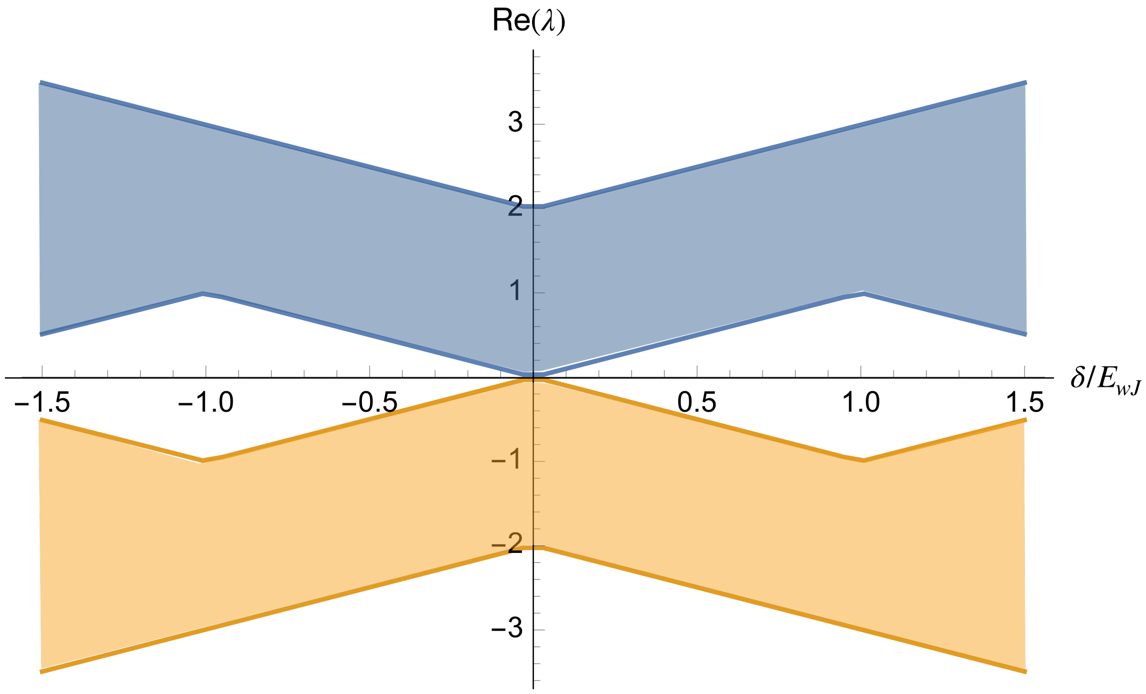

Figure 3.4.: Plot of the real parts of the eigenvalues λ_7 (blue lines) and λ_9 (orange lines), since for all other eigenvalues the real part is either 0 or similar. The real gap closes for $\delta = -2E_{wJ}, 0, 2E_{wJ}$, here we have shown it only in the vicinity of $\delta = 0$, the values of the superconducting phases where the gap closes are $\phi_1 = \pi, \phi_2 = 0$ and $\phi_1 = 0, \phi_2 = \pi$.

Before closing this chapter we would like to reiterate what our preliminary results mean. We have shown that our toy model with symmetric dissipation is topologically non trivial for $-2E_{wJ} < \delta < 2E_{wJ}$, and that this topology is encoded in the open system version of the Chern number, which is well defined even in presence of quasi-particle poisoning. But we have also shown that this Chern number cannot appear in any regular transport measurement. We did this by introducing a counting field in the system Lindbladian and finding the FCS, the form of the Lindbladian with the counting field immediately told us that no cumulant of the transport statistics can reflect this Chern number in an experiment.

4. Utilizing and extending superconducting circuit toolbox to simulate analog event horizons

4.1. Introduction

Unifying quantum mechanics and gravity poses several theoretical [tV74; GS86; Pen14] and experimental challenges [Hos+85; MP88; Lee+20; Wes+21; Ger+11; Eib+13; Rom17; Pin+18; Fei+19; Del+20; Teb+21], which motivates studying analogs of relativistic quantum effects in experimentally accessible systems [BLV11]. Several ideas have therefore been proposed for simulating gravitational effects in solid-state systems – for example, holographic ideas borrowed from string theory [SY93; Sac15; BAK16; KS18; KS19; Jaf+22], or cosmological particle creation [BLV03; FF04; FS04; Jai+07; PFL10; Ste+22], or more directly, using Unruh's proposal of "sonic black holes" [Unr81] as an inspiration to simulate black holes in labs. Along these lines, apparent event horizons and the resulting Hawking radiation have been studied on various platforms [KBW20; STW20; De +21; Nat+09; KHF20; TD19; Lan15; Sab18; Sab16], most notably in ultracold atomic gases [Gar+00; Gar+01; Ste14; Muñ+19; RBF22].

There remain however a number of open questions. First, so far for solid state implementations the metric usually changes only over a finite "healing length". If the surface gravity (for analog black holes surface gravity corresponds to the rate of change of the group velocity with which a signal will move in the given metric [Muñ+19]) is too weak, the resulting small Hawking temperature may thus be below the threshold of the system's intrinsic temperature [Rob12] – an obstacle that (at least up to now) seems to have only been overcome for cold atom simulators [Muñ+19]. Relatedly, systems with an apparent event horizon generically do not have a well-defined ground state, such that any coupling to the environment leads to an instability, making it extremely challenging to distinguish intrinsic radiation due to the horizon (which would actually simulate aspects of a universe with nontrivial spacetime metric) and radiation due to environment induced relaxation. In addition, even in the absence of environment, the closed system can in some platforms be spontaneously unstable [Gar+00; Gar+01]. Furthermore, lattice realizations (which ultimately concerns all solid state systems) add a number of interesting but challenging facets, such as a natural (though possibly artifical) resolution of the trans-Planckian problem [Jac91; Bro+95; SU05; HF23], and most notably, the fact that any event horizon has both black and white hole character, since the dispersion relation in a periodic Brillouin zone must necessarily cross zero at least twice [De +21].

Superconducting circuits are one of the prime candidates for building large-scale quantum hardware [Aru19; Wu 21; Kja+20]. The behaviour of these circuits and their interactions with quantised electromagnetic fields in the microwave range are described by circuit quantum electrodynamics (cQED), a formalism that reduces circuits to lumped elements whose phase and charge are canonically conjugate [YD84; BKD04; UH16; VD17; Bla+04; Bla+07; BGO20; Bla+21; RD22]. The toolbox of superconducting circuits includes nonlinear elements such as Josephson junctions and linear elements such as capacitors and inductors. Our work will also feature nonreciprocal multi-port circuit elements. Classical nonreciprocal elements called gyrators (or their close cousins, circulators), are already widely in use in circuit engineering and signal processing [Abd+13; KSA20; MC15; MC17], whose consistent circuit theoretical description goes back to the work by Tellegen [Tel48]. These are however generally large clunky objects operating in a finite frequency window. Various recent works strive towards a realisation and a consistent description of quantum mechanical gyrators [VD14; Rym+21; Sel+23; VH24]. Moreover, it has recently been realised [VH24; Riw23; MTY24] that the same nonreciprocal behaviour also occurs due to topological transitions in the transport degrees of freedom of multiterminal junctions [Riw+16a; FAB21; Pey+21; Wei+21; Kle+21; HR22], whose size can be on the meso scale and the gyration behavior emerges in the D.C. limit. Over the course of decades, it has been shown that networks of superconducting circuits can give rise to a large number of physical phenomena and imitate various quantum field theories from other domains [KM89; Ust98; Wal+00; Fv01; CAB08; Gla+09; THD12; HTK12; HG19; TD19; Ole+22; WMB24; Flu+12; Wil+11]. However, the exploration of analog gravity phenomena has so far been limited to Hawking-like radiation in Josephson junction arrays [Nat+09; KHF20; Kat+21; Kat21a; Kat21b; Kat+23; TD19; Lan15], which, due to the nature of their proposal leave only little control over the shape of the spacetime geometry, or recreation of a limited class of curved spacetimes by means of flux control of SQUID arrays [Sab18; Sab16].

In this work, we demonstrate that networks of Josephson junctions and gyrators can be used as an engineering tool for simulations of quantum-gravity phenomena with unprecedented tunability capabilities, and generate surprising insights specific to lattice systems. The basic idea is that arrays of these elements result in a (nearly) massless scalar field theory describing a quantum field – the superconducting phases of the charge islands – propagating across a lattice with spatially varying analog spacetime metric. The latter essentially encompasses the local dispersion relation, i.e., the velocities with which right and left signals move with respect to the laboratory frame. Note, however, that although the model consists of quantum fields propagating on a fixed lattice of quantum circuit elements, this does *not* necessarily correspond to the semi-classical limit (i.e. quantum field theory on fixed background spacetime). The fixed laboratory coordinates (space and time of the experimenter implementing the device) do not have to coincide with space or time coordinates emerging from hypothetical observers within the toy universe, see also discussion in the outlook.

To create an apparent horizon we need a boundary between the "normal region" (region where the signals can move in both directions) and a wormhole region where the signals only move in one direction, i.e. a region with overtilted dispersion relation. As it turns out such a region can be created with *negative* inductors, which we propose to achieve by adapting recent insights in flux quench of regular Josephson junctions [YSK19b; RD22]. Tunable $0-\pi$ junctions [PB18; Li+19; Ke+19] may offer an alternative pathway towards negative inductances.

Already for such classical metric profiles, we make a number of important observations specific to lattice simulations. The exceptional tunability of the individual energy scales in the lattice allows to change the analog metric over only a few lattice sites, which would yield for typical charging and Josephson energies Hawking temperatures in the 100mK up to $1K$ range, thus comfortably exceeding usual cryogenic temperatures. But as we show, this comes at the price of a fundamental impossibility to create stable event horizons for strictly discrete lattice systems. Instead, the system becomes unstable right after the quench, resulting in an immediate evaporation starting out from the event horizon. We here embrace this instability, and show how to realize systems with a change of the spacetime over a *single* lattice point, where the rate of change of the metric itself is ill-defined at the horizon (in the style of Refs. [Jac91; Bro+95; SU05], we refer to this change in the metric as being “trans-Planckian”) resulting in a likewise ill-defined Hawking temperature. We thus create a system where the signatures of wormhole collapse are fully disjoint from any finite surface gravity effects at the horizon – and in doing so, provide an answer to the question of what happens at an event horizon in the otherwise highly speculative limit of diverging surface gravity. We show that the instability leads to an accumulation of charge and phase quantum fluctuations, which we expect to be a highly robust signature with respect to environment-induced dissipation, since the latter *reduces* quantum fluctuations (instead of increasing them).

Moreover, we find an instructive loop-hole to the aforementioned ambiguity of black- versus white hole event horizons in lattice systems. Namely, the inductive coupling can go either via nearest or next-to-nearest neighbour nodes. For the former, the dispersion relation inside the wormhole region exhibits an *exceptional point*, such that the eigenspectrum no longer crosses zero energy twice, but instead takes a detour on the complex plane to satisfy periodicity. We thus realize lattice versions of event horizons which are definitely either black- or white hole, but not both. However, this feature radically changes the dynamics in the interior of the wormhole: instead of an evaporation from the horizons outwards the entire wormhole interior evaporates everywhere immediately after the quench.

Lastly, while we mostly consider long chains in the main part of this work, as they provide a clean interpretation of the effects in the context of curved spacetime, we are aware that they may be challenging to realize experimentally. In the outlook, we therefore also propose experiments on only few lattice points as proofs of principle, which already contain much of the pertinent phenomenology present in long chains.

This work started off as a group project and therefore has contributions from all, past and present, group members. T. Herrig and C. Koliofoti contributed to the initial stages of the project and were instrumental in discarding a lot of false starts. A. Kenawy wrote the first version of the code and obtained preliminary numerical results, while O. Kashuba helped with the extension of Klich's determinant formula (see App. E). Also, D. Kruti and C. Koliofoti were of great help in understanding the subtleties of already established results about astrophysical event horizons, while R.-P. Riwar helped with placing this project in context of much larger body of already existing work regarding analog event horizons in condensed matter physics. This chapter of the thesis is organized as follows, section 4.2 is a brief review of scalar field theories on curved spacetime, and a summary of our main accomplishments of this work. In section 4.3 we introduce and study the two circuits that will host the apparent horizons that we wish to investigate, we especially focus on the different effect that negative inductances have on the dispersion relations of these two circuits anticipating the differences between the horizons in them. Section 4.4 is a brief detour, where we expand upon the idea of using flux quench on a Josephson junction to get a negative inductance, and in section 4.5 we study and characterize the horizons in the two aforementioned circuits, by looking at the time evolution of quantum fluctuations of the conjugate charge and the phase difference. In section 4.6 we hypothesize on the long time fate of the analog horizons and argue that the effect of this intrinsic evaporation is easily distinguishable from the effect of coupling to the environment. This section also acts as a bridge to the idea of quantum inductors and using them to observe quantum superpositions of two spacetime geometries, this part of the work is not included in the thesis since its main contibutors are D. Kruti and R.-P. Riwar, but can be found in [Jav+24].

4.2. Curved space time metrics and the circuit simulator

4.2.1. Brief review of field theories with curved spacetime and stability considerations

To set the stage, let us reiterate basic notions related to field theories with nontrivial spacetime metric.

Within this brief review, questions regarding the stability of the considered systems will emerge. To this end, we begin by providing a number of general statements regarding bosonic Hamiltonians (as we focus on scalar bosonic quantum fields). The quantum systems we consider are all described by a Hermitian Hamiltonian. In accordance with Refs. [Gar+00; Gar+01; Nak+08; Min+07], we point out that hermiticity does *not* guarantee stability of the system, due to the special symplectic structure of the Bogoliubov transformation. In particular, two cases need to be distinguished. It may happen that certain eigenvalues are negative, such that the system has no well-defined many-body ground state. Such systems however still evolve in a stable fashion, unless they are coupled to an environment, which will in general lead to a collapse of the system, as negative energy bosonic states can now be occupied by extracting energy from the bath. In the second case, some eigenenergies may become *complex* (again, this is consistent with Hermitian Hamiltonians, see Refs. [Gar+00; Gar+01]). Such systems are spontaneously unstable, as they do not require a coupling to a bath to collapse.

In continuous field theories, the action of a field ϕ in a $d+1$-dimensional spacetime is generally given as

$$S = \frac{1}{2} \int dt d^d x \sqrt{-g}\, g^{\mu\nu} \partial_\mu \phi\, \partial_\nu \phi \ , \tag{4.1}$$

where the metric tensor $g^{\mu\nu}$ can in general depend on all coordinates. Within actual general relativity, the metric tensor of course encompasses the entire causal structure of spacetime. However, it is understood since a long time that a wide variety of nonrelativistic systems (condensed matter and beyond) may be described by an action of the same form, however with typical velocities much below the speed of light. These systems provide an analog spacetime in the sense that $g^{\mu\nu}$ looses its concrete relativistic interpretation.

For simplicity, let us consider $1+1$ dimensions (note that our simulator recipe works also for more spatial dimensions, as we point out in a moment), and focus on metrics that depend only on the position coordinate, i.e., metrics that are stationary in the laboratory frame. Here we write the action explicitly in a matrix form as

$$S = \frac{1}{2} \int dt dx \begin{pmatrix} \partial_t \phi & \partial_x \phi \end{pmatrix} \begin{pmatrix} \frac{1}{u} & \frac{v}{u} \\ \frac{v}{u} & \frac{v^2 - u^2}{u} \end{pmatrix} \begin{pmatrix} \partial_t \phi \\ \partial_x \phi \end{pmatrix} , \tag{4.2}$$

where u and v are two independent functions of x. Note that the matrix representing the spacetime metric has determinant -1, such that the $\sqrt{-g}$ prefactor is here irrelevant. For actions of this form, it is always possible to make a coordinate transformation [Rob12]

$$y = t - \int^x dx' \frac{1}{u(x') + v(x')} \tag{4.3}$$

$$z = t + \int^x dx' \frac{1}{u(x') - v(x')} \ , \tag{4.4}$$

to bring the action into the simple form

$$S = \int dy dz \partial_y \phi\, \partial_z \phi \ . \tag{4.5}$$

In these coordinates, the classical Euler-Lagrange equation is simply $\partial_y \partial_z \phi = 0$, whose solutions are arbitrary superpositions of functions that depend either only on y, or only on z. Transforming back to (t, x)-coordinates via Eqs. (4.3) and (4.4), these two separate solutions correspond to waves propagating locally either with velocity $u + v$ or $u - v$. For constant u, v (and $u > 0$), the theory is readily quantized, yielding the Hamiltonian

$$H = \int dk \omega_k a_k^\dagger a_k \ , \tag{4.6}$$

where for bosonic fields, $[a_k, a_{k'}^\dagger] = \delta(k - k')$. The dispersion relation $\omega_k = u|k| + vk$ readily provides the group velocity of quantum excitations, such that the classical y and z type solutions here correspond to $k > 0$ and $k < 0$, respectively. For $|v| < u$, the system describes a regular analog light cone with H having only positive many-body eigenvalues, where v corresponds to a finite tilt of the dispersion relation.

For $|v| > u$ the dispersion relation is overtilted, such that one of the branches (either $k < 0$ or $k > 0$) has now negative energies. Negative energies are meaningful in the following sense. As already pointed out above, the Hamiltonian H here has in principle no more well-defined ground state – indicating a serious instability. However, the eigenvalues remain real, such that the closed quantum system still evolves in a stable fashion. In particular, with a Galilei transformation [1] by, e.g., $-v$, we can undo the tilt (the dispersion relation goes to $u|k|$) and thus return to a regular Hamiltonian with a well-defined ground state. Consequently, for the closed quantum system, there is nothing special about whether or not a particular branch has negative eigenenergies. Matters are markedly different, once we consider open quantum systems. Here, the Galilei transformation applies to both the system Hamiltonian, as well as to the interaction with the environment. Hence, one cannot change a system from stable to unstable by merely moving with respect to it – thus avoiding what would otherwise be a serious conundrum. However, the inverse may well happen: if we fine tune the parameters of the system such that it implements an overtilted dispersion relation in the laboratory rest frame, the coupling to the environment may indeed be such that the system collapses on very fast time scales (usually given by the typical relaxation rates of the considered quantum hardware).

Returning to spatially varying spacetime metrics, apparent event horizons emerge in this field theory when at a given point v crosses from $|v| < |u|$ to $|v| > |u|$, such that there no longer exist a global transformation to a flat spacetime. Consequently, the system is separated at the horizon into two halves, one with a well-defined ground state (regular or no tilt in the dispersion relation) and one with no ground state (overtilted). In principle, one could now expect already the closed quantum system to be unstable as the two halves could exchange energy (which would thus lead to complex eigenvalues). But as is well known [Rob12], this does not happen for this particular system. Even in the presence of such a horizon, the system is still described by regular, real eigenvalues, such that at least for the closed system, the evolution is still stable (though in general not in a well-defined ground state). The reason for this is that on both sides of the horizon, the above coordinate transformation to (y, z) still applies, such that for these coordinates, there still exist two well-defined branches of the wave solutions moving at different speeds relative to the lab frame. At the horizon, the transition from $|v| < |u|$ to $|v| > |u|$ results in one – but only one – of the two coordinate transformations (either y or z, depending on the sign of v) to be singular. Consequently, the branch without singularity simply moves through the event horizon as if it wasn't there. The other branch (with the singularity) is causally

[1] Galilei transformations are of course allowed for the here considered simulator systems which operate at velocities far below the speed of light.

disconnected at the horizon, because wave solutions come to a stand-still. Hence the left and right hand side of this branch do not couple.

Since the system is however not in a ground state, meaningful quantum measurements are best defined by anchoring all observables to a basis with well-defined ground state. This is commonly done [Rob12] by imagining the system to be prepared (in the distant past) in the ground state of a spacetime metric without horizon (e.g., perfectly flat spacetime). When now defining measurements with respect to the new eigenbasis, Hawking radiation emerges. A frequency decomposition of this radiation reveals that it is of thermal nature, given by the surface gravity – e.g., for constant u, the temperature is thus proportional to the energy scale $\partial_x v$, evaluated at the horizon.

Crucially, while for the closed system (or for the actual universe) it therefore seems plausible to have stable spacetime metrics with horizons and a related thermal Hawking radiation, it has to be noted that for simulators coupled to an environment, the above is a highly precarious situation – precisely because of the lack of a well-defined ground state. For instance, while the branch with the singularity may well be exactly separated at the horizon for the closed system, the overtilted part very likely becomes unstable simply due to coupling with the environment (see our above Galilei transformation argument, respectively its inverse). Moreover, it cannot be excluded that a (ever so slightly) nonlocal coupling to an environment effectively couples the two causally separated branches, such that energy can be exchanged across the singularity via environment-assisted tunneling. As we now go on to lattice simulators, stability concerns only pile up.

4.2.2. Simulation with circuit networks

Here, we summarize our simulation idea by means of quantum circuits, and indicate the main accomplishments of our work.

As we see in Eq. (4.2), for a system to emulate a field moving on a nontrivial spacetime, we need interactions that provide the terms $\sim \dot{\phi}^2$, $\sim \dot{\phi}\,\partial_x\phi$, and $\sim (\partial_x\phi)^2$. Quantum circuit theory [BKD04; VD17; Rym+21; RD22] readily provides elements that (in a certain continuum limit) provide such interactions. For a superconducting node j, a finite capacitance (C_j) provides to the Lagrangian $\mathcal{L}$ an energy contribution of the form

$$\mathcal{L} \to \mathcal{L} + \frac{C_j}{2}\left(\frac{\dot{\phi}_j}{2e}\right)^2 , \tag{4.7}$$

whereas a finite inductance (L_j) between two neighbouring nodes $j+1$ and j provides

$$\mathcal{L} \to \mathcal{L} - \frac{1}{2L_j}\left(\frac{\phi_{j+1}-\phi_j}{2e}\right)^2 . \tag{4.8}$$

In the continuum limit $\phi_j \to \phi(x)$, we indeed get the terms $\sim \dot{\phi}^2$ and $\sim (\partial_x\phi)^2$, respectively.

However, this alone does not provide a tilt of the dispersion relation. This is where gyrators come into play. As pointed out in Ref. [Rym+21], a three-port gyrator, connecting two neighbouring nodes ϕ_{j+1} and ϕ_j to ground (whose phase is set to zero) can be described by the following contribution to the Lagrangian [2],

$$\mathcal{L} \to \mathcal{L} + G_j(\phi_j \dot{\phi}_{j+1} - \dot{\phi}_j \phi_{j+1}) \ , \tag{4.9}$$

where the parameter G is proportional to the transconductance of the gyrator,

$$2eI_j = \frac{\partial \mathcal{L}}{\partial \phi_j} = G_j \dot{\phi}_{j+1} = 2eG_j V_{j+1} \tag{4.10}$$

$$2eI_{j+1} = \frac{\partial \mathcal{L}}{\partial \phi_{j+1}} = -G_j \dot{\phi}_j = -2eG_j V_j \ . \tag{4.11}$$

The gyrator thus has a typical circular transport behaviour, i.e., a voltage at j $(j+1)$ induces a current (with reversed sign) at $j{+}1$ (j). The continuum limit (at least a naive continuum limit, as we discuss in detail below) yields indeed a term of the sought-after form $\sim \dot{\phi}\, \partial_x \phi$ and thus provides a tilt. In fact, it is precisely the above circular transport behaviour, which allows us to develop an illustrative intuitive picture for the physical origin of the tilt. Essentially, the gyrator acts as a "conveyer belt" for plasmon excitations within the chain, transporting signals in opposite directions with different group velocity. Thus it has in essence the same effect as a Galilei transformation (at least in the continuum limit), except that we can in principle control it locally within a given chain by modulating the value of G as a function of j.

The above ingredient list is in principle sufficient to simulate analog spacetime geometries with finite curvature. Also, while 1D and 2D arrays are likely most straightforwardly implemented on a circuit board, with appropriate 3D stacking one could potentially also reach a higher number of spatial dimensions. The above realizations mark a first central accomplishment of this work, where

(i) we identify a minimal set of circuit elements to realize scalar discrete field theories with any shape of stationary analog spacetime geometry.

For illustration purposes and practicality, we stick to 1D arrays in the remainder of this work. However, even in the $1 + 1$ dimensional problem, there are a number of interesting challenges which we attack in the following. As we argue in more detail below, already for flat spacetime, an overtilt (with a negative energy branch) is not straightforward to realize. As can be seen when comparing Eq. (4.2) with the inductor contribution of Eq. (4.8) an overtilt $|v| > u$ requires *negative* inductances. As a second main result (developed in the subsequent section),

(ii) we show how to realize negative inductances via transient flux drive of Josephson junctions, and thus create overtilted dispersion relations and analog (apparent) event horizons.

[2] Note that the gyrator Lagrangian can be subject to gauge transformations, such that its form is not uniquely determined.

This particular implementation of negative inductances via a flux quench is first of all of fundamental interest, as (contrary to other realizations [Gar+00; RBF22]) we do not require a continuous non-equilibrium drive to maintain the event horizons. As we detail further below, the absence of a well-defined ground state is merely the result of an approximation valid at short times. The exact quantum field theory retains a ground state at all times, which will ultimately be reached again via relaxation processes, thus potentially offering the possibility of a complete wormhole evaporation simulation emerging naturally from the hardware. Moreover, the setup we propose allows for a radical change of the spacetime geometry over only a few lattice sites (and as we show in a moment, even over a *single* lattice bond). With the energy scales of the local charging energy given by E_C and when using Josephson junctions as inductive elements E_J, we would thus (at least in principle) be able to reach Hawking temperatures (as defined above) on the order of $\sim \sqrt{E_C E_J}$ which (taking as a typical transmon qubit frequency the value of 1GHz ~ 10GHz) can yield up to 0.1K ~ 1K (which is above typical cryogenic temperatures).

However, in addition to the already mentioned general stability issues related to the environment, the circuit simulation reveals fundamental lattice-specific spontaneous instabilities (due to complex eigenvalues), which are already present when disregarding the environment. We expect those to impede a straightforward observation of thermal Hawking radiation. Instead,

(iii) we propose to directly probe the spontaneous collapse of systems with apparent event horizons by means of accumulating quantum fluctuations, which we argue to be distinguishable from collapse due to dissipative processes.

At any rate, some of the lattice-specific stability issues can be appreciated on the general level here, others will be shown subsequently for a specific model. On a general footing, we see in Eq. (4.2) that any (constant or spatially dependent) local tilt v (which in our simulation would be implemented by constant or spatially varying gyrator parameters G_j) must equally appear in the $(\partial_x \phi)^2$ term, as the corresponding matrix element g^{11} ($\mu, \nu = 1$ is the space-space component) is proportional to $v^2 - u^2$. In other words, a finite nonreciprocity in the circuit needs to be "countered" by a corresponding inductive interaction, in order to realize actions of the form of Eq. (4.2). Consequently, we would need an according spatially dependent tuning of the local inductance profile L_j which matches exactly with the values of G_j. But first of all, such a perfect fine tuning is realistically not possible, such that the condition $g = -1$ is in general only approximately, but never exactly, fulfilled. Hence, the mapping onto Eq. (4.5) is likewise not exact, and we cannot guarantee a perfect causal decoupling across the horizon, and the closed system might become spontaneously unstable over already short time scales. In fact, below we refrain from a simulation with constant metric determinant g (in fact, we will modify the inductances rather than the gyrator values), such that the systems we consider do not map to Eq. (4.5) in the continuum limit. Furthermore, with the Hawking temperature being defined (at least in continuous field theories) as the derivative of the group velocity (i.e., the surface gravity) at the event horizon, there emerges the curious question of what happens to the observables of the system when considering a very sharp (discontinuous) change of the metric at the horizon, and how such a diverging surface gravity is regularized. In what follows we will provide an answer to that question for lattice simulators.

Moreover, there is a deeper issue that our discrete circuit realization unravels, which is true even if perfect tuning of G_j and L_j would be available. To see this, consider first an (infinite) array where all gyrators have the same parameter $G_j = G$. Here, we can reformulate the nonreciprocal part of the Lagrangian as follows,

$$G \sum_j \left(\phi_j \dot{\phi}_{j+1} - \phi_{j+1} \dot{\phi}_j \right) = G \sum_j \dot{\phi}_j \left(\phi_{j-1} - \phi_{j+1} \right) \ . \tag{4.12}$$

Thus, we see that in order to have the correct counter term in the g^{11} component for the lattice, we actually do *not* need nearest neighbour inductive coupling [as indicated in Eq. (4.8)] but instead *next-to-nearest* neighbour coupling, $\sim (\phi_{j+1} - \phi_{j-1})^2$. As further detailed below, because of this fundamental feature of the gyrator element, nearest and next-to-nearest neighbour inductive couplings have fundamentally different stability properties. In particular,

(iv) we find an important loop hole to the ambiguous black and white-hole nature of lattice event horizons (through an exceptional point in the dispersion relation) leading to a fundamentally different behaviour in the wormhole interior.

Finally, when returning to a spatially varying G_j, we can draw another important conclusion. Namely, for a general gyrator Lagrangian of the form

$$\begin{aligned} &\sum_j G_j \left(\phi_j \dot{\phi}_{j+1} - \phi_{j+1} \dot{\phi}_j \right) = \\ &\quad \sum_j \dot{\phi}_j \left(G_{j-1} \phi_{j-1} - G_j \phi_{j+1} \right) \ , \end{aligned} \tag{4.13}$$

it turns out to be impossible to find exact inductive counter terms: as can be seen in the right-hand side of above equation, the Lagrangian can no longer be factored into simple phase differences (due to $G_j \neq G_{j-1}$). The only possibility to counter the above expression in terms of inductive couplings is to add inductors to ground, and thus abandon charge conservation within the array. While charge leakage to ground is very much a potential reality (especially if the realization of the gyrators is not ideal, leading to additional inductive shunts), nonetheless

(v) we conclude that for generic circuits networks, nonreciprocal interactions cannot be exactly countered by charge conserving inductive interactions.

The breaking of charge conservation (which is physical as it corresponds to leakage to ground) effectively provides a mass term in the theory. In fact, we will include a (finite but very small) mass term in the following, but for a different reason: it allows us to deal with the otherwise problematic zero mode in the boson Hamiltonian.

To summarize, items (i) and (v) have already been fully demonstrated within the above general reasoning, and require no further illustration. Items (ii-iv) on the other hand are now explicitly shown in what follows, by considering a concrete setup.

4.3. Setup

We here show with two example circuit models the capability of circuit arrays to engineer nontrivial dispersion relations with analog wormholes. The first proposed circuit consists of an array of J nodes (with periodic boundary conditions, i.e., $J+1 = 1$), interconnected via Josephson junctions in parallel with 3-port gyrators, as depicted in Fig. 4.1a). The complete Lagrangian of the circuit will consist of three parts, namely a capacitive Lagrangian in Eq. (4.7), a gyrator Lagrangian in Eq. (4.9) and a term for the Josephson junctions $\mathcal{L}_J = \sum_{j=1}^{J} E_J \cos\left(\phi_{j+1} - \phi_j + \phi_{\text{ext},j}\right)$. Here, E_J is the Josephson energy and $\phi_{\text{ext},j}$ is the external flux coupling to each Josephson junction. This flux, and its time-dependent control, will play a pivotal role in what follows.

By standard circuit theory methods [BKD04; VD17; CDT24], we find that the Hamiltonian of this array takes the form

$$\begin{aligned}\mathcal{H} = &\sum_{j=1}^{J} E_{\mathrm{C}}\Big[N_j + G(\phi_{j+1} - \phi_{j-1})\Big]^2 \\ &- \sum_{j=1}^{J} E_J \cos(\phi_{j+1} - \phi_j + \phi_{\text{ext},j}),\end{aligned} \tag{4.14}$$

with the charging energy

$$E_{\mathrm{C}} \equiv \frac{(2e)^2}{2C} \ .$$

The number operator N_j and the phase ϕ_j satisfy the canonical commutator $[\phi_{j'}, N_j] = i\delta_{jj'}$.

As stated in the previous section, the stability of circuits where Josephson junctions connect nearest neighbours nodes and the ones where Josephson junctions couple next nearest neighbour nodes is very different. Therefore, to illustrate their differences the second circuit we study has next nearest neighbour connections via Josephson junctions, see Fig. 4.1b). The Hamiltonian for such a circuit is

$$\begin{aligned}\mathcal{H}' = &\sum_{j=1}^{J} E_{\mathrm{C}}\Big[N_j + G(\phi_{j+1} - \phi_{j-1})\Big]^2 \\ &- \sum_{j=1}^{J} E_J' \cos(\phi_{j+1} - \phi_{j-1} + \phi_{\text{ext},j}) \ .\end{aligned} \tag{4.15}$$

Considering the system at low energies (close to the many-body ground state), the phases on the nodes will approach an equilibrium configuration minimizing the total Josephson junction energy of the array. For sufficiently long arrays, we find either $\phi_{j+1} - \phi_j \approx -\phi_{\text{ext},j} + \delta\phi_{j+1} - \delta\phi_j$ (for $\mathcal{H}$) or $\phi_{j+1} - \phi_{j-1} \approx -\phi_{\text{ext},j} + \delta\phi_{j+1} - \delta\phi_{j-1}$ (for $\mathcal{H}'$). Assuming $E_C < E_J$, the quantum fluctuations around the equilibrium value will be small, $\delta\phi_j \ll 1$. Consequently, the Josephson term in Hamiltonians (4.14) and (4.15) can be approximated by

$$\approx \sum_{j=1}^{J} E_L(\delta\phi_{j+1} - \delta\phi_j)^2 + \text{const.}$$

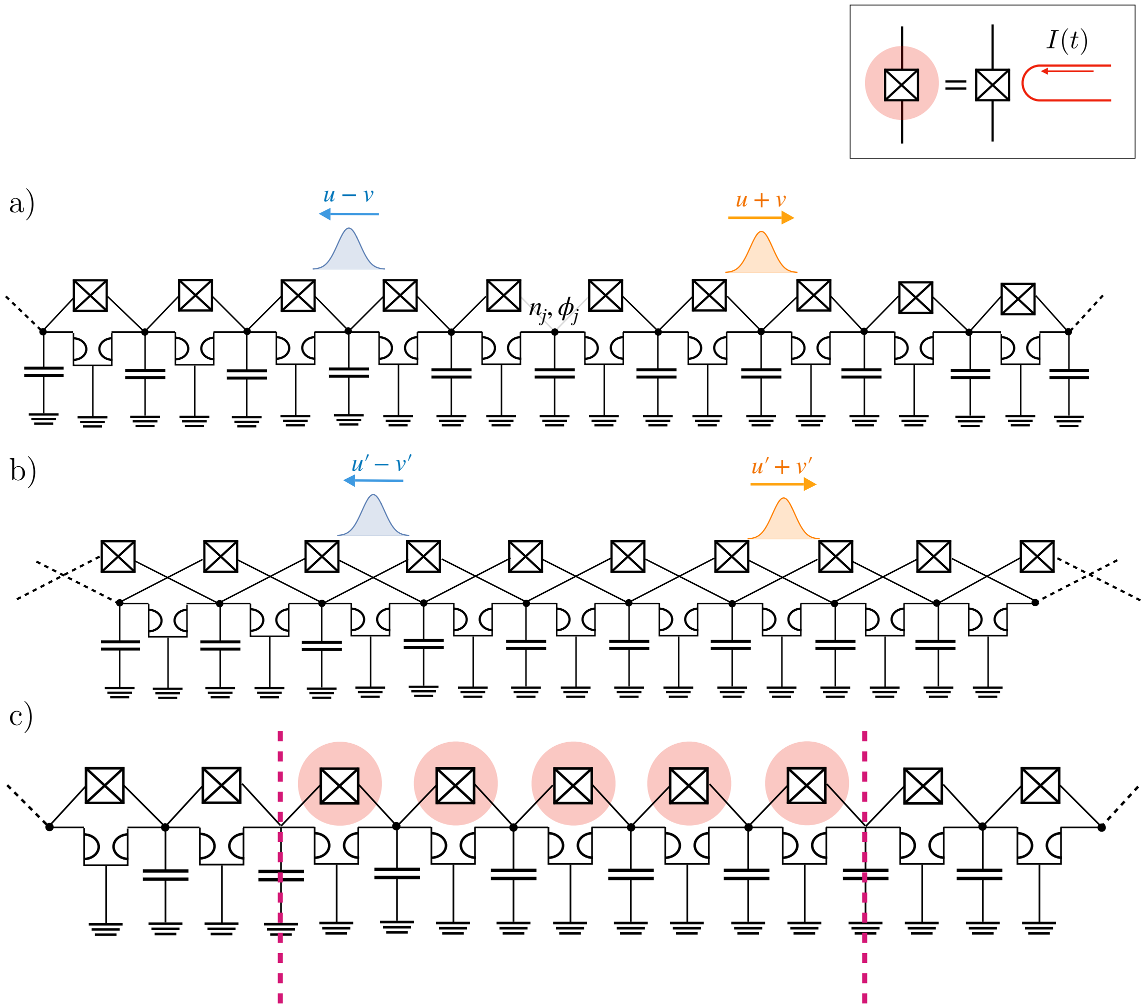

Figure 4.1.: Wormhole simulations with quantum circuits. In circuits a) and b) (nearest and next-to-nearest Josephson coupling, respectively) the presence of gyrators tilts the dispersion relation giving left and right moving wave packets different speeds. The circuit c) is obtained by inverting the signs of a finite connected region inductances of circuit a). This is achieved by a flux quench induced by a localized current (inset), shifting the superconducting phase difference across the junction by π, leading to negative inductance. This creates two boundaries between the normal and over-tilted regions, which act as the apparent horizons. Horizons for the circuit with Josephson junctions connecting next-nearest neighbors b) can be obtained in a similar manner.

$$\approx \sum_{j=1}^{J} E'_L(\delta\phi_{j+1} - \delta\phi_{j-1})^2 + \text{const.}, \tag{4.16}$$

where $\delta\phi_j$ still satisfy the same commutation relations with N_j. The inductive energy is $E_L^{(\prime)} = E_J^{(\prime)}/2$.

With the quadradic approximation of the Josephson energies, the total Hamiltonian describes a noninteracting boson field. Moreover, close to the ground state, the externally applied flux $\phi_{\text{ext},j}$ could be eliminated from the problem. It would therefore seem that neither the nonlinearity of the Josephson junction, nor the external flux play a role. However, as we will show in Sec. 4.4, transient flux-control and the compact cosine behaviour of the Josephson energy will allow us to generate nontrivial features related to quantum gravity. In particular, we will be able to modulate the effective inductive energy E_L highly locally, and in particular, render it negative, allowing for the creation of instabilities that will lead to non-thermal Hawking radiation. Note that the nonlinearity of the Josephson energy was likewise of importance for earlier proposals to measure Hawking-like radiation emerging from soliton excitations in Josephson junction arrays [KHF20]. We will comment on similarities with – but also significant differences to – our approach further below.

For the above conventional non-interacting boson problem, translational invariance allows us to analytically diagonalize the Hamiltonians (4.14) and (4.15), $\mathcal{H}^{(\prime)} = \sum_m \omega_m^{(\prime)} b_m^\dagger b_m$ (where index m goes from $-J/2+1$ to $J/2$), to get the dispersion relations (Appendix C)

$$\begin{aligned} \omega_m &= 2\sqrt{E_C^2\beta_m} + 4E_C G \sin\left(\frac{2\pi m}{J}\right), \\ \omega'_m &= 2\sqrt{E_C^2\beta'_m} + 4E_C G \sin\left(\frac{2\pi m}{J}\right), \end{aligned} \tag{4.17}$$

where b_m ($b_m^\dagger$) are bosonic annihilation (creation) operators satifying $[b_m, b_{m'}^\dagger] = \delta_{mm'}$ and

$$\begin{aligned} \beta_m &= \frac{4E_C G^2 \sin^2\left(\frac{2\pi m}{J}\right) + 4E_L \sin^2\left(\frac{\pi m}{J}\right) + M}{E_C}, \\ \beta'_m &= \frac{4E_C G^2 \sin^2\left(\frac{2\pi m}{J}\right) + 4E'_L \sin^2\left(\frac{2\pi m}{J}\right) + M}{E_C}, \end{aligned} \tag{4.18}$$

where we will set $E'_L = E_L/4$ for the ease of comparing the two spectra in the linear approximation. The quantum number m enumerates the momentum of bosonic excitations, where we can define the wave vector as $k = 2\pi m/J$, such that $\omega_m^{(\prime)} \to w^{(\prime)}(k)$. Note that we have introduced a very small mass term M ($\mathcal{H}^{(\prime)} \to \mathcal{H}^{(\prime)} + M\sum_j \phi_j^2$) to avoid the well-known diagonalization issues with the zero modes. We take whenever possible the limit $M \to 0$. The mass term physically corresponds to a small leakage of supercurrent towards ground, which could, e.g., originate from an imperfect implementation of the gyrator element.

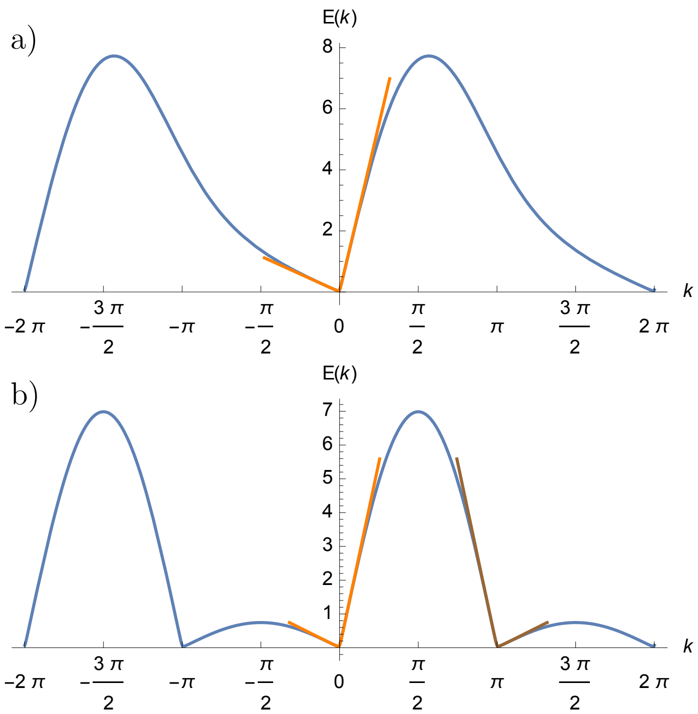

Figure 4.2.: The above two figures show that the low-momentum eigenvalues (blue lines) of the circuit Hamiltonians (4.14) and (4.15) can be approximated by the linear dispersion relation (4.19) (orange lines) at low energies. The branches of the dispersion relation correspond to right and left movers with speeds $u \pm v$. One crucial point about the eigenvalues in b) is that near $k = \pi$ the dispersion relation (brown lines) is the mirror image of the dispersion near $k = 0$, which is a feature that the eigenvalues in a) do not have. Parameters used: $E_\mathrm{C}/E_L = 1.3, E'_L/E_L = 0.25, G = 0.6$, and $J = 50$. To lift the degeneracy at zero energy, a small mass term is used ($\approx 10^{-3}E_L$).

For small k, the system exhibits a linear dispersion relation, [see Figs. 4.2a) and 4.2b)],

$$\omega(k) \approx \omega'(k) \approx 2\sqrt{4E_\mathrm{C}^2G^2 + E_\mathrm{C}E_L}\,|k| + 4E_\mathrm{C}Gk. \tag{4.19}$$

In the relativistic sense, this would correspond to the analog speed of light, where the two branches $k > 0$ and $k < 0$ denote right and left moving signals, respectively [see also Eq. (4.6)]. Importantly, we see in general different analog speeds of light $u + v$ $(u - v)$ for excitations moving to the left, $k < 0$ (right, $k > 0$) [as illustrated in Figure 4.1a) and b)], with $u \propto 2\sqrt{4E_C^2G^2 + E_CE_L}$ and $v \propto 4E_\mathrm{C}G$. A nonzero v corresponds to a tilt of the dispersion relation, which is only possible for a nonzero gyrator, $G \neq 0$, due to the aforementioned "conveyer belt" dynamics.

Moreover, we observe that on this coarse-grained level (small k essentially corresponds to taking the continuum limit of the lattice grid), the two models exhibit the exact same dispersion relation. Note however, that the next-nearest neighbour model hosts a second low-energy point with linear dispersion relation at $k \approx \pi$ [see Fig. 4.2b)]. The dispersion tilt here is always opposite to the one at $k \approx 0$. This feature emerges for the following reason. In the absence of the gyrators, the model $\mathcal{H}'$ has two disjoint low-energy fields for even and odd lattice sites, resulting in a π-periodic Brillouin zone. The gyrators couple these two separate modes, restoring 2π-periodicity with respect to k (due to the alternating tilt), but keeping the two low-energy solutions intact. In essence, while model $\mathcal{H}$ hosts a single low-energy analog light field, model $\mathcal{H}'$ hosts two separate fields with opposite dispersion relation. This detail will play an even more prominent role in what follows.

In order to engineer analog wormholes with event horizons, we need to specifically create a dispersion relation with an *overtilt* where $|v| > u$ – at least in a finite region of the device. Here, our resulting dispersion relation, Eq. (4.19), provides us with a significant challenge: if both the inductive and capacitive energies E_L, E_C are positive, then it can be easily shown that $u > |v|$, independent of the specific parameter values. Consequently, an overtilt must necessarily involve negative capacitances or negative inductances. In the next section, we will explicitly discuss possibilities to render either E_C or E_L negative, and point out in particular, why we expect negative E_L to be the more feasible of the two options.

In the remainder of this section, we proceed by discussing the consequences a negative inductance has on the dispersion relation. As already stated, for small k we thus get an overtilted linear dispersion relation in both models, see Figs. 4.3a) and 4.3b). As the slope of the dispersion relation now has the same sign for both positive and negative k, we get signals propagating in the same direction. If we now join regions with regular ($u > |v|$) and overtilted ($u < |v|$) dispersion relation, we could indeed engineer analog wormholes. But before we embark on that, we need to discuss in detail the behaviour of the dispersion relations, Eq. (4.17), for large k. Namely, when considering the full Brillouin zone (i.e., for $-\pi < k < \pi$), we see that the two models (nearest versus next-nearest neighbour) differ significantly. In particular, for the nearest neighbor coupling, we observe that outside the range $-k_0 < k < k_0$ the dispersion relation becomes complex, see Fig. 4.3a), where k_0 is determined by the condition

$$\sin^2\left(\frac{k_0}{2}\right) = \frac{4E_C G^2 - |E_L|}{4E_C G^2}. \tag{4.20}$$

This transition point is equivalent to an *exceptional point* in the system. Crucially, this finding is in stark contrast to the model circuit where the Josephson junctions connect the next nearest neighbors. Here, for parameter regime $4E_C G^2 + E_L > 0$, we can overtilt the dispersion relation without encountering complex eigenvalues, see Fig. 4.3b).

There are several reasons why both of these models are interesting in their own right. First, let us comment in more detail on stability. In principle, the inversion of inductance (or capacitance for that matter) indicates a spontaneous electrostatic instability. This can be understood already on a much simpler level of a single LC circuit, with a resonance frequency $\sim \sqrt{E_L E_C}$. Swapping the sign of the inductance leads to an imaginary frequency. Note that for transient times, this result is by no

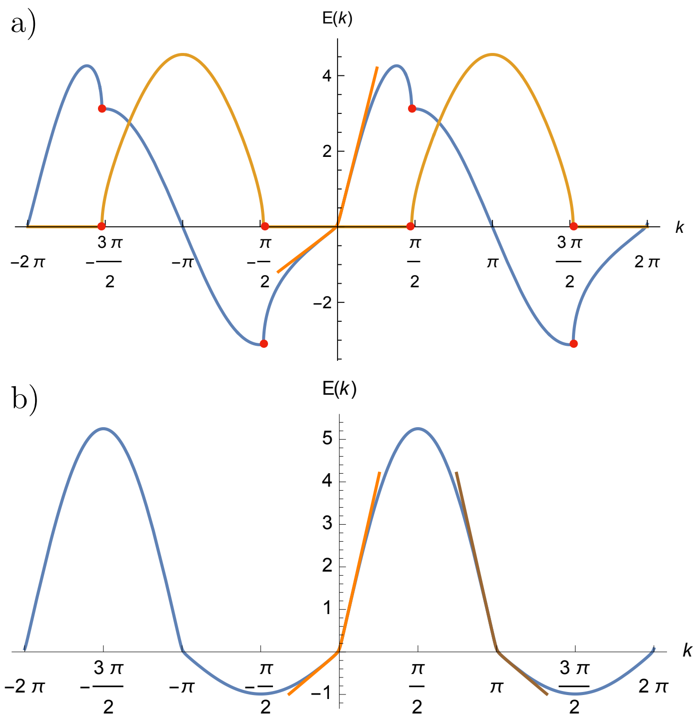

Figure 4.3.: The principle behind the topological loop-hole for black versus white hole horizons in lattice systems via exceptional point. In panels a) and b), we show the complete dispersion of the circuit Hamiltonians (4.14) and (4.15) with negative inductances. When the Josephson junctions connect nearest neighbors, a), the eigenspectrum is complex (blue line represents real part of the eigenvalues and yellow line the imaginary part). The points where the eigenvalues go from real to complex are exceptional points (marked by red dots). Consequently, the spectrum only crosses zero once at $k = 0$, and satisfies the periodicity constraint of the Brillouin zone via a detour in the complex plane. For next nearest neighbor coupling, b), the spectrum is real for all values of k, and crosses zero twice, again with mirror images at $k = 0$ and $k = \pi$. The low momentum eigenvalues (orange line) for both the circuits do show an overtilt, which is required to create a horizon. Parameters are same as in Fig. 4.2, except the signs for E_L and E'_L are flipped.

means problematic (see also Sec. 4.2.1), as such an imaginary frequency corresponds to placing a localized wave function on the tip of an inverted harmonic potential. For transient times, we can by all means obtain physically meaningful results from the Schrödinger equation. In particular, note that such an evolution will result in an exponential blowing up of quantum fluctuations of both canonically conjugate quantities, here, charge and phase (as we will see later also in explicit calculations). This might at first sight seem counterintuitive. The most common situation for generic quantum wave functions is that the uncertainty in one of the two conjugate spaces is inversely proportional to the uncertainty in the other. But note that inverted potentials provide very special wave functions over time that spread both in position (e.g., ϕ) space, as the wave function evolves from the tip of the parabola to both sides, as well as increasing uncertainty in momentum (e.g., N) space, since the particle wave gets more and more accelerated as it rolls down both sides of the inverted parabola. The theory is only problematic in the long-time limit, due to the formal removal of a well-defined ground state. We note that our realization of negative inductances via the inherent nonlinearity of the Josephson effect provides a very neat conceptual realization of instabilities, while (in principle) retaining a well-defined ground state for long times, as we explain in more detail further below. We also note that a recent work [RSB24] has explored a related but distinct concept of negative mass resonators in cQED architectures, by strongly driving a weakly nonlinear superconducting LC circuit [Fan+21], leading effectively to negative susceptibility.

To proceed, we note that in the 1D chain models we consider, there are ways to stabilize the system in spite of negative inductances, in line with the discussion in Sec. 4.2. Indeed, the gyrators play the pivotal role for stabilization: in the Hamiltonians of Eqs. (4.14) and (4.15), when we expand the term in the first line $\sim E_C$, we get an effective inductive element due to a nonzero G, $\sim E_C G^2(\phi_{j+1} - \phi_{j-1})^2$. This is an effective inductive contribution due to the gyrator, which is guaranteed to be positive even when $E_L < 0$ (as long as $E_C > 0$). But as already foreshadowed in Sec. 4.2.2, this effective inductive contribution couples next-nearest neighbour sites. Hence, a negative next-nearest inductor [Eq. (4.14)] can be exactly compensated by a positive next-nearest neighbour contribution of the gyrator. The negative nearest neighbour inductor model [Eq. (4.15)] on the other hand cannot exactly be compensated by the gyrators, hence the presence of the exceptional point.

Let us now take a bit of a more formal perspective on the above observation for generic wormhole simulations, which will allow us to demonstrate one of the central results of this work, see also item (iv) in Sec. 4.2.2. Namely, there is a simple topological connection between overtilted spectra, Brillouin zone sizes, and exceptional points. For discrete lattice implementations the dispersion relation is always 2π periodic in k. Crucially, an overtilted spectrum means that the energies cross from positive to negative values at the transition points $k = 0, 2\pi, \ldots$. If the spectrum is real for all k, then periodicity in momentum space always guarantees that an overtilted spectrum near a certain value of k must have an overtilted partner at another value of k with *opposite tilt direction*, as a periodic spectrum must traverse the zero-energy line an even number of times. Consequently, for any lattice implementation, it seems unavoidable that what appears like a black hole horizon near one value of k, must necessarily have a white hole horizon partner at another value of k. This fact has already been pointed out in the context of analog black-hole simulations in tilted Weyl semimetal structures [De +21]. Our next-nearest neighbour model confirms this expectation, where the overtilt point at $k \approx 0$ has an inverted partner point at $k \approx \pm\pi$, see Fig. 4.3 b). These two k points can be individually addressed when preparing, e.g., Gaussian wave packets centered either around $k \approx 0$ (wave packets that are smooth in j space) and $k \approx \pm\pi$ (wave packets with alternating even-odd signs in j space).

Crucially, the nearest-neighbour model provides an intriguing loop hole: here, the overtilt at $k \approx 0$ has no partner point with inverted tilt, very simply because the dispersion relation satisfies the periodicity constraint in k by taking, in a sense, a "detour" in the complex plane – by courtesy of the exceptional point. Consequently, the spectrum crosses the zero energy line only once. We are thus able to conclude that there is after all a case, where black and white hole horizons can be created independently in a lattice. This comes at the cost of a spontaneous instability within the overtilted region, which, importantly, is present even in the absence of an event horizon. This finding will be of great importance when interpreting the origin of radiation in the presence of event horizons in Sec. 4.5 below.

4.4. Realizing negative inductance through quench

As noted above, an overtilt in the dispersion relation is realized by means of either negative capacitances or negative inductances. We here present ideas for the engineering of both features, and then argue, why we expect the latter to be more feasible, thus demonstrating claim (ii) in Sec. 4.2.2,

Negative (and other nonlinear) capacitances are an interesting topic within quantum circuits, which date back to various pioneering ideas by Little [Lit64] and Landauer [Lan76], and have recently been a focal point of research, either in the form of ferroelectric materials [CJG15; Zub+16; Hof+18; Hof+20], or capacitively-coupled polarizers inducing pairing in quantum dots [Ham+16; Pla+18]. Specifically within the circuit QED context, it has recently been proposed that negative capacitances exist in the sense of an emf-induced renormalization [RD22], or that the charge in the quantum phase slip energy contribution can be fractionalized and thus rendered incommensurate [Her+23a; Her+23b]. There is, however, the problem that negative capacitances correspond to an electrostatic instability, and are thus only meaningful either as partial capacitances (where another capacitance in parallel guarantees total positivity on a given charge island) or in a transient regime. Since we are interested in the latter (after all, Hawking radiation is manifestly a transient feature), this means that the capacitance should have to be tunable on very fast time scales, which seems challenging, especially on the small scales of the here proposed circuit QED architecture.

This is why we move on to ideas on how to bring about a transient behaviour within the inductive (Josephson junction) element. Remember that we focus on a regime of $E_J > E_C$ where the cosine of the Josephson energy can be approximated as a parabola with the inductive energy $E_L \sim E_J$ of an effectively regular linear inductor (rendering the resulting plasmon field effectively non-interacting, as shown above). Nonetheless, we can exploit the nonlinear inductive behaviour. Suppose there is a mechanism, allowing for a fast, transient switch from $-\cos(\phi_j - \phi_{j-1})$ (e.g., for the nearest neighbor model) to $+\cos(\phi_j - \phi_{j-1})$. If that switch occurs sufficiently fast, the circuit degrees of freedom have no time to adjust, such that the many-body wave function immediately after the switch remains localized on what is now the *maximum* (and not the minimum) of the cosine. Expanding for small phase differences localized around said maximum, we can realize a sign switch of the inductive energy, $E_L \to -E_L$, leading to the sought-after overtilt in the dispersion relation (see the orange lines in Fig. 4.2). Specifically, in the next section, we discuss the possibility of applying an inverted inductance only in part of the system to create event horizons separating regions with $u < |v|$ from unquenched regions with $u > |v|$.

Our proposal, thus, requires a mechanism to locally address the Josephson junctions in a way to create connected regions with inverted inductance. We note that so-called tunable $0 - \pi$ junctions are a subject of ongoing research and have multiple proposals for their implementation, including the theoretical proposal about Josephson junctions with a high-spin magnetic impurity sandwiched between two superconductors [PB18], experimental realization in ballistic Dirac semimetal Josephson junctions [Li+19] and another experimental realization in Indium antimonide (InSb) two dimensional electron gases [Ke+19].

We here point out a feasible alternative, where inductance inversion is also possible for regular superconductor-insulator-superconductor Josephson junctions. Namely, a nearby current source can likewise induce a phase shift of π. This idea is based on the results of Ref. [RD22] where a gauge invariant formulation of time-dependent flux driving was derived. Gauge aspects are of utmost importance to understand how time-dependent flux is allocated in circuits involving multiple Josephson junctions, such as SQUIDs or junction arrays [YSK19b; RD22; KR23]. Previous to Ref. [RD22], it was expected that the ordinary lumped element approach to circuit QED is valid in the presence of time-dependent flux. In this standard framework, it was recently shown [YSK19b] that the allocation of the time-dependent flux within the device (and thus, of the induced electric fields) is given by the capacitive network of the involved charge islands. If this observation were generally true, it would be difficult to locally address certain junctions with high local precision, unless the capacitive network would be engineered accordingly. However, as shown in Ref. [RD22], the connection between flux allocation and the capacitive network is valid only in special cases; in general, both device geometry and magnetic field distribution lead to a highly nontrivial flux allocation.

We here adopt this principle to show that the individual junctions can be addressed by small current loops, (one loop per junction) where a time-dependent drive (inset in Fig. 4.1) provides a shift inside the Josephson energies of the form $\cos(\phi_{j+1} - \phi_j + \phi_j^{\text{ext}})$,

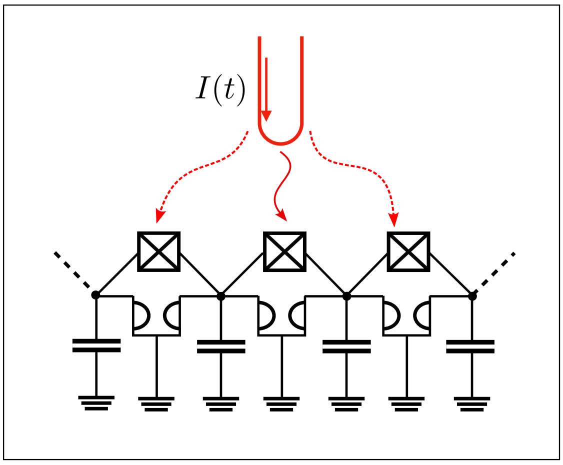

Figure 4.4.: Illustration of non-local effects of the current loop flux drive.

where

$$\phi_j^{\text{ext}} = \frac{2\pi}{\Phi_0} \int_{\mathcal{L}_j} d\mathbf{l} \cdot \mathbf{A} \ . \tag{4.21}$$

Here Φ_0 is the flux quantum and $\mathbf{A}$ is the vector potential in the irrotational gauge [YSK19b; RD22] accounting for the magnetic field emitted by the current carrying loop sources. Note that since the magnetic field decays only as a power law, one may have to take into account non-local effects, that is, the current loop at junction j influences not only the phase drop at junction j but also at the other junctions j', see Fig. 4.4). We can generically write down the equation

$$\phi_j^{\text{ext}}(t) = \sum_{j=1}^{J} \alpha_{j,j'} I_j(t) \ , \tag{4.22}$$

where the matrix α contains the information about the geometric details of the circuit, and accounts for the screening of the magnetic field (Meissner effect) as well as the screening of the induced electric field (Thomas-Fermi screening). In order to know what exact current pulses need to be applied in order to create a desired target phase profile ϕ_j^{ext} (e.g., $\phi_j^{\text{ext}} = \pi$ within a given connected interval, $j_0 < j < j_1$, and $\phi_j^{\text{ext}} = 0$ everywhere else, which gives the black and white hole horizons, see sections below), one simply needs to invert the square matrix α. Generally, we note that for our purposes, the precision requirements are not so stringent: as long as deviations from the target phase profile are small (with respect to π), the inductances in the array are still inverted, resulting in the desired apparent event horizon.

The computation of matrix α is in general a complicated numerical task. We can however provide a rough estimate by assuming the junctions to be arranged in a straight line, and applying the Biot-Savart law (similar in spirit to Ref. [Riw21]). To this end, we assume that each current-carrying wire j is described by a small current

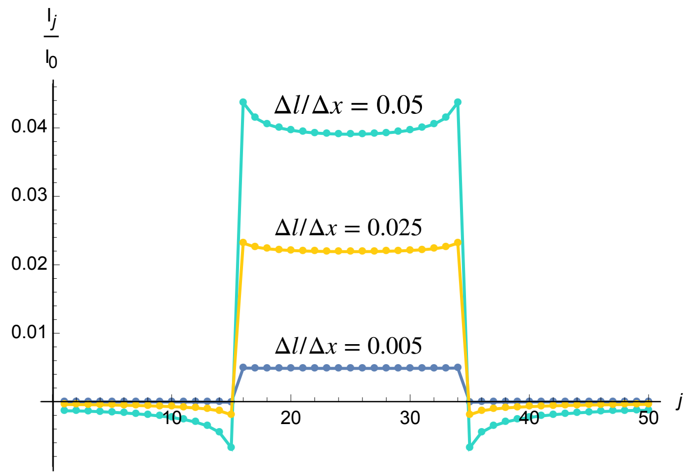

Figure 4.5.: Plot of current profiles for different parameters, in order to create the target phase shift profile of exactly π within a connected region in the junction array (from $j = j_0$ to $j = j_1$). We have plotted three current profiles, that were obtained for a system with 50 sites with $j_0 = 15$ and $j_1 = 35$, with different ratios of Δl to Δx as shown in the graph. The parameter R does not have a significant effect on the nature of the current profile, only on the magnitude of the ration I_j/I_0, hence we set $R/\Delta x = 1$.

element of length ΔL. For small current loops with radius R, we can simply set $\Delta L \sim R$ [3]. Assuming Coulomb gauge (equivalent to the irrotational gauge, up to screening of induced charges on the superconducting surfaces [RD22], which we here neglect for simplicity) we have to solve $\nabla^2 \mathbf{A} = -\mu_0 \mathbf{j}$ with the current density $\mathbf{j}$ for a small current carrying element. Assuming an infinitesimal, delta-like current element $\mathbf{j} \sim \delta(\mathbf{x})$x, and plugging the resulting $\mathbf{A}$ into Eq. (4.22), we find

$$\alpha_{j,j'} \approx \frac{1}{I_0} \frac{R}{\sqrt{\Delta x^2 (j - j')^2 + \Delta l^2}}, \tag{4.23}$$

where Δx is the separation between Josephson junctions, and Δl is the separation between current loop j and junction j. The characteristic current I_0 is given as $I_0^{-1} = \mu_0 \mathcal{L}/(2\Phi_0)$, where $\mathcal{L}$ is the length of path $\mathcal{L}_j$ in Eq. (4.22). It represents the size of the fine structure containing the Josephson junction (Niemayer-Dolan bridge). For a typical size of $\mathcal{L} \sim 10\mu m$, we find $I_0 \sim 10\mu A$ (which is at the upper bound of the current that can usually pass through flux lines). Note that this is a crude upper bound for I_0. Very likely, I_0 is reduced significantly due to screening of the electric field which has here been neglected. We therefore expect that a flip of the phase by $\sim \pi$ is feasible. The other central figure of merit is the speed with which the

[3] Note that the most common designs for flux control, the loops have a radius larger than the separation of the input and output lines, such that the representation of the source as a small current carrying element is strongly simplified. A current source with ring geometry could be more precise, but complicates the here presented estimate.

phase flip can be performed. Defining the ramping time from zero current to target current for a single flux line as Δt_I, the phase flip is guaranteed to be nonadiabatic for $\sqrt{E_C E_J}\Delta t_I < 1$. This requires either the use of sub-GHz qubit designs, similar in spirit to a recent proposal in Ref. [Sel+23], or ultrafast (~ 100 gigasamples per second) arbitrary waveform generators. The latter may cause problems with usual Al-based architecture, but improvements were very recently demonstrated in connection with Nb-based circuits [Anf+24].

For the matrix given in Eq. (4.23), we can explicitly compute a required current profile that needs to be applied in order to swap the phases by $\pm\pi$ within a connected part of the 1D chain. Blue dots in Fig. 4.5 show that if $\Delta l \ll \Delta x$, α is almost perfectly diagonal, such that there is a one-to-one correspondence between the desired target phase profile and the required current profile that has to be applied to the individual loops. Note however that the onset of non-local effects may play a role even for (moderately) small $\Delta l/\Delta x$ (orange and brown dots in Fig. 4.5), where we need to apply a slightly nonlocal current profile to have a sharp, local switch from positive to negative inductances within the 1D chain.

Note that the flux drive may in general not only couple to the Josephson junctions but also to the gyrators shunted in parallel. In accordance with Ref. [RD22], such a stray coupling can be neglected if the surface charges induced by the time-dependent flux drive (these are the charges screening the induced electric field) are mostly allocated near the junction. We expect this scenario to be plausible if junction and gyrator are sufficiently spatially separated with respect to the length scale on which the magnetic field varies. If such a spatial separation cannot be guaranteed, then one would have to take into account the microscopic and geometric details of the gyrator which is beyond the scope of this work.

To conclude this section, we point out similarities and differences to previous proposals creating analog event horizons and Hawking radiation in solid state systems. Specifically, the analog Hawking radiation previously predicted in Josephson junction arrays [KHF20] relies on the creation of solitons, where within the finite extension of the soliton (over many lattice sites), the inductance can likewise be regarded as effectively negative within the soliton profile. The procedure we produce on the other hand involves creating $\pm\pi$ shifts on a connected series of junctions, which in essence corresponds to a tightly packed generation of “half”-solitons with the width of a single lattice site. Our system thus seems arguably much less stable. But first, as indicated already, the nonreciprocity provided by the gyrators allows for a stabilization of the system even with inverted inductors, due to an extra (positive) inductive contribution. Second, the extra tilting mechanism provided by the gyrators allows for the explicit realization of arbitrary (on-demand) spacetime geometries, and in addition, the explicit creation of wormholes with (in principle) distinguishable black and white hole horizons. As for the evolution of the unstable system beyond transient times, we provide some thoughts in Sec. 4.6. Another important difference is that we here have in principle perfect control on the *position* of the horizon, contrary to the solitons studied in Ref. [Nat+09; KHF20], which are autonomously moving with respect to the lab frame. Moreover, we can create an event horizon with the precision of a single lattice site. This is in contrast to all other analog Hawking radiation proposals (cold atoms, circuits, tilted Weyl semimetals), where the analog metric always changes over a finite width (a healing length). This is an interesting caveat specifically regarding the existence of a well-defined Hawking temperature, or more generally, how to make sense of horizons with diverging surface gravity, as already indicated in Sec. 4.2.

4.5. Analog horizons via flux quench

Once the optimization problem of the current profile has been solved, the sign of the Josephson energy can be flipped for a region of the circuits described by the Hamiltonians (4.14) and (4.15), resulting in two horizons in the circuits (Fig. 4.1c). In the presence of horizons, the energy spectrum is in general complex for both nearest and next-to-nearest neighbour implementations.

The presence of tilted dispersion relations and horizons can be probed by means of injecting wave packets within the chains, and probe their time of flight. For example, within an overtilted region, wave packets can only move in one direction. At a white hole horizon, an incoming wave packet comes to a stand still. Such features represent a first experimentally available signature of the nontrivial spacetime geometry. Note that for the time evolution of the wave packets, the distinction between nearest and next-to-nearest neighbour coupling is not that important, under the condition that the experimenter is able to prepare wave packets close to $k \approx 0$ or $k \approx \pi$. These two types of excitations clearly distinguish between black and white hole horizon as they probe only a local part of k space. In addition, aspects of the wormhole stability (or instability) are not immediately visible in the wave packet amplitude (until the moment when the evaporation starts changing the spacetime geometry itself, see also Sec. 4.6 below).

We therefore present in addition a more sophisticated measurement which is able to probe radiation due to instabilities in a more direct fashion. Namely, this section examines how to characterize the system via two point charge and phase correlation functions. As foreshadowed above, while for a stable system, quantum fluctuations remain bounded over time, they start to diverge in the presence of complex eigenvalues. In the quadratic approximation, see Eq. (4.16), it is convenient to express the charge and phase operators for the circuits (4.14) and (4.15), in terms of bosonic operators

$$N_j = \frac{i}{\sqrt{2}}\left(a_j - a_j^\dagger\right), \tag{4.24}$$

$$\phi_j = \frac{1}{\sqrt{2}}\left(a_j + a_j^\dagger\right), \tag{4.25}$$

that obey the following commutation relations $[a_j, a_{j'}^\dagger] = \delta_{jj'}$, $[a_j, a_{j'}] = 0$. Now, calculating the two point correlation functions for charge and phase operators turns into calculating the correlation functions of the form $\langle a_j(t) a_{j'}^\dagger(t')\rangle$, $\langle a_j^\dagger(t) a_{j'}^\dagger(t')\rangle$, $\langle a_j(t) a_{j'}(t')\rangle$, and $\langle a_j^\dagger(t) a_{j'}(t')\rangle$.

We are going to calculate these correlations using two methods: 1) direct diagonalization and 2) an extension of Klich's determinant formula [Kli02]. The reason for the multi-pronged approach will be explained in detail below. To summarize, 1) is in principle very straightforward to implement and program, and is more versatile, as it would allow computing all types of observables, not only correlations. But diagonalization is not applicable in the presence of exceptional points, which is where method 2) comes into play, since it only requires exponentiation of the matrix with exceptional points.

As previously stated, once the system has been quenched, its state is in a highly excited state, were the new ground state is removed from the theory (a well-defined procedure for times sufficiently close to the quench). In order to anchor the theory to a well-defined ground state (necessary to compute observables in a well-defined way), we choose to perform computations with respect to the ground state of the unquenched system. Since the diagonalization of the quenched Hamiltonian is being performed with respect to a state that is in general not its eigenstate, we will need a generalised version of bosonic Bogoliubov transformations. These transformations are discussed in Appendix D.

Implementing the Bogoliubov transformations on the quenched Hamiltonian, mentioned in the previous paragraph, requires diagonalizing a non-Hermitian matrix. This can pose a problem if the matrix has defective eigenvalues (exceptional points). We therefore suggest another method of calculating the correlations after the quench. Consider the following way to write a two point correlation

$$\begin{aligned}\left\langle a_i^\dagger(t)a_j(t)\right\rangle &= \partial_\chi \left\langle e^{\chi a_i^\dagger(t)a_j(t)}\right\rangle_{\chi=0} \\ &= \lim_{\beta\to\infty}\frac{\mathrm{Tr}\left(e^{i\mathcal{H}_> t}e^{\chi a_i^\dagger a_j}e^{-i\mathcal{H}_> t}e^{-\beta\mathcal{H}_<}\right)}{\mathrm{Tr}\left(e^{-\beta\mathcal{H}_<}\right)},\end{aligned} \tag{4.26}$$

where $\mathcal{H}_<$ and $\mathcal{H}_>$ are the unquenched and quenched Hamiltonians respectively. The many body traces in the above expression can be calculated by an extension of Klich's trace-determinant formula. The original formula was introduced to calculate the trace of many body operators by replacing it by a determinant of the corresponding first quantized operator [Kli02]. The extension of this formula is described in appendices E and F. This approach bypasses the problem posed by defective eigenvalues but it is also considerably slower than diagonalization for numerics, hence limiting the size of the systems we can work with. Another important remark: in the derivation (Appendix E) we have to assume the existence of a ground state for a non-Hermitian operator, which is not guaranteed. For some context about diagonalizing quadratic bosonic non-Hermitian operators we also refer the reader to Ref. [KH23], where the concept of third quantization [Pro08] was extended to the bosonic Linblad equation. In Ref. [KH23], the existence of a ground state (or more appropriately, a non-equilibrium steady state) is always guaranteed due to the form of the Lindblad equation. Crucially, we do not have this constraint.

The system we will study here has fifty sites ($J = 100$) with the wormhole located between $j_0 = 30$ and $j_1 = 70$. For convenience, we impose periodic boundaries in position space (i.e., the 1D chain is closed into a loop). The parameters of the system are $|E'_L| = |E_L| = 3.42E_C$, $G = 2.4$ and $M = 3 * 10^{-4}E_C$. As already pointed out, in each of the following figures of correlation functions the result could be obtained by both diagonalization and the generalized Klich determinant. The time steps in the following plots are $\delta t = 0.0031E_C^{-1}$ for the circuit with nearest neighbor coupling and $\delta t = 0.031E_C^{-1}$ for the next-to-nearest neighbor coupling.

First, let us examine the plots of correlation functions for the circuit with only nearest neighbor coupling, Figs. 4.6 and 4.7. We see that both phase and charge quantum fluctuations diverge after the quench. The system has two boundaries (red dotted lines) between the wormhole and the normal regions, that act as the horizons (located at j_0 and j_1). If we initialize low energy excitations (for this circuit this means excitations near $k = 0$) in the region with overtilted dispersion, they move from the left horizon to the right horizon, hence we label them as the black and the white hole horizon respectively. The black hole horizon radiates away with time, as can be inferred by the accumulation of quantum fluctuations near it with time (which indicates presence of radiation), while the white hole horizon does not radiate. This explicitly confirms the previously discussed fact that for the nearest neighbour system, black and white hole horizons are distinguishable. The wormhole region also starts radiating due to the presence of the exceptional point (as likewise already discussed in Sec. 4.3). We observe that the decay in the wormhole interior is much faster than the one induced by the presence of the horizons, which leads to the correlation functions growing much more rapidly *inside* the wormhole, before the black hole horizon show any appreciable decay. Overall, the above thus illustrates the possibility to create lattice simulations of wormholes with distinguishable black and white hole horizons, at the cost of a strong instability of the wormhole interior.

Now, let us focus on the circuit where Josephson junctions connect next nearest neighbors. Low-energy excitations in this circuit can be either near $k = 0$ or $k = \pm\pi$. For excitations (inside the wormhole region) near $k = 0$, similar to the previous circuit, the left boundary (j_0) acts as the black hole horizon and the right one (j_1) as the white hole. In contrast, for excitations near $k = \pm\pi$ the left boundary acts as the white hole horizon and right boundary as the black hole. This symmetry is also reflected in the correlation plots in Figs. 4.8 and 4.9, where we can observe both horizons radiating away identically. Also, the only instability in this circuit is due to the horizons, leading to a much slower collapse.

We can contrast above findings with a numerical calculation on a lattice with increasingly smooth variation of circuit parameters. Naively one would expect that there exists a continuum limit where the lattice theory maps back to the continuous Lagrangian (see Eq. (4.1)), where stable solutions exist (non-complex eigenvalues) and where horizons are unambiguously either black or white holes. Our calculation reveals the following (see Appendix G): while solutions with real-valued eigenfrequencies exist (reproducing thermal Hawking radiation) there remain two caveats. First of all the black/white hole ambiguity remains for the next nearest coupling model – giving rise to radiation close to both $k = 0$ and $k = \pi$ sectors. Secondly, the Boltzmann factor (expressing Hawking radiation) receives a renormalisation that depends

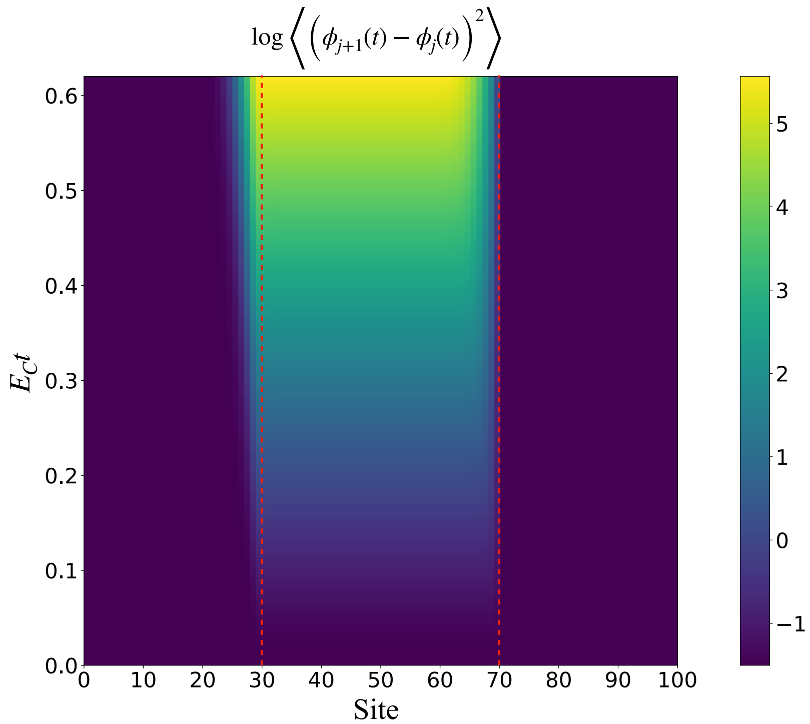

Figure 4.6.: Time evolution of quantum fluctuations of phase difference for a system with Josephson junctions connecting the nearest neighbors. Red dotted lines denote the position of the apparent horizons, i.e., boundaries between the wormhole and normal regions. Here, the fluctuations visibly distinguish between a pure black (pure white) hole horizon, where quantum fluctuations accumulate (or not). More over, the interior between the two horizons is here unstable, such that quantum fluctuations diverge immediately within the entire wormhole region.

strongly on the details of the discretisation, which likewise cannot be removed by simply letting the lattice constant go to zero. Overall we can distinguish three types of field theories, which are all demonstrably distinct from one another. Lattice theories can either be considered in an unstable regime where parameters change abruptly with respect to the lattice constant, or a stable regime with smooth changes. However even the latter does not simply map to the continuous model.

4.6. Perspective on wormhole evaporation over long times and path to quantum inductors

As shown in the previous section, charge and phase fluctuations accumulate very rapidly due to the fundamental instability inherent to the wormhole horizons or interior (in case of nearest neighbour inductive coupling). In particular, the more the system accumulates charge and phase fluctuations over time, the more the quadratic

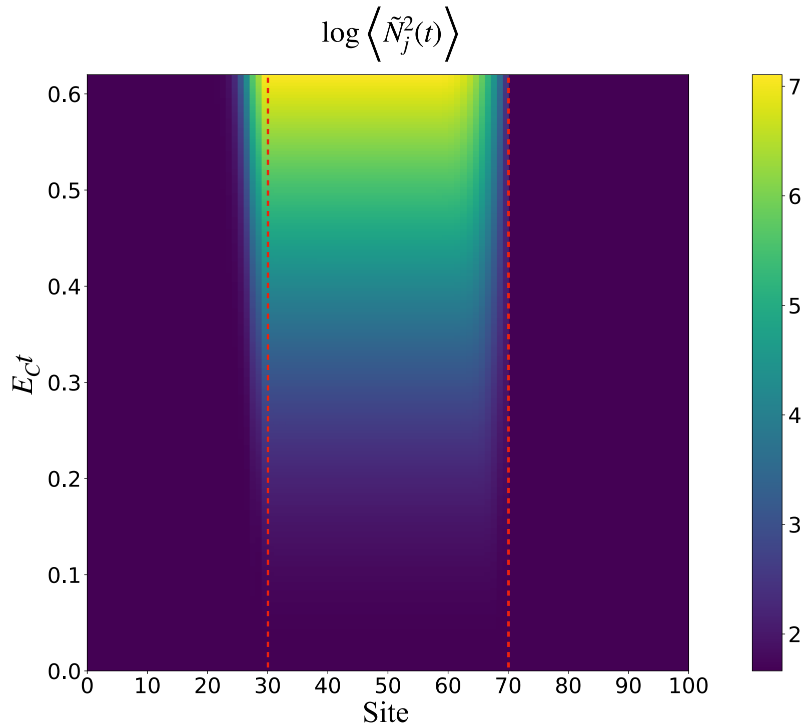

Figure 4.7.: Time evolution of quantum fluctuations of conjugate charge for a system with Josephson junctions connecting the nearest neighbors.

approximation of the Josephson energy becomes inaccurate, such that predicting the system dynamics for long times becomes a much harder task (as the system can no longer be approximated by non-interacting bosons). This is well beyond the scope of the present work. We nonetheless find it illustrative to speculate on a qualitative level about the long term fate of the wormhole – especially as it allows us to distinguish between intrinsic (spontaneous) collapse, and dissipative relaxation. In addition, some of the resulting concepts provide an interesting segue to the subsequent idea: quantum superpositions of the spacetime geometry.

To this end, let us take into account interactions with an environment. For the sake of simplicity and concreteness, we consider the phase difference $\phi_j - \phi_{j-1} + \phi_{\text{ext},j}$ across a single junction. At the beginning of the wormhole quench, this phase difference is either localized around 0 (minimum of the cosine, if the junction is positioned outside the wormhole) or around $\pm\pi$ (maximum of the cosine, inside the wormhole). In the presence of the instability, the quantum fluctuations of this phase difference blow up over time, as shown in the previous section. Now suppose that the environment entangles (either weakly or strongly) with the current across this junction. This means that the phase difference gets spontaneously projected onto a more localized state. Notably, this type of environment-induced process thus *diminishes* quantum fluctuations. We note that the same picture holds in perfect analogy for the accumulation of charge noise quantum fluctuations, respectively, the reduction thereof by a dissipative

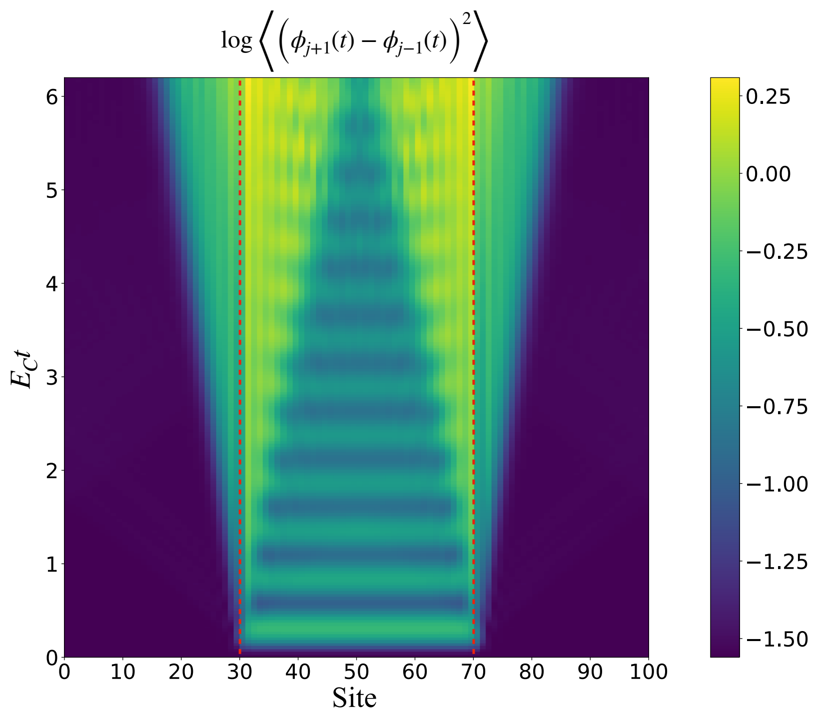

Figure 4.8.: Time evolution of quantum fluctuations of phase difference for a system with Josephson junctions connecting the next-nearest neighbors. Here, (and contrary to Figs. 4.6 and 4.7) both horizons have black as well as white hole character, such that the two horizons are not easily distinguised when considering the spatial dependence of the fluctuations. On the other hand, the wormhole interior is here (at least initially) stable, and quantum fluctuations grow only from the horizons outwards.

process extracting information about the charge.

To proceed, note that the location of the wave function now is no longer at 0 or π, but can be (with a finite probability) at a certain distance from the minimum or maximum. With the new location updated, we again quadratically expand the cosine around the new peak position of the phase difference. Importantly, due to the cosine behaviour of the junction the resulting effective inductance is now different (the curvature of the cosine obviously changes as a function of the position at which it is calculated). Thus, as time progresses, and the phase difference starts to classically diffuse after repeated environment-induced measurements, the effective inductance at a given junction likewise fluctuates classically. At this point, the impact of such dissipative processes could likewise be detectable in time-of-flight measurements of wave packets within the array. At any rate, the most likely long-term outcome is that all phase differences relax to the ground state, equivalent to the complete evaporation of the analog wormhole. We note that for a system on a ring (with periodic boundaries), or a system with a finite mass term (Cooper-pair leakage to ground), the emergence of soliton states might be a possibility.

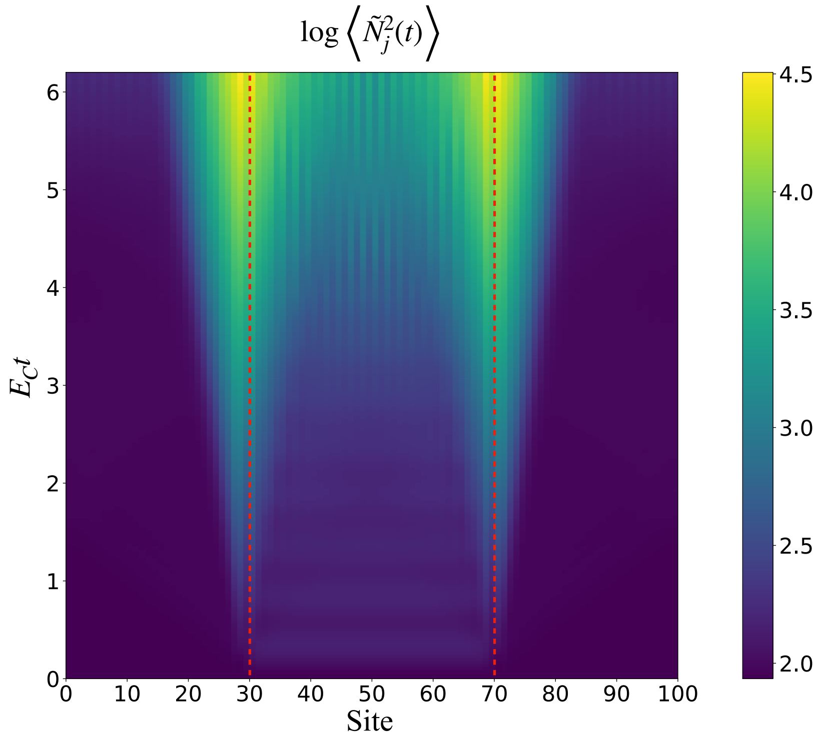

Figure 4.9.: Time evolution of quantum fluctuations of conjugate charge of a system with Josephson junctions connecting the next-nearest neighbors.

Let us repeat that even though the environment will undoubtedly have a big impact on the system dynamics (especially beyond the immediate transient time scale), the experimental signatures could not be more different. Analog Hawking radiation leads to an increase of *quantum* fluctuations, whereas the environment induces *classical* fluctuations. Thus, the observation of the former can distinguish between how the system intrinsically reacts to the creation of an instability, as compared to the impact of external perturbations.

To conclude this section, we consider the very hypothetical case of negligible coupling to the environment, as it reveals an interesting additional idea which we pursue in the remainder of this work. If we assume that the build-up of quantum fluctuations of the phase could progress unimpeded over longer times, the nonlinearity of the Josephson energies results not in classical fluctuations of the effective inductance (as in the previous paragraph), but in a system that has to be interpreted as being in a *quantum* superposition of different effective inductances – a form of quantum superposition of the spacetime geometry itself. However, within the above considered setting, this effect is likely not to survive for very long due to environment-induced decoherence of the quantum fluctuations, and even for a highly protected system, it would be hard to analyse the effect in an unambiguous way. This serves as the motivation for the next part of this project, which is not included in this thesis. We modify the idea of quantum superposition of different effective inductances by not relying on instabilities (and thus not requiring any ultra-fast quenches), but instead on more general notions of Josephson junctions with multiple minimas. This endeavour will on the one hand introduce the notion of a quantum inductance, and with it, a likely more stable version of a quantum superposition of the analog spacetime. As is shown in Sec. VII of [Jav+24] there exists protocols allowing classical signals to entangle with quantum spacetime, marking a highly non-trivial form of backaction between fields and the spacetime they traverse.

4.7. Conclusions and outlook

In this chapter of the thesis we have proposed using quantum circuits to implement analog horizons. Even though it is a well explored concept in solid state systems in general, we here explicitly demonstrate the capacity of superconducting circuits to emulate arbitrary spacetime configurations. By identifying a minimal fundamental set of necessary circuit elements, we further unravel a number of surprising findings pertinent to lattice systems, which allow in particular to create horizons where the change in metric parameters happens at trans-Planckian length scales, allowing us to disentangle the effect of a finite healing length from the effect of a horizon – and in doing so, exploring the extreme regime of horizons with diverging surface gravity. To implement the analog horizons in a quantum circuit, we proposed a general way of creating negative inductances with Josephson junctions transiently driven by nearby current loops. We further uncovered two subtly distinct ways to engineer a region with overtilted dispersion relation, either with inductive coupling of nearest or next-to-nearest neighbour nodes. While for the latter, horizons have a combination of black and white hole character (as is the most usual case in lattices), the former [Eq.(4.14)] hosts two distinct kinds of horizons, one that acts purely as a black hole horizon and the other as a white hole horizon. For this second type of circuit, it is not only the horizons, but also the region between the horizons (wormhole interior) that is unstable due to the presence of an exceptional point. This instability also contributes to the observed radiation (in addition to the evaporation of the horizons) as can be confirmed by tracking the quantum fluctuations of phase difference and conjugate charge with time (Figs. 4.6 and 4.7). In addition to Bogoliubov diagonalization, we used an extension of Klich's trace-determinant formula to obtain the correlation functions numerically. The proof of this extension remains elusive for a general operator, but in the parameter regime where the generalised Bogoliubov transformation is applicable, the results of both numerical methods agree.

In this work, in addition to standard circuit elements, we have also included elements that are still being developed experimentally (such as quantum gyrators), or introduced a new way to realise effective negative inductance, which, although it is based on existing elements and ideas such as Josephson junctions and flux drive, are here proposed to be operated in previously unexplored regimes. We here therefore point at feasible small scale experimental test that can act as proof of principle for the basic physical principles behind the considered physics. For instance, our proposal can be tested on a single transmon, where the qubit frequency becomes imaginary $\sqrt{E_J E_C} \to \sqrt{-E_J E_C}$ for transient times. The resulting accumulation of phase or charge quantum fluctuations (or limits thereof due to coupling to the environment) can thus be tested in an "imaginary" qubit device. Such a study might be also of some fundamental interest, when extending the description of the junction beyond the quadratic approximation, where the expansion around the energy minimum or the energy maximum can be regarded as real and imaginary twins of nonlinear dynamics – ready to be explored in future works. Finally this work also serves as basis for us to develop the idea of quantum inductors and use them to simulate quantum superposition of spacetimes (Sec. VII of [Jav+24]). An idea that as far as we know has been unexplored in condensed matter physics until now.

Bibliography

[12] "Introduction to topological superconductivity and Majorana fermions". In: *Semiconductor Science and Technology* 27.12 (Nov. 2012), p. 124003. DOI: 10.1088/0268-1242/27/12/124003. URL: https://doi.org/10.1088/0268-1242/27/12/124003.

[20] "Direct observation of anyonic braiding statistics". In: *Nature Physics* 16.9 (2020), pp. 931–936. ISSN: 1745-2481. DOI: 10.1038/s41567-020-1019-1. URL: https://doi.org/10.1038/s41567-020-1019-1.

[Abd+13] Baleegh Abdo et al. "Directional Amplification with a Josephson Circuit". In: *Phys. Rev. X* 3 (3 July 2013), p. 031001. DOI: 10.1103/PhysRevX.3.031001. URL: https://link.aps.org/doi/10.1103/PhysRevX.3.031001.

[Anf+24] Alexander Anferov et al. *Superconducting Qubits Above 20 GHz Operating over 200 mK*. 2024. arXiv: 2402.03031 [quant-ph].

[Ari98] D. N. Aristov. "Bosonization for a Wigner-Jordan-like transformation: Backscattering and umklapp processes on a fictitious lattice". In: *Phys. Rev. B* 57 (20 May 1998), pp. 12825–12831. DOI: 10.1103/PhysRevB.57.12825. URL: https://link.aps.org/doi/10.1103/PhysRevB.57.12825.

[Aru19] F. Arute et al. "Quantum supremacy using a programmable superconducting processor". In: *Nature* 574.7779 (2019), pp. 505–510. ISSN: 1476-4687. DOI: 10.1038/s41586-019-1666-5. URL: https://doi.org/10.1038/s41586-019-1666-5.

[AS10] A. Altland and B. D. Simons. *Condensed Matter Field Theory*. Cambridge, UK: Cambridge University Press, 2010.

[ASW84] Daniel Arovas, J. R. Schrieffer, and Frank Wilczek. "Fractional Statistics and the Quantum Hall Effect". In: *Phys. Rev. Lett.* 53 (7 Aug. 1984), pp. 722–723. DOI: 10.1103/PhysRevLett.53.722. URL: https://link.aps.org/doi/10.1103/PhysRevLett.53.722.

[Avi+19] J. Avila et al. "Non-hermitian topology as a unifying framework for the Andreev versus Majorana states controversy". In: *Communications Physics* 2 (Oct. 2019). DOI: 10.1038/s42005-019-0231-8. URL: https://rdcu.be/cOzTW.

[AZ97] Alexander Altland and Martin R. Zirnbauer. "Nonstandard symmetry classes in mesoscopic normal-superconducting hybrid structures". In: *Phys. Rev. B* 55 (2 Jan. 1997), pp. 1142–1161. DOI: 10.1103/PhysRevB.55.1142. URL: https://link.aps.org/doi/10.1103/PhysRevB.55.1142.

[Bac+21] K. M. Backes et al. "A quantum enhanced search for dark matter axions". In: *Nature* 590 (Feb. 2021), pp. 238–242. DOI: 10.1038/s41586-021-03226-7.

[BAK16] Dmitry Bagrets, Alexander Altland, and Alex Kamenev. "Sachdev–Ye–Kitaev model as Liouville quantum mechanics". In: *Nuclear Physics B* 911 (2016), pp. 191–205. ISSN: 0550-3213. DOI: https://doi.org/10.1016/j.nuclphysb.2016.08.002. URL: https://www.sciencedirect.com/science/article/pii/S0550321316302206.

[Bar+13] C-E Bardyn et al. "Topology by dissipation". In: *New Journal of Physics* 15.8 (Aug. 2013), p. 085001. DOI: 10.1088/1367-2630/15/8/085001. URL: https://doi.org/10.1088/1367-2630/15/8/085001.

[Bar+18] Charles-Edouard Bardyn et al. "Probing the Topology of Density Matrices". In: *Phys. Rev. X* 8 (1 Feb. 2018), p. 011035. DOI: 10.1103/PhysRevX.8.011035.

[Bar+20] H. Bartolomei et al. "Fractional statistics in anyon collisions". In: *Science* 368.6487 (2020), pp. 173–177. DOI: 10.1126/science.aaz5601. URL: https://www.science.org/doi/abs/10.1126/science.aaz5601.

[BBK21] Emil J. Bergholtz, Jan Carl Budich, and Flore K. Kunst. "Exceptional topology of non-Hermitian systems". In: *Rev. Mod. Phys.* 93 (1 Feb. 2021), p. 015005. DOI: 10.1103/RevModPhys.93.015005. URL: https://link.aps.org/doi/10.1103/RevModPhys.93.015005.

[BD15] Jan Carl Budich and Sebastian Diehl. "Topology of density matrices". In: *Phys. Rev. B* 91 (16 Apr. 2015), p. 165140. DOI: 10.1103/PhysRevB.91.165140. URL: https://link.aps.org/doi/10.1103/PhysRevB.91.165140.

[Bee91] C. W. J. Beenakker. "Universal limit of critical-current fluctuations in mesoscopic Josephson junctions". In: *Phys. Rev. Lett.* 67 (27 Dec. 1991), pp. 3836–3839. DOI: 10.1103/PhysRevLett.67.3836. URL: https://link.aps.org/doi/10.1103/PhysRevLett.67.3836.

[Bel05] W. Belzig. "Full counting statistics of super-Poissonian shot noise in multilevel quantum dots". In: *Phys. Rev. B* 71 (16 Apr. 2005), p. 161301. DOI: 10.1103/PhysRevB.71.161301. URL: https://link.aps.org/doi/10.1103/PhysRevB.71.161301.

[BGO20] A. Blais, S. M. Girvin, and W. D. Oliver. “Quantum information processing and quantum optics with circuit quantum electrodynamics”. In: *Nat. Phys.* 16 (2020), p. 247. DOI: 10.1038/s41567-020-0806-z. URL: https://doi.org/10.1038/s41567-020-0806-z.

[BGO23] Alexandre Blais, Steven M. Girvin, and William D. Oliver. “Quantum information processing and quantum optics with circuit quantum electrodynamics”. In: *Nature Physics* 16 (Mar. 2023), pp. 247–256. DOI: 10.1038/s41567-020-0806-z.

[BHZ06] B. Andrei Bernevig, Taylor L. Hughes, and Shou-Cheng Zhang. “Quantum Spin Hall Effect and Topological Phase Transition in HgTe Quantum Wells”. In: *Science* 314.5806 (2006), pp. 1757–1761. DOI: 10.1126/science.1133734. eprint: https://www.science.org/doi/pdf/10.1126/science.1133734. URL: https://www.science.org/doi/abs/10.1126/science.1133734.

[BKD04] Guido Burkard, Roger H. Koch, and David P. DiVincenzo. “Multilevel quantum description of decoherence in superconducting qubits”. In: *Phys. Rev. B* 69 (6 Feb. 2004), p. 064503. DOI: 10.1103/PhysRevB.69.064503. URL: https://link.aps.org/doi/10.1103/PhysRevB.69.064503.

[Bla+04] A. Blais et al. “Cavity quantum electrodynamics for superconducting electrical circuits: an architecture for quantum computation”. In: *Phys. Rev. A* 69 (2004), p. 062320. DOI: 10.1103/PhysRevA.69.062320. URL: https://link.aps.org/doi/10.1103/PhysRevA.69.062320.

[Bla+07] A. Blais et al. “Quantum-information processing with circuit quantum electrodynamics”. In: *Phys. Rev. A* 75 (3 Mar. 2007), p. 032329. DOI: 10.1103/PhysRevA.75.032329. URL: https://link.aps.org/doi/10.1103/PhysRevA.75.032329.

[Bla+21] A. Blais et al. “Circuit quantum electrodynamics”. In: *Rev. Mod. Phys.* 93 (2021), p. 025005. DOI: 10.1103/RevModPhys.93.025005. URL: https://link.aps.org/doi/10.1103/RevModPhys.93.025005.

[BLV03] Carlos Barceló, S. Liberati, and Matt Visser. “Probing semiclassical analog gravity in Bose-Einstein condensates with widely tunable interactions”. In: *Phys. Rev. A* 68 (5 Nov. 2003), p. 053613. DOI: 10.1103/PhysRevA.68.053613. URL: https://link.aps.org/doi/10.1103/PhysRevA.68.053613.

[BLV11] Carlos Barceló, Stefano Liberati, and Matt Visser. “Analogue Gravity”. In: *Living Rev. Relativ.* 14.1 (2011), p. 3. DOI: 10.12942/lrr-2011-3. URL: https://doi.org/10.12942/lrr-2011-3.

[BN03] D. A. Bagrets and Yu. V. Nazarov. “Full counting statistics of charge transfer in Coulomb blockade systems”. In: *Phys. Rev. B* 67 (8 Feb. 2003), p. 085316. DOI: 10.1103/PhysRevB.67.085316.

[BP07] H. Breuer and F. Petruccione. *The Theory of Open Quantum Systems.* Oxford University Press, 2007.

[Bra+17] Kay Brandner et al. "Experimental Determination of Dynamical Lee-Yang Zeros". In: *Phys. Rev. Lett.* 118 (18 May 2017), p. 180601. DOI: 10.1103/PhysRevLett.118.180601. URL: https://link.aps.org/doi/10.1103/PhysRevLett.118.180601.

[Bro+95] R. Brout et al. "A primer for black hole quantum physics". In: *Physics Reports* 260.6 (1995), pp. 329–446. ISSN: 0370-1573. DOI: https://doi.org/10.1016/0370-1573(95)00008-5. URL: https://www.sciencedirect.com/science/article/pii/0370157395000085.

[Bru02] Todd A. Brun. "A simple model of quantum trajectories". In: *American Journal of Physics* 70.7 (July 2002), pp. 719–737. ISSN: 0002-9505. DOI: 10.1119/1.1475328. eprint: https://pubs.aip.org/aapt/ajp/article-pdf/70/7/719/7530993/719_1_online.pdf. URL: https://doi.org/10.1119/1.1475328.

[BS01] C. W. J. Beenakker and H. Schomerus. "Counting Statistics of Photons Produced by Electronic Shot Noise". In: *Phys. Rev. Lett.* 86 (4 Jan. 2001), pp. 700–703. DOI: 10.1103/PhysRevLett.86.700. URL: https://link.aps.org/doi/10.1103/PhysRevLett.86.700.

[Bud+19] Jan Carl Budich et al. "Symmetry-protected nodal phases in non-Hermitian systems". In: *Phys. Rev. B* 99 (4 Jan. 2019), p. 041406. DOI: 10.1103/PhysRevB.99.041406. URL: https://link.aps.org/doi/10.1103/PhysRevB.99.041406.

[Bul84] S. A. Bulgadaev. "Phase diagram of a dissipative quantum system". In: *JETP Letters* 39 (6 1984), pp. 315–319.

[BWT12] Jan Carl Budich, Stefan Walter, and Björn Trauzettel. "Failure of protection of Majorana based qubits against decoherence". In: *Phys. Rev. B* 85 (12 Mar. 2012), p. 121405. DOI: 10.1103/PhysRevB.85.121405. URL: https://link.aps.org/doi/10.1103/PhysRevB.85.121405.

[CAB08] Jaeyoon Cho, Dimitris G. Angelakis, and Sougato Bose. "Fractional Quantum Hall State in Coupled Cavities". In: *Phys. Rev. Lett.* 101 (24 Dec. 2008), p. 246809. DOI: 10.1103/PhysRevLett.101.246809. URL: https://link.aps.org/doi/10.1103/PhysRevLett.101.246809.

[CAH00] Aashish A. Clerk, Vinay Ambegaokar, and Selman Hershfield. "Andreev scattering and the Kondo effect". In: *Phys. Rev. B* 61 (5 Feb. 2000), pp. 3555–3562. DOI: 10.1103/PhysRevB.61.3555. URL: https://link.aps.org/doi/10.1103/PhysRevB.61.3555.

[Cat+11] G. Catelani et al. "Relaxation and frequency shifts induced by quasiparticles in superconducting qubits". In: *Phys. Rev. B* 84 (6 Aug. 2011), p. 064517. DOI: 10.1103/PhysRevB.84.064517. URL: https://link.aps.org/doi/10.1103/PhysRevB.84.064517.

[CDT24] Alessandro Ciani, David P. DiVincenzo, and Barbara M. Terhal. *Lecture Notes on Quantum Electrical Circuits*. TU Delft OPEN Publishing, Jan. 2024. ISBN: 9789463668149. DOI: `10.59490/tb.85`. URL: `http://dx.doi.org/10.59490/tb.85`.

[Chi+16] Ching-Kai Chiu et al. "Classification of topological quantum matter with symmetries". In: *Rev. Mod. Phys.* 88 (3 Aug. 2016), p. 035005. DOI: `10.1103/RevModPhys.88.035005`. URL: `https://link.aps.org/doi/10.1103/RevModPhys.88.035005`.

[Cho+04] Mahn-Soo Choi et al. "Kondo effect and Josephson current through a quantum dot between two superconductors". In: *Phys. Rev. B* 70 (2 July 2004), p. 020502. DOI: `10.1103/PhysRevB.70.020502`. URL: `https://link.aps.org/doi/10.1103/PhysRevB.70.020502`.

[CJG15] Gustau Catalan, David Jiménez, and Alexei Gruverman. "Negative capacitance detected". In: *Nat. Mater.* 14.2 (Feb. 1, 2015), pp. 137–139. ISSN: 1476-4660. DOI: `https://doi.org/10.1038/nmat4195`. URL: `https://doi.org/10.1038/nmat4195`.

[Cle+10] A. A. Clerk et al. "Introduction to quantum noise, measurement, and amplification". In: *Rev. Mod. Phys.* 82 (2 Apr. 2010), pp. 1155–1208. DOI: `10.1103/RevModPhys.82.1155`. URL: `https://link.aps.org/doi/10.1103/RevModPhys.82.1155`.

[Cle+20] A. A. Clerk et al. "Hybrid quantum systems with circuit quantum electrodynamics". In: *Nature Physics* 16 (Mar. 2020), pp. 257–267. DOI: `10.1038/s41567-020-0797-9`.

[CLM01] J. C. Cuevas, A. Levy Yeyati, and A. Martín-Rodero. "Kondo effect in normal-superconductor quantum dots". In: *Phys. Rev. B* 63 (9 Feb. 2001), p. 094515. DOI: `10.1103/PhysRevB.63.094515`. URL: `https://link.aps.org/doi/10.1103/PhysRevB.63.094515`.

[Con+12] L. Debora Contreras-Pulido et al. "Time scales in the dynamics of an interacting quantum dot". In: *Phys. Rev. B* 85 (7 Feb. 2012), p. 075301. DOI: `10.1103/PhysRevB.85.075301`. URL: `https://link.aps.org/doi/10.1103/PhysRevB.85.075301`.

[Cot02] Audrey Cottet. "Implementation of a Quantum Bit in a Superconducting Circuit". PhD thesis. 2002.

[Cre+06] James D. Cresser et al. "Measurement master equation". In: *Optics Communications* 264.2 (2006). Quantum Control of Light and Matter, pp. 352–361. ISSN: 0030-4018. DOI: `https://doi.org/10.1016/j.optcom.2006.02.061`. URL: `https://www.sciencedirect.com/science/article/pii/S0030401806004962`.

[De +21] Christophe De Beule et al. "Artificial event horizons in Weyl semimetal heterostructures and their non-equilibrium signatures". In: *SciPost Physics* 11.5 (2021), p. 095.

[de-+97] R. de-Picciotto et al. “Direct observation of a fractional charge”. In: *Nature* 389 (Sept. 1997). URL: http://dx.doi.org/10.1038/38241.

[Del+20] Uroš Delić et al. “Cooling of a levitated nanoparticle to the motional quantum ground state”. In: *Science* 367.6480 (2020), pp. 892–895. URL: https://doi.org/10.1126/science.aba3993.

[DFM22] Kun Ding, Chen Fang, and Guancong Ma. “Non-Hermitian topology and exceptional-point geometries”. In: *Nature Reviews Physics* 4.12 (2022), pp. 745–760.

[Die+11] Sebastian Diehl et al. “Topology by dissipation in atomic quantum wires”. In: *Nature Physics* 7.12 (Oct. 2011), pp. 971–977. DOI: 10.1038/nphys2106.

[Din+18] Kun Ding et al. “Experimental Demonstration of an Anisotropic Exceptional Point”. In: *Phys. Rev. Lett.* 121 (8 Aug. 2018), p. 085702. DOI: 10.1103/PhysRevLett.121.085702. URL: https://link.aps.org/doi/10.1103/PhysRevLett.121.085702.

[Dir+11] Travis Dirks et al. “Transport through Andreev bound states in a graphene quantum dot”. In: *Nature Physics* 7.5 (2011), pp. 386–390. ISSN: 1745-2481. DOI: 10.1038/nphys1911. URL: https://doi.org/10.1038/nphys1911.

[DS18] Niklas Dittmann and Janine Splettstoesser. “Finite-frequency noise of interacting single-electron emitters: Spectroscopy with higher noise harmonics”. In: *Phys. Rev. B* 98 (11 Sept. 2018), p. 115414. DOI: 10.1103/PhysRevB.98.115414. URL: https://link.aps.org/doi/10.1103/PhysRevB.98.115414.

[Eib+13] Sandra Eibenberger et al. “Matter–wave interference of particles selected from a molecular library with masses exceeding 10000 amu”. In: *Physical Chemistry Chemical Physics* 15.35 (2013), pp. 14696–14700. URL: https://doi.org/10.1039/C3CP51500A.

[EKB19] Elisabet Edvardsson, Flore K. Kunst, and Emil J. Bergholtz. “Non-Hermitian extensions of higher-order topological phases and their biorthogonal bulk-boundary correspondence”. In: *Phys. Rev. B* 99 (8 Feb. 2019), p. 081302. DOI: 10.1103/PhysRevB.99.081302.

[El-+18] Ramy El-Ganainy et al. “Non-Hermitian physics and PT symmetry”. In: *Nature Physics* 14.1 (2018), pp. 11–19.

[Eng+17] G. Engelhardt et al. “Random-walk topological transition revealed via electron counting”. In: *Phys. Rev. B* 96 (24 Dec. 2017), p. 241404. DOI: 10.1103/PhysRevB.96.241404.

[Eri+17] Erik Eriksson et al. “Topological transconductance quantization in a four-terminal Josephson junction”. In: *Phys. Rev. B* 95 (7 Feb. 2017), p. 075417. DOI: 10.1103/PhysRevB.95.075417. URL: https://link.aps.org/doi/10.1103/PhysRevB.95.075417.

[FAB21] Valla Fatemi, Anton R. Akhmerov, and Landry Bretheau. “Weyl Josephson circuits”. In: *Phys. Rev. Research* 3 (1 Mar. 2021), p. 013288. DOI: 10.1103/PhysRevResearch.3.013288. URL: https://link.aps.org/doi/10.1103/PhysRevResearch.3.013288.

[Fan+21] F. Fani Sani et al. “Level attraction and idler resonance in a strongly driven Josephson cavity”. In: *Phys. Rev. Res.* 3 (4 Nov. 2021), p. 043111. DOI: 10.1103/PhysRevResearch.3.043111. URL: https://link.aps.org/doi/10.1103/PhysRevResearch.3.043111.

[FEG17] Liang Feng, Ramy El-Ganainy, and Li Ge. “Non-Hermitian photonics based on parity–time symmetry”. In: *Nature Photonics* 11.12 (Dec. 1, 2017), pp. 752–762. ISSN: 1749-4893. DOI: 10.1038/s41566-017-0031-1. URL: https://doi.org/10.1038/s41566-017-0031-1.

[Fei+19] Yaakov Y Fein et al. “Quantum superposition of molecules beyond 25 kDa”. In: *Nature Physics* 15.12 (2019), pp. 1242–1245. URL: https://doi.org/10.1038/s41567-019-0663-9.

[FF04] Petr O. Fedichev and Uwe R. Fischer. ““Cosmological” quasiparticle production in harmonically trapped superfluid gases”. In: *Phys. Rev. A* 69 (3 Mar. 2004), p. 033602. DOI: 10.1103/PhysRevA.69.033602. URL: https://link.aps.org/doi/10.1103/PhysRevA.69.033602.

[FG13] Christian Flindt and Juan P. Garrahan. “Trajectory Phase Transitions, Lee-Yang Zeros, and High-Order Cumulants in Full Counting Statistics”. In: *Phys. Rev. Lett.* 110 (5 Jan. 2013), p. 050601. DOI: 10.1103/PhysRevLett.110.050601.

[FHS05] Takahiro Fukui, Yasuhiro Hatsugai, and Hiroshi Suzuki. “Chern Numbers in Discretized Brillouin Zone: Efficient Method of Computing (Spin) Hall Conductances”. In: *Journal of the Physical Society of Japan* 74.6 (2005), pp. 1674–1677. DOI: 10.1143/JPSJ.74.1674. eprint: https://doi.org/10.1143/JPSJ.74.1674. URL: https://doi.org/10.1143/JPSJ.74.1674.

[FK07] Liang Fu and C. L. Kane. “Topological insulators with inversion symmetry”. In: *Phys. Rev. B* 76 (4 July 2007), p. 045302. DOI: 10.1103/PhysRevB.76.045302. URL: https://link.aps.org/doi/10.1103/PhysRevB.76.045302.

[FK08] Liang Fu and C. L. Kane. “Superconducting Proximity Effect and Majorana Fermions at the Surface of a Topological Insulator”. In: *Phys. Rev. Lett.* 100 (9 Mar. 2008), p. 096407. DOI: 10.1103/PhysRevLett.100.096407. URL: https://link.aps.org/doi/10.1103/PhysRevLett.100.096407.

[FK09] Liang Fu and C. L. Kane. “Josephson current and noise at a superconductor quantum-spin-Hall-insulator superconductor junction”. In: *Phys. Rev. B* 79 (16 Apr. 2009), p. 161408. DOI: 10.1103/PhysRevB.79.161408. URL: https://link.aps.org/doi/10.1103/PhysRevB.79.161408.

[FKM07] Liang Fu, C. L. Kane, and E. J. Mele. “Topological Insulators in Three Dimensions”. In: *Phys. Rev. Lett.* 98 (10 Mar. 2007), p. 106803. DOI: 10.1103/PhysRevLett.98.106803. URL: https://link.aps.org/doi/10.1103/PhysRevLett.98.106803.

[FL81] Daniel S. Fisher and Patrick A. Lee. “Relation between conductivity and transmission matrix”. In: *Phys. Rev. B* 23 (12 June 1981), pp. 6851–6854. DOI: 10.1103/PhysRevB.23.6851. URL: https://link.aps.org/doi/10.1103/PhysRevB.23.6851.

[Fli+09] C. Flindt et al. “Universal oscillations in counting statistics”. In: *Proceedings of the National Academy of Sciences* 106.25 (2009), pp. 10116–10119. DOI: 10.1073/pnas.0901002106. URL: https://www.pnas.org/doi/abs/10.1073/pnas.0901002106.

[Flu+12] E. Flurin et al. “Generating Entangled Microwave Radiation Over Two Transmission Lines”. In: *Phys. Rev. Lett.* 109 (18 Oct. 2012), p. 183901. DOI: 10.1103/PhysRevLett.109.183901. URL: https://link.aps.org/doi/10.1103/PhysRevLett.109.183901.

[FR98] Rosario Fazio and Roberto Raimondi. “Resonant Andreev Tunneling in Strongly Interacting Quantum Dots”. In: *Phys. Rev. Lett.* 80 (13 Mar. 1998), pp. 2913–2916. DOI: 10.1103/PhysRevLett.80.2913. URL: https://link.aps.org/doi/10.1103/PhysRevLett.80.2913.

[FS04] Uwe R. Fischer and Ralf Schützhold. “Quantum simulation of cosmic inflation in two-component Bose-Einstein condensates”. In: *Phys. Rev. A* 70 (6 Dec. 2004), p. 063615. DOI: 10.1103/PhysRevA.70.063615. URL: https://link.aps.org/doi/10.1103/PhysRevA.70.063615.

[Fut+09] David Futterer et al. “Nonlocal Andreev transport through an interacting quantum dot”. In: *Phys. Rev. B* 79 (5 Feb. 2009), p. 054505. DOI: 10.1103/PhysRevB.79.054505. URL: https://link.aps.org/doi/10.1103/PhysRevB.79.054505.

[Fut+13] David Futterer et al. “Renormalization effects in interacting quantum dots coupled to superconducting leads”. In: *Phys. Rev. B* 87 (1 Jan. 2013), p. 014509. DOI: 10.1103/PhysRevB.87.014509. URL: https://link.aps.org/doi/10.1103/PhysRevB.87.014509.

[Fv01] Rosario Fazio and Herre van der Zant. “Quantum phase transitions and vortex dynamics in superconducting networks”. In: *Physics Reports* 355.4 (2001), pp. 235–334. ISSN: 0370-1573. DOI: https://doi.org/10.1016/S0370-1573(01)00022-9. URL: https://www.sciencedirect.com/science/article/pii/S0370157301000229.

[Gao+21] Yvonne Y. Gao et al. “Practical Guide for Building Superconducting Quantum Devices”. In: *PRX Quantum* 2 (4 Nov. 2021), p. 040202. DOI: 10.1103/PRXQuantum.2.040202. URL: https://link.aps.org/doi/10.1103/PRXQuantum.2.040202.

[Gar+00] Luis Javier Garay et al. “Sonic analog of gravitational black holes in Bose-Einstein condensates”. In: *Physical Review Letters* 85.22 (2000), p. 4643. URL: https://doi.org/10.1103/PhysRevLett.85.4643.

[Gar+01] Luis Javier Garay et al. “Sonic black holes in dilute Bose-Einstein condensates”. In: *Physical Review A* 63.2 (2001), p. 023611. URL: https://doi.org/10.1103/PhysRevA.63.023611.

[GC11] G. Goldstein and C. Chamon. “Decay rates for topological memories encoded with Majorana fermions”. In: *Phys. Rev. B* 84 (20 Nov. 2011), p. 205109. DOI: 10.1103/PhysRevB.84.205109. URL: https://link.aps.org/doi/10.1103/PhysRevB.84.205109.

[Ger+11] Stefan Gerlich et al. “Quantum interference of large organic molecules”. In: *Nature communications* 2.1 (2011), pp. 1–5. URL: https://doi.org/10.1038/ncomms1263.

[GGM10] D. B. Gutman, Yuval Gefen, and A. D. Mirlin. “Full Counting Statistics of a Luttinger Liquid Conductor”. In: *Phys. Rev. Lett.* 105 (25 Dec. 2010), p. 256802. DOI: 10.1103/PhysRevLett.105.256802.

[Gla+09] Sergey Gladchenko et al. “Superconducting nanocircuits for topologically protected qubits”. In: *Nature Physics* 5.1 (Jan. 1, 2009), pp. 48–53. ISSN: 1745-2481. DOI: 10.1038/nphys1151. URL: https://doi.org/10.1038/nphys1151.

[GS86] Marc H. Goroff and Augusto Sagnotti. “The ultraviolet behavior of Einstein gravity”. In: *Nuclear Physics B* 266.3 (1986), pp. 709–736. ISSN: 0550-3213. DOI: https://doi.org/10.1016/0550-3213(86)90193-8. URL: https://www.sciencedirect.com/science/article/pii/0550321386901938.

[Gu+17] Xiu Gu et al. “Microwave photonics with superconducting quantum circuits”. In: *Physics Reports* 718-719 (2017), pp. 1–102. ISSN: 0370-1573. DOI: https://doi.org/10.1016/j.physrep.2017.10.002. URL: https://www.sciencedirect.com/science/article/pii/S0370157317303290.

[Gus+06] S. Gustavsson et al. “Counting Statistics of Single Electron Transport in a Quantum Dot”. In: *Phys. Rev. Lett.* 96 (7 Feb. 2006), p. 076605. DOI: 10.1103/PhysRevLett.96.076605.

[Hal88] F. D. M. Haldane. “Model for a Quantum Hall Effect without Landau Levels: Condensed-Matter Realization of the "Parity Anomaly"”. In: *Phys. Rev. Lett.* 61 (18 Oct. 1988), pp. 2015–2018. DOI: 10.1103/PhysRevLett.61.2015. URL: https://link.aps.org/doi/10.1103/PhysRevLett.61.2015.

[Ham+16] A. Hamo et al. “Electron attraction mediated by Coulomb repulsion”. In: *Nature* 535.7612 (July 1, 2016), pp. 395–400. ISSN: 1476-4687. DOI: https://doi.org/10.1038/nature18639. URL: https://doi.org/10.1038/nature18639.

[Har+20] Fenner Harper et al. “Topology and Broken Symmetry in Floquet Systems”. In: *Annual Review of Condensed Matter Physics* 11.Volume 11, 2020 (2020), pp. 345–368. ISSN: 1947-5462. DOI: https://doi.org/10.1146/annurev-conmatphys-031218-013721. URL: https://www.annualreviews.org/content/journals/10.1146/annurev-conmatphys-031218-013721.

[Hat97] Y Hatsugai. “Topological aspects of the quantum Hall effect”. In: *Journal of Physics: Condensed Matter* 9.12 (Mar. 1997), p. 2507. DOI: 10.1088/0953-8984/9/12/003. URL: https://dx.doi.org/10.1088/0953-8984/9/12/003.

[Hec+11] B. van Heck et al. “Coulomb stability of the 4π-periodic Josephson effect of Majorana fermions”. In: *Phys. Rev. B* 84 (18 Nov. 2011), p. 180502. DOI: 10.1103/PhysRevB.84.180502. URL: https://link.aps.org/doi/10.1103/PhysRevB.84.180502.

[Hei04] W D Heiss. “Exceptional points of non-Hermitian operators”. In: *Journal of Physics A: Mathematical and General* 37.6 (Jan. 2004), pp. 2455–2464. DOI: 10.1088/0305-4470/37/6/034. URL: https://doi.org/10.1088/0305-4470/37/6/034.

[Hei12] W D Heiss. “The physics of exceptional points”. In: *Journal of Physics A: Mathematical and Theoretical* 45.44 (Oct. 2012), p. 444016. DOI: 10.1088/1751-8113/45/44/444016. URL: https://doi.org/10.1088/1751-8113/45/44/444016.

[Her+10] L. G. Herrmann et al. "Carbon Nanotubes as Cooper-Pair Beam Splitters". In: *Phys. Rev. Lett.* 104 (2 Jan. 2010), p. 026801. DOI: 10.1103/PhysRevLett.104.026801. URL: https://link.aps.org/doi/10.1103/PhysRevLett.104.026801.

[Her+23a] T. Herrig et al. "Quasiperiodic circuit quantum electrodynamics". In: *npj Quantum Information* 9.1 (Nov. 14, 2023), p. 116. ISSN: 2056-6387. DOI: 10.1038/s41534-023-00786-6. URL: https://doi.org/10.1038/s41534-023-00786-6.

[Her+23b] Tobias Herrig et al. *Emulating moiré materials with quasiperiodic circuit quantum electrodynamics.* 2023. arXiv: 2310.15103 [cond-mat.mes-hall].

[HF23] Caio C. Holanda Ribeiro and Uwe R. Fischer. "Impact of trans-Planckian excitations on black-hole radiation in dipolar condensates". In: *Phys. Rev. D* 107 (12 June 2023), p. L121502. DOI: 10.1103/PhysRevD.107.L121502. URL: https://link.aps.org/doi/10.1103/PhysRevD.107.L121502.

[HG19] Manuel Houzet and Leonid I. Glazman. "Microwave Spectroscopy of a Weakly Pinned Charge Density Wave in a Superinductor". In: *Phys. Rev. Lett.* 122 (23 June 2019), p. 237701. DOI: 10.1103/PhysRevLett.122.237701. URL: https://link.aps.org/doi/10.1103/PhysRevLett.122.237701.

[HG97] F. W. J. Hekking and L. I. Glazman. "Quantum fluctuations in the equilibrium state of a thin superconducting loop". In: *Phys. Rev. B* 55 (10 Mar. 1997), pp. 6551–6558. DOI: 10.1103/PhysRevB.55.6551. URL: https://link.aps.org/doi/10.1103/PhysRevB.55.6551.

[HH11] Yi Chen Hu and Taylor L. Hughes. "Absence of topological insulator phases in non-Hermitian *PT*-symmetric Hamiltonians". In: *Phys. Rev. B* 84 (15 Oct. 2011), p. 153101. DOI: 10.1103/PhysRevB.84.153101. URL: https://link.aps.org/doi/10.1103/PhysRevB.84.153101.

[Hil+11] Bastian Hiltscher et al. "Adiabatic pumping in a double-dot Cooper-pair beam splitter". In: *Phys. Rev. B* 84 (15 Oct. 2011), p. 155403. DOI: 10.1103/PhysRevB.84.155403. URL: https://link.aps.org/doi/10.1103/PhysRevB.84.155403.

[HK10] M. Z. Hasan and C. L. Kane. "Colloquium: Topological insulators". In: *Rev. Mod. Phys.* 82 (4 Nov. 2010), pp. 3045–3067. DOI: 10.1103/RevModPhys.82.3045. URL: https://link.aps.org/doi/10.1103/RevModPhys.82.3045.

[HK15] P.C. Hohenberg and A.P. Krekhov. "An introduction to the Ginzburg–Landau theory of phase transitions and nonequilibrium patterns". In: *Physics Reports* 572 (2015). An introduction to the Ginzburg–Landau theory of phase transitions and nonequilibrium patterns, pp. 1–42. ISSN: 0370-1573. DOI: https://doi.org/10.1016/j.physrep.2015.01.001.

URL: https://www.sciencedirect.com/science/article/pii/S0370157315000514.

[Hlu+21] Anton V Hlushchenko et al. “Multimode $\mathcal{PT}$-symmetry thresholds and third-order exceptional points in coupled dielectric waveguides with loss and gain”. In: *Journal of Optics* 23.12 (Nov. 2021), p. 125002. DOI: 10.1088/2040-8986/ac31d4. URL: https://dx.doi.org/10.1088/2040-8986/ac31d4.

[Hof+10] L. Hofstetter et al. “Ferromagnetic Proximity Effect in a Ferromagnet–Quantum-Dot–Superconductor Device”. In: *Phys. Rev. Lett.* 104 (24 June 2010), p. 246804. DOI: 10.1103/PhysRevLett.104.246804. URL: https://link.aps.org/doi/10.1103/PhysRevLett.104.246804.

[Hof+18] Michael Hoffmann et al. “Ferroelectric negative capacitance domain dynamics”. In: *Journal of Applied Physics* 123.18 (2018), p. 184101. DOI: https://doi.org/10.1063/1.5030072. URL: https://doi.org/10.1063/1.5030072.

[Hof+20] Michael Hoffmann et al. “What’s next for negative capacitance electronics?” In: *Nat. Electron.* 3.9 (Sept. 1, 2020), pp. 504–506. ISSN: 2520-1131. DOI: https://doi.org/10.1038/s41928-020-00474-9. URL: https://doi.org/10.1038/s41928-020-00474-9.

[Hos+85] J. K. Hoskins et al. “Experimental tests of the gravitational inverse-square law for mass separations from 2 to 105 cm”. In: *Phys. Rev. D* 32 (12 Dec. 1985), pp. 3084–3095. DOI: 10.1103/PhysRevD.32.3084. URL: https://link.aps.org/doi/10.1103/PhysRevD.32.3084.

[HR22] T. Herrig and R.-P. Riwar. “Cooper-pair transistor as a minimal topological quantum circuit”. In: *Phys. Rev. Research* 4 (1 Jan. 2022), p. 013038. DOI: 10.1103/PhysRevResearch.4.013038. URL: https://link.aps.org/doi/10.1103/PhysRevResearch.4.013038.

[HS21] Pertti J. Hakonen and Edouard B. Sonin. “Comment on “Absence of a Dissipative Quantum Phase Transition in Josephson Junctions””. In: *Phys. Rev. X* 11 (1 Mar. 2021), p. 018001. DOI: 10.1103/PhysRevX.11.018001. URL: https://link.aps.org/doi/10.1103/PhysRevX.11.018001.

[HS22] Markus Heckschen and Björn Sothmann. “Pair-amplitude dynamics in strongly coupled superconductor–quantum dot hybrids”. In: *Phys. Rev. B* 105 (4 Jan. 2022), p. 045420. DOI: 10.1103/PhysRevB.105.045420. URL: https://link.aps.org/doi/10.1103/PhysRevB.105.045420.

[Hsi+08] D. Hsieh et al. “A topological Dirac insulator in a quantum spin Hall phase”. In: *Nature* 452.7190 (2008), pp. 970–974. DOI: 10.1038/nature06843. URL: https://doi.org/10.1038/nature06843.

[HTK12] Andrew A. Houck, Hakan E. Türeci, and Jens Koch. "On-chip quantum simulation with superconducting circuits". In: *Nature Physics* 8.4 (Apr. 1, 2012), pp. 292–299. ISSN: 1745-2481. DOI: 10.1038/nphys2251. URL: https://doi.org/10.1038/nphys2251.

[IAC13] Dmitri A Ivanov, Alexander G Abanov, and Vadim V Cheianov. "Counting free fermions on a line: a Fisher-Hartwig asymptotic expansion for the Toeplitz determinant in the double-scaling limit". In: *Journal of Physics A: Mathematical and Theoretical* 46.8 (Feb. 2013), p. 085003. DOI: 10.1088/1751-8113/46/8/085003. URL: https://doi.org/10.1088/1751-8113/46/8/085003.

[Imu+02] K.-I. Imura et al. "Conductance of one-dimensional quantum wires". In: *Phys. Rev. B* 66 (3 July 2002), p. 035313. DOI: 10.1103/PhysRevB.66.035313. URL: https://link.aps.org/doi/10.1103/PhysRevB.66.035313.

[Jac91] Theodore Jacobson. "Black-hole evaporation and ultrashort distances". In: *Phys. Rev. D* 44 (6 Sept. 1991), pp. 1731–1739. DOI: 10.1103/PhysRevD.44.1731. URL: https://link.aps.org/doi/10.1103/PhysRevD.44.1731.

[Jaf+22] Daniel Jafferis et al. "Traversable wormhole dynamics on a quantum processor". In: *Nature* 612.7938 (Dec. 1, 2022), pp. 51–55. ISSN: 1476-4687. DOI: 10.1038/s41586-022-05424-3. URL: https://doi.org/10.1038/s41586-022-05424-3.

[Jai+07] Piyush Jain et al. "Analog model of a Friedmann-Robertson-Walker universe in Bose-Einstein condensates: Application of the classical field method". In: *Phys. Rev. A* 76 (3 Sept. 2007), p. 033616. DOI: 10.1103/PhysRevA.76.033616. URL: https://link.aps.org/doi/10.1103/PhysRevA.76.033616.

[Jav+24] M. A. Javed et al. *Utilizing and extending superconducting circuit toolbox to simulate analog quantum gravity*. 2024. arXiv: 2406.01261 [cond-mat.mes-hall]. URL: https://arxiv.org/abs/2406.01261.

[Jos74] B. D. Josephson. "The discovery of tunnelling supercurrents". In: *Rev. Mod. Phys.* 46 (2 Apr. 1974), pp. 251–254. DOI: 10.1103/RevModPhys.46.251. URL: https://link.aps.org/doi/10.1103/RevModPhys.46.251.

[JSR23] Mohammad Atif Javed, Jakob Schwibbert, and Roman-Pascal Riwar. "Fractional Josephson effect versus fractional charge in superconducting–normal metal hybrid circuits". In: *Phys. Rev. B* 107 (3 Jan. 2023), p. 035408. DOI: 10.1103/PhysRevB.107.035408. URL: https://link.aps.org/doi/10.1103/PhysRevB.107.035408.

[Kan98] Kicheon Kang. “Kondo resonance, Coulomb blockade, and Andreev transport through a quantum dot”. In: *Phys. Rev. B* 58 (15 Oct. 1998), pp. 9641–9643. DOI: 10.1103/PhysRevB.58.9641. URL: https://link.aps.org/doi/10.1103/PhysRevB.58.9641.

[Kap+19] M. Kapfer et al. “A Josephson relation for fractionally charged anyons”. In: *Science* 363.6429 (2019), pp. 846–849. DOI: 10.1126/science.aau3539.

[Kat+21] Haruna Katayama et al. “Solitonic black holes induced by magnetic solitons in a dc-SQUID array transmission line coupled with a magnetic chain”. In: *Phys. Rev. D* 103 (6 Mar. 2021), p. 066025. DOI: 10.1103/PhysRevD.103.066025. URL: https://link.aps.org/doi/10.1103/PhysRevD.103.066025.

[Kat+23] Haruna Katayama et al. “Analog black-white hole solitons in traveling wave parametric amplifiers with superconducting nonlinear asymmetric inductive elements”. In: *Phys. Rev. Res.* 5 (2 June 2023), p. L022055. DOI: 10.1103/PhysRevResearch.5.L022055. URL: https://link.aps.org/doi/10.1103/PhysRevResearch.5.L022055.

[Kat21a] Haruna Katayama. “Designed Analogue Black Hole Solitons in Josephson Transmission Lines”. In: *IEEE Transactions on Applied Superconductivity* 31.5 (2021), pp. 1–5. DOI: 10.1109/TASC.2021.3058076.

[Kat21b] Haruna Katayama. “Quantum-circuit black hole lasers”. In: *Scientific Reports* 11 (2021), p. 19137. DOI: 10.1038/s41598-021-98456-0. URL: https://doi.org/10.1038/s41598-021-98456-0.

[Kau+21] Kuljeet Kaur et al. “Spin-Boson Quantum Phase Transition in Multilevel Superconducting Qubits”. In: *Phys. Rev. Lett.* 127 (23 Dec. 2021), p. 237702. DOI: 10.1103/PhysRevLett.127.237702. URL: https://link.aps.org/doi/10.1103/PhysRevLett.127.237702.

[Kaw+19a] Kohei Kawabata et al. “Symmetry and Topology in Non-Hermitian Physics”. In: *Phys. Rev. X* 9 (4 Oct. 2019), p. 041015. DOI: 10.1103/PhysRevX.9.041015. URL: https://link.aps.org/doi/10.1103/PhysRevX.9.041015.

[Kaw+19b] Kohei Kawabata et al. “Topological unification of time-reversal and particle-hole symmetries in non-Hermitian physics”. In: *Nature Communications* 10.1 (2019), p. 297. DOI: 10.1038/s41467-018-08254-y. URL: https://doi.org/10.1038/s41467-018-08254-y.

[KBW20] Yaron Kedem, Emil J Bergholtz, and Frank Wilczek. “Black and white holes at material junctions”. In: *Physical Review Research* 2.4 (2020), p. 043285.

[KDP80] K. v. Klitzing, G. Dorda, and M. Pepper. "New Method for High-Accuracy Determination of the Fine-Structure Constant Based on Quantized Hall Resistance". In: *Phys. Rev. Lett.* 45 (6 Aug. 1980), pp. 494–497. DOI: 10.1103/PhysRevLett.45.494. URL: https://link.aps.org/doi/10.1103/PhysRevLett.45.494.

[Ke+19] Chung Ting Ke et al. "Ballistic superconductivity and tunable π–junctions in InSb quantum wells". In: *Nature Communications* 10 (Aug. 2019), p. 3764. DOI: https://doi.org/10.1038/s41467-019-11742-4. URL: https://www.nature.com/articles/s41467-019-11742-4.

[KF94] C. L. Kane and Matthew P. A. Fisher. "Nonequilibrium noise and fractional charge in the quantum Hall effect". In: *Phys. Rev. Lett.* 72 (5 Jan. 1994), pp. 724–727. DOI: 10.1103/PhysRevLett.72.724. URL: https://link.aps.org/doi/10.1103/PhysRevLett.72.724.

[KH23] Steven Kim and Fabian Hassler. "Third quantization for bosons: symplectic diagonalization, non-Hermitian Hamiltonian, and symmetries". In: *Journal of Physics A: Mathematical and Theoretical* 56.38 (Sept. 2023), p. 385303. DOI: 10.1088/1751-8121/acf177. URL: https://dx.doi.org/10.1088/1751-8121/acf177.

[KHF20] Haruna Katayama, Noriyuki Hatakenaka, and Toshiyuki Fujii. "Analogue Hawking radiation from black hole solitons in quantum Josephson transmission lines". In: *Phys. Rev. D* 102 (8 Oct. 2020), p. 086018. DOI: 10.1103/PhysRevD.102.086018. URL: https://link.aps.org/doi/10.1103/PhysRevD.102.086018.

[KHR22] Ahmed Kenawy, Fabian Hassler, and Roman-Pascal Riwar. "Electromotive force in driven topological quantum circuits". In: *Phys. Rev. B* 106 (3 July 2022), p. 035430. DOI: 10.1103/PhysRevB.106.035430. URL: https://link.aps.org/doi/10.1103/PhysRevB.106.035430.

[Kim98] H J Kimble. "Strong interactions of single atoms and photons in cavity QED". In: *Physica Scripta* T76 (Jan. 1998), p. 127. DOI: 10.1238/Physica.Topical.076a00127. URL: https://dx.doi.org/10.1238/Physica.Topical.076a00127.

[Kit01] A Yu Kitaev. "Unpaired Majorana fermions in quantum wires". In: *Physics-Uspekhi* 44.10S (Oct. 2001), pp. 131–136. DOI: 10.1070/1063-7869/44/10s/s29. URL: https://doi.org/10.1070/1063-7869/44/10s/s29.

[Kit09] Alexei Kitaev. "Periodic table for topological insulators and superconductors". In: *AIP Conference Proceedings* 1134.1 (May 2009), pp. 22–30. ISSN: 0094-243X. DOI: 10.1063/1.3149495. eprint: https://pubs.aip.org/aip/acp/article-pdf/1134/1/22/11584243/22_1_online.pdf. URL: https://doi.org/10.1063/1.3149495.

[Kja+20] M. Kjaergaard et al. “Superconducting Qubits: current State of Play”. In: *Annu. Rev. Condens. Matter Phys.* 11.1 (2020), p. 369. DOI: 10.1146/annurev-conmatphys-031119-050605. URL: https://doi.org/10.1146/annurev-conmatphys-031119-050605.

[Kle+20] R. L. Klees et al. “Microwave Spectroscopy Reveals the Quantum Geometric Tensor of Topological Josephson Matter”. In: *Phys. Rev. Lett.* 124 (19 May 2020), p. 197002. DOI: 10.1103/PhysRevLett.124.197002. URL: https://link.aps.org/doi/10.1103/PhysRevLett.124.197002.

[Kle+21] R. L. Klees et al. “Ground-state quantum geometry in superconductor–quantum dot chains”. In: *Phys. Rev. B* 103 (1 Jan. 2021), p. 014516. DOI: 10.1103/PhysRevB.103.014516. URL: https://link.aps.org/doi/10.1103/PhysRevB.103.014516.

[Kli02] I. Klich. *Full Counting Statistics: An elementary derivation of Levitov's formula*. 2002. arXiv: cond-mat/0209642 [cond-mat.mes-hall].

[KM05] C. L. Kane and E. J. Mele. “Quantum Spin Hall Effect in Graphene”. In: *Phys. Rev. Lett.* 95 (22 Nov. 2005), p. 226801. DOI: 10.1103/PhysRevLett.95.226801. URL: https://link.aps.org/doi/10.1103/PhysRevLett.95.226801.

[KM89] Yuri S. Kivshar and Boris A. Malomed. “Dynamics of solitons in nearly integrable systems”. In: *Rev. Mod. Phys.* 61 (4 Oct. 1989), pp. 763–915. DOI: 10.1103/RevModPhys.61.763. URL: https://link.aps.org/doi/10.1103/RevModPhys.61.763.

[KOB19] Thomas Kiendl, Felix von Oppen, and Piet W. Brouwer. “Proximity-induced gap in nanowires with a thin superconducting shell”. In: *Phys. Rev. B* 100 (3 July 2019), p. 035426. DOI: 10.1103/PhysRevB.100.035426. URL: https://link.aps.org/doi/10.1103/PhysRevB.100.035426.

[Koc+09] Jens Koch et al. “Charging Effects in the Inductively Shunted Josephson Junction”. In: *Phys. Rev. Lett.* 103 (21 Nov. 2009), p. 217004. DOI: 10.1103/PhysRevLett.103.217004. URL: https://link.aps.org/doi/10.1103/PhysRevLett.103.217004.

[Kön+07] Markus König et al. “Quantum Spin Hall Insulator State in HgTe Quantum Wells”. In: *Science* 318.5851 (2007), pp. 766–770. DOI: 10.1126/science.1148047. eprint: https://www.science.org/doi/pdf/10.1126/science.1148047. URL: https://www.science.org/doi/abs/10.1126/science.1148047.

[Kon+22] Phatthamon Kongkhambut et al. "Observation of a continuous time crystal". In: *Science* 377.6606 (2022), pp. 670–673. DOI: 10.1126/science.abo3382. eprint: https://www.science.org/doi/pdf/10.1126/science.abo3382. URL: https://www.science.org/doi/abs/10.1126/science.abo3382.

[Kön99] Jürgen König. "Quantum Fluctuations in the Single-Electron Transistor". PhD thesis. 1999.

[KR19] Michael J. Kastoryano and Mark S. Rudner. "Topological transport in the steady state of a quantum particle with dissipation". In: *Phys. Rev. B* 99 (12 Mar. 2019), p. 125118. DOI: 10.1103/PhysRevB.99.125118. URL: https://link.aps.org/doi/10.1103/PhysRevB.99.125118.

[KR23] Christina Koliofoti and Roman-Pascal Riwar. "Compact description of quantum phase slip junctions". In: *npj Quantum Information* 9.1 (2023), p. 125. ISSN: 2056-6387. DOI: 10.1038/s41534-023-00790-w. URL: https://doi.org/10.1038/s41534-023-00790-w.

[KS18] Alexei Kitaev and S Josephine Suh. "The soft mode in the Sachdev-Ye-Kitaev model and its gravity dual". In: *Journal of High Energy Physics* 2018.5 (2018), pp. 1–68.

[KS19] Alexei Kitaev and S Josephine Suh. "Statistical mechanics of a two-dimensional black hole". In: *Journal of High Energy Physics* 2019.5 (2019), pp. 1–56.

[KSA20] Ahmed Kord, Dimitrios L. Sounas, and Andrea Alù. "Microwave Nonreciprocity". In: *Proceedings of the IEEE* 108.10 (2020), pp. 1728–1758. DOI: 10.1109/JPROC.2020.3006041.

[Kun+18] Flore K. Kunst et al. "Biorthogonal Bulk-Boundary Correspondence in Non-Hermitian Systems". In: *Phys. Rev. Lett.* 121 (2 July 2018), p. 026808. DOI: 10.1103/PhysRevLett.121.026808.

[KYZ16] Vladimir V. Konotop, Jianke Yang, and Dmitry A. Zezyulin. "Nonlinear waves in $\mathcal{PT}$-symmetric systems". In: *Rev. Mod. Phys.* 88 (3 July 2016), p. 035002. DOI: 10.1103/RevModPhys.88.035002. URL: https://link.aps.org/doi/10.1103/RevModPhys.88.035002.

[Lac+19] Dany Lachance-Quirion et al. "Hybrid quantum systems based on magnonics". In: *Applied Physics Express* 12.7 (June 2019), p. 070101. DOI: 10.7567/1882-0786/ab248d. URL: https://dx.doi.org/10.7567/1882-0786/ab248d.

[Lan15] Xiao-Gang Lan. "Measuring Hawking Radiation of a Kerr-Newman Black Hole in a Superconducting Transmission Line". In: *International Journal of Theoretical Physics* 54.1 (2015), pp. 116–122. ISSN: 1572-9575. DOI: 10.1007/s10773-014-2207-5. URL: https://doi.org/10.1007/s10773-014-2207-5.

[Lan76] R. Landauer. “Can capacitance be negative?” In: *Collect. Phenom.* 2 (1976), pp. 167–170.

[Lau81] R. B. Laughlin. “Quantized Hall conductivity in two dimensions”. In: *Phys. Rev. B* 23 (10 May 1981), pp. 5632–5633. DOI: 10.1103/PhysRevB.23.5632. URL: https://link.aps.org/doi/10.1103/PhysRevB.23.5632.

[Lau83] R. B. Laughlin. “Anomalous Quantum Hall Effect: An Incompressible Quantum Fluid with Fractionally Charged Excitations”. In: *Phys. Rev. Lett.* 50 (18 May 1983), pp. 1395–1398. DOI: 10.1103/PhysRevLett.50.1395. URL: https://link.aps.org/doi/10.1103/PhysRevLett.50.1395.

[Lee+20] J. G. Lee et al. “New Test of the Gravitational $1/r^2$ Law at Separations down to 52 μm”. In: *Phys. Rev. Lett.* 124 (10 Mar. 2020), p. 101101. DOI: 10.1103/PhysRevLett.124.101101. URL: https://link.aps.org/doi/10.1103/PhysRevLett.124.101101.

[Les+20] Raphaël Lescanne et al. “Irreversible Qubit-Photon Coupling for the Detection of Itinerant Microwave Photons”. In: *Phys. Rev. X* 10 (2 May 2020), p. 021038. DOI: 10.1103/PhysRevX.10.021038. URL: https://link.aps.org/doi/10.1103/PhysRevX.10.021038.

[LGL05] Roman Lutchyn, Leonid Glazman, and Anatoly Larkin. “Quasiparticle decay rate of Josephson charge qubit oscillations”. In: *Phys. Rev. B* 72 (1 July 2005), p. 014517. DOI: 10.1103/PhysRevB.72.014517. URL: https://link.aps.org/doi/10.1103/PhysRevB.72.014517.

[Li+19] Chuan Li et al. “Zeeman-Effect-Induced $0-\pi$ Transitions in Ballistic Dirac Semimetal Josephson Junctions”. In: *Phys. Rev. Lett.* 123 (2 July 2019), p. 026802. DOI: 10.1103/PhysRevLett.123.026802. URL: https://link.aps.org/doi/10.1103/PhysRevLett.123.026802.

[Li+23] Aodong Li et al. “Exceptional points and non-Hermitian photonics at the nanoscale”. In: *Nature Nanotechnology* 18 (July 2023), pp. 706–720. DOI: 10.1038/s41565-023-01408-0.

[Lia+21] Qing Liao et al. “Experimental Measurement of the Divergent Quantum Metric of an Exceptional Point”. In: *Phys. Rev. Lett.* 127 (10 Sept. 2021), p. 107402. DOI: 10.1103/PhysRevLett.127.107402. URL: https://link.aps.org/doi/10.1103/PhysRevLett.127.107402.

[Lid20] Daniel A. Lidar. *Lecture Notes on the Theory of Open Quantum Systems.* 2020. arXiv: 1902.00967 [quant-ph]. URL: https://arxiv.org/abs/1902.00967.

[Lin+13] Netanel H. Lindner et al. “Topological Floquet spectrum in three dimensions via a two-photon resonance”. In: *Phys. Rev. B* 87 (23 June 2013), p. 235131. DOI: 10.1103/PhysRevB.87.235131. URL: https://link.aps.org/doi/10.1103/PhysRevB.87.235131.

[Lit64] W. A. Little. “Possibility of Synthesizing an Organic Superconductor”. In: *Phys. Rev.* 134 (6A June 1964), A1416–A1424. DOI: `https://doi.org/10.1103/PhysRev.134.A1416`. URL: `https://link.aps.org/doi/10.1103/PhysRev.134.A1416`.

[Liu+10] R-B Liu et al. “Dynamics revealed by correlations of time-distributed weak measurements of a single spin”. In: *New Journal of Physics* 12.1 (Jan. 2010), p. 013018. DOI: `10.1088/1367-2630/12/1/013018`. URL: `https://doi.org/10.1088/1367-2630/12/1/013018`.

[Liu+23] Tongjun Liu et al. “Photonic metamaterial analogue of a continuous time crystal”. In: *Nature Physics* 19 (July 2023), pp. 986–991. DOI: `10.1038/s41567-023-02023-5`.

[LLL96] Leonid S. Levitov, Hyunwoo Lee, and Gordey B. Lesovik. “Electron counting statistics and coherent states of electric current”. In: *Journal of Mathematical Physics* 37.10 (1996), pp. 4845–4866. DOI: `10.1063/1.531672`.

[LM12] Juha Leppäkangas and Michael Marthaler. “Fragility of flux qubits against quasiparticle tunneling”. In: *Phys. Rev. B* 85 (14 Apr. 2012), p. 144503. DOI: `10.1103/PhysRevB.85.144503`. URL: `https://link.aps.org/doi/10.1103/PhysRevB.85.144503`.

[LM77] J. M. Leinaas and J. Myrheim. “On the theory of identical particles”. In: *Il Nuovo Cimento B (1971-1996)* 37.1 (1977), pp. 1–23. ISSN: 1826-9877. DOI: `10.1007/BF02727953`. URL: `https://doi.org/10.1007/BF02727953`.

[LMC20] Simon Lieu, Max McGinley, and Nigel R. Cooper. “Tenfold Way for Quadratic Lindbladians”. In: *Phys. Rev. Lett.* 124 (4 Jan. 2020), p. 040401. DOI: `10.1103/PhysRevLett.124.040401`. URL: `https://link.aps.org/doi/10.1103/PhysRevLett.124.040401`.

[LRS14] Fuxiang Li, Jie Ren, and Nikolai A. Sinitsyn. “Quantum Zeno effect as a topological phase transition in full counting statistics and spin noise spectroscopy”. In: *EPL* 105.2 (2014), p. 27001. DOI: `10.1209/0295-5075/105/27001`. URL: `https://doi.org/10.1209/0295-5075/105/27001`.

[LSD10] Roman M. Lutchyn, Jay D. Sau, and S. Das Sarma. “Majorana Fermions and a Topological Phase Transition in Semiconductor-Superconductor Heterostructures”. In: *Phys. Rev. Lett.* 105 (7 Aug. 2010), p. 077001. DOI: `10.1103/PhysRevLett.105.077001`. URL: `https://link.aps.org/doi/10.1103/PhysRevLett.105.077001`.

[MAA09] John M. Martinis, M. Ansmann, and J. Aumentado. "Energy Decay in Superconducting Josephson-Junction Qubits from Nonequilibrium Quasiparticle Excitations". In: *Phys. Rev. Lett.* 103 (9 Aug. 2009), p. 097002. DOI: 10.1103/PhysRevLett.103.097002. URL: https://link.aps.org/doi/10.1103/PhysRevLett.103.097002.

[MAG16] Eric J. Meier, Fangzhao Alex An, and Bryce Gadway. "Observation of the topological soliton state in the Su–Schrieffer–Heeger model". In: *Nature Communications* 7.1 (2016), p. 13986.

[Man+09] Vladimir E. Manucharyan et al. "Fluxonium: Single Cooper-Pair Circuit Free of Charge Offsets". In: *Science* 326.5949 (2009), pp. 113–116. DOI: 10.1126/science.1175552. URL: https://science.sciencemag.org/content/326/5949/113.

[Mat+14] Clemens Matthiesen et al. "Full counting statistics of quantum dot resonance fluorescence". In: *Scientific Reports* 4.1 (May 9, 2014), p. 4911. ISSN: 2045-2322. DOI: 10.1038/srep04911. URL: https://doi.org/10.1038/srep04911.

[MB07] J. E. Moore and L. Balents. "Topological invariants of time-reversal-invariant band structures". In: *Phys. Rev. B* 75 (12 Mar. 2007), p. 121306. DOI: 10.1103/PhysRevB.75.121306. URL: https://link.aps.org/doi/10.1103/PhysRevB.75.121306.

[MB21] Ipsita Mandal and Emil J. Bergholtz. "Symmetry and Higher-Order Exceptional Points". In: *Phys. Rev. Lett.* 127 (18 Oct. 2021), p. 186601. DOI: 10.1103/PhysRevLett.127.186601. URL: https://link.aps.org/doi/10.1103/PhysRevLett.127.186601.

[MC15] A. Metelmann and A. A. Clerk. "Nonreciprocal Photon Transmission and Amplification via Reservoir Engineering". In: *Phys. Rev. X* 5 (2 June 2015), p. 021025. DOI: 10.1103/PhysRevX.5.021025. URL: https://link.aps.org/doi/10.1103/PhysRevX.5.021025.

[MC17] A. Metelmann and A. A. Clerk. "Nonreciprocal quantum interactions and devices via autonomous feedforward". In: *Phys. Rev. A* 95 (1 Jan. 2017), p. 013837. DOI: 10.1103/PhysRevA.95.013837. URL: https://link.aps.org/doi/10.1103/PhysRevA.95.013837.

[MC18] Max McGinley and Nigel R. Cooper. "Topology of One-Dimensional Quantum Systems Out of Equilibrium". In: *Phys. Rev. Lett.* 121 (9 Aug. 2018), p. 090401. DOI: 10.1103/PhysRevLett.121.090401. URL: https://link.aps.org/doi/10.1103/PhysRevLett.121.090401.

[MC19] Max McGinley and Nigel R. Cooper. "Classification of topological insulators and superconductors out of equilibrium". In: *Phys. Rev. B* 99 (7 Feb. 2019), p. 075148. DOI: 10.1103/PhysRevB.99.075148. URL: https://link.aps.org/doi/10.1103/PhysRevB.99.075148.

[MH17] Julia S. Meyer and Manuel Houzet. “Nontrivial Chern Numbers in Three-Terminal Josephson Junctions”. In: *Phys. Rev. Lett.* 119 (13 Sept. 2017), p. 136807. DOI: 10.1103/PhysRevLett.119.136807. URL: https://link.aps.org/doi/10.1103/PhysRevLett.119.136807.

[Min+07] Makoto Mine et al. “Quantum field theoretical description of unstable behavior of trapped Bose–Einstein condensates with complex eigenvalues of Bogoliubov–de Gennes equations”. In: *Annals of Physics* 322.10 (2007), pp. 2327–2349. ISSN: 0003-4916. DOI: https://doi.org/10.1016/j.aop.2007.01.008. URL: https://www.sciencedirect.com/science/article/pii/S0003491607000152.

[MP88] VP Mitrofanov and OI Ponomareva. “Experimental test of gravitation at small distances”. In: *Sov. Phys. JETP* 67.10 (1988), p. 1963. URL: http://jetp.ras.ru/cgi-bin/dn/e_067_10_1963.pdf.

[MPS15] Simon Malzard, Charles Poli, and Henning Schomerus. “Topologically Protected Defect States in Open Photonic Systems with Non-Hermitian Charge-Conjugation and Parity-Time Symmetry”. In: *Phys. Rev. Lett.* 115 (20 Nov. 2015), p. 200402. DOI: 10.1103/PhysRevLett.115.200402. URL: https://link.aps.org/doi/10.1103/PhysRevLett.115.200402.

[MTY24] F.J. Matute-Cañadas, L. Tosi, and A. Levy Yeyati. “Quantum Circuits with Multiterminal Josephson-Andreev Junctions”. In: *PRX Quantum* 5 (2 May 2024), p. 020340. DOI: 10.1103/PRXQuantum.5.020340. URL: https://link.aps.org/doi/10.1103/PRXQuantum.5.020340.

[Muñ+19] Juan Ramón Muñoz de Nova et al. “Observation of thermal Hawking radiation and its temperature in an analogue black hole”. In: *Nature* 569 (2019), pp. 688–691. DOI: https://doi.org/10.1038/s41586-019-1241-0. URL: https://doi.org/10.1038/s41586-019-1241-0.

[Mur+20] A. Murani et al. “Absence of a Dissipative Quantum Phase Transition in Josephson Junctions”. In: *Phys. Rev. X* 10 (2 Apr. 2020), p. 021003. DOI: 10.1103/PhysRevX.10.021003. URL: https://link.aps.org/doi/10.1103/PhysRevX.10.021003.

[Mur+21] A. Murani et al. “Reply to “Comment on ‘Absence of a Dissipative Quantum Phase Transition in Josephson Junctions’””. In: *Phys. Rev. X* 11 (1 Mar. 2021), p. 018002. DOI: 10.1103/PhysRevX.11.018002. URL: https://link.aps.org/doi/10.1103/PhysRevX.11.018002.

[MY20] Ari Mizel and Yariv Yanay. “Right-sizing fluxonium against charge noise”. In: *Phys. Rev. B* 102 (1 July 2020), p. 014512. DOI: 10.1103/PhysRevB.102.014512. URL: https://link.aps.org/doi/10.1103/PhysRevB.102.014512.

[Nak+08] Y. Nakamura et al. “Condition for emergence of complex eigenvalues in the Bogoliubov–de Gennes equations”. In: *Phys. Rev. A* 77 (4 Mar. 2008), p. 043601. DOI: `10.1103/PhysRevA.77.043601`. URL: `https://link.aps.org/doi/10.1103/PhysRevA.77.043601`.

[Nak58] Sadao Nakajima. “On Quantum Theory of Transport Phenomena: Steady Diffusion”. In: *Progress of Theoretical Physics* 20.6 (Dec. 1958), pp. 948–959. ISSN: 0033-068X. DOI: `10.1143/PTP.20.948`. URL: `https://doi.org/10.1143/PTP.20.948`.

[Nat+09] P. D. Nation et al. “Analogue Hawking Radiation in a dc-SQUID Array Transmission Line”. In: *Phys. Rev. Lett.* 103 (8 Aug. 2009), p. 087004. DOI: `10.1103/PhysRevLett.103.087004`. URL: `https://link.aps.org/doi/10.1103/PhysRevLett.103.087004`.

[NB02] Yu. V. Nazarov and D. A. Bagrets. “Circuit Theory for Full Counting Statistics in Multiterminal Circuits”. In: *Phys. Rev. Lett.* 88 (19 Apr. 2002), p. 196801. DOI: `10.1103/PhysRevLett.88.196801`.

[NBW21] K. Nestmann, V. Bruch, and M. R. Wegewijs. “How Quantum Evolution with Memory is Generated in a Time-Local Way”. In: *Phys. Rev. X* 11 (2 May 2021), p. 021041. DOI: `10.1103/PhysRevX.11.021041`. URL: `https://link.aps.org/doi/10.1103/PhysRevX.11.021041`.

[NN81] H.B. Nielsen and M. Ninomiya. “A no-go theorem for regularizing chiral fermions”. In: *Physics Letters B* 105.2 (1981), pp. 219–223. ISSN: 0370-2693. DOI: `https://doi.org/10.1016/0370-2693(81)91026-1`. URL: `http://www.sciencedirect.com/science/article/pii/0370269381910261`.

[Ole+22] Nikita A. Olekhno et al. “Topological transitions driven by quantum statistics and their electrical circuit emulation”. In: *Phys. Rev. B* 105 (20 May 2022), p. 205113. DOI: `10.1103/PhysRevB.105.205113`. URL: `https://link.aps.org/doi/10.1103/PhysRevB.105.205113`.

[Ort+15] Christoph P. Orth et al. “Non-Abelian parafermions in time-reversal-invariant interacting helical systems”. In: *Phys. Rev. B* 91 (8 Feb. 2015), p. 081406. DOI: `10.1103/PhysRevB.91.081406`. URL: `https://link.aps.org/doi/10.1103/PhysRevB.91.081406`.

[OY19] Ryo Okugawa and Takehito Yokoyama. “Topological exceptional surfaces in non-Hermitian systems with parity-time and parity-particle-hole symmetries”. In: *Phys. Rev. B* 99 (4 Jan. 2019), p. 041202. DOI: `10.1103/PhysRevB.99.041202`. URL: `https://link.aps.org/doi/10.1103/PhysRevB.99.041202`.

[Özt+21] Fahri Emre Öztürk et al. “Observation of a non-Hermitian phase transition in an optical quantum gas”. In: *Science* 372.6537 (2021), pp. 88–91. DOI: 10.1126/science.abe9869. eprint: https://www.science.org/doi/pdf/10.1126/science.abe9869. URL: https://www.science.org/doi/abs/10.1126/science.abe9869.

[PB18] Subhajit Pal and Colin Benjamin. “Tuning the $0-\pi$ Josephson junction with a magnetic impurity: Role of tunnel contacts, exchange coupling, $e-e$ interactions and high-spin states.” In: *Scientific Reports* 8 (Mar. 2018), p. 5208. DOI: https://doi.org/10.1038/s41598-018-23517-w. URL: https://www.nature.com/articles/s41598-018-23517-w.

[Pek+13] Jukka P. Pekola et al. “Single-electron current sources: Toward a refined definition of the ampere”. In: *Reviews of Modern Physics* 85.4 (Oct. 2013), pp. 1421–1472. DOI: 10.1103/RevModPhys.85.1421. URL: https://link.aps.org/doi/10.1103/RevModPhys.85.1421.

[Pen14] Roger Penrose. “On the Gravitization of Quantum Mechanics 1: Quantum State Reduction”. In: *Foundations of Physics* 44.5 (May 1, 2014), pp. 557–575. ISSN: 1572-9516. DOI: 10.1007/s10701-013-9770-0. URL: https://doi.org/10.1007/s10701-013-9770-0.

[Per95] A. Peres. *Quantum Theory: Concepts and Method*. Kluwer Academic Publishers, 1995.

[Pey+21] L. Peyruchat et al. “Transconductance quantization in a topological Josephson tunnel junction circuit”. In: *Phys. Rev. Research* 3 (1 Mar. 2021), p. 013289. DOI: 10.1103/PhysRevResearch.3.013289. URL: https://link.aps.org/doi/10.1103/PhysRevResearch.3.013289.

[PFL10] Angus Prain, Serena Fagnocchi, and Stefano Liberati. “Analogue cosmological particle creation: Quantum correlations in expanding Bose-Einstein condensates”. In: *Phys. Rev. D* 82 (10 Nov. 2010), p. 105018. DOI: 10.1103/PhysRevD.82.105018. URL: https://link.aps.org/doi/10.1103/PhysRevD.82.105018.

[PGK07] Marco G Pala, Michele Governale, and Jürgen König. “Nonequilibrium Josephson and Andreev current through interacting quantum dots”. In: *New Journal of Physics* 9.8 (Aug. 2007), pp. 278–278. DOI: 10.1088/1367-2630/9/8/278. URL: https://doi.org/10.1088/1367-2630/9/8/278.

[PGL00] K.-V. Pham, M. Gabay, and P. Lederer. “Fractional excitations in the Luttinger liquid”. In: *Phys. Rev. B* 61 (24 June 2000), pp. 16397–16422. DOI: 10.1103/PhysRevB.61.16397. URL: https://link.aps.org/doi/10.1103/PhysRevB.61.16397.

[Pin+18] H Pino et al. “On-chip quantum interference of a superconducting microsphere”. In: *Quantum Science and Technology* 3.2 (2018), p. 025001. URL: https://doi.org/10.1088/2058-9565/aa9d15.

[Pis04] F. Pistolesi. "Full counting statistics of a charge shuttle". In: *Phys. Rev. B* 69 (24 June 2004), p. 245409. DOI: 10.1103/PhysRevB.69.245409. URL: https://link.aps.org/doi/10.1103/PhysRevB.69.245409.

[Pla+18] B. A. Placke et al. "Attractive and driven interactions in quantum dots: Mechanisms for geometric pumping". In: *Phys. Rev. B* 98 (8 Aug. 2018), p. 085307. DOI: https://doi.org/10.1103/PhysRevB.98.085307. URL: https://link.aps.org/doi/10.1103/PhysRevB.98.085307.

[Poz12] D. M. Pozar. *Microwave Engineering.* Hoboken, NJ: Wiley, 2012.

[Pro08] Tomaž Prosen. "Third quantization: a general method to solve master equations for quadratic open Fermi systems". In: *New Journal of Physics* 10.4 (Apr. 2008), p. 043026. DOI: 10.1088/1367-2630/10/4/043026. URL: https://dx.doi.org/10.1088/1367-2630/10/4/043026.

[Pro10] Tomaž Prosen. "Spectral theorem for the Lindblad equation for quadratic open fermionic systems". In: *Journal of Statistical Mechanics: Theory and Experiment* 2010.07 (July 2010), P07020. DOI: 10.1088/1742-5468/2010/07/P07020. URL: https://dx.doi.org/10.1088/1742-5468/2010/07/P07020.

[PWS] T. Pluecker, M. R. Wegewijs, and J. Splettstoesser. *Meter calibration and the geometric pumping process in open quantum systems.* arXiv: 1711.10431v1 [cond-mat.mes-hall].

[PWS17] T. Pluecker, M. R. Wegewijs, and J. Splettstoesser. "Gauge freedom in observables and Landsberg's nonadiabatic geometric phase: Pumping spectroscopy of interacting open quantum systems". In: *Phys. Rev. B* 95 (15 Apr. 2017), p. 155431. DOI: 10.1103/PhysRevB.95.155431. URL: https://link.aps.org/doi/10.1103/PhysRevB.95.155431.

[Qi+09] Xiao-Liang Qi et al. "Time-Reversal-Invariant Topological Superconductors and Superfluids in Two and Three Dimensions". In: *Phys. Rev. Lett.* 102 (18 May 2009), p. 187001. DOI: 10.1103/PhysRevLett.102.187001. URL: https://link.aps.org/doi/10.1103/PhysRevLett.102.187001.

[QZ11] Xiao-Liang Qi and Shou-Cheng Zhang. "Topological insulators and superconductors". In: *Rev. Mod. Phys.* 83 (4 Oct. 2011), pp. 1057–1110. DOI: 10.1103/RevModPhys.83.1057. URL: https://link.aps.org/doi/10.1103/RevModPhys.83.1057.

[RA00] A. V. Rozhkov and Daniel P. Arovas. "Interacting-impurity Josephson junction: Variational wave functions and slave-boson mean-field theory". In: *Phys. Rev. B* 62 (10 Sept. 2000), pp. 6687–6691. DOI: 10.1103/PhysRevB.62.6687. URL: https://link.aps.org/doi/10.1103/PhysRevB.62.6687.

[RB82] R. Rajaraman and J.S. Bell. "On solitons with half integral charge". In: *Physics Letters B* 116.2 (1982), pp. 151–154. ISSN: 0370-2693. DOI: `https://doi.org/10.1016/0370-2693(82)90996-0`. URL: `https://www.sciencedirect.com/science/article/pii/0370269382909960`.

[RBF22] Caio C. Holanda Ribeiro, Sang-Shin Baak, and Uwe R. Fischer. "Existence of steady-state black hole analogs in finite quasi-one-dimensional Bose-Einstein condensates". In: *Phys. Rev. D* 105 (12 June 2022), p. 124066. DOI: `10.1103/PhysRevD.105.124066`. URL: `https://link.aps.org/doi/10.1103/PhysRevD.105.124066`.

[RC19] R. -P. Riwar and G. Catelani. "Efficient quasiparticle traps with low dissipation through gap engineering". In: *Physical Review B* 100.14 (Oct. 2019), pp. 144514–. DOI: `10.1103/PhysRevB.100.144514`. URL: `https://link.aps.org/doi/10.1103/PhysRevB.100.144514`.

[RD22] R. -P. Riwar and D. P. DiVincenzo. "Circuit quantization with time-dependent magnetic fields for realistic geometries". In: *npj Quantum Information* 8.1 (2022), p. 36. ISSN: 2056-6387. DOI: `10.1038/s41534-022-00539-x`. URL: `https://doi.org/10.1038/s41534-022-00539-x`.

[Ris+13] D. Ristè et al. "Millisecond charge-parity fluctuations and induced decoherence in a superconducting transmon qubit". In: *Nature Communications* 4.1 (2013), p. 1913. ISSN: 2041-1723. DOI: `10.1038/ncomms2936`. URL: `https://doi.org/10.1038/ncomms2936`.

[Riw+16a] Roman-Pascal Riwar et al. "Multi-terminal Josephson junctions as topological matter". In: *Nature Communications* 7.1 (2016), p. 11167. DOI: `10.1038/ncomms11167`. URL: `https://doi.org/10.1038/ncomms11167`.

[Riw+16b] Roman-Pascal Riwar et al. "Multi-terminal Josephson junctions as topological matter". In: *Nature Communications* 7.1 (2016), p. 11167. ISSN: 2041-1723. DOI: `10.1038/ncomms11167`. URL: `https://doi.org/10.1038/ncomms11167`.

[Riw19] Roman-Pascal Riwar. "Fractional charges in conventional sequential electron tunneling". In: *Phys. Rev. B* 100 (24 Dec. 2019), p. 245416. DOI: `10.1103/PhysRevB.100.245416`. URL: `https://link.aps.org/doi/10.1103/PhysRevB.100.245416`.

[Riw21] Roman-Pascal Riwar. "Charge quantization and detector resolution". In: *SciPost Phys.* 10 (4 2021), p. 93. DOI: `10.21468/SciPostPhys.10.4.093`. URL: `https://scipost.org/10.21468/SciPostPhys.10.4.093`.

[Riw23] R. -P. Riwar. *Discrete control of capacitance in quantum circuits*. 2023. arXiv: `2306.00587 [cond-mat.supr-con]`. URL: `https://arxiv.org/abs/2306.00587`.

[RL09] M. S. Rudner and L. S. Levitov. "Topological Transition in a Non-Hermitian Quantum Walk". In: *Phys. Rev. Lett.* 102 (6 Feb. 2009), p. 065703. DOI: 10.1103/PhysRevLett.102.065703. URL: https://link.aps.org/doi/10.1103/PhysRevLett.102.065703.

[RL10] M. S. Rudner and L. S. Levitov. "Phase transitions in dissipative quantum transport and mesoscopic nuclear spin pumping". In: *Phys. Rev. B* 82 (15 Oct. 2010), p. 155418. DOI: 10.1103/PhysRevB.82.155418. URL: https://link.aps.org/doi/10.1103/PhysRevB.82.155418.

[RL12] Diego Rainis and Daniel Loss. "Majorana qubit decoherence by quasi-particle poisoning". In: *Phys. Rev. B* 85 (17 May 2012), p. 174533. DOI: 10.1103/PhysRevB.85.174533. URL: https://link.aps.org/doi/10.1103/PhysRevB.85.174533.

[RLL] Mark S. Rudner, Michael Levin, and Leonid S. Levitov. *Survival, decay, and topological protection in non-Hermitian quantum transport.* arXiv: 1605.07652v1 [cond-mat.mes-hall].

[RN04] Alessandro Romito and Yu. V. Nazarov. "Full counting statistics of Cooper pair shuttling". In: *Phys. Rev. B* 70 (21 Dec. 2004), p. 212509. DOI: 10.1103/PhysRevB.70.212509. URL: https://link.aps.org/doi/10.1103/PhysRevB.70.212509.

[Rob12] Scott J Robertson. "The theory of Hawking radiation in laboratory analogues". In: *Journal of Physics B: Atomic, Molecular and Optical Physics* 45.16 (Aug. 2012), p. 163001. DOI: 10.1088/0953-4075/45/16/163001. URL: https://dx.doi.org/10.1088/0953-4075/45/16/163001.

[Roc+13] B. Roche et al. "A two-atom electron pump". In: *Nature Communications* 4.1 (2013), p. 1581. ISSN: 2041-1723. DOI: 10.1038/ncomms2544. URL: https://doi.org/10.1038/ncomms2544.

[Rom17] Oriol Romero-Isart. "Coherent inflation for large quantum superpositions of levitated microspheres". In: *New Journal of Physics* 19.12 (2017), p. 123029. URL: https://doi.org/10.1088/1367-2630/aa99bf.

[Roy08] Rahul Roy. *Topological superfluids with time reversal symmetry.* 2008. arXiv: 0803.2868 [cond-mat.mes-hall]. URL: https://arxiv.org/abs/0803.2868.

[RS13] Jie Ren and N. A. Sinitsyn. "Braid group and topological phase transitions in nonequilibrium stochastic dynamics". In: *Phys. Rev. E* 87 (5 May 2013), p. 050101. DOI: 10.1103/PhysRevE.87.050101.

[RSB24] I. C. Rodrigues, G. A. Steele, and D. Bothner. "Photon Pressure with an Effective Negative Mass Microwave Mode". In: *Phys. Rev. Lett.* 132 (20 May 2024), p. 203603. DOI: 10.1103/PhysRevLett.132.203603. URL: https://link.aps.org/doi/10.1103/PhysRevLett.132.203603.

[RSK13] Roman-Pascal Riwar, Janine Splettstoesser, and Jürgen König. "Zero-frequency noise in adiabatically driven interacting quantum systems". In: *Phys. Rev. B* 87 (19 May 2013), p. 195407. DOI: 10.1103/PhysRevB.87.195407. URL: https://link.aps.org/doi/10.1103/PhysRevB.87.195407.

[Rym+21] Martin Rymarz et al. "Hardware-Encoding Grid States in a Nonreciprocal Superconducting Circuit". In: *Phys. Rev. X* 11 (1 Feb. 2021), p. 011032. DOI: 10.1103/PhysRevX.11.011032. URL: https://link.aps.org/doi/10.1103/PhysRevX.11.011032.

[Ryu+10] Shinsei Ryu et al. "Topological insulators and superconductors: tenfold way and dimensional hierarchy". In: *New Journal of Physics* 12.6 (June 2010), p. 065010. DOI: 10.1088/1367-2630/12/6/065010. URL: https://dx.doi.org/10.1088/1367-2630/12/6/065010.

[Sab16] Carlos Sabín. "Quantum simulation of traversable wormhole spacetimes in a dc-SQUID array". In: *Phys. Rev. D* 94 (8 Oct. 2016), p. 081501. DOI: 10.1103/PhysRevD.94.081501. URL: https://link.aps.org/doi/10.1103/PhysRevD.94.081501.

[Sab18] Carlos Sabín. "One-dimensional sections of exotic spacetimes with superconducting circuits". In: *New Journal of Physics* 20.5 (May 2018), p. 053028. DOI: 10.1088/1367-2630/aac0db. URL: https://dx.doi.org/10.1088/1367-2630/aac0db.

[Sac15] Subir Sachdev. "Bekenstein-Hawking Entropy and Strange Metals". In: *Phys. Rev. X* 5 (4 Nov. 2015), p. 041025. DOI: 10.1103/PhysRevX.5.041025. URL: https://link.aps.org/doi/10.1103/PhysRevX.5.041025.

[Sam+97] L. Saminadayar et al. "Observation of the $e/3$ Fractionally Charged Laughlin Quasiparticle". In: *Phys. Rev. Lett.* 79 (13 Sept. 1997), pp. 2526–2529. DOI: 10.1103/PhysRevLett.79.2526. URL: https://link.aps.org/doi/10.1103/PhysRevLett.79.2526.

[San+16] Pablo San-Jose et al. "Majorana bound states from exceptional points in non-topological superconductors". In: *Scientific Reports* 6 (Feb. 2016). DOI: 10.1038/srep21427. URL: https://rdcu.be/c0zRe.

[Sch+08] Andreas P. Schnyder et al. "Classification of topological insulators and superconductors in three spatial dimensions". In: *Phys. Rev. B* 78 (19 Nov. 2008), p. 195125. DOI: 10.1103/PhysRevB.78.195125. URL: https://link.aps.org/doi/10.1103/PhysRevB.78.195125.

[Sch20] Jakob Schwibbert. *Topological phases in the FCS of a hybrid superconductor-normal metal quantum circuit.* Master thesis, RWTH Aachen. Aug. 2020.

[Sch83] Albert Schmid. “Diffusion and Localization in a Dissipative Quantum System”. In: *Phys. Rev. Lett.* 51 (17 Oct. 1983), pp. 1506–1509. DOI: 10.1103/PhysRevLett.51.1506. URL: https://link.aps.org/doi/10.1103/PhysRevLett.51.1506.

[Sel+23] Lev-Arcady Sellem et al. *A GKP qubit protected by dissipation in a high-impedance superconducting circuit driven by a microwave frequency comb*. 2023. arXiv: 2304.01425 [quant-ph].

[Sha+08] M. D. Shaw et al. “Kinetics of nonequilibrium quasiparticle tunneling in superconducting charge qubits”. In: *Phys. Rev. B* 78 (2 July 2008), p. 024503. DOI: 10.1103/PhysRevB.78.024503. URL: https://link.aps.org/doi/10.1103/PhysRevB.78.024503.

[SK14] Soller, H. and Komnik, A. “Full counting statistics of interacting quantum dots contacted by a normal metal and a superconductor”. In: *EPL* 106.3 (2014), p. 37009. DOI: 10.1209/0295-5075/106/37009. URL: https://doi.org/10.1209/0295-5075/106/37009.

[SKB09] Gernot Schaller, Gerold Kießlich, and Tobias Brandes. “Transport statistics of interacting double dot systems: Coherent and non-Markovian effects”. In: *Phys. Rev. B* 80 (24 Dec. 2009), p. 245107. DOI: 10.1103/PhysRevB.80.245107. URL: https://link.aps.org/doi/10.1103/PhysRevB.80.245107.

[SMH22] Sarath Sankar, Julia S. Meyer, and Manuel Houzet. “Josephson effect in superconductor/normal-dot/superconductor junctions driven out of equilibrium by quasiparticle injection”. In: *Phys. Rev. B* 105 (13 Apr. 2022), p. 134515. DOI: 10.1103/PhysRevB.105.134515. URL: https://link.aps.org/doi/10.1103/PhysRevB.105.134515.

[Smi+22] W. C. Smith et al. “Magnifying Quantum Phase Fluctuations with Cooper-Pair Pairing”. In: *Phys. Rev. X* 12 (2 Apr. 2022), p. 021002. DOI: 10.1103/PhysRevX.12.021002. URL: https://link.aps.org/doi/10.1103/PhysRevX.12.021002.

[Sot+10] Björn Sothmann et al. “Probing the exchange field of a quantum-dot spin valve by a superconducting lead”. In: *Phys. Rev. B* 82 (9 Sept. 2010), p. 094514. DOI: 10.1103/PhysRevB.82.094514. URL: https://link.aps.org/doi/10.1103/PhysRevB.82.094514.

[Sot+14] Björn Sothmann et al. “Unconventional superconductivity in double quantum dots”. In: *Phys. Rev. B* 90 (22 Dec. 2014), p. 220501. DOI: 10.1103/PhysRevB.90.220501. URL: https://link.aps.org/doi/10.1103/PhysRevB.90.220501.

[Spl+10] Janine Splettstoesser et al. “Charge and spin dynamics in interacting quantum dots”. In: *Phys. Rev. B* 81 (16 Apr. 2010), p. 165318. DOI: 10.1103/PhysRevB.81.165318. URL: https://link.aps.org/doi/10.1103/PhysRevB.81.165318.

[Ste+01] A. Steinbach et al. “Direct Measurement of the Josephson Supercurrent in an Ultrasmall Josephson Junction”. In: *Phys. Rev. Lett.* 87 (13 Sept. 2001), p. 137003. DOI: 10.1103/PhysRevLett.87.137003. URL: https://link.aps.org/doi/10.1103/PhysRevLett.87.137003.

[Ste+07] Hadar Steinberg et al. “Charge fractionalization in quantum wires”. In: *Nature Physics* 4 (Dec. 2007), p. 116. DOI: 10.1038/nphys810. URL: https://doi.org/10.1038/nphys810.

[Ste+22] Jeff Steinhauer et al. “Analogue cosmological particle creation in an ultracold quantum fluid of light”. In: *Nature Communications* 13.1 (2022), p. 2890. ISSN: 2041-1723. DOI: 10.1038/s41467-022-30603-1. URL: https://doi.org/10.1038/s41467-022-30603-1.

[Ste14] Jeff Steinhauer. “Observation of self-amplifying Hawking radiation in an analogue black-hole laser”. In: *Nature Physics* 10.11 (Nov. 1, 2014), pp. 864–869. ISSN: 1745-2481. DOI: 10.1038/nphys3104. URL: https://doi.org/10.1038/nphys3104.

[STW20] Raphael P Schmit, Bruno G Taketani, and Frank K Wilhelm. “Quantum simulation of particle creation in curved space-time”. In: *Plos one* 15.3 (2020), e0229382.

[SU05] Ralf Schützhold and William G. Unruh. “Hawking Radiation in an Electromagnetic Waveguide?” In: *Phys. Rev. Lett.* 95 (3 July 2005), p. 031301. DOI: 10.1103/PhysRevLett.95.031301. URL: https://link.aps.org/doi/10.1103/PhysRevLett.95.031301.

[SW12] R. B. Saptsov and M. R. Wegewijs. “Fermionic superoperators for zero-temperature nonlinear transport: Real-time perturbation theory and renormalization group for Anderson quantum dots”. In: *Phys. Rev. B* 86 (23 Dec. 2012), p. 235432. DOI: 10.1103/PhysRevB.86.235432. URL: https://link.aps.org/doi/10.1103/PhysRevB.86.235432.

[SY93] Subir Sachdev and Jinwu Ye. “Gapless spin-fluid ground state in a random quantum Heisenberg magnet”. In: *Phys. Rev. Lett.* 70 (21 May 1993), pp. 3339–3342. DOI: 10.1103/PhysRevLett.70.3339. URL: https://link.aps.org/doi/10.1103/PhysRevLett.70.3339.

[TD19] Zehua Tian and Jiangfeng Du. “Analogue Hawking radiation and quantum soliton evaporation in a superconducting circuit”. In: *Eur. Phys. J. C.* 79.12 (2019), p. 994. ISSN: 1434-6052. DOI: 10.1140/epjc/s10052-019-7514-9. URL: https://doi.org/10.1140/epjc/s10052-019-7514-9.

[Teb+21] Felix Tebbenjohanns et al. “Quantum control of a nanoparticle optically levitated in cryogenic free space”. In: *Nature* 595.7867 (2021), pp. 378–382. URL: https://doi.org/10.1038/s41586-021-03617-w.

[Tel48] B.D.H. Tellegen. “The Gyrator, a New Electric Network Element.” In: *Philips Research Reports* 3 (1948), pp. 81–101.

[THD12] Barbara M. Terhal, Fabian Hassler, and David P. DiVincenzo. “From Majorana fermions to topological order”. In: *Phys. Rev. Lett.* 108 (26 June 2012), p. 260504. DOI: `10.1103/PhysRevLett.108.260504`. URL: `https://link.aps.org/doi/10.1103/PhysRevLett.108.260504`.

[Thi+03] Axel Thielmann et al. “Shot noise in tunneling transport through molecules and quantum dots”. In: *Phys. Rev. B* 68 (11 Sept. 2003), p. 115105. DOI: `10.1103/PhysRevB.68.115105`. URL: `https://link.aps.org/doi/10.1103/PhysRevB.68.115105`.

[Thi+05a] Axel Thielmann et al. “Cotunneling Current and Shot Noise in Quantum Dots”. In: *Phys. Rev. Lett.* 95 (14 Sept. 2005), p. 146806. DOI: `10.1103/PhysRevLett.95.146806`. URL: `https://link.aps.org/doi/10.1103/PhysRevLett.95.146806`.

[Thi+05b] Axel Thielmann et al. “Super-Poissonian noise, negative differential conductance, and relaxation effects in transport through molecules, quantum dots, and nanotubes”. In: *Phys. Rev. B* 71 (4 Jan. 2005), p. 045341. DOI: `10.1103/PhysRevB.71.045341`. URL: `https://link.aps.org/doi/10.1103/PhysRevB.71.045341`.

[Tho+82] D. J. Thouless et al. “Quantized Hall Conductance in a Two-Dimensional Periodic Potential”. In: *Phys. Rev. Lett.* 49 (6 Aug. 1982), pp. 405–408. DOI: `10.1103/PhysRevLett.49.405`. URL: `https://link.aps.org/doi/10.1103/PhysRevLett.49.405`.

[Tin04] Michael Tinkham. *Introduction to Superconductivity.* 2nd ed. Dover Publications, June 2004. ISBN: 0486435032. URL: `http://www.worldcat.org/isbn/0486435032`.

[Tra+04] Björn Trauzettel et al. “Appearance of Fractional Charge in the Noise of Nonchiral Luttinger Liquids”. In: *Phys. Rev. Lett.* 92 (22 June 2004), p. 226405. DOI: `10.1103/PhysRevLett.92.226405`. URL: `https://link.aps.org/doi/10.1103/PhysRevLett.92.226405`.

[TSG82] D. C. Tsui, H. L. Stormer, and A. C. Gossard. “Two-Dimensional Magnetotransport in the Extreme Quantum Limit”. In: *Phys. Rev. Lett.* 48 (22 May 1982), pp. 1559–1562. DOI: `10.1103/PhysRevLett.48.1559`. URL: `https://link.aps.org/doi/10.1103/PhysRevLett.48.1559`.

[Tsu24] Naoto Tsuji. “Floquet states”. In: *Encyclopedia of Condensed Matter Physics (Second Edition)*. Ed. by Tapash Chakraborty. Second Edition. Oxford: Academic Press, 2024, pp. 967–980. ISBN: 978-0-323-91408-6. DOI: `https://doi.org/10.1016/B978-0-323-90800-9.00241-9`. URL: `https://www.sciencedirect.com/science/article/pii/B9780323908009002419`.

[tV74] G. ’t Hooft and M. J. G. Veltman. “One loop divergencies in the theory of gravitation”. In: *Annales de l’institut Henri Poincaré. Section A, Physique Théorique* 20 (1974), p. 69.

[Ubb+12] Niels Ubbelohde et al. “Measurement of finite-frequency current statistics in a single-electron transistor”. In: *Nature Communications* 3 (Jan. 2012), p. 612. DOI: 10.1038/ncomms1620.

[UH16] Jascha Ulrich and Fabian Hassler. “Dual approach to circuit quantization using loop charges”. In: *Phys. Rev. B* 94 (9 Sept. 2016), p. 094505. DOI: 10.1103/PhysRevB.94.094505. URL: https://link.aps.org/doi/10.1103/PhysRevB.94.094505.

[Unr81] W. G. Unruh. “Experimental Black-Hole Evaporation?” In: *Phys. Rev. Lett.* 46 (21 May 1981), pp. 1351–1353. DOI: 10.1103/PhysRevLett.46.1351. URL: https://link.aps.org/doi/10.1103/PhysRevLett.46.1351.

[Ust98] A. V. Ustinov. “Solitons in Josephson junctions”. In: *Physica D: Nonlinear Phenomena* 123.1-4 (1998), pp. 315–329.

[VD14] Giovanni Viola and David P. DiVincenzo. “Hall Effect Gyrators and Circulators”. In: *Phys. Rev. X* 4 (2 May 2014), p. 021019. DOI: 10.1103/PhysRevX.4.021019. URL: https://link.aps.org/doi/10.1103/PhysRevX.4.021019.

[VD17] Uri Vool and Michel Devoret. “Introduction to quantum electromagnetic circuits”. In: *International Journal of Circuit Theory and Applications* 45.7 (2017), pp. 897–934. DOI: https://doi.org/10.1002/cta.2359. URL: https://onlinelibrary.wiley.com/doi/abs/10.1002/cta.2359.

[VH24] Pauli Virtanen and Tero T. Heikkilä. “Nonreciprocal Josephson Linear Response”. In: *Phys. Rev. Lett.* 132 (4 Jan. 2024), p. 046002. DOI: 10.1103/PhysRevLett.132.046002. URL: https://link.aps.org/doi/10.1103/PhysRevLett.132.046002.

[Vij+12] R. Vijay et al. “Stabilizing Rabi oscillations in a superconducting qubit using quantum feedback”. In: *Nature* 490.7418 (2012), pp. 77–80. ISSN: 1476-4687. DOI: 10.1038/nature11505. URL: https://doi.org/10.1038/nature11505.

[VMY03] E. Vecino, A. Martín-Rodero, and A. Levy Yeyati. “Josephson current through a correlated quantum level: Andreev states and π junction behavior”. In: *Phys. Rev. B* 68 (3 July 2003), p. 035105. DOI: 10.1103/PhysRevB.68.035105. URL: https://link.aps.org/doi/10.1103/PhysRevB.68.035105.

[Wal+00] A Wallraff et al. “Whispering vortices”. In: *Physical review letters* 84.1 (2000), p. 151.

[Wal+04] A. Wallraff et al. “Strong coupling of a single photon to a superconducting qubit using circuit quantum electrodynamics”. In: *Nature* 431.7005 (2004), pp. 162–167. ISSN: 1476-4687. DOI: 10.1038/nature02851. URL: https://doi.org/10.1038/nature02851.

[Wan+] Zhi Wang et al. *Transport theory for topological Josephson junctions with a Majorana qubit*. DOI: 10.48550/ARXIV.2204.09923. arXiv: 2204.09923. URL: https://arxiv.org/abs/2204.09923.

[Wei+21] H. Weisbrich et al. "Second Chern Number and Non-Abelian Berry Phase in Topological Superconducting Systems". In: *PRX Quantum* 2 (1 Jan. 2021), p. 010310. DOI: 10.1103/PRXQuantum.2.010310. URL: https://link.aps.org/doi/10.1103/PRXQuantum.2.010310.

[Wen17] G. Wendin. "Quantum information processing with superconducting circuits: a review". In: *Reports on Progress in Physics* 80.10 (Sept. 2017), p. 106001. DOI: 10.1088/1361-6633/aa7e1a. URL: https://doi.org/10.1088/1361-6633/aa7e1a.

[Wes+21] Tobias Westphal et al. "Measurement of gravitational coupling between millimetre-sized masses". In: *Nature* 591.7849 (2021), pp. 225–228. URL: https://www.nature.com/articles/s41586-021-03250-7.

[Wie+22] Benjamin J. Wieder et al. "Topological materials discovery from crystal symmetry". In: *Nature Reviews Materials* 7.3 (2022), pp. 196–216. DOI: 10.1038/s41578-021-00380-2. URL: https://doi.org/10.1038/s41578-021-00380-2.

[Wil+11] C. M. Wilson et al. "Observation of the dynamical Casimir effect in a superconducting circuit". In: *Nature* 479.7373 (Nov. 1, 2011), pp. 376–379. ISSN: 1476-4687. DOI: 10.1038/nature10561. URL: https://doi.org/10.1038/nature10561.

[Wil82] Frank Wilczek. "Quantum Mechanics of Fractional-Spin Particles". In: *Phys. Rev. Lett.* 49 (14 Oct. 1982), pp. 957–959. DOI: 10.1103/PhysRevLett.49.957. URL: https://link.aps.org/doi/10.1103/PhysRevLett.49.957.

[WJS19] H. C. Wu, L. Jin, and Z. Song. "Inversion symmetric non-Hermitian Chern insulator". In: *Phys. Rev. B* 100 (15 Oct. 2019), p. 155117. DOI: 10.1103/PhysRevB.100.155117. URL: https://link.aps.org/doi/10.1103/PhysRevB.100.155117.

[WK17] Stephan Weiss and Jürgen König. "Odd-triplet superconductivity in single-level quantum dots". In: *Phys. Rev. B* 96 (6 Aug. 2017), p. 064529. DOI: 10.1103/PhysRevB.96.064529. URL: https://link.aps.org/doi/10.1103/PhysRevB.96.064529.

[WMB24] Matteo M Wauters, Lorenzo Maffi, and Michele Burrello. "Engineering a Josephson junction chain for the simulation of the clock model". In: *arXiv preprint arXiv:2408.14549* (2024). URL: https://www.arxiv.org/abs/2408.14549.

[Wu 21] Y. Wu et al. “Strong Quantum Computational Advantage Using a Superconducting Quantum Processor”. In: *Phys. Rev. Lett.* 127 (2021), p. 180501. DOI: 10.1103/PhysRevLett.127.180501. URL: https://link.aps.org/doi/10.1103/PhysRevLett.127.180501.

[Xia+21] Shiqiang Xia et al. “Higher-order exceptional point and Landau–Zener Bloch oscillations in driven non-Hermitian photonic Lieb lattices”. In: *APL Photonics* 6.12 (Dec. 2021), p. 126106. ISSN: 2378-0967. DOI: 10.1063/5.0069633. eprint: https://pubs.aip.org/aip/app/article-pdf/doi/10.1063/5.0069633/14055975/126106_1_online.pdf. URL: https://doi.org/10.1063/5.0069633.

[XVL17] Hong-Yi Xie, Maxim G. Vavilov, and Alex Levchenko. “Topological Andreev bands in three-terminal Josephson junctions”. In: *Phys. Rev. B* 96 (16 Oct. 2017), p. 161406. DOI: 10.1103/PhysRevB.96.161406. URL: https://link.aps.org/doi/10.1103/PhysRevB.96.161406.

[XVL18] Hong-Yi Xie, Maxim G. Vavilov, and Alex Levchenko. “Weyl nodes in Andreev spectra of multiterminal Josephson junctions: Chern numbers, conductances, and supercurrents”. In: *Phys. Rev. B* 97 (3 Jan. 2018), p. 035443. DOI: 10.1103/PhysRevB.97.035443. URL: https://link.aps.org/doi/10.1103/PhysRevB.97.035443.

[YD84] Bernard Yurke and John S. Denker. “Quantum network theory”. In: *Phys. Rev. A* 29 (3 Mar. 1984), pp. 1419–1437. DOI: 10.1103/PhysRevA.29.1419. URL: https://link.aps.org/doi/10.1103/PhysRevA.29.1419.

[YSK19a] Xinyuan You, J. A. Sauls, and Jens Koch. “Circuit quantization in the presence of time-dependent external flux”. In: *Phys. Rev. B* 99 (17 May 2019), p. 174512. DOI: 10.1103/PhysRevB.99.174512. URL: https://link.aps.org/doi/10.1103/PhysRevB.99.174512.

[YSK19b] Xinyuan You, J. A. Sauls, and Jens Koch. “Circuit quantization in the presence of time-dependent external flux”. In: *Phys. Rev. B* 99 (17 May 2019), p. 174512. DOI: 10.1103/PhysRevB.99.174512. URL: https://link.aps.org/doi/10.1103/PhysRevB.99.174512.

[YTW16] Zhizhou Yu, Gao-Min Tang, and Jian Wang. “Full-counting statistics of transient energy current in mesoscopic systems”. In: *Phys. Rev. B* 93 (19 May 2016), p. 195419. DOI: 10.1103/PhysRevB.93.195419. URL: https://link.aps.org/doi/10.1103/PhysRevB.93.195419.

[YU20] Zongping Gong Yuto Ashida and Masahito Ueda. “Non-Hermitian physics”. In: *Advances in Physics* 69.3 (2020), pp. 249–435. DOI: 10.1080/00018732.2021.1876991. eprint: https://doi.org/10.1080/00018732.2021.1876991. URL: https://doi.org/10.1080/00018732.2021.1876991.

[Zir96] Martin R. Zirnbauer. “Riemannian symmetric superspaces and their origin in random-matrix theory”. In: *Journal of Mathematical Physics* 37.10 (Oct. 1996), pp. 4986–5018. ISSN: 0022-2488. DOI: 10.1063/1.531675. eprint: https://pubs.aip.org/aip/jmp/article-pdf/37/10/4986/19056249/4986_1_online.pdf. URL: https://doi.org/10.1063/1.531675.

[ZK14a] Fan Zhang and C. L. Kane. “Anomalous topological pumps and fractional Josephson effects”. In: *Phys. Rev. B* 90 (2 July 2014), p. 020501. DOI: 10.1103/PhysRevB.90.020501. URL: https://link.aps.org/doi/10.1103/PhysRevB.90.020501.

[ZK14b] Fan Zhang and C. L. Kane. “Time-Reversal-Invariant Z_4 Fractional Josephson Effect”. In: *Phys. Rev. Lett.* 113 (3 July 2014), p. 036401. DOI: 10.1103/PhysRevLett.113.036401. URL: https://link.aps.org/doi/10.1103/PhysRevLett.113.036401.

[Zub+16] Pavlo Zubko et al. “Negative capacitance in multidomain ferroelectric superlattices”. In: *Nature* 534.7608 (June 1, 2016), pp. 524–528. ISSN: 1476-4687. DOI: 10.1038/nature17659. URL: https://doi.org/10.1038/nature17659.

[Zwa60] Robert Zwanzig. “Ensemble Method in the Theory of Irreversibility”. In: *The Journal of Chemical Physics* 33.5 (1960), pp. 1338–1341. DOI: 10.1063/1.1731409. eprint: https://doi.org/10.1063/1.1731409. URL: https://doi.org/10.1063/1.1731409.

A. Extracting derivatives of eigenvalues from experiments

In the main text, we argue that the χ-derivatives of eigenvalues λ can be extracted from experimental data. We here briefly explain this statement. It is rooted in the first definition of FCS with time-local current measurements, as explained in Sec. 2.4.1 of the main text. Here, one measures the cumulants, as defined in Eqs. (2.15) and (2.16). The moment and cumulant generating functions can be expressed in terms of the eigenmodes of $L(\chi, \phi)$ as

$$
\begin{aligned}
m(\chi, \tau) &= e^{\tau c(\chi, \phi, \tau)} \equiv \operatorname{tr}\left[e^{L(\chi, \phi)\tau} \rho_0\right] \\
&= \sum_n e^{\lambda_n(\chi, \phi)\tau} \underbrace{\operatorname{tr}\left[|n(\chi, \phi)) (n(\chi, \phi)| \rho_0\right]}_{e^{\alpha_n(\chi, \phi)}} \\
&= \sum_n e^{\lambda_n(\chi, \phi)\tau + \alpha_n(\chi, \phi)} \\
&= e^{\lambda_0(\chi, \phi)\tau + \alpha_0(\chi, \phi)} + \sum_{n \neq 0} e^{\lambda_n(\chi, \phi)\tau + \alpha_n(\chi, \phi)}
\end{aligned} \tag{A.1}
$$

where $\lambda_n(\chi, \phi)$ are the eigenvalues of $L(\chi, \phi)$ while $|n(\chi, \phi))$ and $(n(\chi, \phi)|$ are its right and left eigenvectors, respectively. We know that $\lambda_0(0, \phi) = 0$ and $\alpha_0(0, \phi) = 0$ if ρ_0 is the stationary state. The moment and cumulant generating functions can be expanded about $\chi = 0$. For notational simplicity, we omit the addition of the $(-i)^k$ prefactor for the k-th cumulant, and we likewise neglect the elementary charge prefactor e. Note that the physically measurable cumulants C_k in the main text and the below defined c_k are related as $C_k = (-ie)^k c_k$. At any rate, we find

$$
\begin{aligned}
m(\chi, \phi, \tau) &\approx m_0(\phi, \tau) + \chi m_1(\phi, \tau) + \frac{1}{2}\chi^2 m_2(\phi, \tau) + \ldots \\
m_k(\phi, \tau) &= \partial_\chi^k m(\chi, \phi, \tau)\Big|_{\chi \to 0} \\
c(\chi, \phi, \tau) &\approx c_0(\phi, \tau) + \chi c_1(\phi, \tau) + \frac{1}{2}\chi^2 c_2(\phi, \tau) + \ldots \\
c_k(\phi, \tau) &= \partial_\chi^k c(\chi, \phi, \tau)\Big|_{\chi \to 0}
\end{aligned} \tag{A.2}
$$

Now we can define the derivatives of the cumulant generating function in terms of the derivatives of the moment generating function via the natural logarithm

$$
\frac{1}{\tau}\ln\left[1 + \chi m_1(\phi, \tau) + \frac{1}{2}\chi^2 m_2(\phi, \tau) + \ldots\right] = c_0(\phi, \tau) + \chi c_1(\phi, \tau) + \frac{1}{2}\chi^2 c_2(\phi, \tau) + \ldots
$$

$$\ln\left[1+\chi m_1(\phi,\tau)+\frac{1}{2}\chi^2 m_2(\phi,\tau)+\dots\right]\approx \chi m_1(\phi,\tau)+\frac{1}{2}\chi^2\left[m_2(\phi,\tau)-m_1^2(\phi,\tau)\right]+\dots\ , \tag{A.3}$$

where we have used the Maclaurin series expansion $\ln(1+x)=x-x^2/2+x^3/3-\dots$. An order by order comparison yields the well-known relationships

$$\begin{aligned} c_0(\phi,\tau)&=0\\ c_1(\phi,\tau)&=\frac{1}{\tau}m_1(\phi,\tau)\\ c_2(\phi,\tau)&=\frac{1}{\tau}\left[m_2(\phi,\tau)-m_1^2(\phi,\tau)\right] \end{aligned} \tag{A.4}$$

To proceed we now have to find the relation between the derivatives of moment generating function and the derivatives of eigenvalues. For the latter, we get

$$\begin{aligned} \lambda_n(\chi,\phi)\tau+\alpha_n(\chi,\phi)\approx{}&\left[\lambda_n^{(0)}(\phi)+\chi\lambda_n^{(1)}(\phi)+\frac{1}{2}\chi^2\lambda_n^{(2)}(\phi)\right]\tau\\ &+\left[\alpha_n^{(0)}(\phi)+\chi\alpha_n^{(1)}(\phi)+\frac{1}{2}\chi^2\alpha_n^{(2)}(\phi)\right]+\dots \end{aligned} \tag{A.5}$$

where $\lambda_n^{(k)}(\phi)=\partial_\chi\lambda_n(\chi,\phi)\big|_{\chi\to 0}$, and the same for $\alpha_n^{(k)}(\phi)$. Plugging this expansion of λ and α into the definition of the moment generating function, we get

$$m_0(\phi,\tau)=1 \tag{A.6}$$

$$\begin{aligned} m_1(\phi,\tau)&=\sum_n e^{\lambda_n^{(0)}(\phi)\tau+\alpha_n^{(0)}(\phi)}\left[\lambda_n^{(1)}(\phi)\tau+\alpha_n^{(1)}(\phi)\right]\\ m_2(\phi,\tau)&=\sum_n e^{\lambda_n^{(0)}(\phi)\tau+\alpha_n^{(0)}(\phi)}\left[\lambda_n^{(2)}(\phi)\tau+\alpha_n^{(2)}(\phi)+\left(\lambda_n^{(1)}(\phi)\tau+\alpha_n^{(1)}(\phi)\right)^2\right]\ . \end{aligned} \tag{A.7}$$

Finally we can write the cumulants in terms of derivatives of eigenvalues

$$\begin{aligned} c_1(\phi,\tau)={}&\sum_n e^{\lambda_n^{(0)}(\phi)\tau}e^{\alpha_n^{(0)}(\phi)}\left[\lambda_n^{(1)}(\phi)+\frac{1}{\tau}\alpha_n^{(1)}(\phi)\right]\\ c_2(\phi,\tau)={}&\sum_n e^{\lambda_n^{(0)}(\phi)\tau}e^{\alpha_n^{(0)}(\phi)}\left[\lambda_n^{(2)}(\phi)+2\lambda_n^{(1)}(\phi)\alpha_n^{(1)}(\phi)+\left[\lambda_n^{(1)}(\phi)\right]^2\tau+\frac{1}{\tau}\left(\alpha_n^{(2)}(\phi)+\left[\alpha_n^{(1)}(\phi)\right]^2\right)\right]\\ &-\sum_{nn'} e^{\lambda_n^{(0)}(\phi)\tau}e^{\lambda_{n'}^{(0)}(\phi)\tau}\Bigg[e^{\alpha_n^{(0)}(\phi)}\lambda_n^{(1)}(\phi)e^{\alpha_{n'}^{(0)}(\phi)}\lambda_{n'}^{(1)}(\phi)\tau+e^{\alpha_n^{(0)}(\phi)}\lambda_n^{(1)}(\phi)e^{\alpha_{n'}^{(0)}(\phi)}\alpha_{n'}^{(1)}(\phi)\\ &+e^{\alpha_n^{(0)}(\phi)}\alpha_n^{(1)}(\phi)e^{\alpha_{n'}^{(0)}(\phi)}\lambda_{n'}^{(1)}(\phi)+\frac{1}{\tau}e^{\alpha_n^{(0)}(\phi)}\alpha_n^{(1)}(\phi)e^{\alpha_{n'}^{(0)}(\phi)}\alpha_{n'}^{(1)}(\phi)\Bigg] \end{aligned} \tag{A.8}$$

Just to briefly confirm, in the long time limit $\tau\to\infty$, the second cumulant becomes $c_2(\phi,\tau)=-\lambda_0^{(2)}(\phi)$. Now, the idea is the following. The quantities c_1 and c_2 are measurable as a function of τ, when performing a finite frequency evaluation of current and noise. Then, all quantities which have a distinct time-evolution (be it due to a different exponential decay due to λ_n or due to a prefactor with a different power-law in τ) can be distinguished and extracted in principle by fitting of the τ-dependent data, by an appropriately chosen fitting function.

Consequently, in addition to the decay rates λ_n^0, the following terms can be individually extracted from the experimental data. For the first cumulant, these are

$$o_{1,n} = e^{\alpha_n^{(0)}(\phi)} \lambda_n^{(1)}(\phi) \tag{A.9}$$

$$o_{2,n} = e^{\alpha_n^{(0)}(\phi)} \alpha_n^{(1)}(\phi) \ . \tag{A.10}$$

From the second cumulant, we can independently extract

$$o_{3,n} = e^{\alpha_n^{(0)}(\phi)} \lambda_n^{(2)}(\phi) + 2e^{\alpha_n^{(0)}(\phi)} \lambda_n^{(1)}(\phi)\, \alpha_n^{(1)}(\phi) \tag{A.11}$$

$$o_{4,n} = e^{\alpha_n^{(0)}(\phi)} \left[\lambda_n^{(1)}(\phi)\right]^2 \tag{A.12}$$

$$o_{5,n} = e^{\alpha_n^{(0)}(\phi)} \left(\alpha_n^{(2)}(\phi) + \left[\alpha_n^{(1)}(\phi)\right]^2\right). \tag{A.13}$$

Finally by taking different combination of these expressions we can get the first and second order corrections of *all* eigenvalues, that is

$$\lambda_n^{(1)}(\phi) = \frac{o_{4,n}}{o_{1,n}} \ , \tag{A.14}$$

and

$$\lambda_n^{(2)}(\phi) = \frac{(o_{1,n} o_{3,n} - 2 o_{2,n} o_{4,n})\, o_{4,n}}{o_{n,1}^3} \ . \tag{A.15}$$

These individual results can be stitched together to get $\lambda_n(\chi) \approx \lambda_n^{(0)} + \chi \lambda_n^{(1)} + \frac{1}{2}\chi^2 \lambda_n^{(2)}$, which we plot in Fig. 2.9a in the main text for $\lambda_\pm$. While in principle, this procedure allows us to analytically continue the eigenvalues from $\chi = 0$ to finite χ, we see that this continuation fails to converge if there is a topological phase transition from zero χ to finite χ, unless one measures cumulants up to infinite order in k, which is a prohibitive requirement.

B. Calculation of the transmission coefficient for the squid detector

In the main text, we describe an all-circuit realization of continuous weak measurement of the supercurrent. The decisive figure of merit is the transmission coefficient of incoming waves towards the SQUID detector. To calculate this transmission coefficient, we start from the Hamiltonian description of the SQUID detector given in Eqs. (2.31-2.33), and first diagonalize the Hamiltonians for the left and right conductor lines, i.e. H_L and H_R, using the following mode expansion

$$\begin{aligned} q_{j,L/R} &= -\frac{i}{\sqrt{2}} \int_0^\pi \frac{dk}{\pi} \left(\frac{C_0}{L_0}\right)^{1/4} \sqrt{2\sin\left(\frac{|k|}{2}\right)} \cos\left(k(j-1/2)\right) \left[a_{k,L/R} - a^\dagger_{k,L/R}\right] \\ \frac{\varphi_{j,L/R}}{2e} &= \frac{1}{\sqrt{2}} \int_0^\pi \frac{dk}{\pi} \left(\frac{L_0}{C_0}\right)^{1/4} \frac{1}{\sqrt{2\sin\left(\frac{|k|}{2}\right)}} \cos\left(k(j-1/2)\right) \left[a_{k,L/R} + a^\dagger_{k,L/R}\right] \end{aligned} \tag{B.1}$$

The free Hamiltonians becomes

$$H_0 = H_L \otimes \mathbb{I}_R + \mathbb{I}_L \otimes H_R = \omega_0 \int_0^\pi \frac{dk}{\pi} \sin\left(\frac{k}{2}\right) a^\dagger_{k,L} a_{k,L} \otimes \mathbb{I}_R + \mathbb{I}_L \otimes \omega_0 \int_0^\pi \frac{dk}{\pi} \sin\left(\frac{k}{2}\right) a^\dagger_{k,R} a_{k,R} \ . \tag{B.2}$$

We note that in the continuum limit (vanishing size of islands j), we recover a linear dispersion relation $\sim \omega_0 k$. For now we keep finite size effects, and take the continuum limit at an appropriate later time.

Consequently, the interaction term can be expressed in terms of these bosonic operators as follows,

$$\begin{aligned} V &= \gamma \left(\frac{\varphi_1 - \varphi_0}{2e}\right)^2 \\ &= \frac{\gamma}{4} \sqrt{\frac{L_0}{C_0}} \int_0^\pi \int_0^\pi \frac{dk dk'}{(2\pi)^2} \frac{\cos\left(\frac{k}{2}\right)\cos\left(\frac{k'}{2}\right)}{\sqrt{\sin\left(\frac{k}{2}\right)\sin\left(\frac{k'}{2}\right)}} \left[\mathbb{I}_L \otimes a_{k,R} + \mathbb{I}_L \otimes a^\dagger_{k,R} - a_{k,L} \otimes \mathbb{I}_R - a^\dagger_{k,L} \otimes \mathbb{I}_R\right] \\ &* \left[\mathbb{I}_L \otimes a_{k',R} + \mathbb{I}_L \otimes a^\dagger_{k',R} - a_{k',L} \otimes \mathbb{I}_R - a^\dagger_{k',L} \otimes \mathbb{I}_R\right] \end{aligned} \tag{B.3}$$

We can now deploy the following important simplification. We will be considering an incoming signal at a certain energy focussing on the limit of elastic interaction (neglecting a small chance that the boson may be absorbed by the main circuit). In addition, we perform a rotation wave approximation, discarding the pair-wise creation (annihilation) terms $\sim a^\dagger a^\dagger$ ($\sim aa$). This allows us to work in the single particle picture, the relevant states being $|0,k\rangle$ and $|k,0\rangle$, where the first (second) states corresponds to a single particle eigenstate of H_L (H_R). The corresponding Green's functions are

$$
\begin{aligned}
(G_{k,k'})_{LL} &= \langle k,0| \frac{1}{E-H+i0^+} |k',0\rangle \\
(G_{k,k'})_{LR} &= \langle k,0| \frac{1}{E-H+i0^+} |0,k'\rangle \\
(G_{k,k'})_{RL} &= \langle 0,k| \frac{1}{E-H+i0^+} |k',0\rangle \\
(G_{k,k'})_{RR} &= \langle 0,k| \frac{1}{E-H+i0^+} |0,k'\rangle
\end{aligned}
\tag{B.4}
$$

According to the Fisher-Lee formula [FL81], for the transmission coefficient we need to find $(G_{k,k'})_{RL}$. We can write the Dyson equation as

$$
(G_{k,k'})_{RL} = \langle 0,k| \frac{1}{E-H+i0^+} |k',0\rangle = \langle 0,k| \frac{1}{E-H_0+i0^+} |k',0\rangle + \langle 0,k| \frac{1}{E-H_0+i0^+} V \frac{1}{E-H+i0^+} |k',0\rangle
\tag{B.5}
$$

Since we consider only processes in V conserving the total boson number, we can insert the identity operator for single particle subspace

$$
\begin{aligned}
\mathbb{I}_L &= \int_0^\pi \frac{dk}{2\pi} |k,0\rangle \langle k,0| \\
\mathbb{I} = \mathbb{I}_L \oplus \mathbb{I}_R &= \int_0^\pi \frac{dk_1}{2\pi} |k_1,0\rangle \langle k_1,0| + \int_0^\pi \frac{dk_2}{2\pi} |0,k_2\rangle \langle 0,k_2| \ .
\end{aligned}
\tag{B.6}
$$

to get

$$
\begin{aligned}
(G_{k,k'})_{RL} = {} & \langle 0,k| \frac{1}{E-H_0+i0^+} |k',0\rangle \\
& + \langle 0,k| \frac{1}{E-H_0+i0^+} \int_0^\pi \frac{dk_1}{2\pi} |k_1,0\rangle \langle k_1,0| V \int_0^\pi \frac{dk_3}{2\pi} |k_3,0\rangle \langle k_3,0| \frac{1}{E-H+i0^+} |k',0\rangle \\
& + \langle 0,k| \frac{1}{E-H_0+i0^+} \int_0^\pi \frac{dk_1}{2\pi} |k_1,0\rangle \langle k_1,0| V \int_0^\pi \frac{dk_4}{2\pi} |0,k_4\rangle \langle 0,k_4| \frac{1}{E-H+i0^+} |k',0\rangle \\
& + \langle 0,k| \frac{1}{E-H_0+i0^+} \int_0^\pi \frac{dk_2}{2\pi} |0,k_2\rangle \langle 0,k_2| V \int_0^\pi \frac{dk_3}{2\pi} |k_3,0\rangle \langle k_3,0| \frac{1}{E-H+i0^+} |k',0\rangle \\
& + \langle 0,k| \frac{1}{E-H_0+i0^+} \int_0^\pi \frac{dk_2}{2\pi} |0,k_2\rangle \langle 0,k_2| V \int_0^\pi \frac{dk_4}{2\pi} |0,k_4\rangle \langle 0,k_4| \frac{1}{E-H+i0^+} |k',0\rangle
\end{aligned}
\tag{B.7}
$$

Assuming weak tunneling, we may deploy a perturbation theory up to first order in the interaction V. To this end, we set $H = H_0$ on the right side of Eq.B.5, to get

$$\begin{aligned}(G_{k,k'})_{RL} &\approx \langle 0,k| \frac{1}{E-H_0+i0^+} |k',0\rangle + \langle 0,k| \frac{1}{E-H_0+i0^+} V \frac{1}{E-H_0+i0^+} |k',0\rangle \\ &= \frac{1}{E-\omega_k+i0^+} \langle 0,k| V |k',0\rangle \frac{1}{E-\omega_{k'}+i0^+} \end{aligned} \tag{B.8}$$

Since without the interaction term V, there cannot be any coupling between the left and right side of the system, the free Green's function connecting the left and right momenta is zero, i.e.

$$\langle 0,k| \frac{1}{E-H_0+i0^+} |k',0\rangle = 0 \ . \tag{B.9}$$

This leaves us with the task of computing the interaction term

$$\begin{aligned}\langle 0,k| V |k',0\rangle &= \frac{\gamma}{4}\sqrt{\frac{L_0}{C_0}} \int_0^\pi \int_0^\pi \frac{dk_1 dk_2}{(2\pi)^2} \frac{\cos\left(\frac{k_1}{2}\right)\cos\left(\frac{k_2}{2}\right)}{\sqrt{\sin\left(\frac{k_1}{2}\right)\sin\left(\frac{k_2}{2}\right)}} \langle 0| \otimes \langle 0| a_{k,R} \left[\mathbb{I}_L \otimes a_{k_1,R} + \mathbb{I}_L \otimes a^\dagger_{k_1,R}\right. \\ &\left. - a_{k_1,L} \otimes \mathbb{I}_R - a^\dagger_{k_1,L} \otimes \mathbb{I}_R\right] \left[\mathbb{I}_L \otimes a_{k_2,R} + \mathbb{I}_L \otimes a^\dagger_{k_2,R} - a_{k_2,L} \otimes \mathbb{I}_R - a^\dagger_{k_2,L} \otimes \mathbb{I}_R\right] a^\dagger_{k',L} |0\rangle \otimes |0\rangle \\ &= -\frac{\gamma}{4}\sqrt{\frac{L_0}{C_0}} \int_0^\pi \int_0^\pi dk_1 dk_2 \frac{\cos\left(\frac{k_1}{2}\right)\cos\left(\frac{k_2}{2}\right)}{\sqrt{\sin\left(\frac{k_1}{2}\right)\sin\left(\frac{k_2}{2}\right)}} \left[\delta(k_2-k')\delta(k_1-k) + \delta(k_1-k')\delta(k_2-k)\right] \\ &= -\frac{\gamma}{2}\sqrt{\frac{L_0}{C_0}} \frac{\cos\left(\frac{k}{2}\right)\cos\left(\frac{k'}{2}\right)}{\sqrt{\sin\left(\frac{k}{2}\right)\sin\left(\frac{k'}{2}\right)}} \end{aligned} \tag{B.10}$$

Hence to first order we get

$$(G_{k,k'})_{RL} = -\frac{\gamma}{2}\sqrt{\frac{L_0}{C_0}} \frac{1}{E-\omega_k+i0^+} \frac{\cos\left(\frac{k}{2}\right)\cos\left(\frac{k'}{2}\right)}{\sqrt{\sin\left(\frac{k}{2}\right)\sin\left(\frac{k'}{2}\right)}} \frac{1}{E-\omega_{k'}+i0^+} \ . \tag{B.11}$$

Let us connect the above Green's function to a Green's function in position space, using the following transformation

$$|j\rangle = \int_0^\pi \frac{dk}{\pi} \cos\left(k\left(j-1/2\right)\right) |k\rangle \tag{B.12}$$

The position space Green's function is

$$\langle 0,j| \frac{1}{E-H+i0^+} |j',0\rangle = -\frac{\gamma}{2}\sqrt{\frac{L_0}{C_0}} \int_0^\pi \int_0^\pi \frac{dk dk'}{\pi^2} \cos\left(k\left(j-1/2\right)\right) (G_{k,k'})_{RL} \cos\left(k'\left(j'-1/2\right)\right) \tag{B.13}$$

Hence the transmission coefficient using Eq. (2.35) is

$$t^L = iv\frac{\gamma}{2}\sqrt{\frac{L_0}{C_0}} \lim_{j\to\infty, j'\to-\infty} \langle 0,j| \frac{1}{E-H_0+i0^+} |j',0\rangle e^{-ik_E(j-j')}$$

$$= iv\frac{\gamma}{8}\sqrt{\frac{L_0}{C_0}}\lim_{j\to\infty}\left(\int_0^{\pi}\frac{dk}{\pi}\frac{e^{-ik/2}e^{i(k-k_E)j}+e^{ik/2}e^{-i(k+k_E)j}}{E-2\omega_0\sin\left(\frac{k}{2}\right)+i0^+}\frac{\cos\left(k/2\right)}{\sqrt{\sin\left(k/2\right)}}\right)$$
$$*\lim_{j'\to-\infty}\left(\int_0^{\pi}\frac{dk'}{\pi}\frac{e^{-ik'/2}e^{i(k'+k_E)j'}+e^{ik'/2}e^{-i(k'-k_E)j'}}{E-2\omega_0\sin\left(\frac{k'}{2}\right)+i0^+}\frac{\cos\left(k'/2\right)}{\sqrt{\sin\left(k'/2\right)}}\right) \tag{B.14}$$

where k_E is the wave vector corresponding to the energy at which the signal travels, $E = 2\omega_0\sin(k_E/2)$. Let us focus on the first integral

$$\int_0^{\pi}\frac{dk}{\pi}\frac{e^{-ik/2}e^{i(k-k_E)j}+e^{ik/2}e^{-i(k+k_E)j}}{E-2\omega_0\sin\left(\frac{k}{2}\right)+i0^+}\frac{\cos\left(k/2\right)}{\sqrt{\sin\left(k/2\right)}}\approx e^{-ik_Ej}\int_0^{\pi}\frac{dk}{\pi}\frac{e^{-ik/2}e^{ikj}}{E-2\omega_0\sin\left(\frac{k}{2}\right)+i0^+}\frac{\cos\left(k/2\right)}{\sqrt{\sin\left(k/2\right)}} \tag{B.15}$$

where we have ignored the term $e^{-i(k+k_E)j}$ as it will become highly oscillatory in the limit $j\to\infty$. We furthermore consider energies sufficiently low, such that we can also make a linear approximation for the sine and cosine functions

$$e^{-ik_Ej}\int_0^{\pi}\frac{dk}{\pi}\frac{e^{-ik/2}e^{ikj}}{E-2\omega_0\sin\left(\frac{k}{2}\right)+i0^+}\frac{\cos\left(k/2\right)}{\sqrt{\sin\left(k/2\right)}}\approx\frac{e^{-ik_Ej}}{\omega_0}\int_0^{\infty}\frac{dk}{\pi}\frac{e^{ikj}}{k_E-k+i0^+}\sqrt{\frac{2}{k}}\,. \tag{B.16}$$

This is in accordance with taking the continuum limit, i.e., the dimensions of the islands j approaching zero.

To evaluate the remaining integral, we perform a contour integral in complex k-space, where the contour is a quarter circle in the first quadrant centered at the origin and with radius R, hence

$$\oint_C\frac{dz}{\pi}\frac{e^{izj}}{k_E-z+i0^+}\sqrt{\frac{2}{z}}=\int_0^R\frac{dk}{\pi}\frac{e^{ikj}}{k_E-k+i0^+}\sqrt{\frac{2}{k}}+\int_{\theta=0}^{\pi/2}\frac{iRe^{i\theta}d\theta}{\pi}\frac{e^{ijR(\cos\theta+i\sin\theta)}}{k_E-Re^{i\theta}+i0^+}\sqrt{\frac{2}{Re^{i\theta}}}$$
$$+\int_R^0\frac{idk}{\pi}\frac{e^{-kj}}{k_E-ik+i0^+}\sqrt{\frac{2}{ik}}\,. \tag{B.17}$$

The left-hand side of the above can be evaluated using Residue theorem, to get

$$\begin{aligned}\oint_C\frac{dz}{\pi}\frac{e^{izj}}{k_E-z+i0^+}\sqrt{\frac{2}{z}}&=\frac{2\pi i}{\pi}\lim_{z\to k_E+i0^+}\left(z-(k_E+i0^+)\right)\frac{e^{izj}}{k_E+i0^+-z}\sqrt{\frac{2}{z}}\\&=-2ie^{i(k_E+i0^+)j}\sqrt{\frac{2}{k_E+i0^+}}\\&=-2ie^{ik_Ej}\sqrt{\frac{2}{k_E}}\end{aligned} \tag{B.18}$$

To evaluate the right-hand side, we take the limit $R\to\infty$, hence the angular integral goes to zero, which gives us

$$\int_0^{\infty}\frac{dk}{\pi}\frac{e^{ikj}}{k_E-k+i0^+}\sqrt{\frac{2}{k}}=\sqrt{2i}\int_0^{\infty}\frac{dk}{\pi}\frac{e^{-kj}}{k_E-ik}\sqrt{\frac{1}{k}}-2ie^{ik_Ej}\sqrt{\frac{2}{k_E}}$$

$$= \sqrt{2} * \frac{ie^{ijk_E}\mathrm{erfc}\left(\sqrt{j}\sqrt{ik_E}\right)}{\sqrt{k_E}} - 2ie^{ik_Ej}\sqrt{\frac{2}{k_E}} \ . \tag{B.19}$$

Hence

$$\begin{aligned}\int_0^\pi \frac{dk}{\pi}\frac{e^{-ik/2}e^{i(k-k_E)j} + e^{ik/2}e^{-i(k+k_E)j}}{E - 2\omega_0\sin\left(\frac{k}{2}\right) + i0^+}\frac{\cos(k/2)}{\sqrt{\sin(k/2)}} &\approx e^{-ik_Ej}\left(ie^{ijk_E}\mathrm{erfc}\left(\sqrt{j}\sqrt{ik_E}\right)\sqrt{\frac{2}{k_E}} - 2ie^{ik_Ej}\sqrt{\frac{2}{k_E}}\right) \\ &= i\mathrm{erfc}\left(\sqrt{j}\sqrt{ik_E}\right)\sqrt{\frac{2}{k_E}} - 2i\sqrt{\frac{2}{k_E}} \ .\end{aligned} \tag{B.20}$$

Similarly for the second integral we get

$$\int_0^\pi \frac{dk'}{\pi}\frac{e^{-ik'/2}e^{i(k'+k_E)j'} + e^{ik'/2}e^{-i(k'-k_E)j'}}{E - 2\omega_0\sin\left(\frac{k'}{2}\right) + i0^+}\frac{\cos(k'/2)}{\sqrt{\sin(k'/2)}} \approx i\mathrm{erfc}\left(\sqrt{-j'}\sqrt{ik_E}\right)\sqrt{\frac{2}{k_E}}-2i\sqrt{\frac{2}{k_E}} \ . \tag{B.21}$$

Finally the transmission coefficient is

$$\begin{aligned}t^L &= iv\frac{\gamma}{8\omega_0^2}\sqrt{\frac{L_0}{C_0}}\lim_{j\to\infty}\left(i\mathrm{erfc}\left(\sqrt{j}\sqrt{ik_E}\right)\sqrt{\frac{2}{k_E}} - 2i\sqrt{\frac{2}{k_E}}\right)\lim_{j'\to-\infty}\left(i\mathrm{erfc}\left(\sqrt{-j'}\sqrt{ik_E}\right)\sqrt{\frac{2}{k_E}} - 2i\sqrt{\frac{2}{k_E}}\right) \\ &= -i\frac{\gamma L_0}{k_E} \ ,\end{aligned} \tag{B.22}$$

where $v = \omega_0\cos(k_E/2) \approx \omega_0$. The error function parts in both the integrals goes to zero in the respective limits. We thus arrive at Eq. (2.36) in the main text.

C. Josephson junction array with gyrators

Here we solve a JJ array with gyrators

$$\mathcal{H} = \sum_{j=1}^{J} \Big[N_j + G(\phi_{j+1} - \phi_{j-1}) \Big]^2 + E_L \left(\phi_{j+1} - \phi_j\right)^2 + M\phi_j^2 \ , \tag{C.1}$$

and periodic boundary conditions, where we have introduced a mass term to regularize the zero mode. Define the fourier transform as follows

$$\begin{aligned} N_k &= \frac{1}{\sqrt{J}} \sum_{j=1}^{J} e^{ik_m j} N_j \ , \\ \phi_k &= \frac{1}{\sqrt{J}} \sum_{j=1}^{J} e^{-ik_m j} \phi_j \ , \\ k_m &= \frac{2\pi m}{J} \ , \end{aligned} \tag{C.2}$$

where $m \in \{-J/2+1, -J/2+2, ..., J/2\}$. The Hamiltonian can now be written as

$$\mathcal{H} = E_C \sum_{m=-\frac{J}{2}+1}^{\frac{J}{2}} \left[N_m N_{-m} + i2G \sin\left(\frac{2\pi m}{J}\right) \{N_m, \phi_m\} + \beta_m \phi_m \phi_{-m} \right] \ , \tag{C.3}$$

where

$$\beta_m = \frac{4E_C G^2 \sin^2\left(\frac{2\pi m}{J}\right) + 4E_L \sin^2\left(\frac{\pi m}{J}\right) + M}{E_C},$$

and $\{,\cdot\}$ denotes the anti-commutator. Now, we write the Fourier transformed charge and phase operators in terms of bosonic annihilation and creation operators

$$N_m = \frac{i}{\sqrt{2}} \left(a_{-m} - a_m^\dagger\right) \ , \tag{C.4}$$

$$\phi_m = \frac{1}{\sqrt{2}} \left(a_m + a_{-m}^\dagger\right) \ , \tag{C.5}$$

that obey the following commutation relations $[a_m, a_{m'}^\dagger] = \delta_{mm'}$, $[a_m, a_{m'}] = 0$. Finally, the Hamiltonian becomes

$$\mathcal{H} = \frac{E_C}{2} \sum_{m=1}^{\frac{J}{2}-1} \begin{pmatrix} a_m^\dagger & a_{-m}^\dagger & a_m & a_{-m} \end{pmatrix} H_m \begin{pmatrix} a_m \\ a_{-m} \\ a_m^\dagger \\ a_{-m}^\dagger \end{pmatrix} + \frac{E_C}{2} \begin{pmatrix} a_0^\dagger & a_0 \end{pmatrix} h \begin{pmatrix} a_0 \\ a_0^\dagger \end{pmatrix} + \frac{E_C}{2} \begin{pmatrix} a_{\frac{J}{2}}^\dagger & a_{\frac{J}{2}} \end{pmatrix} h' \begin{pmatrix} a_{\frac{J}{2}} \\ a_{\frac{J}{2}}^\dagger \end{pmatrix} \ ,$$

$$\mathcal{H} = \sum_{m=1}^{\frac{J}{2}-1} \mathcal{H}_{1,m} + \mathcal{H}_2 + \mathcal{H}_3 \ , \tag{C.6}$$

where

$$H_m = (\beta_m + 1)\,\mathbb{I}_4 + 4G \sin\left(\frac{2\pi m}{J}\right)\begin{pmatrix} \sigma_z & 0 \\ 0 & \sigma_z \end{pmatrix} + (\beta_m - 1)\begin{pmatrix} 0 & \sigma_x \\ \sigma_x & 0 \end{pmatrix} \ , \tag{C.7}$$

$$h = (\beta_0 + 1)\,\mathbb{I}_2 + (\beta_0 - 1)\,\sigma_x \ , \tag{C.8}$$

$$h' = \left(\beta_{\frac{J}{2}} + 1\right)\mathbb{I}_2 + \left(\beta_{\frac{J}{2}} - 1\right)\sigma_x. \tag{C.9}$$

$\mathbb{I}_n$ is a n-dimensional identity matrix while σ_z and σ_x are Pauli matrices. We will focus on diagonalization of $\mathcal{H}_{1,m}$ in eq.(C.6), the same formalism can be used for the other parts.

We will use the diagonalization of $\mathcal{H}_{1,m}$ to outline some general properties of a Bosonic Bogoliubov transformation. Our goal is to find new operators, $b_m, b_m^\dagger$ such that

$$\mathcal{H}_{1,m} = \frac{E_C}{2}\begin{pmatrix} b_m^\dagger & b_{-m}^\dagger & b_m & b_{-m} \end{pmatrix}\tau_z \Lambda_m \begin{pmatrix} b_m \\ b_{-m} \\ b_m^\dagger \\ b_{-m}^\dagger \end{pmatrix} \ , \tag{C.10}$$

where Λ_m is a diagonal matrix, and the new operators still satisfy the Bosonic commutation relations. This entails finding a matrix Q_m such that

$$\Lambda_m = Q_m^{-1}\tau_z H_m Q_m, \tag{C.11}$$

where

$$\tau_z = \begin{pmatrix} \mathbb{I}_2 & 0 \\ 0 & -\mathbb{I}_2 \end{pmatrix}.$$

Since the column vector and the row vector in eq.(A10) are related by Hermitian conjugation, this imposes the following condition

$$Q_m^{-1} = \tau_z Q_m^\dagger \tau_z. \tag{C.12}$$

Moreover the column (and the row) in eq.(A10) has internal structure as well, the bottom half of the column contains Hermitian conjugates of the upper half, this results in the following conditions

$$Q_m^* = \tau_x Q_m \tau_x, \tag{C.13}$$

$$\Lambda_m = -\tau_x \Lambda_m \tau_x, \tag{C.14}$$

where

$$\tau_x = \begin{pmatrix} 0 & \mathbb{I}_2 \\ \mathbb{I}_2 & 0 \end{pmatrix}.$$

Finally, we can write

$$\mathcal{H}_{1,m} = \frac{E_C}{2} \begin{pmatrix} a_m^\dagger & a_{-m}^\dagger & a_m & a_{-m} \end{pmatrix} \tau_z Q_m \tau_z \tau_z \Lambda_m Q_m^{-1} \begin{pmatrix} a_m \\ a_{-m} \\ a_m^\dagger \\ a_{-m}^\dagger \end{pmatrix} \tag{C.15}$$

$$= \frac{E_C}{2} \begin{pmatrix} b_m^\dagger & b_{-m}^\dagger & b_m & b_{-m} \end{pmatrix} \tau_z \Lambda_m \begin{pmatrix} b_m \\ b_{-m} \\ b_m^\dagger \\ b_{-m}^\dagger \end{pmatrix}. \tag{C.16}$$

The above procedure of Bogoliubov transformation is only applicable if Λ_m is a real matrix, for complex matrix we will develop the procedure in the next section.

The complete diagonalized Hamiltonian is

$$\mathcal{H} = \sum_{m=-\frac{J}{2}+1}^{\frac{J}{2}} \omega_m b_m^\dagger b_m, \tag{C.17}$$

$$\omega_m = 2\sqrt{E_C^2 \beta_m} + 4E_C G \sin\left(\frac{2\pi m}{J}\right). \tag{C.18}$$

We also investigate the arrays where the Josephson junction connects next nearest neighbors, the Hamiltonian for such a system will be

$$\mathcal{H}' = \sum_{j=1}^{J} \left[N_j + G(\phi_{j+1} - \phi_{j-1})\right]^2 + E_L\left(\phi_{j+1} - \phi_{j-1}\right)^2 + M\phi_j^2. \tag{C.19}$$

This Hamiltonian can be diagonalized in a similar way to get

$$\mathcal{H}' = \sum_{m=-\frac{J}{2}+1}^{\frac{J}{2}} \omega_m b_m^\dagger b_m, \tag{C.20}$$

$$\omega_m = 2\sqrt{E_C^2 \beta_m} + 4E_C G \sin\left(\frac{2\pi m}{J}\right), \tag{C.21}$$

$$\beta_m = \frac{4\left(E_C G^2 + E_L\right)\sin^2\left(\frac{2\pi m}{J}\right) + M}{E_C}.$$

D. Bogoliubov transformation for calculating correlations after quench

Consider the following Hamiltonian

$$\mathcal{H} = \sum_{j=1}^{J} \left[N_j + G(\phi_{j+1} - \phi_{j-1}) \right]^2 + E_{L,j} \left(\phi_{j+1} - \phi_j \right)^2 + M\phi_j^2. \tag{D.1}$$

The term $E_{L,j}$ indicates that the inductance can vary with site. Since there is no translational invariance, we cannot use Fourier transform, instead we write the phase and charge operators in terms of Bosonic annihilation and creation operators

$$N_j = \frac{i}{\sqrt{2}} \left(a_j - a_j^\dagger \right), \tag{D.2}$$

$$\phi_j = \frac{1}{\sqrt{2}} \left(a_j + a_j^\dagger \right), \tag{D.3}$$

that obey the following commutation relations $[a_j, a_{j'}^\dagger] = \delta_{jj'}$, $[a_j, a_{j'}] = 0$. This allows us to write the Hamiltonian as

$$\mathcal{H} = \mathbf{a}^\dagger H \mathbf{a}, \tag{D.4}$$

where $\mathbf{a} = \begin{pmatrix} a_1 & \cdots & a_J & a_1^\dagger & \cdots & a_J^\dagger \end{pmatrix}^T$.

We begin with the unquenched Hamiltonian, where $E_{L,j} = E_L$, this is the same Hamiltonian that we solved in appendix C, this time in position space, we can still follow the same steps and diagonalize it without going to the Fourier space to get

$$\begin{aligned}
\mathcal{H}_< &= \mathbf{a}^\dagger H_< \mathbf{a} \\
&= \mathbf{a}^\dagger Z Q Z Z \Lambda_< Q^{-1} \mathbf{a} \\
&= \mathbf{b}^\dagger Z \Lambda_< \mathbf{b} && \text{(D.5)} \\
&= \sum_{j=1}^{J} \left(\lambda_{<,j} b_j^\dagger b_j + \lambda_{<,j} b_j b_j^\dagger \right). && \text{(D.6)}
\end{aligned}$$

Here

$$Z = \begin{pmatrix} \mathbb{I}_J & 0 \\ 0 & -\mathbb{I}_J \end{pmatrix},$$

and operators $\mathbf{b}^{(\dagger)}$ have the same commutation relations as $\mathbf{a}^{(\dagger)}$. The matrix Q satisfies the conditions in eq.(C.12) and (C.13), while the diagonal matrix $\Lambda_<$ satisfies the eq.(C.14). In position space the Hamiltonian does not break down into independent blocks of $4*4$ matrices, therefore the size of the matrices in the above equations have to be changed appropriately.

Now we quench the system such that

$$E_{L,j} = \begin{cases} -E_L & j_0 < j < j_1, \\ E_L & \text{everywhere else}, \end{cases} \tag{D.7}$$

for some arbitrary j_0 and j_1. The quenched Hamiltonian can be written as

$$\begin{aligned} \mathcal{H}_> &= \mathbf{a}^\dagger H_> \mathbf{a} \\ &= \mathbf{a}^\dagger Z P Z Z \Lambda_> P^{-1} \mathbf{a}. \end{aligned} \tag{D.8}$$

The diagonal matrix $\Lambda_>$ is not necessarily real, therefore the eq.(C.12) and (C.13) doesn't hold, but these conditions translate to conditions on the first quantized matrix as

$$H_> = H_>^\dagger, \tag{D.9}$$
$$H_>^T = X H_> X, \tag{D.10}$$
$$X = \begin{pmatrix} 0 & \mathbb{I}_J \\ -\mathbb{I}_J & 0 \end{pmatrix}.$$

which still hold true. From this we can get some new properties

$$P^{-1} = Z X P^T X Z, \tag{D.11}$$
$$\Lambda_> = -X \Lambda_> X, \tag{D.12}$$
$$\Lambda_> = M^{-1} \Lambda_>^* M, \tag{D.13}$$

where $M = Z P^\dagger Z P$. One might notice that eq.(D.11) is just the combination of eq.(C.12) and (C.13). The unquenched Hamiltonian can now be written as

$$\mathcal{H}_> = \mathbf{c}^\bullet Z_{2J} \Lambda_> \mathbf{c} \tag{D.14}$$
$$= \sum_{j=1}^{J} \left(\lambda_{>,j} c_j^\bullet c_j + \lambda_{>,j} c_j c_j^\bullet \right), \tag{D.15}$$

where

$$\begin{aligned} \mathbf{c}^\bullet &= \begin{pmatrix} c_1^\bullet & \cdots & c_J^\bullet & c_1 & \cdots & c_J \end{pmatrix} \\ \mathbf{c} &= \begin{pmatrix} c_1 & \cdots & c_J & c_1^\bullet & \cdots & c_J^\bullet \end{pmatrix}^T. \end{aligned}$$

The new operators obey the following commutation relations $[c_j, c_{j'}^\bullet] = \delta_{jj'}$, $[c_j, c_{j'}] = 0$, $[c_j^\bullet, c_{j'}^\bullet] = 0$. These relations closely resemble Bosonic commutation relations, but it is important to note that the operators $c_j^\bullet$ and c_j are not related by Hermitian conjugation.

Any two point correlation of charge and phase operators can be written as a linear combination of two point correlators of the $\mathbf{a}^{(\dagger)}$ operators, hence we focus on finding the following correlation matrix

$$F(t,t') \equiv \left\langle \mathbf{a}(t)\mathbf{a}^\dagger(t') \right\rangle, \tag{D.16}$$

where the average is taken over the ground state of the equilibrium system. For a total number of J sites F is a $2J * 2J$ matrix with the substructure form

$$F(t,t') = \begin{pmatrix} A(t,t') & B(t,t') \\ C(t,t') & D(t,t') \end{pmatrix}, \tag{D.17}$$

where A, B, C and D are block matrices of dimensions $J * J$ that contain the correlations of the form $\left\langle a_j(t)a_{j'}^\dagger(t') \right\rangle$,$\left\langle a_j^\dagger(t)a_{j'}^\dagger(t') \right\rangle$,$\left\langle a_j(t)a_{j'}(t') \right\rangle$ and $\left\langle a_j^\dagger(t)a_{j'}(t') \right\rangle$ respectively.

First let us calculate the correlation matrix for unquenched Hamiltonian

$$F_<(t,t') = Q\left\langle \mathbf{b}(t)\mathbf{b}^\dagger(t') \right\rangle ZQ^{-1}Z. \tag{D.18}$$

In this step we have used the fact that the matrices Q and Z_{2J} commute with many-body operator $\mathcal{H}_<$. Since the ground state of unquenched Hamiltonian is defined as $b_i\left|0\right\rangle = 0 \ \forall i$, we get

$$F_<(t,t') = Qe^{-i2(t-t')\Lambda_<}\frac{\mathbb{I}_{2J}+Z}{2}Q^{-1}Z. \tag{D.19}$$

Now we focus on the case where we quench the system. Namely, we prepare the system in a ground state of a different Hamiltonian $\mathcal{H}_<$ for times $t < 0$, and immediately switch the system to the Hamiltonian $\mathcal{H}_>$ at time $t = 0$ (and let it evolve for subsequent $t > 0$). Using the previous results we can finally write down the correlation matrix

$$\begin{aligned} F_>(t,t') &= \left\langle \mathbf{a}(t)\mathbf{a}^\dagger(t') \right\rangle \\ &= P\left\langle \mathbf{c}(t)\mathbf{c}^\bullet(t') \right\rangle ZP^{-1}Z \\ &= Pe^{-i2\Lambda_>t}\left\langle \mathbf{c}\mathbf{c}^\bullet \right\rangle e^{i2\Lambda_>t'}ZP^{-1}Z \\ &= Pe^{-i2\Lambda_>t}P^{-1}\left\langle \mathbf{a}\mathbf{a}^\dagger \right\rangle ZPe^{i2\Lambda_>t'}P^{-1}Z \\ &= Pe^{-i2\Lambda_>t}P^{-1}Q\left\langle \mathbf{b}\mathbf{b}^\dagger \right\rangle ZQ^{-1}Pe^{i2\Lambda_>t'}P^{-1}Z \\ &= Pe^{-i2\Lambda_>t}P^{-1}Q\frac{\mathbb{I}_{2J}+Z}{2}Q^{-1}Pe^{i2\Lambda_>t'}P^{-1}Z \\ &= e^{-i2H_>t}Q\frac{\mathbb{I}_{2J}+Z}{2}Q^{-1}e^{i2H_>t'}Z. \end{aligned} \tag{D.20}$$

E. Klich's determinant formula

Consider two second quantized operators $\hat{A}$ and $\hat{B}$, such that

$$\hat{A} = \sum_{i,j} \langle i| A |j\rangle d_i^\dagger d_j,$$
$$\hat{B} = \sum_{i,j} \langle i| B |j\rangle d_i^\dagger d_j,$$

where A and B are first the quantized operators and the states $|i\rangle$ span the corresponding single particle Hilbert space. Then it can be shown that [Kli02]

$$\mathrm{Tr}\left(e^{\hat{A}} e^{\hat{B}}\right) = \det\left(1 - \xi e^{A} e^{B}\right)^{-\xi}, \tag{E.1}$$

where $\xi = 1$ for Bosons and $\xi = -1$ for Fermions (the creation and annihilation operators satisfy $d_i d_j^\dagger - \xi d_j^\dagger d_i = \delta_{ij}$).

We are going to derive a similar formula for operators that also contain terms of the form $d_i d_j$ and $d_i^\dagger d_j^\dagger$, we will work with Bosonic operators, the formula for Fermionic operators can be derived in a similar way.

Consider an operator (not necessarily Hermitian) that can be written in terms of Bosonic creation and annihilation operators as follows

$$\hat{A} = \sum_{i,j=1}^{J} a_i^\dagger A_{ij}^{(0)} a_j + \frac{1}{2} a_i^\dagger A_{ij}^{(1)} a_j^\dagger + \frac{1}{2} a_i A_{ij}^{(2)} a_j = \frac{1}{2}\mathcal{A} - \frac{1}{2}\mathrm{tr} A^{(0)}, \tag{E.2}$$

(note: Tr is the trace for a many body operator while tr is the normal trace for a matrix), here

$$\mathcal{A} = \mathbf{a}^\dagger A \mathbf{a},$$
$$A = \begin{pmatrix} A^{(0)} & A^{(1)} \\ A^{(2)} & A^{(0)T} \end{pmatrix}.$$

The matrices $A^{(1)}$ and $A^{(2)}$ can always be written as symmetric matrices due to the Bosonic commutation relations. This leads to the following property

$$XAX = A^T. \tag{E.3}$$

To calculate the trace of this many body operator, we can diagonalize ZA but since it is not Hermitian, there is no guarantee that it is diagonalizable. Instead we find Schur's decomposition of ZA i.e.

$$ZA = U \Lambda U^\dagger, \tag{E.4}$$

where U is a unitary matrix and Λ is an upper triangular matrix with eigenvalues of ZA on its diagonal. Schur's decomposition allows us to arrange the eigenvalues in any order we want on the diagonal of Λ, we will choose the following arrangement

$$\mathrm{Diag}\Lambda = \begin{pmatrix} \lambda_1 & \cdots & \lambda_J & -\lambda_J & \cdots & -\lambda_1 \end{pmatrix}, \tag{E.5}$$

the above arrangement is possible because the eigenvalues of ZA come in pairs of $(\lambda, -\lambda)$, this fact can be ascertained from the following property

$$\begin{aligned} &\text{if } (ZA - \lambda)^m |\lambda\rangle = 0 \\ \implies &|\lambda\rangle^T ZX (ZA + \lambda)^m = 0, \end{aligned} \tag{E.6}$$

for $m \geq 1$, the $m \neq 1$ cases correspond to generalized eigenvectors. The specific arrangement of eigenvalues in eq.(E.5) also imposes a specific structure on the matrix U, which is

$$U = \begin{pmatrix} |\lambda_1\rangle & \cdots & |\lambda_J\rangle & XZ|\lambda_J\rangle^* & \cdots & XZ|\lambda_1\rangle^* \end{pmatrix}, \tag{E.7}$$

where $|\lambda_i\rangle$ is the (generalized) eigenvector corresponding to the eigenvalue λ_i. The eigenvectors are normalized as follows

$$|\lambda_i\rangle^\dagger |\lambda_j\rangle = \delta_{ij}. \tag{E.8}$$

Now we return to the problem of calculating the trace of the many body operator, for that

$$\begin{aligned} \mathcal{A} &= \mathbf{a}^\dagger A \mathbf{a} \\ &= \mathbf{a}^\dagger ZUZZ\Lambda U^\dagger \mathbf{a} \\ &= \begin{pmatrix} c_1^\bullet & \cdots & c_J^\bullet & c_J & \cdots & c_1 \end{pmatrix} Z\Lambda \begin{pmatrix} c_1 & \cdots & c_J & c_J^\bullet & \cdots & c_1^\bullet \end{pmatrix}^T, \end{aligned} \tag{E.9}$$

and the commutation relations for the new operators are $[c_j, c_{j'}^\bullet] = \delta_{jj'}$, $[c_j, c_{j'}] = 0$, $[c_j^\bullet, c_{j'}^\bullet] = 0$. Finally,

$$\mathcal{A} = \sum_{i=1}^{J} \lambda_i \left(c_i^\bullet c_i + c_i c_i^\bullet\right) + \sum_{i,j=1}^{J} N_{ij} c_i^\bullet c_j^\bullet + \sum_{i<j,i=1}^{J} R_{ij} c_i^\bullet c_j, \tag{E.10}$$

where the terms N_{ij} and R_{ij} encompass the non-diagonal terms of the upper triangular matrix Λ.

Define two states $\langle 0|_L$ and $|0\rangle_R$ such that

$$\langle 0|_L\, c_i^\bullet = 0 \;\forall i, \tag{E.11}$$
$$c_i\, |0\rangle_R = 0 \;\forall i. \tag{E.12}$$

Then it is easy to see that the operator $\sum_{i=1}^J c_i^\bullet c_i$ acts as a number operator. We can define a basis for a Fock space in terms of the following states

$$|n_1, n_2, \cdots, n_J\rangle = \frac{c_1^{\bullet\, n_1} c_2^{\bullet\, n_2} \cdots c_J^{\bullet\, n_J}}{\sqrt{n_1! n_2! \cdots n_J!}} |0\rangle_R, \tag{E.13}$$

$$\langle\langle n_1, n_2, \cdots, n_J| = \langle 0|_L \frac{c_1{}^{n_1} c_2{}^{n_2} \cdots c_J{}^{n_J}}{\sqrt{n_1! n_2! \cdots n_J!}}. \tag{E.14}$$

The states are normalized such that

$$\langle\langle n_1, n_2, \cdots, n_J| \, |m_1, m_2, \cdots, m_J\rangle = \delta_{n_1,m_1}\delta_{n_2,m_2}\cdots\delta_{n_J,m_J}, \tag{E.15}$$

and the resolution of the identity on the Fock space is

$$\hat{\mathcal{I}} = \sum_{n_1=0}^{\infty} \cdots \sum_{n_J=0}^{\infty} |n_1, n_2, \cdots, n_J\rangle \, \langle\langle n_1, n_2, \cdots, n_J| \, . \tag{E.16}$$

The trace of the exponential of the many body operator can now be written as

$$\begin{aligned}
\mathrm{Tr} e^{\hat{A}} &= e^{-\mathrm{tr} A^{(0)}/2} \mathrm{Tr} e^{\mathcal{A}/2} \\
&= e^{-\mathrm{tr} A^{(0)}/2} \sum_{n_1=0}^{\infty} \cdots \sum_{n_J=0}^{\infty} \langle\langle n_1, n_2, \cdots, n_J| \, e^{\mathcal{A}/2} \, |n_1, n_2, \cdots, n_J\rangle \\
&= \sum_{n_1=0}^{\infty} \cdots \sum_{n_J=0}^{\infty} \langle\langle n_1, n_2, \cdots, n_J| \, e^{\sum_{i=1}^{J} \lambda_i (c_i^{\bullet} c_i + c_i c_i^{\bullet})/2} \, |n_1, n_2, \cdots, n_J\rangle \\
&= \prod_{i=1}^{J} \frac{e^{\lambda_i/2}}{1 - e^{\lambda_i}}.
\end{aligned} \tag{E.17}$$

The terms $\sum_{i,j=1}^{J} N_{ij} c_i^{\bullet} c_j^{\bullet}$ and $\sum_{i<j,i=1}^{J} R_{ij} c_i^{\bullet} c_j$ change the number states in such a way that no combination of them with each other or themselves can contribute to the trace, therefore the only term that contributes is $\sum_{i=1}^{J} \lambda_i \left(c_i^{\bullet} c_i + c_i c_i^{\bullet}\right)$. This was the reason why we chose a specific arrangement of eigenvalues in eq.(E.5).

We can write eq.(C18) as

$$\mathrm{Tr} e^{\hat{A}} = e^{-\mathrm{tr} A^{(0)}/2} \det(1 - U U^{\dagger} Z e^{Z A/2})^{-1}, \tag{E.18}$$

which doesn't appear to be universal on account of the appearance of the matrix U, instead we will work with the following formula

$$\left[\mathrm{Tr} e^{\hat{A}}\right]^2 = \det(Z) e^{-\mathrm{tr} A^{(0)}} \det(1 - e^{Z A})^{-1}. \tag{E.19}$$

We still don't have an expression which is analogous to the eq.(E.1), to derive such an expression, consider another operator $\hat{B}$ that can be written in a form similar to eq.(E.2), then it can be shown that

$$\left[\frac{1}{2}\mathcal{A}, \frac{1}{2}\mathcal{B}\right] = \frac{1}{2}\mathcal{C}, \tag{E.20}$$

where

$$\mathcal{C} = \mathbf{a}^{\dagger} Z \left[Z A, Z B\right] \mathbf{a}.$$

Using the Baker-Campbell-Hausdorff we can get our final expression as

$$\left[\mathrm{Tr}\left(e^{\hat{A}} e^{\hat{B}}\right)\right]^2 = \det(Z) e^{-\mathrm{tr}(A^{(0)} + B^{(0)})} \det(1 - e^{Z A} e^{Z B})^{-1}. \tag{E.21}$$

F. Correlation matrix from Klich's determinant formula

This section gives the expressions used to calculate the equal time correlation matrix after the quench $F_>(t,t)$, using the formulas developed in the last section. Before we give the general expressions, first let us note a result that will be used in the rest of the section

$$\begin{aligned}
\lim_{\beta\to\infty}\left[\frac{\mathrm{Tr}\left(e^{\hat{A}}e^{-\beta\mathcal{H}_<}\right)}{\mathrm{Tr}\left(e^{-\beta\mathcal{H}_<}\right)}\right]^2 &= \lim_{\beta\to\infty} e^{-\mathrm{tr}A^{(0)}}\frac{\det(1-e^{ZA}e^{-\beta ZH_<})^{-1}}{\det(1-e^{-\beta ZH_<})^{-1}} \\
&= \lim_{\beta\to\infty} e^{-\mathrm{tr}A^{(0)}}\det\left(\frac{1}{1-e^{-\beta\Lambda_<}}-Q^{-1}e^{ZA}Q\frac{e^{-\beta\Lambda_<}}{1-e^{-\beta\Lambda_<}}\right)^{-1} \\
&= e^{-\mathrm{tr}A^{(0)}}\det\left(\frac{\mathbb{I}_{2J}+Z}{2}+Q^{-1}e^{ZA}Q\frac{\mathbb{I}_{2J}-Z}{2}\right)^{-1}, \qquad \text{(F.1)}
\end{aligned}$$

where the diagonal matrix $\Lambda_<$ of dimensions $2J$ has positive eigenvalues in the first half on the diagonal and negative eigenvalues in the second half.

Now let us write down the expressions for elements of the correlation matrix

$$\begin{aligned}
F_{>,ij}(t,t) = \left\langle \mathbf{a}^\dagger(t)_i\mathbf{a}(t)_j\right\rangle &= \partial_\chi\left\langle e^{\chi\mathbf{a}^\dagger(t)_i\mathbf{a}(t)_j}\right\rangle_{\chi=0} \\
&\approx \lim_{\delta\chi\to 0}\frac{\left\langle e^{\delta\chi\mathbf{a}^\dagger(t)_i\mathbf{a}(t)_j}\right\rangle - 1}{\delta\chi} \\
&= \lim_{\delta\chi\to 0}\frac{\sqrt{\left\langle e^{\delta\chi\mathbf{a}^\dagger(t)_i\mathbf{a}(t)_j}\right\rangle^2} - 1}{\delta\chi} \\
&= \lim_{\delta\chi\to 0}\frac{\sqrt{\lim_{\beta\to\infty}\frac{\mathrm{Tr}(e^{i\mathcal{H}_>t}e^{\hat{\chi}}e^{-i\mathcal{H}_>t}e^{-\beta\mathcal{H}_<})^2}{\mathrm{Tr}(e^{-\beta\mathcal{H}_<})^2}} - 1}{\delta\chi}, \qquad \text{(F.2)}
\end{aligned}$$

where we have defined the operator $\hat{\chi}$ as follows

$$\begin{aligned}
\hat{\chi} &= \delta\chi\left(\frac{1}{2}\mathbf{a}^\dagger M\mathbf{a} \pm \frac{1}{2}\mathrm{tr}M^{(0)}\right), \\
M &= \begin{pmatrix} M^{(0)} & M^{(1)} \\ M^{(2)} & \left(M^{(0)}\right)^T \end{pmatrix}, \qquad \text{(F.3)}
\end{aligned}$$

such that

$$M^{(1)} = \left(M^{(1)}\right)^T,$$

$$M^{(2)} = \left(M^{(2)}\right)^T .$$

The elements of the matrix M and the plus or minus sign in the definition of $\hat{\chi}$ depend on the value of the indices i and j.

$$F_{>,ij}(t,t) = \lim_{\delta\chi\to 0} \frac{\sqrt{\lim_{\beta\to\infty} \frac{\mathrm{Tr}\left(e^{i\mathcal{H}_>t} e^{\hat{\chi}} e^{-i\mathcal{H}_>t} e^{-\beta\mathcal{H}_<}\right)^2}{\mathrm{Tr}\left(e^{-\beta\mathcal{H}_<}\right)^2}} - 1}{\delta\chi}$$

$$= \lim_{\delta\chi\to 0} \frac{\sqrt{\lim_{\beta\to\infty} \frac{e^{\pm\delta\chi \mathrm{tr} M^{(0)}} \det\left(1 - e^{iZ_{2J}H_>t} e^{\delta\chi Z_{2J} M} e^{-iZ_{2J}H_>t} e^{-\beta Z_{2J} H_<}\right)^{-1}}{\det\left(1 - e^{-\beta Z_{2J} H_<}\right)^{-1}}} - 1}{\delta\chi}, \quad \text{(F.4)}$$

$$\text{(F.5)}$$

where we have used Eq.(E.21). Expanding the exponentials upto first order in $\delta\chi$, and using the identity $\det(\mathbb{I} + \epsilon A) \approx 1 + \epsilon \mathrm{tr}(A) + \mathcal{O}(\epsilon^2)$, we get

$$F_{>,ij}(t,t) = \lim_{\delta\chi\to 0} \frac{e^{\pm\delta\chi \mathrm{tr}\frac{M^{(0)}}{2}} \left(1 + \frac{\delta\chi}{2} \mathrm{tr}\left[Q^{-1} e^{iZH_>t} Z M e^{-iZH_>t} Q \left(\mathbb{I}_{2J} - Z\right)\right]\right)^{-1/2} - 1}{\delta\chi}. \quad \text{(F.6)}$$

If $\mathrm{tr} M^{(0)} = 0$

$$\begin{aligned} F_{>,ij}(t,t) &= \lim_{\delta\chi\to 0} \frac{\left(1 + \frac{\delta\chi}{2} \mathrm{tr}\left[Q^{-1} e^{iZH_>t} Z M e^{-iZH_>t} Q \left(\mathbb{I}_{2J} - Z\right)\right]\right)^{-1/2} - 1}{\delta\chi} \\ &\approx \lim_{\delta\chi\to 0} \frac{1 - \frac{\delta\chi}{4} \mathrm{tr}\left[Q^{-1} e^{iZH_>t} Z M e^{-iZH_>t} Q \left(\mathbb{I}_{2J} - Z\right)\right] - 1}{\delta\chi} \\ &= -\frac{\mathrm{tr}\left[Q^{-1} e^{iZH_>t} Z M e^{-iZH_>t} Q \left(\mathbb{I}_{2J} - Z\right)\right]}{4}. \end{aligned} \quad \text{(F.7)}$$

instead if $\mathrm{tr} M^{(0)} = 1$ with a negative sign in the definition of $\hat{\chi}$

$$\begin{aligned} F_{>,ij}(t,t) &= \lim_{\delta\chi\to 0} \frac{e^{-\frac{\delta\chi}{2}} \left(1 + \frac{\delta\chi}{2} \mathrm{tr}\left[Q^{-1} e^{iZH_>t} Z M e^{-iZH_>t} Q \left(\mathbb{I}_{2J} - Z\right)\right]\right)^{-1/2} - 1}{\delta\chi} \\ &\approx \lim_{\delta\chi\to 0} \frac{e^{-\frac{\delta\chi}{2}} - e^{-\frac{\delta\chi}{2}} \frac{\delta\chi}{4} \mathrm{tr}\left[Q^{-1} e^{iZH_>t} Z M e^{-iZH_>t} Q \left(\mathbb{I}_{2J} - Z\right)\right] - 1}{\delta\chi} \\ &= -\frac{1}{2} - \frac{\mathrm{tr}\left[Q^{-1} e^{iZH_>t} Z M e^{-iZH_>t} Q \left(\mathbb{I}_{2J} - Z\right)\right]}{4}. \end{aligned} \quad \text{(F.8)}$$

and finally if $\mathrm{tr} M^{(0)} = 1$ with a plus sign in the definition of $\hat{\chi}$

$$\begin{aligned} F_{>,ij}(t,t) &= \lim_{\delta\chi\to 0} \frac{e^{\frac{\delta\chi}{2}} \left(1 + \frac{\delta\chi}{2} \mathrm{tr}\left[Q^{-1} e^{iZH_>t} Z M e^{-iZH_>t} Q \left(\mathbb{I}_{2J} - Z\right)\right]\right)^{-1/2} - 1}{\delta\chi} \\ &\approx \lim_{\delta\chi\to 0} \frac{e^{\frac{\delta\chi}{2}} - e^{\frac{\delta\chi}{2}} \frac{\delta\chi}{4} \mathrm{tr}\left[Q^{-1} e^{iZH_>t} Z M e^{-iZH_>t} Q \left(\mathbb{I}_{2J} - Z\right)\right] - 1}{\delta\chi} \end{aligned}$$

$$= \frac{1}{2} - \frac{\mathrm{tr}\left[Q^{-1}e^{iZH_{>}t}ZMe^{-iZH_{>}t}Q\left(\mathbb{I}_{2J} - Z\right)\right]}{4}. \tag{F.9}$$

The matrix M and the operator $\hat{\chi}$ will have the following forms depending on the indices i and j.

- $i \leq J, j \leq J$:

  The matrices $M^{(1)}$ and $M^{(2)}$ will only contain zeros, and

$$M^{(0)}_{lk} = \begin{cases} 0 & l \neq i, k \neq j, \\ 1 & l = i, k = j, \end{cases}$$
$$\hat{\chi} = \delta\chi\left(\frac{1}{2}\mathbf{a}^\dagger M\mathbf{a} - \frac{1}{2}\mathrm{tr}M^{(0)}\right), \tag{F.10}$$

  the indices l and k run from 1 to J. Here, $\mathrm{tr}M^{(0)} = 1$ only if $i = j$ otherwise it's zero.

- $i \leq J, j > J$:

  The matrices $M^{(0)}$ and $M^{(2)}$ will only contain zeros, and

$$M^{(1)}_{lk} = \begin{cases} 1 & l = j - J, k = i, \\ 1 & l = i, k = j - J, \\ 0 & \text{every other element}, \end{cases}$$
$$\hat{\chi} = \delta\chi\frac{1}{2}\mathbf{a}^\dagger M\mathbf{a}. \tag{F.11}$$

  Here, $\mathrm{tr}M^{(0)}$ is always zero.

- $i > J, j \leq J$:

  The matrices $M^{(0)}$ and $M^{(1)}$ will only contain zeros, and

$$M^{(2)}_{lk} = \begin{cases} 1 & l = j, k = i - J, \\ 1 & l = i - J, k = j, \\ 0 & \text{every other element}, \end{cases}$$
$$\hat{\chi} = \delta\chi\frac{1}{2}\mathbf{a}^\dagger M\mathbf{a}. \tag{F.12}$$

  Again, $\mathrm{tr}M^{(0)}$ is always zero.

- $i > J, j > J$:

  The matrices $M^{(1)}$ and $M^{(2)}$ will only contain zeros, and

$$M^{(0)}_{lk} = \begin{cases} 0 & l \neq i - J, k \neq j - J, \\ 1 & l = i - J, k = j - J, \end{cases}$$
$$\hat{\chi} = \delta\chi\left(\frac{1}{2}\mathbf{a}^\dagger M\mathbf{a} + \frac{1}{2}\mathrm{tr}M^{(0)}\right). \tag{F.13}$$

  Here, $\mathrm{tr}M^{(0)} = 1$ only if $i = j$ otherwise it's zero.

G. Hawking-Unruh radiation on a lattice

In this appendix we argue that the Hawking radiation can indeed be obtained on a lattice if the change in the parameters of the system, equivalently the change in metric, is smooth enough (with some restrictions). However as also pointed out in the main text, there will be essential differences between continuum and lattice models. To begin let us consider the following Lagrangian

$$\mathcal{L} = \int dx \left(\frac{1}{2u}\dot{\phi}^2 - \frac{v(x)}{u}\dot{\phi}\partial_x\phi + \frac{v^2(x) - u^2}{2u}\left(\partial_x\phi\right)^2 \right), \tag{G.1}$$

this form of Lagrangian is what most works on analog horizons try to emulate [Rob12], an important aspect of this field theory is that the determinant of the metric remains constant. This is in contrast to our proposal, where we only modulate the inductance with position, which does not conserve the determinant of the metric in the continuum limit. But our goal here is to compare the result of lattice realisations and continuum realisations, and since most existing continuum proposals for analog horizons use this particular field theory, therefore we stick to this one.

Now we set this field theory on a one dimensional infinite lattice, the discretised version of the Lagrangian is

$$\mathcal{L} = \frac{\Delta x}{u}\sum_j \dot{\phi}_j^2 - \sum_j \frac{v_j}{u}\dot{\phi}_j\left(\phi_{j+1} - \phi_{j-1}\right) - \sum_j \frac{u^2 - v_j^2}{4u\Delta x}\left(\phi_{j+1} - \phi_{j-1}\right)^2, \tag{G.2}$$

also note that since we consider next-to-nearest neighbour coupling, in order to avoid any issues due to instabilities that do not arise from the presence of a horizon, also in this model the lattice constant is best defined as $2\Delta x$. The conjugate field is

$$\pi_j = \frac{1}{2\Delta x}\frac{\partial\mathcal{L}}{\partial\dot{\phi}_j} = \frac{1}{u}\dot{\phi}_j - \frac{v_j}{2u\Delta x}\left(\phi_{j+1} - \phi_{j-1}\right), \tag{G.3}$$

hence using the Legendre transform we can write the Hamiltonian

$$\mathcal{H} = 2\Delta x\frac{u}{2}\sum_j \pi_j^2 + \frac{v_j}{2}\sum_j \left\{\pi_j, \left(\phi_{j+1} - \phi_{j-1}\right)\right\} + \sum_j \frac{u}{4\Delta x}\left(\phi_{j+1} - \phi_{j-1}\right)^2. \tag{G.4}$$

Now the equations of motion will be

$$2\Delta x\ddot{\phi}_j = v_{j+1}\dot{\phi}_{j+1} - v_{j-1}\dot{\phi}_{j-1} + v_j\left(\dot{\phi}_{j+1} - \dot{\phi}_{j-1}\right) - \frac{u^2 - v_{j-1}^2}{2\Delta x}\left(\phi_j - \phi_{j-2}\right) - \frac{u^2 - v_{j+1}^2}{2\Delta x}\left(\phi_j - \phi_{j+2}\right), \tag{G.5}$$

for the translationally invariant case ($v_j = v$) this reduces to

$$2\Delta x\ddot{\phi}_j = 2v\left(\dot{\phi}_{j+1} - \dot{\phi}_{j-1}\right) - \frac{u^2 - v^2}{2\Delta x}\left(2\phi_j - \phi_{j-2} - \phi_{j+2}\right). \tag{G.6}$$

Using the following ansatz $\phi_j(t) = e^{i\omega t}e^{ik\Delta x j}$, we get the dispersion relation

$$\omega_\pm(k) = v\frac{\sin(k\Delta x)}{\Delta x} \pm u\left|\frac{\sin(k\Delta x)}{\Delta x}\right|, \tag{G.7}$$

in the limit $\Delta x \to 0$, this yields the same dispersion relation as in the continuum case. Additionally in this dispersion relation the sector near $k = 0$ and $k = \pi$ mirror each other which is reminiscent of the dispersion relation in Eq. (4.17).

We now come to the inhomogeneous system, since the Lagrangian is still time independent we can still write the ansatz $\phi_j(t) = e^{i\omega t}\phi_j$, which gives us the following recurrence relation

$$\begin{aligned}-\omega^2\frac{2\Delta x}{u}\phi_j = {}& i\omega\frac{v_{j+1}}{u}\phi_{j+1} - i\omega\frac{v_{j-1}}{u}\phi_{j-1} + i\omega\frac{v_j}{u}\left(\phi_{j+1} - \phi_{j-1}\right) - \frac{u^2 - v_{j-1}^2}{2u\Delta x}\left(\phi_j - \phi_{j-2}\right) \\ &- \frac{u^2 - v_{j+1}^2}{2u\Delta x}\left(\phi_j - \phi_{j+2}\right),\end{aligned} \tag{G.8}$$

which we can re-write as

$$\begin{aligned}\phi_{j+2} = {}& \phi_j - \frac{4\omega^2\Delta x^2}{u^2 - v_{j+1}^2}\phi_j + \frac{2i\omega\Delta x}{u^2 - v_{j+1}^2}\left(v_{j-1}\phi_{j-1} - v_{j+1}\phi_{j+1}\right) - \frac{2i\omega\Delta x}{u^2 - v_{j+1}^2}v_j\left(\phi_{j+1} - \phi_{j-1}\right) \\ &+ \frac{u^2 - v_{j-1}^2}{u^2 - v_{j+1}^2}\left(\phi_j - \phi_{j-2}\right).\end{aligned} \tag{G.9}$$

We are interested in the solution to this recurrence relation for the following profile

$$v_j = \begin{cases} v_0 & j \to -\infty, \\ v_1 & j \to \infty, \end{cases} \tag{G.10}$$

such that $v_0 < u < v_1$. With this profile of the parameter v_j, in the asymptotically left region the signals will move in both left and right directions while in asymptotically right region the signals will only move towards right, and somewhere in the boundary between these two region for some j' we will have $v_{j'} \leq u < v_{j'+1}$, this is the event horizon.

In general solving the recurrence relation in Eq.(G.9) for an arbitrary profile of v_j is not analytically possible, therefore we will tackle this problem numerically. We use a linear profile for the parameter v_j such that

$$v_j = \begin{cases} 0 & j < -J, \\ v_{\max}\frac{j+J}{2J} & -J \leq j \leq J, \\ v_{\max} & j > J, \end{cases} \tag{G.11}$$

where $v_{\max} = \frac{2u}{1-\frac{\alpha}{J}}$ and $\alpha < J$ is a real number that decides the details of discretisation of v_j with respect to u. For example, if $\alpha = 0$ then $v_{j=0} = u$, or if $\alpha = 0.5$ then u will lie exactly in middle of $v_{j'}$ and $v_{j'+1}$. The justification for using a linear profile is that in the continuum limit if the change in metric across the horizon is smooth, then we can always approximate this change in the region near the horizon as linear.

To construct scattering modes for the Hamiltonian we start with the following incoming plane wave

$$\phi_{\text{in}} = \sum_{j<-J} e^{ik\Delta xj} \quad 0 < k\Delta x \ll 1, \tag{G.12}$$

in the region with $v_j = 0$ and energy $\omega_+(k) = u\sin(k\Delta x)/\Delta x$. Using the recurrence relation we obtain the transmitted mode as shown in Fig. G.1, from this we conclude that the scattering modes with positive energy are of the form

$$\phi_k = \sum_{j<-J} e^{ik\Delta xj} + C(\omega_{k,+}) \sum_{j\geq -J} \left(e^{i\widetilde{k}\Delta xj} + e^{i(\pi-\widetilde{k}\Delta x)j} \right), \tag{G.13}$$

where

$$\widetilde{k} = \frac{1}{\Delta x} \arcsin \frac{\omega_{k,+}\Delta x}{v_{\max} - u}, \tag{G.14}$$

is obtained by energy matching and $C(\omega_{k,+})$ is a constant depending on the energy of the incoming wave. To extract the form of the constant $C(\omega_{k,+})$, we use the plot in Fig. G.2 (a) and find that

$$C(\omega_{k,+}) = \gamma e^{\frac{\pi}{a}\omega_{k,+}}. \tag{G.15}$$

The factor $e^{\pi\omega_{k,+}/a}$ is the expected Hawking factor where a is the analog surface gravity, which should be given by the derivative of the group velocity across the horizon, and indeed from Fig. G.2 (b) we can see that

$$a = \frac{v_{\max}}{2J\Delta x}, \tag{G.16}$$

i.e. it is the discrete derivative of the group velocity. In contrast to the continuum version of this problem we also have the γ term in addition to the Hawking factor ($e^{\pi\omega_{k,+}/a}$). As alluded to in the main text γ depends on the exact details of the discretisation of v_j, if $\alpha = 0.5$ and therefore u lies exactly in the middle of some $v_{j'}$ and $v_{j'+1}$ then $\gamma = 1$, as we change α and therefore the asymmetry of u with respect to $v_{j'}$ and $v_{j'+1}$, the value of γ changes and becomes infinite for $\alpha = 0$ (see Fig. G.2 (b)). This can also be seen from the recurrence relation in Eq.(G.9), where if some $v_j = u$, the equation becomes non-analytic. Another thing we can gleam from Eq. (G.13) is that the incoming mode scatters into two different modes with same energy but for one of them its momentum is near $\widetilde{k} = 0$ and for the other one the momentum is near $\widetilde{k} = \pi$. This in turn implies that even for the case of smooth variation of parameters, in a lattice model, the ambiguity between black/white hole nature of the horizon still remains.

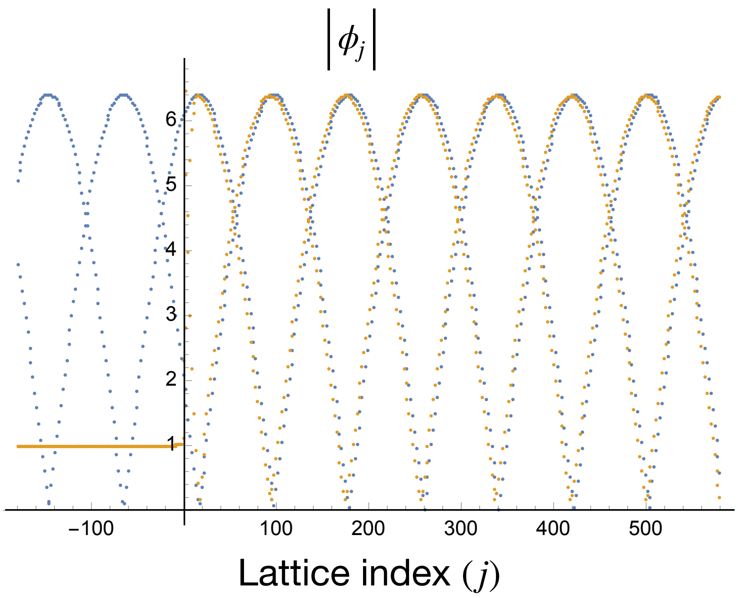

Figure G.1.: In this figure we have plotted the absolute value of ϕ_j as a function of j. Since the incoming mode was chosen to be a plane wave therefore we see $|\phi_j| = 1$ for $j < -J$. The transmitted mode (orange dotted lines), obtained numerically, shows a beating pattern. To confirm that the beating pattern is produced by a wave vector near $\widetilde{k} = 0$ and the other one near $\widetilde{k} = \pi$, we have also plotted a function $A\left(e^{i\widetilde{k}\Delta x j} + e^{i\left(\pi - \widetilde{k}\Delta x\right)j)}\right)$ on the same figure. We see that the theoretical and numerical transmitted modes agree with each other if we scale the theoretical one appropriately using the constant A.

a)

b)

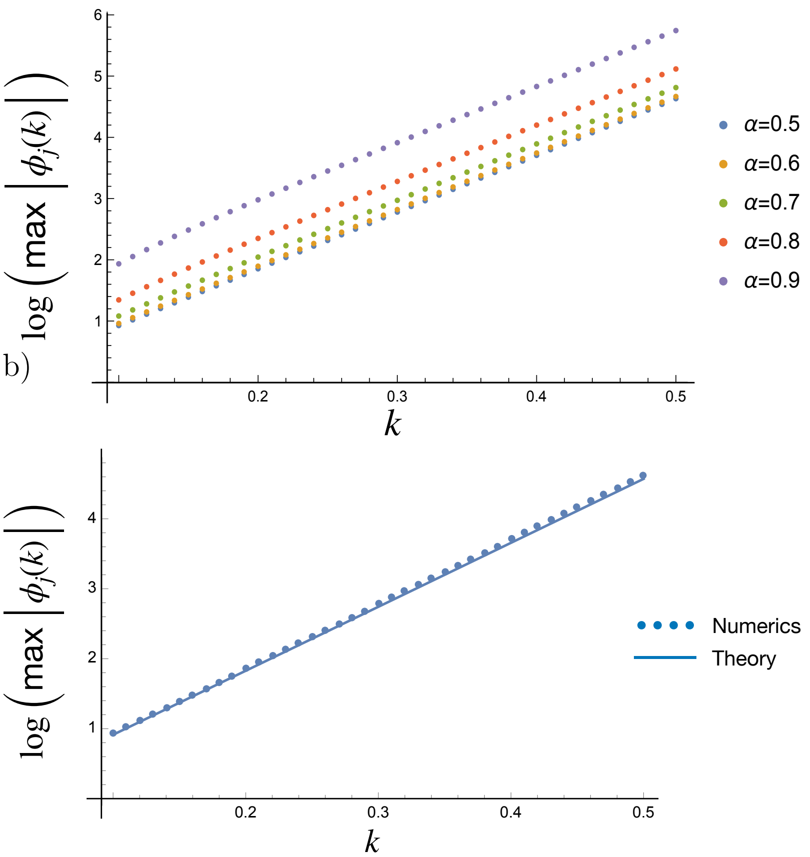

Figure G.2.: a) In this figure we have plotted the logarithm of maximum of $|\phi_j(k)|$, where k is the wave vector of the incoming mode, against k to extract the constant $C(\omega_{k,+})$. Note that only the transmitted mode has been plotted. We see that for different values of α the log plots differ by their intercepts, this is the factor γ that depends on the details of discretisation of v_j. b) Here we have isolated the plot of $\alpha = 0.5$, such that $\gamma = 1.0$, to confirm that our theoretical prediction of the surface gravity $a = v_{\max}/2J\Delta x$ matches the numerical calculation, which we can see it indeed does.